THE UNIVERSITY
of EDINBURGH

THE UNIVERSITY of EDINBURGH
Centre for Inflammation Research

Strategies for Earlier Diagnosis of Endometrial Cancer: Targeting Endometrial Hyperplasia

Peter Andrew Sanderson MB ChB MRCOG

Thesis submitted for the degree of Doctor of Philosophy

The University of Edinburgh

March 2019

CANCER RESEARCH UK | EDINBURGH CENTRE

Declaration

I declare that this thesis was composed by myself, that the work contained herein is my own except where explicitly stated otherwise in the text, and that this work has not been submitted for any other degree or professional qualification except as specified.

Parts of this work have been published in [*Peter A. Sanderson, Hilary O.D. Critchley, Alistair R.W. Williams, Mark J. Arends, Philippa T.K. Saunders; New concepts for an old problem: the diagnosis of endometrial hyperplasia, Human Reproduction Update, Volume 23, Issue 2, 1 March 2017, Pages 232–254*].

Peter Andrew Sanderson

March 2019

Acknowledgements

First and foremost, I wish to thank Professor Philippa Saunders. Philippa has been a constant source of encouragement, advice and expertise during my research fellowship. Philippa is a brilliant, world-class scientist and a leader in her field, I consider myself very lucky to be part of her laboratory group. The skills and knowledge that I have developed over the course of the last 4 years are immeasurable, and none of what I have achieved would have been possible were it not for Philippa taking a chance on me – the O&G trainee from Sheffield, who had not picked up a pipette before!

I am also exceptionally grateful to Professors Mark Arends and Hilary Critchley, both of whom have provided invaluable guidance and support, both scientifically and clinically, throughout my fellowship. A very special thanks must go to Professor Alistair Williams. This PhD project would not have been possible without Alistair. He is an exceptionally patient, kind and knowledgeable teacher, with a wealth of academic experience and unwavering research enthusiasm. One of the most valuable parts of this fellowship was the time spent with Alistair analysing endometrial samples over a double-headed microscope.

I have had the privilege to work alongside some fantastic people within the Saunders lab. Frances Collins has literally taught me everything, from cell culture to Taqman – her research experience is second to none and I would particularly like to thank her for her assistance and constant optimism with the cell culture work in chapter 5. Many thanks also go to Arantza, for sharing her wealth of knowledge about immunohistochemistry, her patience during antibody optimisations and for performing the staining for the mismatch match repair proteins detailed in chapter 4. I am grateful to all past and present members of the Saunders group including; Bianca, Yannis, Doug, Phoebe, Olympia, Fiona, and Erin for creating a welcoming and fun working environment. Each of them has helped in some way towards this thesis, be it with words of encouragement, troubleshooting advice or simply proclaiming the phrase “that’s science!” when experiments did not quite go as planned.

Additional thanks go to Professor Simon Herrington for helping to reclassify the endometrial hyperplasia specimens, Dr Pamela Brown and Ms Linda Ferguson for creating the lentiviral vectors, Lyndsey Boswell in SuRF histology for the automated PTEN staining, to Cancer Research UK for funding my fellowship and to all the patients who donated tissue samples. Finally, I would like to thank my parents for their continued support and my wife, Tracie, for her patience, understanding and continual belief in me.

Abstract

Endometrial cancer (EC) is the most common gynaecological malignancy in the developed world, with approximately 9000 new cases reported annually within the UK (2013-2015). Incidence rates of EC have been steadily climbing over the last decade, with a notably steep increase described in the 40 to 49-year-old age group, most likely as a consequence of rising rates of obesity. Endometrial hyperplasia (EH) is a uterine pathology which is characterised by an increase in the endometrial gland-to-stroma ratio when compared to endometrium from the proliferative phase of the menstrual cycle. The clinical significance of EH lies in its association with progression to endometrioid endometrial cancer and 'atypical' forms of EH are widely considered to be premalignant lesions.

The overarching objective of the studies described in this thesis was to use cellular and molecular approaches to improve our capacity for earlier diagnosis of EC, through targeting and enhancing our understanding of EH. The following aims were addressed:

1. To develop a human EH tissue resource and utilise this to evaluate the current methods used to classify EH and predict its progression to EC.

2. To characterise key molecular changes within EH lesions so that they can be used to extend and enhance pathological classification of EH.

3. To explore *in vitro* models of the endometrium and investigate the role of PTEN and ARID1A in endometrial epithelial cell proliferation.

The results obtained herein provide novel insight into the diagnostic reproducibility of the two prominent EH pathological classification systems; i) the well-known and widely used World Health Organisation 1994 (WHO94) classification and ii) the more recent Endometrioid Intraepithelial Neoplasia (EIN)/WHO2014 iteration. Following an extensive retrospective review of patient medical records, a human tissue resource was established from samples held within The Lothian NRS Human Annotated Bioresource. Archival tissue sections from n=125 individual patient samples, that were pathologically diagnosed and coded as EH lesions based on the WHO94 criteria, were identified. A dual, blinded, expert gynaecological pathologist review was subsequently carried out. Interobserver percentage agreement for each of the expert pathologists and the original WHO94 based diagnosis was 56.0 % (n=70) and 48.8 % (n=61) respectively. Upon reclassification using the EIN/WHO2014 classification system, EIN lesions were identified in 52/125 patients, with increased interobserver agreement

noted between the expert pathologists (67.2 %, n=84). The EIN/WHO2014 classification system also appeared to improve upon the WHO94 system when predicting progression to EC.

Investigation of EH lesions for molecular changes pertinent to endometrial carcinogenesis revealed significant differences in the immunohistochemical expression pattern of the tumour suppressor PTEN, and the transcription factors PAX2 and HAND2 between EIN and benign EH lesions. These data may, pending further validation studies, lend favourably to their use as a diagnostic pathological aid. Somewhat unexpectedly, the frequency of defects in mismatch repair protein (dMMR) expression was considerably less than hypothesised amongst EIN lesions. This was surprising given that dMMR are reported in approximately 25-30 % of somatic ECs.

An accepted risk factor for the development of both EH and EC is exposure to 'unopposed oestrogens' i.e. oestrogen without progesterone opposition. A novel *in vitro* model was created utilising EC cell lines to investigate the proliferative effects of silencing two commonly mutated genes within both EHs and ECs, namely PTEN and ARID1A, and also the overexpression of oestrogen receptor alpha (ERα). Cellular manipulation of gene expression for ERα, PTEN and ARID1A was performed. Findings demonstrated a significant increase in EC cell proliferation with knockdown of PTEN and to a lesser extent ARID1A, when compared to EC cells transfected with a scrambled sequence. The addition of a functional ERα to the knockdown models did not appear to increase cell proliferation in this context.

In conclusion, novel data described herein highlights the current difficulties in achieving a reproducible diagnosis for EH. The use of immunohistochemistry identified changes in protein expression, which together with automated tissue analysis and *in vitro* studies, were used to complement and extend our understanding of premalignant changes in the endometrium. These findings have implications for the clinical management of women diagnosed with EH, as well as the development of a personalised approach to monitoring of women at increased risk of progression to EC.

Lay Summary

The inner lining layer of the womb is called the endometrium and it is made up of many different types of cells. The endometrium undergoes monthly structural changes, called 'the menstrual cycle' and this is controlled by chemical structures called hormones. The two main female hormones are oestrogen and progesterone. Cancer of the endometrium is the most common reproductive cancer to affect women in the developed world and it is strongly associated with being overweight or obese.

Too much oestrogen without progesterone can cause the endometrium to grow and become abnormally thickened. This can occur, either 1) as a woman nears the menopause (natural cessation of periods), 2) due to an underlying medical condition, 3) due to hormonal medications or 4) due to obesity. Abnormal growth and thickening of the endometrium is called endometrial hyperplasia (EH) and this condition has a wide variety of appearances when viewed with a microscope. In its most abnormal form EH may develop into endometrial cancer (EC).

The studies described in this thesis explore how EH is classified and investigate strategies to aid in its diagnosis. The results presented demonstrate problems in reproducibly diagnosing EH using traditional classification methods. These problems arise because at a microscopic level, it can be difficult to separate worrying EH features that are high-risk for future cancer development, from benign EH features caused by high levels of oestrogen exposure. We demonstrate that a newer classification system which uses strict criteria improves on its predecessors. In addition, further findings suggest that this newer classification system may be enhanced using a pathology technique called immunohistochemistry, which allows changes in the presence of proteins between benign and pre-cancerous types of EH to be directly visualised in tissue samples with a microscope. Finally, using a model system of endometrial cancer cells, we have discovered that two commonly altered genes in both EC and EH (i.e. the codes present in the cells that controls the cell behaviour) may affect endometrial cell growth.

With rates of EC continuing to rise, especially in younger pre-menopausal woman, our hope is that though improved understanding of EH (as a potential pre-cancerous condition), strategies for the earlier diagnosis of EC can be developed.

Publications, presentations and posters relating to this thesis

Publication

Peter A. Sanderson, Hilary O.D. Critchley, Alistair R.W. Williams, Mark J. Arends, Philippa T.K. Saunders; **New concepts for an old problem: the diagnosis of endometrial hyperplasia**, Human Reproduction Update, Volume 23, Issue 2, 1 March 2017, Pages 232–254.

Oral Presentations

Endometrial Hyperplasia: Diagnostic reproducibility and use of novel immunohistochemical biomarkers. TENS Obstetrical & Gynaecological Society. October 2018, Dumfries and Galloway. **Rachel Morrison memorial prize winner.**

Early Diagnosis & Treatment Strategies for Endometrial Cancer. CRUK Annual Senior Nurses Meeting. Edinburgh, May 2015. **Invited speaker.**

Poster Presentations

Endometrial hyperplasia diagnostic reproducibility and use of immunohistochemical biomarkers. British Gynaecological Cancer Society Annual Meeting. June 2017, Glasgow.

A Diagnosis of Endometrial Hyperplasia: Where are we now? Winter meeting of the Pathological Society. January 2017, London.

Characterising Endometrial Hyperplasias: The role of immunohistochemistry and pathological classification to gauge neoplastic potential. Royal College of Obstetricians and Gynaecologists Annual Academic Meeting. March 2016, London.

Table of Contents

Table of Figures

List of Tables

List of Abbreviations

Abbreviation	
17β-HSDs	7β-Hydroxysteroid dehydrogenase
4-OHT	4-Hydroxytamoxifen
ACOG	American college of Obstetrics and Gynecology
AKT	Protein kinase B
ARID1A	AT-rich interactive domain-containing protein 1A
AUB	Abnormal uterine bleeding
BGSE	British Society for Gynaecological Endoscopy
BMI	Body mass index
BRCA1	Breast cancer type 1 susceptibility protein
BRCA2	Breast cancer type 2 susceptibility protein
BSA	Bovine serum albumin
BSO	Bilateral salpingo-oophorectomy
CAH	Complex atypical hyperplasia
CNA	Copy number alteration
CD10	Neprilysin
CH	Complex hyperplasia
CI	Confidence interval
CL	Corpus luteum
CMV	Cytomegalovirus
CTNNB1	β-catenin
CYC	CYCLE gene
DAB	3,3′-Diaminobenzidine
DAPI	4′,6-diamidino-2-phenylindole
DMEM	Dulbecco's Modified Eagle Medium
dMMR	Disordered mismatch repair
DMSO	Dimethyl sulfoxide
DNA	Deoxyribonucleic acid
DPBS	Dulbecco's phosphate-buffered saline
DPE	Disordered proliferative endometrium
E_1	Oestrone
E_2	Oestradiol
E_3	Oestriol
EC	Endometrial cancer
EDTA	Ethylenediaminetetraacetic acid
EEC	Endometrioid endometrial cancer
EH	Endometrial hyperplasia
EIN	Endometrioid intraepithelial neoplasia
EIN-EMP	Endometrioid intraepithelial neoplasia - endometrial polyp
ERα	Oestrogen receptor alpha
ERβ	Oestrogen receptor beta
ET	Endometrial thickness
FACS	Fluorescence activated cell sorting
FCS	Foetal calf serum
FFPE	Formalin-fixed paraffin-embedded
FIGO	Fédération Internationale de Gynécologie et d'Obstétrique
FSH	Follicle stimulating hormone
GFP	Green fluorescent protein

GnRH	Gonadotropin-releasing hormone
GOI	Gene of interest
H&E	Haematoxylin and eosin
HAC	Hierarchical agglomerative clustering
HAND2	Heart and Neural Crest Derivatives Expressed 2
HBOC	Hereditary breast and ovarian cancer
HER2	Human epidermal growth factor receptor 2
HIER	Heat induced epitope retrieval
HNPCC	Hereditary nonpolyposis colorectal cancer
HP	Hyperplastic polyp
HPA	Hypothalamic pituitary axis
HRP	Horseradish peroxidase
HRT	Hormone replacement therapy
HwA	Hyperplasia without atypia
ICI	Fulvestrant (Faslodex)
IF	Immunofluorescence
IHC	Immunohistochemistry
IMB	Intermenstrual bleeding
IRES	Internal ribosome entry site
k	Kappa
LH	Luteinising hormone
LNG-IUS	Levonorgestrel intrauterine system
LVSI	Lymphovascular space invasion
miRNA	Micro-ribonucleic acid
MLH1	MutL homolog 1,
MME	Membrane Metalloendopeptidase
MMR	Mismatch repair
MSH2	MutS Homolog 2
MSH6	MutS Homolog 6
NaCl	Sodium chloride
NAS	Normal animal serum
NBF	Neutral buffered formalin
opre	Optimised post-translational response element
p53	TP53 or tumour protein 53
PAX2	Paired box gene 2
PBS	Phosphate buffered saline
PCK	Pan-cytokeratin
PCOS	Polycystic ovarian syndrome
PECs	Primary epithelial cells
PTEN	Phosphatase and tensin homolog
PFS	Progression free survival
PI3K	Phosphoinositide 3-kinases
PIP_2	Phosphatidylinositol 4,5-bisphosphate
PIP_3	Phosphatidylinositol (3,4,5)-trisphosphate
PMB	Post-menopausal bleeding
PMS2	Mismatch repair endonuclease PMS2
POLE	DNA Polymerase Epsilon
PPT	Propyl pyrazole trio
PVDF	Polyvinylidene difluoride
RCOG	Royal college of Obstetricians and Gynaecologists
RFP	Red fluorescent protein
Rho	Rho family of GTPases
RNA	Ribonucleic acid

ROCK	Rho-associated protein kinase
ROI	Region of interest
RPMI	Roswell Park Memorial Institute medium
SAH	Simple atypical hyperplasia
Scr-miR	Scrambled micro-ribonucleic acid
SERM	Selective oestrogen receptor modulator
SH	Simple hyperplasia
SHBG	Sex hormone binding globulin
SuRF	Shared university research facility
SWI/SNF	SWItch/Sucrose Non-Fermentable
TBS	Tris buffered saline
TU	Transduction unit
UK	United Kingdom
VPS	Volume percentage stroma
WHO	World Health Organisation

Chapter 1

1 Literature Review

1.1 Introduction

Endometrial cancer (EC) is the most common gynaecological malignancy in the developed world and the 4th most common cancer to affect UK women (Ferlay *et al.*, 2015). Incidence rates are reported to be rising, with approximately 8500 new cases registered in the UK in 2015 (Cancer Research UK, 2018). Most EC cases occur in postmenopausal women; however, age specific incidence increases steeply from 45-49 years (Figure. 1-1) (Cancer Research UK, 2018).

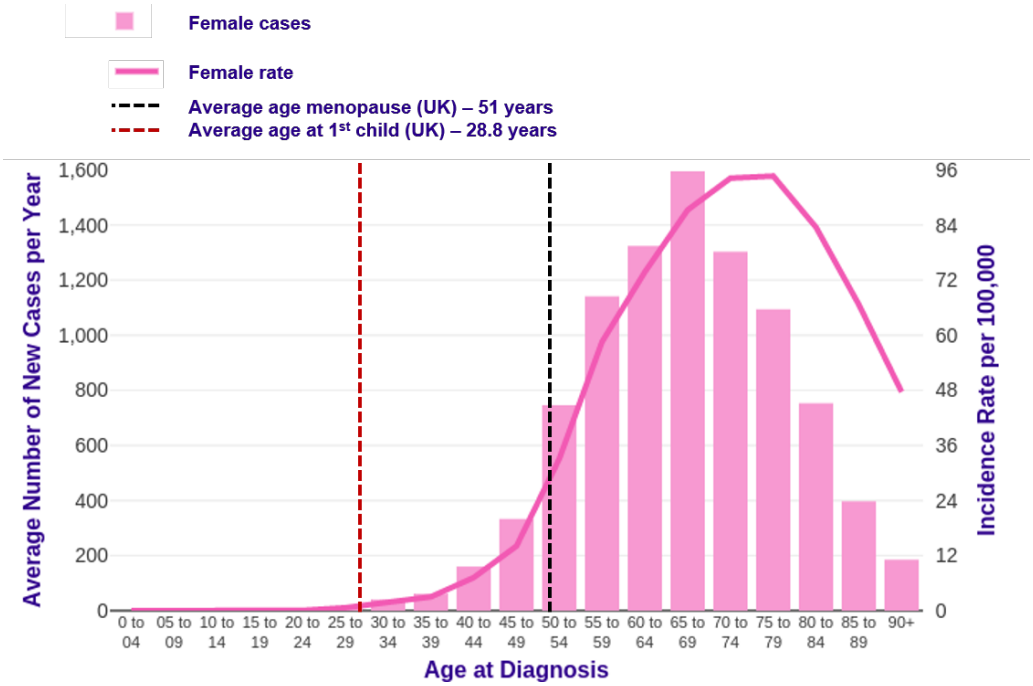

Figure 1-1: UK Uterine cancer statistics 2013-2015. The average number of new cases per year and age-specific incidence rates per 100,000 population for all uterine cancers, UK, 2013-2015. Red dashed line represents the average age a UK woman will have her first child (28.8 years in 2016 (Haines, 2017)). Black dashed line represents the average age of menopause in UK women (51 years (Dunneram *et al.*, 2018)). Adapted from Cancer Research UK, 2018.

A significant risk factor for this increase in incidence is the current obesity epidemic, and EC ranks highest amongst all cancers in its association with obesity (Mackintosh and Crosbie, 2013). If diagnosed and treated whilst confined to the uterus (International Federation

of Gynecology and Obstetrics (FIGO) stage I and II disease) EC carries an excellent prognosis with high curability. Endometrial hyperplasia (EH) is an 'umbrella' term representing a heterogenous spectrum of morphologically abnormal endometrial lesions and the condition shares many risk factors with EC. When cytological atypia (a variety of abnormal nuclear features including; loss of 'axial polarity', unusual / clumped shapes that may be rounded with irregular nuclear contours, noticeable nucleoli, and cleared or dense chromatin) is present within EH lesions there is a substantial risk of a coincident or subsequent diagnosis of endometrioid EC (Ellenson *et al.*, 2011). There is an increasing need for individualised risk stratification and personalised treatment approaches within EC care, especially for younger women who may wish to preserve fertility and for those at a high risk of surgical morbidity. To ensure robust and early diagnosis advancing our understanding of EH as a premalignant lesion is required.

1.2 The normal human endometrium and menstrual cycle

The human endometrium is a dynamic, multicellular tissue structure which forms the inner lining layer of the uterus. During the reproductive years of a woman's life it responds to fluctuating levels of ovarian sex-steroid hormones, undergoing cyclical proliferation and decidualisation ready to support a developing pregnancy (Jabbour *et al.*, 2006). When pregnancy implantation does not occur, the endometrium is shed (menstruation) and without loss of function or scarring it rapidly repairs and restores tissue integrity, ready to begin the process again (Critchley and Maybin, 2011). Abnormal sex-steroid hormone exposure and coexisting pathology can have significant effects on both the structure and function of the endometrium, leading to abnormal uterine bleeding (AUB) and in some cases neoplasia (Maybin and Critchley, 2015).

1.2.1 Structure of the human endometrium

The endometrium lines the uterine cavity and it is surrounded by an outer layer of smooth muscle known as the myometrium (Figure. 1-2). The endometrium is structurally divided into two distinct layers (Figure. 1-2); a luminal (inner) functional layer and a basal layer that is adjacent to the myometrium (Bartelmez, 1957). It is the functional layer that breaks down and is shed during menstruation, however both layers have been proven to contribute to the cyclical regeneration process (Gaide Chevronnay *et al.*, 2009).

The endometrium is comprised of several cell types, which include luminal and glandular epithelial cells and a multicellular stromal compartment. The stromal compartment contains 'fibroblast-like' cells, vascular and lymphatic channels as well as a diverse population of immune cells, the numbers of which fluctuate across the cycle (King, 2000; Maybin and Critchley, 2015; Rogers, 1996). Endometrial blood vessels become heavily coiled in the latter half of the menstrual cycle and consist of endothelial cells with surrounding pericytes (Rogers, 1996). Endometrial lymphatics are suggested to be sparsely distributed in the functional layer, with larger lymph vessels found within the basal layer (Donoghue *et al.*, 2007). Tumour invasion of the lymphovascular space (LVSI) is considered to be a poor prognosticator for EC (Briët *et al.*, 2005).

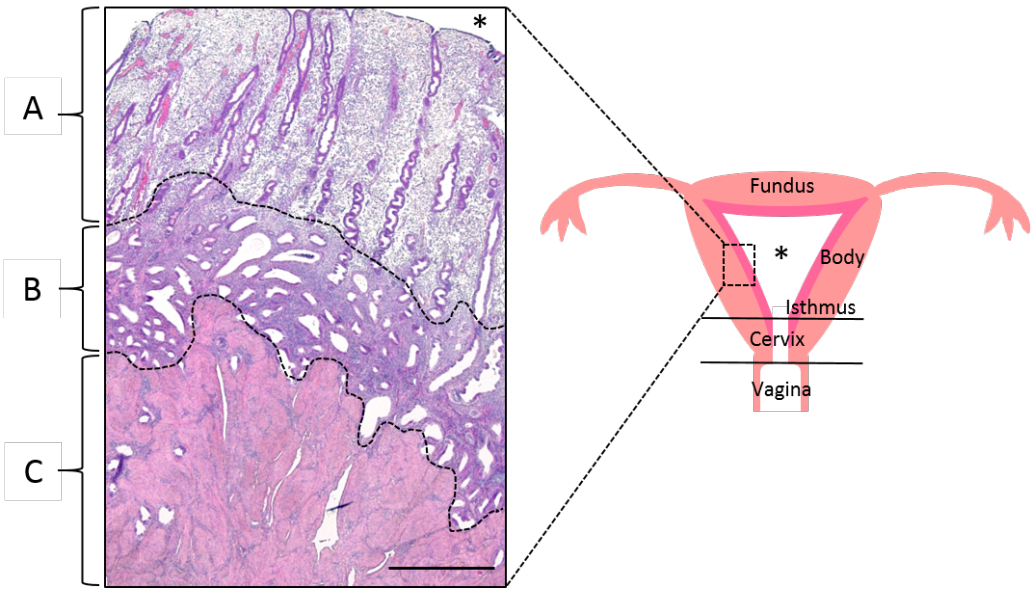

Figure 1-2: Schematic representation of the human uterus and representative histology. The human uterus is divided anatomically into four regions, the fundus, the body, the isthmus and the cervix. The human uterus contains a single uterine cavity (*). The inner lining layer of the human uterus is the endometrium which is divided into: A) an inner/luminal functional layer 'functionalis' and B) a basal layer 'basalis'. The outer smooth muscle layer of the uterus (C) is the myometrium. Representative haematoxylin and eosin (H&E) histological image from the secretory phase of the menstrual cycle kindly provided by Dr Ioannis Simitsidellis, University of Edinburgh. 1000µm scale bar.

1.2.2 The human menstrual cycle

The human menstrual cycle can be considered as having two synchronous aspects: 1) the ovarian cycle - governing the preparation of endocrine tissue and the release of an oocyte and 2) the endometrial cycle - governing the preparation and maintenance of the uterine lining.

1.2.2.1 The ovarian cycle

The menstrual cycle is controlled by ovarian sex-steroid hormones and mediated by feedback loops as part of the hypothalamic-pituitary-ovarian axis (HPA). The average human menstrual cycle lasts from 28-35 days (Sherman and Korenman, 1975; Treloar *et al.*, 1967). The ovarian cycle is divided into two phases: 1) the follicular phase (~14-21 days duration) and 2) the luteal phase (14 days duration) (Figure. 1-2).

The follicular phase begins following the onset of menses (day 1), whereby there is a progressive, pulsatile increase in gonadotrophin-releasing hormone (GnRH) from the hypothalamus and a subsequent slow increase in both serum follicle-stimulating hormone (FSH) and luteinising hormone (LH) concentrations (Bates and Bowling, 2013). The increase in FSH stimulates growth and survival of a cohort of antral follicles within the ovary, which increase their expression of aromatase (Turner *et al.*, 2002) and secrete oestradiol (E_2) (Johnson, 2007). This secreted E_2 provides negative feedback to the HPA to lower FSH and LH secretion, preventing further follicle stimulation. Large follicles require less FSH to survive than smaller ones and so a dominant follicle emerges (Johnson, 2007). Serum oestradiol concentration continues to rise, and a sudden mid-cyclical surge occurs (Adams *et al.*, 1994). This surge represents a switch from negative to positive HPA feedback, resulting in release of LH by the pituitary that can be detected as a rapid rise in serum LH levels in the circulation (Adams *et al.*, 1994). It marks the beginning of the luteal phase of the cycle and also corresponds with ovulation (Figure. 1-3).

After ovulation, transformation of the ovulatory follicle into the corpus luteum (CL) results in the production of high levels of the hormone progesterone, which gradually increases in the mid- to late-luteal phase (Bates and Bowling, 2013) (Figure. 1-3). The CL also produces E_2 and Inhibin A (Stocco *et al.*, 2007). These hormones provide negative feedback on the HPA. If pregnancy does not occur, the CL degenerates, precipitating a fall in circulating concentrations of progesterone and oestrogen with the onset of menses. The HPA axis is

released from negative feedback, causing FSH and LH levels to start to rise and begin the next cycle.

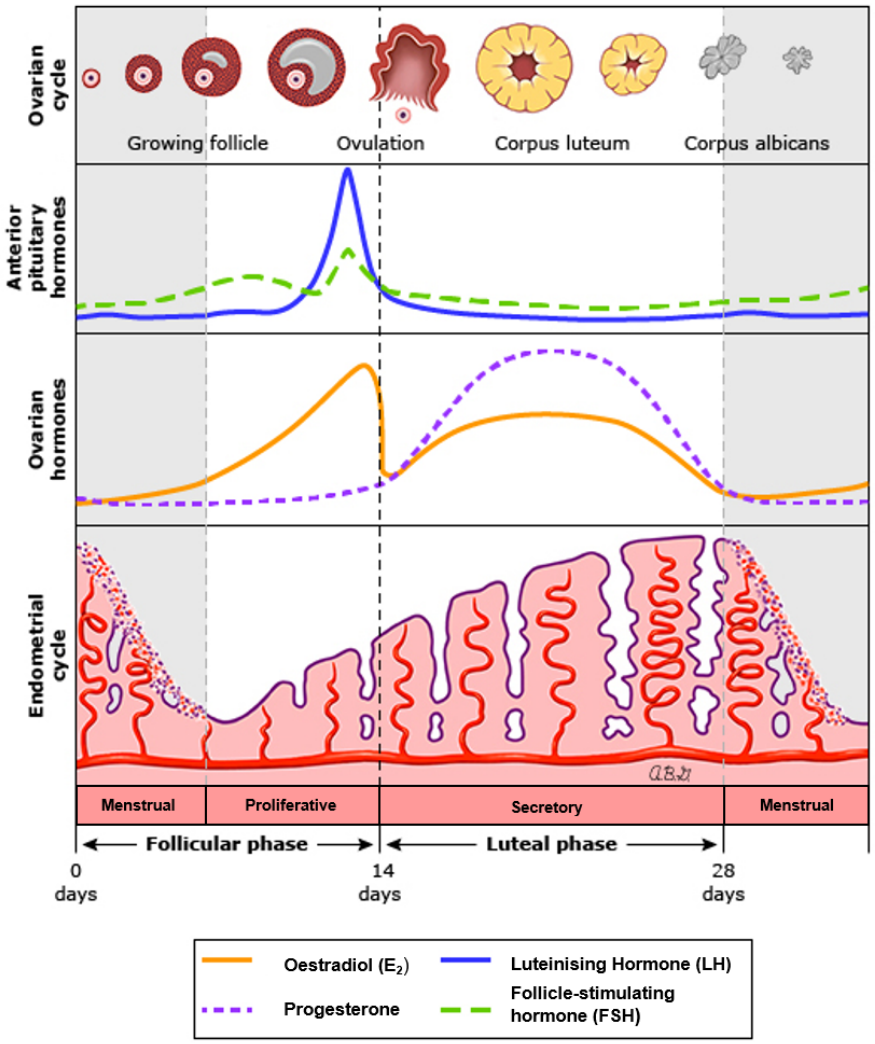

Figure 1-3: The human menstrual cycle. Schematic figure demonstrating the changes in sex-steroid hormone levels during the human menstrual cycle, with the corresponding physiological changes in the endometrium and ovary. In response to FSH a dominant follicle develops with a concomitant increase in the secretion of oestradiol. Following ovulation, oestradiol levels fall rapidly, and the corpus luteum secretes progesterone. Should a pregnancy not establish, regression of the corpus luteum leads to withdrawal of ovarian hormones resulting in menstruation. Image adapted from www.uptodate.com (Graphic 62189 Version 4.0) (UpToDate inc, 2019)

1.2.2.2 The endometrial cycle - proliferative phase

The proliferative phase of the human menstrual cycle commences immediately after menstruation and lasts until ovulation. Under the stimulation of oestrogens, predominantly E_2, proliferation of the epithelial, stromal and vascular cell compartments occurs, resulting in a two-to-three-fold increase in endometrial thickness (ET) by the time of ovulation (Fleischer *et al.*, 1986). In the early-proliferative phase (~ days 4-7 of a 28-day cycle) the endometrium is characterised by a thin luminal epithelium and straight, short and narrow endometrial glands with numerous mitoses present (Noyes *et al.*, 1975). The stromal compartment is compact, and the stromal cells exhibit large nuclei and scanty cytoplasm (Noyes *et al.*, 1975). The mid-proliferative phase (~ days 8-10 of a 28-day cycle), sees the formation of a taller columnar luminal epithelium and elongated curving glands with a 'looser' stromal structure (Figure. 1-4A) (Noyes *et al.*, 1975). Glandular epithelium shows stratification of nuclei – this is characteristic of proliferative phase, and disappears in the secretory phase, when nuclei are situated in a single row close to the basement membrane. By the late-proliferative phase (~ days 10-14 of a 28-day cycle, the luminal epithelium undulates, and the glands appear tortuous with a pseudostratified appearance (Noyes *et al.*, 1975).

1.2.2.3 The endometrial cycle - the secretory phase

The secretory phase of the endometrial cycle begins after ovulation, with the luteal production of progesterone dominating the endocrine environment. The secretory phase is normally divided into three stages: 1) early (days 14-18 of a 28-day cycle), 2) mid (days 19-23) and 3) late (days 24-28). In the early-secretory phase, subnuclear vacuolation of the glandular epithelium becomes prominent and the glands become tortuous in shape (Noyes *et al.*, 1975). The mid-secretory phase (Figure. 1-4B) sees a single layer of rounded nuclei at the base of the epithelial cells, the vacuoles having slipped past and expelled their contents into the gland lumen; the high glycogen content of these secretions aids potential blastocyst survival prior to implantation (Noyes *et al.*, 1975). Within the functional layer changes in the size and shape of the stromal cells become apparent and there is marked oedema. The late-secretory phase is characterised by further transformation of stromal cells (decidualisation) particularly those found under the luminal epithelium and adjacent to the arterioles, further maturation and differentiation of the vasculature (spiral arterioles) and a discernible increase in the numbers of immune cells including uterine natural killer cells and macrophages (King, 2000; Maybin and Critchley, 2015; Noyes *et al.*, 1975).

1.2.2.4 The endometrial cycle - the menstrual phase

In the absence of a pregnancy, withdrawal of oestrogens and progesterone culminates in piece-meal shedding of the functionalis layer of the endometrium (Garry *et al.*, 2009). Blood 'lakes' become apparent, with fragmented stromal cells and inflammatory exudate (Figure 1-4C) (Noyes *et al.*, 1975). These appearances rapidly become generalised and the luminal surface has a ragged and torn appearance with several gland openings (Garry *et al.*, 2009).

1.2.2.5 Postmenopausal endometrial life

There is a progressive failure of ovarian function and a decline in ovarian oestrogen production towards the end of reproductive life, culminating in the permanent cessation of menstruation. Menopause is officially diagnosed following 12-months of amenorrhoea without any other pathological or physical cause (Harlow *et al.*, 2012). The menopausal transition, or 'peri-menopause', occurs after the reproductive years, but before menopause, and is characterised by irregular menstrual cycles, endocrine changes, and vasomotor symptoms (McKinlay *et al.*, 1992). Histologically, the postmenopausal endometrium should appear atrophic, with a cuboidal or columnar epithelium with no mitotic figures (Pernick, 2017). Endometrial glands are usually tubular or cystic. The stroma appears inactive with variable collagenisation and minimal mitotic activity (Pernick, 2017).

1.2.3 The 'unopposed oestrogen' hypothesis

The primary source of oestrogen in postmenopausal life is from adrenal androgens that have been converted by aromatase enzymes to oestrone (E_1) in adipose tissue (Kaaks *et al.*, 2002; Simpson, 2003). Notably, obese postmenopausal individuals have been reported to have higher levels of circulating oestrogen (Moley and Colditz, 2016). In postmenopausal women, any excess oestrogen is not moderated by progesterone and is therefore considered to be 'unopposed.' The same principle applies to women experiencing extended periods of anovulation (e.g. individuals with polycystic ovarian syndrome PCOS or those experiencing a protracted 'peri-menopause') who lack regular luteal phase progesterone (Dumesic and Lobo, 2013). Individuals with a chronic absence of progesterone with continuous exposure to 'unopposed' oestrogen are at risk of EH and EC due to the proliferative and anti-apoptotic effects of oestrogens (Lewis-Wambi and Jordan, 2009). Progesterone, be it physiologically

released, or administered exogenously, has been suggested to 'protect' the endometrium from the proliferative effects of oestrogen (Greenblatt *et al.*, 1982; Kim *et al.*, 2013).

1.3 Abnormal uterine bleeding (AUB)

Abnormal uterine bleeding (AUB) is a common gynaecological condition accounting for ~ 1/3 of all referrals to a gynaecologist (Spencer and Whitehead, 1999). AUB refers to any uterine bleeding which is of abnormal quantity (individualised approach used to define 'excessive' blood loss that affects patient quality of life), duration or schedule (Spencer and Whitehead, 1999; Whitaker and Critchley, 2016). It incorporates heavy menstrual bleeding (HMB), intermenstrual bleeding (IMB) and postmenopausal bleeding (PMB) patterns. In 2011, the International Federation of Gynecology and Obstetrics (FIGO) introduced new terminology to classify the causes of AUB, abbreviated by the acronym PALM-COEIN (Table. 1-1) (Munro *et al.*, 2011). EC and EH are classified according to PALM-COEIN as AUB-M. Both conditions commonly present with postmenopausal bleeding (PMB) (~ 90 %), although only around 10 % of women with PMB will have EC. Women with AUB over 45-years of age, or those with irregular bleeding or failure of treatment over 45-years of age, require endometrial sampling to rule out the presence of EH or EC (Sundar *et al.*, 2017). Prompt referral for gynaecological assessment is mandatory for any episode of PMB.

Table 1-1: The 2011 FIGO PALM-COEIN classification of abnormal uterine bleeding (AUB).

Structural entities (PALM)	**Non-structural entities (COEIN)**
Polyp	**C**oagulopathy
Adenomyosis	**O**vulatory dysfunction
Leiomyoma (Fibroids)	**E**ndometrial
Malignancy & hyperplasia	**I**atrogenic
	Not otherwise classified

Reproduced from Munro *et al.*, 2011.

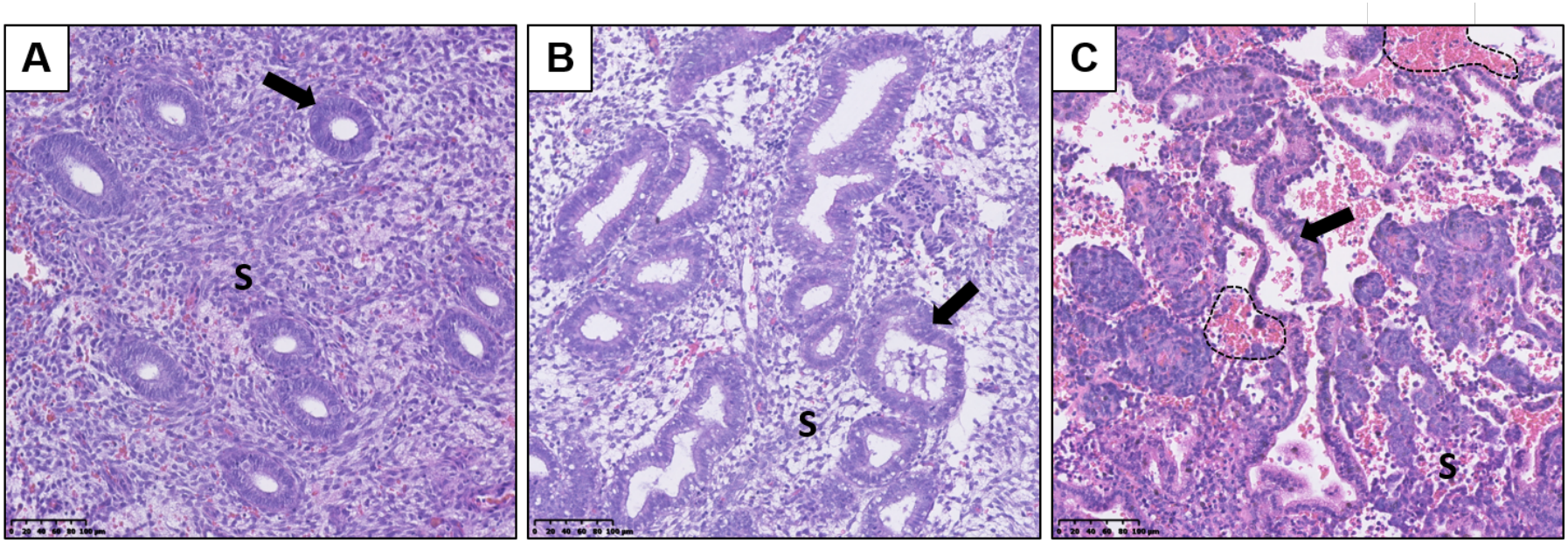

Figure 1-4: Representative haematoxylin and eosin (H&E) stained tissue sections from across the human menstrual cycle. Representative images from human endometrial tissue samples obtained during the course of the studies described herein. A) Mid-proliferative phase endometrium. Small, uniform and rounded endometrial glands arrowed, with compact endometrial stroma (S). B) Mid-secretory phase endometrium with nuclei towards the base of the endometrial glands (arrowed) and vacuoles transitioning from a sub-nuclear position to the luminal surface to expel glycogen rich secretions. The stroma (S) demonstrates marked oedema, with small almost 'naked' nuclei and filamentous cytoplasm. C) Menstrual phase endometrium with blood 'lakes' (circled), fragmented stromal cells (S) and torn, opened glands (arrowed). Magnification – see scale bar.

1.4 Endometrial Cancer

As touched on above, endometrial cancer (EC) is the most common gynaecological malignancy affecting women in developed countries (Ferlay *et al.*, 2015). The incidence of EC is steadily increasing; largely owing to an aging population and escalating rates of obesity (Ferlay *et al.*, 2015; Renehan *et al.*, 2010; Wise *et al.*, 2016). In spite of the frequency of the disease, awareness amongst the general population is low and EC research is somewhat underfunded relative to its societal burden (Carter and Nguyen, 2012). If diagnosed and treated in its early stages (International Federation of Gynaecology and Obstetrics, [FIGO] stages I and II), EC 5-year survival figures stand at approximately 92 % and 75 % respectively (Creasman *et al.*, 2006; Murali *et al.*, 2014). Women diagnosed with advanced EC (FIGO stages III and IV) have 5-year survival figures described at 57-66 % and 20-26 % respectively (Murali *et al.*, 2014). As discussed above, the majority of women with EC will present clinically with symptoms of AUB, in addition EC can also present as persistent postmenopausal discharge, as abdominal endometrial cells on cervical cytology or as an incidental finding. Established risk factors for the development of EC are listed in Table 1-2.

1.4.1 Endometrial cancer pathology

ECs have traditionally been pathologically described via a dualistic model, dividing them into ‘type 1’ and ‘type 2’ cancers based upon their clinical, metabolic and histological features (Bokhman, 1983). Type 1 ECs incorporate most of tumours seen and include the endometrioid adenocarcinomas, which account for >80 % of all ECs. Type 1 ECs are considered oestrogen-dependent and are frequently associated with EH, they are characteristically seen in post-menopausal obese women. Type 1 ECs are assigned a grade (1-3) depending on the degree of differentiation and nuclear features, with grade 1 representing slow growing tumours with low metastatic potential and grade 3 representing tumours with poor differentiation and an aggressive phenotype. Differential expression of oestrogen receptors alpha and beta has been demonstrated in type 1 ECs according to tumour grade (Collins *et al.*, 2009). Type 1 ECs are strongly associated with conditions contributing to unopposed oestrogen exposure (Table. 1-2), in addition to nulliparity and insulin resistance. Furthermore, some evidence has also been presented intimating a role for endocrine disrupting chemicals (EDCs) in EC development (reviewed in Gibson and Saunders, 2014). At a molecular level, type 1 ECs frequently harbour mutations in the genes *PTEN, KRAS, CTNNB1 and PIK3CA* (Murali et al., 2014).

Table 1-2: Established risk factors for the development of 'type 1' endometrial cancer.

Risk factor category	Risk factor	Comments
Non-modifiable	Age	Incidence highest in females aged 75 to 79[1]
	Family history	Suggested higher risk if first degree relative affected by EC
Menstrual	Postmenopausal status	90 % of women with EC will present with PMB
	Early menarche	11 % higher in parous women aged under 13 at menarche[1]
	Late menopause	34 % higher in nulliparous women aged 50-54 at menopause[1]
	Prolonged perimenopause	Suggested increased risk of EC proportional to duration that oestrogens are inadequately opposed[2]
	Null parity	35-42 % higher in nulliparous women[1]
Co-morbid conditions	Obesity	34 % higher in overweight (BMI 25-30) women, and 2.5 times higher in obese (BMI 30+) women[1]
	Diabetes mellitus	40-81 % higher in diabetics compared with non-diabetics[1]
	Polycystic ovarian syndrome (PCOS)	2.8 times higher[1]
	Oestrogen secreting tumours	e.g. Granulosa cell tumours
Iatrogenic	Oestrogen only HRT	2.3 times higher risk of EC with use[1]
	Tamoxifen therapy	Risk higher in postmenopausal women and is dose and duration dependent[3]
	Exogenous oestrogen exposure	2.1-2.7 times higher in women with the high circulating oestrogen levels[1]
Others	Physical inactivity	Likely related to obesity
	Hereditary	Lynch, HBOC and Cowden's Syndromes

[1](Cancer Research UK, 2018a), [2](Hale *et al.*, 2002), [3] (Mourits *et al.*, 2001). BMI = Body mass index, PCOS = polycystic ovarian syndrome, PMB = post-menopausal bleeding, HBOC = Hereditary breast and ovarian cancer syndrome, EC = Endometrial cancer

Conversely, type 2 ECs tend to be oestrogen-independent and include the clinically aggressive ‘serous’, ‘clear cell’ and ‘mixed-cell’ histological subtypes. Type 2 ECs are high-grade tumours by definition. Type 2 ECs are not associated with the same risk factors as type 1 ECs and are more often associated with endometrial atrophy in the postmenopausal woman rather than with EH (Abu-Rustum *et al.*, 2010; Creasman *et al.*, 2006; Matias-Guiu and Prat, 2013). Type 2 ECs are associated with a much poorer clinical prognosis as they also have a high tendency for extra-uterine spread. At a molecular level type 2 ECs are associated with *HER2* amplification and recurrent *TP53* mutations (Matias-Guiu and Prat, 2013).

Despite the seemingly intuitive division of ECs into these two types, this dichotomous classification is far from perfect. There is a significant overlap between type 1 and type 2 ECs. For example, 10 % - 19 % of endometrioid ECs are deemed high-grade and have clinical, histopathological, and molecular features that are more akin to type 2 ECs (Brinton *et al.*, 2013; Voss *et al.*, 2012). Mixed histological patterns incorporating endometrioid and serous morphology also exist (Mackenzie *et al.*, 2015).

EC normally presents as a primary tumour, however in very rare cases it may be metastatic from another malignancy (e.g. breast, ovary, lung, stomach, colorectal, and melanoma). ECs usually spread by direct extension into surrounding structures (myometrium, cervix and vagina), with deeper infiltration eventually leading to a breach of the uterine serosa and invasion of the parametria. Haematogenous and trans-tubal spread may also occur, with the lungs being the most common site for distant metastasis. Lymph node involvement is related to the depth of tumour invasion into the myometrium and the grade of the tumour (Chi *et al.*, 2008). Lymphatic spread usually follows an anatomical distribution with involvement of the pelvic lymph nodes (internal and external iliac, obturator nodes) and the para-aortic nodal chain.

1.4.1.1 Hereditary endometrial cancer

Lynch syndrome (hereditary non-polyposis colorectal cancer (HNPCC) syndrome) is an hereditary condition which increases a woman’s risk of EC. Women with Lynch Syndrome have up to an ~80 % life-time risk of developing colon cancer, followed by an ~60 % life-time risk of developing EC and an ~10 % risk of developing other cancers (including but not exhaustive of; ovarian, pelvi-calyceal/ureteric, gastric, small intestinal, skin, brain and hepato-biliary tumours) (Bonadona *et al.*, 2011; ten Broeke *et al.*, 2015). This autosomal dominant syndrome is caused by a germline (inheritable, i.e. present in gametes) mutation in one or more

of the DNA mismatch repair genes (*MLH1*, *MSH2*, *MSH6* and *PMS2*). Cowden's Syndrome is an autosomal dominant syndrome caused by a germline mutation in the *PTEN* gene which has life-time risk of ~20-30 % for developing EC and other cancers as well as hamartomas (Gammon *et al.*, 2016). Hereditary breast–ovarian cancer syndrome (HBOC) is due to inherited pathogenic mutations in the *BRCA1* and *BRCA2* genes, and confers high risks of breast carcinoma, ovarian serous cancer, as well as other cancers including serous carcinoma of the endometrium.

1.4.2 2009 FIGO endometrial cancer staging

In the UK, current staging of ECs currently utilises the 2009 International Federation of Gynecology and Obstetrics (FIGO) system (Table. 1-3). Staging for EC is surgical because the condition is predominantly treated with surgery. The 2009 FIGO staging system does not require peritoneal cytology in its staging criteria since the prognostic significance of cytology is limited to cases of extrauterine spread, where positive cytology is associated with a poorer outcome.

1.4.3 The Cancer Genome Atlas (TCGA) molecular classification of endometrial cancers

In 2013, an integrated molecular classification drawing on proteomic, genomic and transcriptomic analyses of over 370 ECs was performed by The Cancer Genome Atlas (TCGA) and resulted in new insights into EC subtypes (Kandoth *et al.*, 2013). Briefly, employing array-based and sequencing methodologies, four major EC groups were characterised: i) Ultramutated cancers with DNA polymerase epsilon (*POLE*) mutations (7 %), ii) Hypermutated cancers with microsatellite instability due to *MLH1* promoter methylation (28 %), iii) ECs with low mutation rate and low frequency of DNA copy-number alterations (CNA, 39 %) and iv) ECs with low mutation rate but high-frequency DNA CNA (26 %) (Kandoth *et al.*, 2013). The TCGA data generated interest as the authors discovered that EC patients in the ultramutated group harbouring *POLE* mutations (more commonly seen in grade 3 endometrioid ECs in their cohort) had a less clinically aggressive course and improved progression-free survival when compared with patients in the other the three groups (Figure. 1-5) (Kandoth et al., 2013).

Table 1-3: International Federation of Gynecology and Obstetrics (FIGO) endometrial cancer staging system 2009.

FIGO Stage	Descriptor
Stage I	**Tumour limited to the corpus uteri**
IA	No or less than half myometrial invasion
IB	Invasion equal to or more than half of the myometrium
Stage II	**Tumour invades the cervical stroma but does not spread beyond the uterus***
Stage III	**Local and/or regional spread of tumour**
IIIA	Tumour invades the serosa of the corpus uteri and/or adenexas
IIIB	Vaginal and/or parametrial involvement
IIIC	Metastases to the pelvis and/or para-aortic lymph nodes
IIIC1	Positive pelvic lymph nodes
IIIC2	Positive para-aortic lymph nodes with or without positive pelvic lymph nodes
Stage IV	**Tumour invasion of bladder and/or bowel mucosa and/or distant metastases**
IVA	Tumour invasion of bladder and/or bowel mucosa
IVB	Distant metastases, including intra-abdominal metastases and or inguinal lymph nodes

Grading is reported addition to stage: either G1, G2 or G3, Positive cytology to be reported separately without changing the stage, *Endocervical glandular involvement should only be considered as stage I. Adapted from Creasman, 2009.

Since adjuvant treatment would routinely be offered to women in this group, it is unclear whether this group may be overtreated with adjuvant treatment and would do well regardless (due to their *POLE* status) or whether the favourable outcomes are secondary to their tumours being more susceptible to the adjuvant treatment.

All four TCGA groups contained some low-grade endometrioid ECs, suggesting that the genomic profiles of ECs can be markedly different even in tumours which have similar histological appearances. Furthermore, many of the grade 3 endometrioid ECs within the TCGA cohort had genomic profiles similar to serous carcinomas (i.e. *p53* mutations and high copy number alterations (CNAs)), extending the existing argument as to whether high-grade endometrioid ECs should be grouped with other high grade serous ECs and considered as a 'type 2' tumour (Alvarez *et al.*, 2012). In 2014, Meng *et al* reported that *POLE* mutations could function as a prognostic marker for management of grade 3 endometrioid EC (Meng *et al.*, 2014).

A suggested mechanism for the TCGA observations is that ECs with *POLE* mutations have a favourably enhanced antitumour T-cell response combined with an enrichment of antigenic neopeptides (van Gool *et al.*, 2015). Given the expense and technical expertise required when undertaking molecular classification of ECs, surrogate and clinically applicable methods for use with formalin-fixed paraffin-embedded (FFPE) tissues have been proposed (Talhouk *et al.*, 2015). Through analysis of 152 historic ECs using a combination of p53 immunohistochemistry (as a surrogate marker for copy number status), MMR (MLH1, MSH2, MSH6, PMS2) immunohistochemistry and *POLE* mutation analysis, Talhouk and colleagues were able to replicate the survival curves as demonstrated by the TGCA (Talhouk *et al.*, 2015).

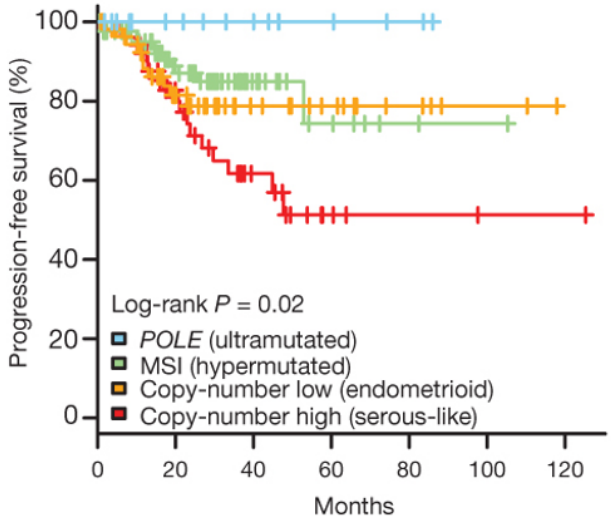

Figure 1-5: Kaplan-Meier progression-free survival (PFS) curves from the TCGA EC cohort. *POLE*-mutant tumours have significantly better PFS, while copy number high tumours have the poorest outcome. Image adapted from Kandoth *et al.*, 2013.

1.5 Endometrial Hyperplasia

Endometrial hyperplasia (EH) is a gynaecological condition which is primarily characterised by abnormal proliferation of the endometrial glandular epithelium. EH is widely recognised to precede the development of endometrioid EC, with atypical EH (synonymously known as endometrial intraepithelial neoplasia (EIN)) considered a direct pre-cursor lesion (Ellenson *et al.*, 2011). It is unsurprising therefore that many of the EC risk factors (Table 1-2) are also risk factors for EH. Histologically, the condition represents a range of morphological abnormalities, resulting in an increase in the endometrial gland-to-stroma ratio when compared to endometrium from the proliferative phase of the menstrual cycle (Ellenson *et al.*, 2011; Kurman *et al.*, 2014). The aberrant endometrial glands can vary greatly in size, shape and may exhibit cytological atypia. In developed countries the incidence of EH stands at approximately 200,000 cases per annum (Chandra *et al.*, 2016). However, this is likely an underestimation since epidemiological registry data on EH patients are not routinely recorded (unlike cancer diagnoses) and so statistical information can vary greatly between institutions.

It is generally accepted that most cases of EH will develop due to chronic exposure of the endometrium by oestrogens unopposed by a progestin (Trimble *et al.*, 2012). As such, EH is relatively uncommon during the reproductive years in women who have a regular menstrual cycle (Ellenson *et al.*, 2011). Women affected by EH will normally have a history of persistent anovulation, exogenous 'un-opposed' oestrogen exposure or obesity (Figure. 1-6). The majority of women with EH will present clinically with AUB. Lidor and colleagues reported a study of n=226 women with PMB, noting that EH was the cause in 15 % of the participants, whilst genital tract atrophy was the commonest associated cause overall (56 %) (Lidor *et al.*, 1986). Although stimulation of the endometrium by oestrogens is considered the basis for developing EH, other causes such as immunosuppression and infection have been implicated (Bobrowska *et al.*, 2006). A retrospective study of 45 immunosuppressed renal graft recipients with AUB found a two-fold increase in the incidence of EH (69 % vs. 33 %) compared to non-transplanted immunocompetent controls (Bobrowska *et al.*, 2006).

The clinical relevance of a diagnosis of EH relates to a future risk of progression to endometrioid EC and it is generally accepted that cytological atypia is the principal histological characteristic when assessing EHs for malignant potential (Ellenson *et al.*, 2011). When atypia is present, it has been estimated that progression to EC can take approximately 4 to 7 years (Gusberg and Kaplan, 1963; Kurman *et al.*, 1985). Not all EH will progress to malignancy; some EHs occur secondary to oestrogenic proliferation without an underlying

malignant mechanism. These patients may be asymptomatic and, in some cases, the EH may regress without ever being detected.

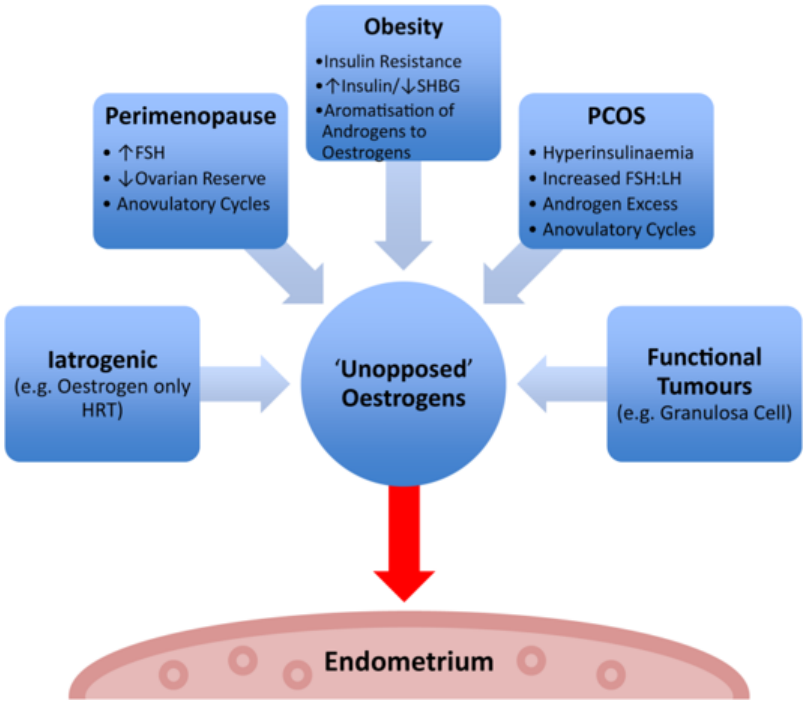

Figure 1-6: Factors contributing to 'unopposed' oestrogen stimulation of the endometrium in endometrial hyperplasia (EH). PCOS = Polycystic ovarian syndrome (Stein-Leventhal syndrome), FSH = follicle stimulation hormone, FSH: LH = follicle stimulating hormone to luteinising hormone ratio, SHBG = sex hormone binding globulin, HRT = hormone replacement therapy. Figure reproduced from Sanderson *et al.*, 2017.

1.5.1 Terminology and classification of endometrial hyperplasia

The terminology and classification of EH has undergone multiple iterations over the past several decades, each system aiming to correlate EH histological features with the risk of progression to endometrioid EC (Chandra *et al.*, 2016). The two prominent classification systems currently in use are: 1) The World Health Organisation (WHO) system, established in 1994 with revision in 2003, which is heavily used within current clinical gynaecological practice and 2) The Endometrial Intraepithelial Neoplasia (EIN) system, introduced in 2000 (Mutter, 2000) and which has recently been endorsed by the WHO in 2014 as part of their most recent classification of tumours of the female reproductive organs (Kurman *et al.*, 2014).

1.5.1.1 The World Health Organisation (WHO) 1994 Classification

In 1994, the WHO proposed a classification system based upon the histological features of EH lesions, in an attempt to stratify EHs based on their potential for malignant transformation (Scully *et al.*, 1994). This system centres around the glandular/stromal architectural configuration of the endometrium (which is defined as being either simple or complex, compared with proliferative endometrium) and the presence or absence of glandular cytological atypia. Four groups were suggested: 1) Simple hyperplasia without atypia (SH) 2) Complex hyperplasia without atypia (CH) 3) Simple atypical hyperplasia (SAH) 4) Complex atypical hyperplasia (CAH) (Table. 1-4).

These groups appeared to correlate with long-term follow-up studies of patients diagnosed with EH that had been conducted previously (Ferenczy and Gelfand, 1989; Kurman *et al.*, 1985). The most influential of these studies was reported by Kurman *et al* in 1985 (Kurman *et al.*, 1985). In this study the authors performed a retrospective analysis of 170 'untreated' EH patients whom had been diagnosed with EH on uterine curettage. The mean follow-up period for women was 13.4 years, during which time a hysterectomy was not performed before 1 year following the index diagnosis. Thirteen of the 170 women in the study progressed to EC during the follow-up period, of which 8% (n=1) had SAH and 29% (n=10) had CAH on initial curettage (Kurman *et al.*, 1985). Subsequent research has corroborated the findings of Kurman *et al* demonstrating that cytological atypia is the most important feature when evaluating EH lesions for malignant potential (Baak *et al.*, 2001; Ferenczy and Gelfand, 1989; Lacey, Ioffe, *et al.*, 2008).

Cytological atypia can be seen in both simple and complex EH architectural arrangements, although SAH is very rarely seen, leading some to question its reproducibility and clinical relevance as a category of EH (Bergeron *et al.*, 1999; Kendall *et al.*, 1998). Abnormal mitotic figures distinctive of atypia include; scattered chromosomes, disrupted metaphase plates or tri/multipolar appearances. Cellular cytoplasm volume can vary, and a large number of eosinophils can be present in regions demonstrating atypia (Ellenson *et al.*, 2011). When first introduced the WHO94 system was considered a significantly novel approach to EH classification since it correlated the histological features of EH lesions with clinical outcome data (Baak and Mutter, 2005). However, the subjective nature of this system has meant that significant diagnostic variation occurs between pathologists and overall diagnostic reproducibility is reportedly poor (Skov et al. 1997; Kendall et al. 1998). Cytological atypia is also not always uniformly seen across individual EH proliferations and subjective atypia grading scales, i.e. mild, moderate and severe are adopted by some, adding

further confusion especially when translating the scheme to clinical management (Kendall *et al.*, 1998). In a study by Trimble and colleagues, 289 endometrial sample specimens with a community diagnosis of atypical EH were re-reviewed by specialised gynaecological pathologists using WHO94 criteria; 25 % of cases were downgraded to less severe histology than atypical EH, and 29 % were upgraded to EC (Trimble *et al.*, 2006).

Table 1-4: The World Health Organisation (WHO) 1994 classification of endometrial hyperplasia. Adapted from Sanderson *et al.*, 2017.

WHO94 Categories	Histological & Cytological Features
Simple hyperplasia without atypia (SH)	• Irregularly shaped and sized glands • Cystic dilatation • Abundant cellular stroma • No back to back crowding • Nuclear pseudo-stratified glands but no nuclear atypia • Variable mitotic activity
Simple atypical hyperplasia (SAH)	• As per SH including nuclear atypia
Complex hyperplasia without atypia (CH)	• Crowded glands – can be complex or tubular, with or without dilatation • Sparse intervening stroma • Oval, bland nuclei with uniform shape • Variable mitotic activity
Complex atypical hyperplasia (CAH)	• Tightly packed glands • Very little intervening stroma • Nuclear atypia

1.5.1.2 The Endometrial Intraepithelial Neoplasia (EIN) 2000 classification system

A multicenter European study was conducted in 1999 by Bergeron and colleagues to assess both intra and inter-observer variability between expert pathologists in the diagnosis of 56 endometrial samples utilising the WHO94 classification system (Bergeron *et al.*, 1999). The authors reported significant disagreement in the diagnoses of CH and atypical hyperplasia (combining SAH and CAH) between pathologists (Bergeron *et al.*, 1999). They concluded that histological classification should be simplified, suggesting that two groups be used; a

combined category for SH and CH, referred to as 'hyperplasia' and a combined category for atypical hyperplasia (SAH and CAH) and well-differentiated adenocarcinoma called 'endometrial neoplasia.' The rational for this is that by utilising two groups, one benign and one neoplastic, reproducibility would be increased, and a two-tier system would align easily with potential therapeutic interventions i.e. medical or surgical (Bergeron *et al.*, 1999).

Research in the 1980s, spearheaded by Jan Baak and colleagues, developed a prognostic tool designed to predict EC progression risk based upon computerised morphometric analysis of the histological features seen within EH lesions (Ausems *et al.*, 1985). It was proposed that by combining pathological analysis of nuclear and architectural features with morphometric analysis, prognostic value could be increased (Baak *et al.*, 1988). This work culminated in the development of a weighted likelihood ratio called the 'D-score'. The D-score centres on three key EH features: 1) volume percentage of stroma, 2) outer surface density of the glands (reflecting gland branching / convolution) and 3) the standard deviation of the shortest nuclear axis within glandular cells, i.e. nuclear atypicality (Baak *et al.*, 1988; Baak and Mutter, 2005). The following equation is used:

> *"D-score = 0.6229 + 0.0439 × (volume percentage stroma) − 3.9934 × Ln (standard deviation shortest nuclear axis) − 0.1592 × (glands outer surface density)" (Baak et al., 1988).*

By applying the D-score, hyperplastic biopsies with a score less than or equal to 1 have a high rate of progression to EC, whereas biopsies with a score greater than 1 almost never progress to EC (Baak *et al.*, 1992, 2001). This system has been reported to have high diagnostic reproducibility (Baak and Mutter, 2005). Advances in molecular genetics, at around a similar time to the progress being made with morphometric analysis, recognised a shared monoclonal pattern of development between atypical EH lesions and ECs (Jovanovic *et al.*, 1996). This monoclonal pattern describes a situation whereby mutated cells with a growth advantage proliferate to the detriment of their neighbours, forming mutant clonal expansions stemming from a common progenitor (Jovanovic *et al.*, 1996). Through the application of morphometric analysis, EH samples can be separated into monoclonal lesions (D-score $\leq$1, i.e. a high risk of progression to endometrioid EC) and polyclonal lesions (D-Score >1, low risk lesions, deemed to be reactive to an abnormal hormone environment) (Baak and Mutter, 2005).

Acknowledging the aforementioned reproducibility deficiencies within the WHO94 classification system, the Endometrial Collaborative Group introduced the concept of

Endometrial Intraepithelial Neoplasia (EIN) in 2000 (Mutter, 2000). This system incorporated the advances in morphometric understanding and recognised the novel molecular research occurring in the field of endometrial precancers at the time (Jovanovic *et al.*, 1996; Mutter, 2000; Mutter *et al.*, 1996). The EIN classification system divides hyperplastic endometrial lesions into two groups: 1) endometrial hyperplasia and 2) Endometrial Intraepithelial Neoplasia (EIN).

EIN is defined as a monoclonal proliferation of architecturally and cytologically altered premalignant endometrial glands, which are prone to transformation to endometrioid EC (Mutter, 2000). This is in contrast to non-neoplastic, polyclonal lesions, which encompass a spectrum of changes ranging from disordered proliferative endometrium to non-atypical hyperplasia. These 'benign' lesions that occur reactively due to a proliferative oestrogenic stimulus i.e. a response to anovulatory cycles or exogenous estrogen exposure - an 'endocrine effect' (Mutter, 2000). The EIN concept proposes that initial genetic alterations within EH occur at a level undetectable by standard light microscopy. It is hypothesized that these 'latent' genetically mutated cells could be present for several years in normal cycling endometrium (Mutter *et al.*, 2007). Through the accrual of further genetic damage, higher-risk mutant clones assert themselves phenotypically as they have a proliferative advantage, demonstrating architectural and cytological features indicative of EIN. It has been inferred that endocrine modifiers of EC (e.g. unopposed oestrogens) can act upon the latent and EIN phases to alter the balance of cancer progression *versus* lesion involution (Mutter *et al.*, 2007).

Since morphometric 'clonality' analysis cannot be performed on diagnostic specimens routinely in most pathology laboratories, the EIN classification system adopts surrogate criteria (Table. 1-5) which emulate what the D-score achieves, however they can be assessed quickly using routine light microscopy on haematoxylin and eosin (H&E) stained EH specimens (Owings and Quick, 2014). The EIN system of EH classification signified a conceptual shift from the long-held belief that oestrogen-driven endometrial proliferation, with increasing glandular architectural complexity and accumulating cytological atypia gradually leads to the development of endometrioid EC. The EIN system recognises that EH lesions can have a several appearances that may include an emergent premalignant clone (EIN) within an oestrogen stimulated hyperplastic background. The notion of separating these two events, mutational activation and oestrogenic promotion, permits histological examination of the two components separately and gives a comprehensible model of the multistep carcinogenic process that is similar to that described in many other tissue types (Vineis *et al.*, 2010)

The EIN system has been suggested to be highly reproducible between observers and straightforward to establish in standard pathological practice (Kane and Hecht, 2012; Usubutun *et al.*, 2012). EIN categories do not correspond directly to specific categories in the WHO94 system and since both systems are governed by different rules the two systems are not directly comparable (Mutter, 2000). However, there is some recognisable overlap, with most SH and some CH falling into the EH category and many CH and most CAHs falling into the EIN category.

Table 1-5: Haematoxylin and eosin section diagnostic criteria for Endometrial Intraepithelial Neoplasia (EIN)

EIN Criterion	Comments
Architecture	Area of glands exceeds that of stroma (VPS <55 %).
Cytology	Cytology differs between architecturally crowded focus and background.
Diameter >1 mm	Maximum linear dimension of the lesion exceeds 1 mm.
Exclude mimics	Benign conditions with overlapping criteria: basalis, secretory, polyps, repair, etc.
Exclude Cancer	Carcinoma if maze-like meandering glands, solid areas, or appreciable cribriforming.

NB: All criteria must be met in order for a diagnosis of EIN to be made.
VPS = volume percentage stroma.
Reproduced with permission from Baak and Mutter, 2005.

1.5.1.3 The World Health Organisation (WHO) 2014 Classification

In 2014 the WHO made significant changes to their EH classification system, simplifying their 4-tier 1994 classification into a 2-tier classification (Kurman *et al.*, 2014). The architectural component of simple or complex was removed and instead recommendations were made to refer to EH as either 1) hyperplasia without atypia (HwA) or 2) atypical hyperplasia (Kurman *et al.*, 2014). For the first time the WHO recognised the EIN concept, refashioning the term to 'Endometrioid Intraepithelial Neoplasia', an adjustment on the original, to reflect that EIN is the precursor lesion to endometrioid EC and not to serous EC

(Kurman *et al.*, 2014). The new WHO2014 classification refers to the premalignant endometrioid lesion as atypical hyperplasia / EIN and views the two terms synonymously.

1.5.2 Predicting progression of endometrial hyperplasia to endometrial cancer

As reviewed in Sanderson *et al.*, 2017, understanding the pathogenesis and classifying EHs permits stratification of women at risk of progression to endometrioid EC, enabling necessary treatment in an appropriate and timely fashion. Several studies have investigated progression rates from EH to malignancy (Feldman *et al.*, 1994; Horn *et al.*, 2004; Lindahl and Willén, 1994; Tabata *et al.*, 2001; Terakawa *et al.*, 1997) however, many lack sufficient controls and/or demonstrate under-powering of EC cases which limits the conclusions that can be drawn in many cases.

The aforementioned study by Kurman *et al* in 1985 is widely cited for its estimates of progression of EH to endometrioid EC based on a retrospective analysis of 170 women between 1940 and 1970 (Kurman *et al.*, 1985). Classification in this study used what would eventually become the WHO94 system and published rates of progression of 1% (SH), 3% (CH), 8% (SAH) and 29% (CAH) respectively for the four categories (Kurman *et al.*, 1985). The differences in progression between the four groups were not statistically significant and given the small number of EC patients and lack of controls, the results cannot be extrapolated to form true rates of progression (Ellenson *et al.*, 201; Lacey, Ioffe, *et al.*, 2008). Lacey *et al* conducted a nested case-control study in 2007. The authors analysed 138 cases of EH (and 241 matched controls) which progressed to EC at least 1 year following index EH diagnosis. They demonstrated a 40 % probability of developing EC following a diagnosis of atypical hyperplasia (incorporating both simple and complex variants), compared to a 10 % probability when atypia was not present (Lacey, Ioffe, *et al.*, 2008). Lacey *et al* commented on the need to increase sensitivity and specificity when diagnosing atypical hyperplasia and to find methods of identifying the rare non-atypical EH lesions that are also likely to progress to EC (Lacey, Ioffe, *et al.*, 2008).

The D-score has consistently been reported to have high levels of sensitivity and specificity when evaluating EH lesions for risk of progression to EC. Baak *et al,* in their 2001 prospective multicentre evaluation, quote a sensitivity of 100 % and specificity 82 % when the D-score was used by technicians to analyse 132 EH cases for EC progression risk in a blinded settling (Baak *et al.*, 2001). Furthermore, the D-score has shown high reproducibility between

users (Kendall *et al.*, 1998) and in a retrospective study by Orbø *et al,* over a 10-20 year follow-up period, the D-score was found to be significantly more accurate and sensitive in predicting EC than the WHO94 classification system (Orbø *et al.*, 2000). Hecht *et al* analysed the use of the D-score compared to EIN criteria in their 2005 retrospective study of 97 EH biopsies. They demonstrated that subjective EIN assessment correlates well with objective morphometric analysis. All of the EH that progressed to EC occurred in patients whose endometrial biopsies were deemed high risk by both methods, although interestingly n=15 samples were given a D-score of ≤ 1 (i.e. high risk) and yet subjectively classified as non-EIN (Hecht *et al.*, 2005). D-score based morphometry however, especially when computerised, is not without financial cost (Baak and Mutter, 2005). Whilst the long-term benefit may offset the initial expenditure and training time, a significant limitation is that not all institutions will be able to meet this financial outlay or have the necessary computer infrastructure in place to permit its use. Furthermore, in spite of the strength of the computerised D-score assessment, the accuracy of the method still needs to be refined. For example, is it reported that overlapping nuclei might result in higher values of the shortest nuclear axis, either higher or lower SD values, and consequently a lower or higher D-score (Ørbo A, Baak JPA, *et al.,* 2000).

Clinical outcome data by Baak *et al* has suggested that 41 % of women diagnosed with EIN will develop EC within 12 months. The mostly likely explanation for this is the presence of a concurrent EC that was not sampled on initial biopsy. Those women who do not develop EC within 12 months have a reported 45-fold increased future risk of EC developing (Baak, Mutter, *et al.*, 2005). Baak *et al,* also argued that of the women who do go on to develop EC, the preceding lesion is more likely to be EIN rather than atypical hyperplasia (Baak, Mutter, *et al.*, 2005). The authors referring to the finding that some EH lesions classified as non-atypical hyperplasia under the WHO system actually meet EIN criteria and as such should be deemed premalignant.

In contrast, a later study in 2008 reported that both EIN and atypical hyperplasia have similar risks of progression to EC when followed-up for 12 months after an EH diagnosis (Lacey, Mutter, *et al.*, 2008). Salman *et al* concluded along similar lines in their 2010 study. They retrospectively found that atypical or complex atypical EH and EIN had similar sensitivities and negative predictive values for the presence of coexistent EC in the pre-operative biopsies of 49 women (Salman *et al.*, 2010). Importantly, they add the caveat that the EIN system may be preferred in centres without an experienced gynae-pathologist in order to minimise diagnostic errors given its use of objective diagnostic criteria (Salman *et al.*, 2010).

1.5.3 Management of endometrial hyperplasia

Clinical management of EH and follow-up should be customised to each woman, taking into account baseline risk factors, symptomatology, fertility wishes and response to treatment (Committee on Gynecologic Practice, 2015; Gallos *et al.*, 2016). Three management options are available, including conservative surveillance, progestin therapy or hysterectomy. All treatment approaches should be accompanied by addressing baseline risk factors in an attempt to remove or limit the source of unopposed oestrogen stimulation, i.e. correcting ovulatory dysfunction, weight loss in the obese, evaluation of iatrogenic oestrogen sources, e.g. HRT and tamoxifen.

Where there is a high risk of concurrent or future EC progression (i.e. EIN) and where there are no absolute contraindications (i.e. unsuitable surgical candidate due to co-morbidities or a wish to retain fertility), total hysterectomy should always be recommended as the first-line treatment, (Committee on Gynecologic Practice, 2015; Gallos *et al.*, 2016). Surveillance alone should only be undertaken if an established risk factor has been corrected and where the risk of occult EC or progression to EC is low (Gallos *et al.*, 2016).

Progestin therapy has been demonstrated to be effective by multiple studies in achieving regression of HwA (Gallos *et al.*, 2012; Gunderson *et al.*, 2012; Montz *et al.*, 2002; Randall and Kurman, 1997; Reed *et al.*, 2009). Progesterone counterbalances the mitogenic effects of oestrogens and induces secretory differentiation of the endometrium (Kim and Chapman-Davis, 2010). Delivery of progestins is challenging due to the short half-life and doses that are required. Regional practice varies on the route of progestin administration, however both continuous oral and local intrauterine (levonorgestrel-releasing intrauterine system (LNG-IUS), e.g. Mirena® (Bayer Pharmaceuticals, Germany) are reported to be effective in achieving regression of HwA (Gallos *et al.*, 2016).

When cytological atypia is present, there is a higher incidence of failure of progestin management (Ferenczy and Gelfand, 1989). A meta-analysis by Gallos and colleagues, incorporated 14 studies with a total of 151 women with atypical hyperplasia treated with progestins (varying routes), reporting a regression rate of 86 % and a relapse rate of 26 %, median follow-up was 11-77 months (Gallos *et al.*, 2012). A further meta-analysis by an Australian group included 12 studies, with 117 women with CAH treated with progestins and found a relapse rate of 20.1 % over a 45-month median follow-up period (Baker *et al.*, 2012). Both the American College of Obstetricians and Gynecologists (ACOG) and the UK Royal College of Obstetricians and Gynaecologists (RCOG) have issued guidelines / opinion papers

detailing management of EH (Committee on Gynecologic Practice, 2015; Gallos *et al.*, 2016). The RCOG advice includes a management algorithm for EH, detailing preferred treatment and advising on the timing of endometrial biopsy for patients undergoing conservative surveillance and medical management (Figure. 1-7) (Gallos *et al.*, 2016).

Overleaf: Figure 1-7: Current UK guidelines on the management of endometrial hyperplasia. Algorithm adapted from the joint RCOG / BSGE joint Green-top guideline (Gallos *et al.*, 2016). Key below.

a. Risk factors include obesity, HRT (hormone replacement therapy) regimens, tamoxifen therapy and anovulation.
b. Consider ovarian conservation according to age, menopausal status and patient preferences. In addition to non-regression of EH or persistence of AUB symptoms following nonsurgical treatments, a total hysterectomy may be indicated where there are (i) adverse effects associated with medical treatment, (ii) concerns over compliance with treatment or follow-up, or (iii) patient preferences e.g. high levels of anxiety.
c. The follow-up interval should be customised to each woman, taking into account baseline risk factors, associated symptoms and response to treatment.
d. Regression – non-hyperplastic or non-malignant endometrial sample or non-diagnostic endometrial sample from an appropriately placed endometrial sampling device; persistence – no regression or progression of initial EH subtype after 3 or more months; progression – development of AH or EC; relapse – recurrence of EH or AH after one or more negative EB result(s).
e. In general, advise continuation of the LNG-IUS for the duration of its 5-year use, especially if EH associated with AUB or other baseline risk factors and no adverse effects.
f. Start medical management if EH not treated initially. The decision to persist with medical management should be taken after careful consideration and thorough discussion with the woman regarding the risks and benefits of prolonged medical treatment compared with total hysterectomy with or without BSO. Persistence beyond 12 months is associated with a significant risk of underlying malignancy and a high risk of failure to regress such that a total hysterectomy with or without BSO should be recommended.
g. At discharge, inform the woman of her estimated individual risk of recurrence, of the need to continue any risk-reducing strategies and to present for an urgent review if any further episodes of AUB.
h. Review the appropriateness of ongoing endometrial surveillance, continuation of medical management or total hysterectomy with or without BSO based on factors such as baseline risk factors including BMI, AUB symptoms, fertility requirements, compliance with treatment and follow-up, medical comorbidities and risk–benefit ratio for total hysterectomy with or without BSO.

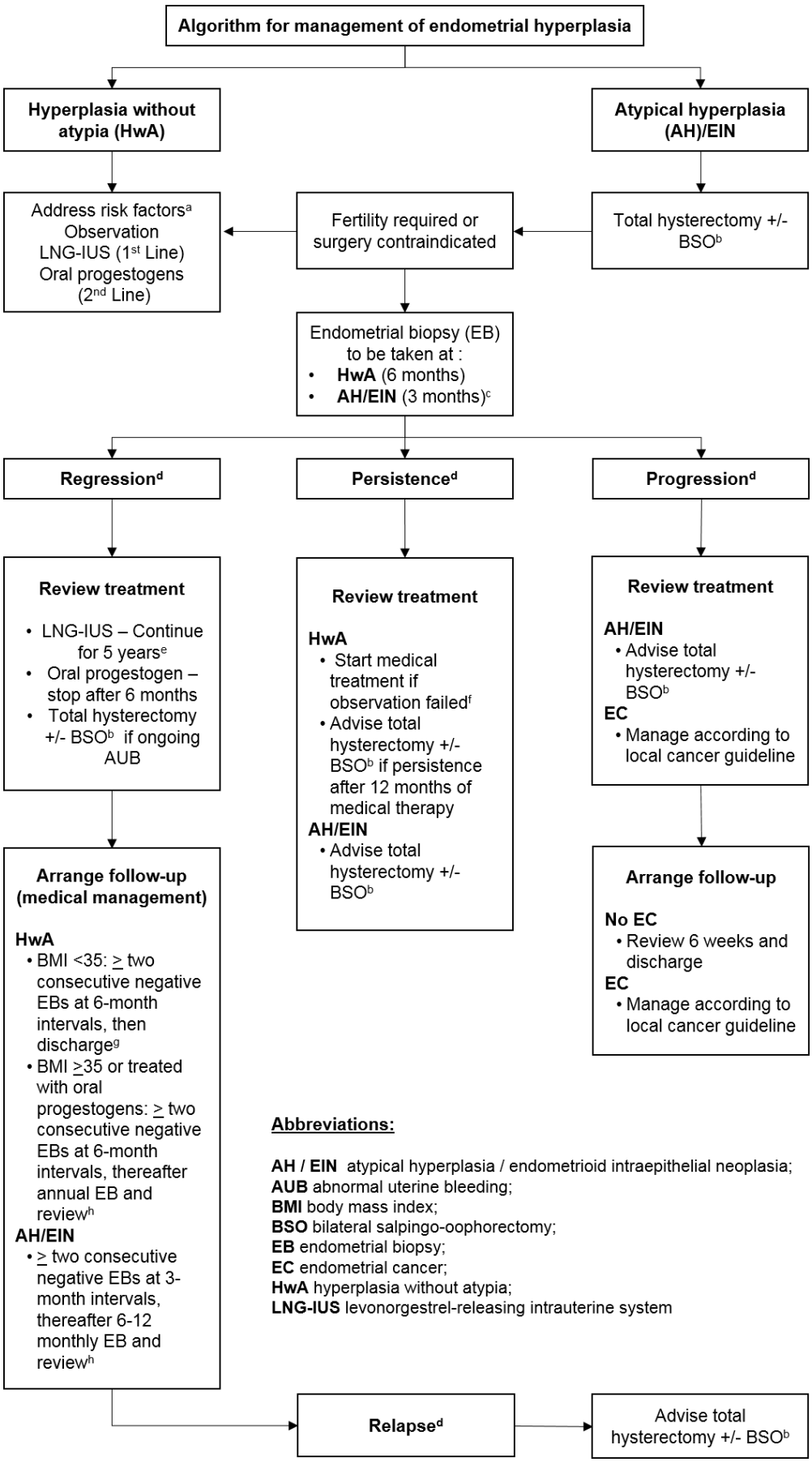
Algorithm for management of endometrial hyperplasia
Hyperplasia without atypia (HwA)
Atypical hyperplasia (AH)/EIN
Address risk factors[a]
Observation
LNG-IUS (1st Line)
Oral progestogens (2nd Line)
Fertility required or surgery contraindicated
Total hysterectomy +/- BSO[b]
Endometrial biopsy (EB) to be taken at :
• HwA (6 months)
• AH/EIN (3 months)[c]
Regression[d]
Persistence[d]
Progression[d]
Review treatment
• LNG-IUS – Continue for 5 years[e]
• Oral progestogen – stop after 6 months
• Total hysterectomy +/- BSO[b] if ongoing AUB
Review treatment
HwA
• Start medical treatment if observation failed[f]
• Advise total hysterectomy +/- BSO[b] if persistence after 12 months of medical therapy
AH/EIN
• Advise total hysterectomy +/- BSO[b]
Review treatment
AH/EIN
• Advise total hysterectomy +/- BSO[b]
EC
• Manage according to local cancer guideline
Arrange follow-up (medical management)
HwA
• BMI <35: ≥ two consecutive negative EBs at 6-month intervals, then discharge[g]
• BMI ≥35 or treated with oral progestogens: ≥ two consecutive negative EBs at 6-month intervals, thereafter annual EB and review[h]
AH/EIN
• ≥ two consecutive negative EBs at 3-month intervals, thereafter 6-12 monthly EB and review[h]
Arrange follow-up
No EC
• Review 6 weeks and discharge
EC
• Manage according to local cancer guideline
Abbreviations:
AH / EIN atypical hyperplasia / endometrioid intraepithelial neoplasia;
AUB abnormal uterine bleeding;
BMI body mass index;
BSO bilateral salpingo-oophorectomy;
EB endometrial biopsy;
EC endometrial cancer;
HwA hyperplasia without atypia;
LNG-IUS levonorgestrel-releasing intrauterine system
Relapse[d]
Advise total hysterectomy +/- BSO[b]

1.6 Molecular alterations in endometrial hyperplasia

Atypical hyperplasia / EIN lesions have been found to harbour several molecular alterations similar to those described in endometrioid EC. These commonly include; somatic alterations in the tumour suppressor gene, *PTEN* and other constituent genes of the PI3K/AKT/mTOR pathway (Hayes *et al.*, 2006; Sun, Enomoto, *et al.*, 2001, 2002), in addition to microsatellite instability (Hardisson *et al.*, 2003; Nieminen *et al.*, 2009). Numerous alterations in candidate genes have also been found, the vast majority as a result of immunohistochemical studies (reviewed in Sanderson *et al.*, 2017).

The focus of the following review surrounds molecular alterations detected using immunohistochemical biomarkers. An EH diagnosis currently requires endometrial tissue sampling for histological confirmation. In the future, alternative non-invasive biomarker approaches, such as blood, urine and cervical smear cytology may become more commonplace, since they are starting to gain momentum in the diagnosis/screening of other gynaecological conditions, e.g. endometriosis and cervical screening (Fassbender, *et al.,* 2015, Sargent, *et al.,* 2019). Currently however, immunohistochemistry is widely used technique and there is a plethora of literature information detailing application of the technique in both EH and EC tissues. Despite this abundance of data, there are currently no adequately robust molecular biomarker candidates that can be used on their own to aid diagnosis of EH or that are able to predict progression of EH to endometrioid EC. The following section summarises information available for several of the prominent immunohistochemical candidates reported in the current literature and reviews their suitability as biomarker candidates.

1.6.1 Tumour Suppressors

1.6.1.1 Phosphatase and Tensin Homolog (PTEN)

Phosphatase and tensin homolog (*PTEN*) is a tumour suppressor gene located on chromosome 10q23 that encodes a dual-specificity phosphatase with both protein and lipid actions (Latta and Chapman, 2002). PTEN protein helps to regulate cellular proliferation and apoptosis via inhibition of Akt (formally Protein Kinase B), whereby its enzymatic activity dephosphorylates Phosphatidylinositol (3,4,5)-trisphosphate (PIP_3) to Phosphatidylinositol 4,5-bisphosphate (PIP_2) (Slomovitz and Coleman, 2012). Furthermore, loss-of-function mutations of *PTEN* have also been reported to increase endometrial glandular proliferation via the PI3K/AKT/mTOR pathway (Daikoku *et al.*, 2008; Hayes *et al.*, 2006). PTEN has been

demonstrated to be inactivated by other mechanisms across several somatic cancer types, including promotor methylation (Wiencke *et al.*, 2007), micro-RNA interference (Kim *et al.*, 2010), phosphorylation (Poliseno *et al.*, 2010) and delocalization from the plasma membrane (Silva *et al.*, 2008). Due to its high frequency of inactivation in carcinogenesis, *PTEN* is ranked as the second most mutated tumour suppressor gene after *p53* (Georgescu, 2010). Evidence for an association with EH and endometrioid EC has been inferred from results obtained using heterozygous *Pten* knockout mice, in which all females developed signs of EH by 6 months of age (Stambolic *et al.*, 2000).

PTEN protein expression has been assessed across the normal menstrual cycle, with immunoexpression observed to be more intense in both the glandular epithelium and stromal compartments during the proliferative phase (plausibly influencing proliferation), whilst there is an apparent decrease in the glandular epithelial compartment during the secretory phase (Mutter, Lin, *et al.,* 2000). Numerous studies have investigated PTEN immunohistochemical expression in EH and EC, with mixed reports regarding expression patterns. Several authors have reported that loss of endometrial glandular PTEN protein expression is more frequent in endometrioid EC and EIN compared to proliferative endometrium and benign EH (Baak, van Diermen, *et al.*, 2005; Monte *et al.*, 2010; Mutter, *et al.*, 2000; Steinbakk, Malpica, *et al.*, 2011). Mutter and colleagues determined that *PTEN* mutations were evident in up to 55 % of EIN lesions (whereby the formation of a truncated protein resulted in loss of immunohistochemical PTEN expression) and suggested that *PTEN* inactivation is an early event in EC carcinogenesis (Mutter, Lin, *et al.*, 2000).

Xiong *et al,* suggested that loss of PTEN expression is not a robust diagnostic marker of EIN, since they described complete PTEN protein loss occurring in only 38 % of EIN lesions (Xiong *et al.*, 2010). Furthermore, Cirpan *et al*, demonstrated no significant difference in 'complete-loss' of PTEN protein expression between proliferative endometrium, EIN and endometrioid EC, with minor differences demonstrated due to 'incomplete-loss' of PTEN expression (Cirpan *et al.*, 2006). These two studies raise the question as to what constitutes 'complete-loss' of PTEN protein expression within an EH lesion, a discussion point considered by Allinson *et al* in their 2008 review who noted that some researchers regard PTEN-null expression as a single negative gland within a lesion whilst others consider only a more extensive expression loss (Allison *et al.*, 2008).

Authors using WHO94 criteria have reported along similar lines to their counterparts using EIN criteria (Erkanli *et al.*, 2006; Kapucuoglu *et al.*, 2007; Lee *et al.*, 2012; Sarmadi *et al.*, 2009). Lee *et al,* found PTEN expression loss in endometrioid EC and CAH was higher

than in SH. Kapucuoglu and colleagues, echoed this finding, however they noted no significant differences in PTEN protein expression between CAH and EC, nor between individual EH groups (Kapucuoglu *et al.*, 2007). One study examining a small group of samples (n=11) showed no significant difference between normal endometrium or EH (Kimura, Watanabe, *et al.*, 2004). However, this study analysed PTEN nuclear staining via a histoscore system rather than reporting PTEN loss of expression, as is the usual convention (Kimura, Watanabe, *et al.*, 2004).

Isolated PTEN-null glands have also been demonstrated within macroscopically normal premenopausal endometrial samples in a reported 43 % of cases (Mutter *et al.*, 2001). These glands do not express PTEN protein due to a genetic mutation and/or deletion and notably they persist between menstrual cycles (Mutter *et al.*, 2001). The Mutter group has previously designated these mutant PTEN glands as 'latent precancers,' suggesting that with accrual of further genetic damage they may transition into phenotypically recognisable pre-malignant lesions (Monte *et al.*, 2010; Mutter, 2000; Mutter *et al.*, 2014). However, subsequent work suggests only a small proportion of these microscopically normal, PTEN-null glands will progress to endometrioid EC (Ayhan *et al.*, 2015). Further work by the Mutter group in 2014 compared PTEN immunohistochemistry between endometrial samples from a cohort of women with EIN or endometrioid EC, as well as histologically benign biopsies taken from the same women (matched non-neoplastic controls were included) (Mutter *et al.*, 2014). Where PTEN-null glands were identified in both the index neoplastic biopsy and historic 'normal' biopsy, DNA sequencing was performed on both samples for comparative PTEN somatic mutation analysis. Results demonstrated that in only 6.7 % of cases the PTEN-null, microscopically normal glands were the direct progenitors of the high risk neoplasia subsequently detected (Mutter *et al.*, 2014).

The role of PTEN has also been investigated in the context of treatments for EH and early stage endometrioid EC. As discussed above, progestins are a medical treatment for EH and can also be considered where hysterectomy is contraindicated for high risk EH-lesions (Committee on Gynecologic Practice, 2015; Gallos *et al.*, 2016). Attempts to reverse baseline risk EH factors, e.g. obesity, should also be made. Building on earlier work from the Mutter group, Zheng *et al* tested the hypothesis that progestin therapy preferentially leads to clearance of immunohistochemically detected PTEN-null endometrial glands, concluding that progestins promote PTEN-null gland involution, albeit in their small (n=17, of which n=5 were diagnosed as EIN) sample set (Zheng *et al.*, 2004). Ørbo *et al* compared the LNG-IUS to oral progesterone as treatment for EH in their 2015 multicentre randomised control trial and

evaluated clearance of PTEN-null glands (Ørbo *et al.*, 2015). The group reported significantly higher rates of clearance of PTEN-null glands with intrauterine progestin delivery (58 % regression and 4% persistence of PTEN-null glands) and noted that PTEN-null gland clearance was also significantly related to regression of EH / therapy response (Ørbo *et al.*, 2015). Furthermore, in a study of n=72 women undergoing bariatric surgery with concomitant endometrial tissue assessment before and after surgery-induced weight loss, n=12 (24 %) of the baseline endometrial biopsies contained PTEN-null glands (MacKintosh *et al.*, 2019). Of these PTEN-null baseline biopsies, n=5 were diagnosed as having atypical hyperplasia (MacKintosh *et al.*, 2019). PTEN-null glands regressed in n=4 of these patients by 12-months post bariatric surgery-induced weight loss, albeit only n=1 without any addition hormonal or surgical intervention (MacKintosh *et al.*, 2019).

In terms of evaluating the role of PTEN protein expression to predict progression of EH to endometrioid EC, Steinbakk and colleagues noted lower PTEN expression in EC samples than in EH samples and using a univariant analysis suggested that PTEN negativity in EH was prognostic of progression to EC (p=0.026) (Steinbakk, Malpica, *et al.*, 2011). Conversely, Lacey *et al* argued that loss of PTEN expression in EH was neither sensitive nor specific in predicting progression to EC (Lacey, Ioffe, *et al.*, 2008). Baak and colleagues tested the hypothesis that PTEN inactivation may stratify EC progression risk among EHs classified by means of the morphometric D-score (Baak, van Diermen, *et al.*, 2005). They demonstrated that all EH cases that progressed to EC were PTEN-null, however only 16 % of all PTEN-null cases progressed to EC (Baak, van Diermen, *et al.*, 2005). They concluded that the prognostic power of PTEN could be increased when combined with tissue analysis using the morphometric D-score (Baak, van Diermen, *et al.*, 2005).

Two studies of women who had a concurrent/coexisting EC after a biopsy result of EH were more divisive. Pavlakis *et al,* noted that loss of PTEN expression on its own was not predictive of concurrent EC, however that changed when analysed in conjunction with a finding of marked nuclear atypia within an EIN lesion (Pavlakis *et al.*, 2010). Ørbo *et al,* found loss of function of PTEN was more likely in EH lesions when a concurrent EC was present or when EC subsequently developed (Ørbo *et al.*, 2003).

1.6.1.2 Tumour Protein p53

Tumour protein p53, or simply p53, is a protein encoded by the *TP53* gene that in humans is located on the short arm of chromosome 17 (17p13.1) (Isobe *et al.*, 1986). *TP53* is

the most commonly mutated gene in human cancers (Schultheis *et al.*, 2016). The majority of mutations affecting *TP53* in human tumours are missense, and primarily affect the DNA-binding domain of the protein (Schultheis *et al.*, 2016). *TP53* is considered a tumour suppressor gene and the wild-type p53 protein has several functions; it can activate DNA repair after damage (Berchuck *et al.*, 1994), can cause cell-cycle inhibition at the G1/S checkpoint to allow DNA to be repaired (Agarwal *et al.*, 1995), it can initiate apoptosis in the event of irreparable cell damage and it is essential for the senescence response to short telomeres (Deng *et al.*, 2008; Ozkara and Corakci, 2004). Mutant p53 proteins lose their tumour suppressor functions and many of these mutant p53 proteins then acquire oncogenic properties that enable them to promote invasion, metastasis, proliferation and cell survival (Muller and Vousden, 2013).

In ECs, most *TP53* mutations are reported to be missense and are generally detected in serous / 'type 2' ECs. They are associated with the formation of a functionally defective p53 protein that is more stable, with a longer half-life than the wild-type p53 protein (Soong *et al.*, 1996). In the TCGA dataset *TP53* mutations were found in 15 % of endometrioid ECs and 88 % of serous ECs (Kandoth *et al.*, 2013). Variations in the type and pattern of *TP53* mutations were also observed across the TCGA dataset between the different EC histological groups, including hotspot mutations (frequent in the serous ECs), frameshift / nonsense mutations and a subset of *TP53* mutations co-occurring with a *PTEN* mutation that were more frequently seen in endometrioid ECs than the serous ECs (Schultheis *et al.*, 2016).

The missense mutated p53 protein product usually accumulates and is detected as overexpression in cell nuclei using immunohistochemistry. Typically, wild-type p53 in cells cannot be detected by immunohistochemistry; however, if p53 is stabilised, due to overexpression in normal cells in response to DNA damage, a positive immunohistochemistry reaction (usually focal, weak and heterogeneous) can be detected in the absence of any mutation (Soong *et al.*, 1996). To further complicate matters, deletions or frame-shift mutations of *TP53* can lead to a truncated/altered protein that lacks epitopes recognized by specific antibodies so a completely negative p53 immunohistochemistry reaction may also indicate a gene abnormality (Garg *et al.*, 2010).

Several studies have assessed p53 immunohistochemical expression in EH and EC. Horrée and colleagues noted p53 expression gradually increasing from nearly all negative cells in inactive endometrium, through to EH where only a few cells were positive, with the highest expression seen in ECs (Horrée *et al.*, 2007). Both Cinel *et al* and Elhafey *et al* demonstrated

higher expression scores in atypical hyperplasias, with the highest expression scores in non-endometrioid EC (Cinel *et al.*, 2002; Elhafey *et al.*, 2001).

In terms of using p53 as a marker of progression from EH to EC, Steinbakk and colleagues performed a retrospective analysis and demonstrated that 2 out of 8 patients who developed EC from EH had ≤1% positivity for p53, which using a univariant analysis they found was prognostic of progression (p=0.038). Although, given the small number of patients progressing to EC captured by this study the confidence interval is notably wide (0.9-23.2) (Steinbakk, Malpica, *et al.*, 2011).

1.6.1.3 AT-rich interactive domain-containing protein 1A (ARID1A)

AT-rich interactive domain-containing protein 1A (ARID1A), also known BAF250A, is an important component of the SWItch/Sucrose Non-Fermentable (SWI/SNF) nucleosome remodeling complex. It is encoded by *ARID1A* which is located on chromosome 1p36.11 (Takeda *et al.*, 2016). The SWI/SNF complex is involved in the regulation of cellular differentiation, tissue development, and DNA repair (Guan, Mao, *et al.*, 2011; Werner *et al.*, 2012). *ARID1A* is required for SWI/SNF complexes to suppress DNA synthesis and as such ARID1A is considered a tumour suppressor since it regulates cell proliferation and functions to prevent genomic instability (Mao and Shih, 2013). Mutations of *ARID1A* have been described in approximately 29-40 % of cases of EC (Guan, Mao, *et al.*, 2011; Kandoth *et al.*, 2013; Wiegand *et al.*, 2011). *ARID1A* mutations are normally insertions or deletions that lead to the formation of truncated proteins (Guan, Mao, *et al.*, 2011).

Mao and colleagues performed an immunohistochemical investigation of 246 endometrial tissue samples spanning a range from normal cycling endometrium, to CAH and high-grade endometrioid EC (Mao *et al.*, 2013). They specifically analysed tissues for 'clonal' loss of ARID1A, in addition to complete loss of expression across the entire tissue section (Mao *et al.*, 2013). The authors reported that all samples of normal endometrium retained ARID1A protein expression, with 16 % (n=38) of CAH demonstrating clonal but not complete loss of protein expression. Complete loss of expression of ARID1A increased with EC tumour grade, from 25 % (n=88) in low-grade to 44 % (n=55) in high-grade endometrioid tumours (Mao *et al.*, 2013). The same group went on to compare ARID1A expression, along with that of PTEN and the proliferation marker Ki67, utilising a cohort of 114 endometrial samples with a diagnosis of atypical hyperplasia / EIN (Ayhan *et al.*, 2015). They noted that all specimens (n=17) with focal ARID1A loss also exhibited concurrent loss of PTEN expression and that this was correlated with a significant increase in proliferation when compared to adjacent areas

in the same tissue without concurrent loss of both markers (Ayhan *et al.*, 2015). The authors used these findings to suggest that ARID1A may act to prevent PTEN inactivation from furthering cellular proliferation in the transition from pre-malignancy to EC (Ayhan *et al.*, 2015).

Werner *et al* adopted a semi-quantitative intensity staining score when analysing ARID1A expression in their retrospective study of 679 endometrial tissue samples (n=436 endometrioid ECs, n=38 EH). Their findings echoed those of Mao *et al* demonstrating a stepwise reduction in staining intensity of ARID1A with progression from hyperplasia without atypia (no loss of protein expression) to hyperplasia with atypia (16 % loss of expression, n=6) and endometrioid tumours (19 % loss of expression, n=84) (Werner *et al.*, 2012).

1.6.2 Transcription Factors

1.6.2.1 Paired Box 2 Protein (PAX2)

Paired Box 2 Gene (*PAX2*) is a member of a large family of paired box genes which globally are implicated in transcriptional regulation during the process of embryogenesis (Mansouri *et al.*, 1994; Ryan *et al.*, 1995) The interest in paired box (PAX) genes as a predictor of EH/EC has been stimulated by reports that they can act as proto-oncogenes through regulation of cell proliferation, survival and apoptosis (reviewed in Robson *et al.*, 2006). Further reports have suggested that *PAX2* is activated by oestrogen and tamoxifen in endometrial cancer-derived cells and EC cell lines but not in the normal endometrium and that *PAX2* is able to promote the growth of EC cells (Shang, 2007; Wu *et al.*, 2005). *PAX2* gene expression has been connected to the normal growth of the central nervous system, eyes, ears, and urogenital system (Allison *et al.*, 2012). Expression of PAX2 protein has been described as a marker of the Müllerian duct derivatives (Fallopian tubes, uterus, cervix, and upper vagina) (Tong *et al.*, 2006). According to Tong *et al*, epithelial cells within the uterine glands normally demonstrate nuclear expression of PAX2 (Tong *et al.*, 2006).

Loss of PAX2 immunoexpression has been implicated in the development of EIN by several authors and has found potential utility as a tool when diagnosing difficult EIN cases (e.g. where there is no ‘normal’ tissue in a sample to act as in internal control when assessing nuclear morphology) (Quick *et al.*, 2012). Joiner and colleagues built on these recommendations (Quick *et al.*, 2012) and compared the WHO94 and EIN classification systems for EH using PAX2 immunohistochemistry (Joiner *et al*., 2015). In their study the authors considered complete loss of nuclear staining, or ‘reduced’ nuclear staining as

compared to background endometrium, to be indicative of reduced PAX2 bioactivity (Joiner *et al.*, 2015). Reduced PAX2 expression was noted in 92 % (33/36) of EIN cases and 88 % (22/25) of atypical EHs. Although the authors concluded that loss of PAX2 immunoexpression is a useful finding when deciding whether lesions are premalignant, they also advocated careful comparison to H&E sections when considering the findings (Joiner *et al.*, 2015)

Loss of PAX2 expression was also found in 71 % (37/52) of EIN cases by Monte *et al* and in 74 % (40/56) of atypical EHs by Allison *et al* (Allison *et al.*, 2012; Monte *et al.*, 2010). Allison *et al* proposed that PAX2 loss occurs early in the process of endometrial carcinogenesis as they did not detect loss of expression in their proliferative or secretory endometrial samples. They added the caveat that the expression pattern does not discriminate between diagnostic categories of EH since its expression is ubiquitously lost amongst all EH groups (Allison *et al.*, 2012). Monte *et al* also corroborated this, adding that the greatest stepwise change in PAX2 expression occurs between normal and premalignant endometrium (Monte *et al.*, 2010). Alternative findings are presented by Kahraman *et al*, suggesting an increase in PAX2 expression with progression from premalignant states to EC (Kahraman *et al.*, 2012).

1.6.2.2 Heart and neural crest derivatives expressed transcript 2 (HAND2)

Heart and neural crest derivatives expressed transcript 2 (HAND2) belongs to the basic helix-loop-helix (bHLH) family of transcription factors; it plays crucial roles during embryological cardiac morphogenesis (VanDusen *et al.*, 2014) and knockout mice are infertile due to failure of implantation (Li *et al.*, 2011). In mice, *Hand2* has been shown to be a progesterone receptor-regulated gene and its expression in endometrial stromal cells inhibits epithelial cell proliferation via suppression of several fibroblast growth factors (FGFs) (Li *et al.*, 2011).

When Jones and colleagues conducted a comprehensive epigenome-transcriptome-interactome analysis, they found HAND2 was at the centre of the most highly ranked differential hotspot in EC (Jones *et al*., 2013), leading them to propose that epigenetic deregulation of HAND2 was a crucial step in endometrial carcinogenesis. They reported that methylation of the *HAND2* promoter was increased in pre-malignant endometrial lesions when compared to normal endometrium and that this was associated with a reduction in HAND2 expression (Jones *et al.,* 2013).

Buell-Gutbrod et al. also hypothesised that HAND2 plays a role in the development of EH and type 1 endometrioid EC (Buell-Gutbrod *et al.,* 2015). In their immunohistochemical study, 56 archival hysterectomy specimens with a known pathological diagnosis of either disordered proliferative endometrium, simple or complex hyperplasia with or without atypia and EC were investigated for expression of HAND2 (Buell-Gutbrod *et al.,* 2015). Results demonstrated a statistically significant ($P<0.001$) reduction in the stromal expression of HAND2 between benign endometrium and both simple and complex hyperplasia with atypia and EC (Buell-Gutbrod *et al.,* 2015). However, there was no statistically significant difference between benign endometrium and simple hyperplasia without atypia or disordered proliferative endometrium (Buell-Gutbrod *et al.,* 2015). The authors remarked that the HAND2 antibody cannot distinguish between simple hyperplasia with atypia, complex hyperplasia with atypia and EC (Buell-Gutbrod *et al.,* 2015).

1.6.3 DNA mismatch repair (MMR)

The role of the DNA mismatch repair (MMR) system is to correct for 'mismatches' (i.e. mismatched base-pairs such as G-A) and small insertions/deletions (InDels) that are mostly caused by errors during DNA replication and sometimes by other forms of DNA damage. DNA mismatches may occur in any DNA sequence, whereas InDels occur in regions of repetitive nucleotide sequences (e.g. AAAAAAAAAA… or CACACACA…) called microsatellites, leading to an expansion or reduction in length of those microsatellites termed microsatellite instability (MSI). Both mismatches and altered microsatellites are normally repaired by a functioning MMR system, but if there is defective mismatch repair (dMMR) as occurs in tumours in Lynch Syndrome, then they remain unrepaired and such cells have a 100x-1000x fold increased mutation rate and microsatellite instability (MSI) (Diaz-Padilla *et al.*, 2013; Poulogiannis *et al.*, 2010). MSI is a characteristic feature of Lynch Syndrome-associated EC and other cancers. Defective mismatch repair (dMMR) arises in Lynch syndrome as a result of inactivation of any one of the four main MMR genes (*MLH1, MSH2, MSH6* and *PMS2*) by inheritance of one mutated MMR allele (the cause of Lynch Syndrome) together with acquired mutation or deletion of the other copy of the same MMR gene in a cell, often a neoplastic precursor cell that may go on to evolve into a tumour (Eshleman and Markowitz, 1996; Poulogiannis *et al.*, 2010). Defective mismatch repair can also occur spontaneously in tumours of patients who do not have Lynch syndrome, and this is almost always due to acquired *MLH1* promoter hypermethylation that leads to silencing of *MLH1* expression, which is found in ~ 25-30 % of EC cases (Hecht and Mutter, 2006).

Inactivation of any of the MMR genes (including *MLH1, MSH2, MSH6* and *PMS2*) can cause MSI (Eshleman and Markowitz, 1996; Poulogiannis *et al.*, 2010). The National Cancer Institute (NCI) consensus or 'Bethesda' panel was established as a panel of microsatellite markers to be used to diagnose MSI. Although initially designed for colorectal cancer, the system has also been adopted for use in the endometrium (Boland *et al.*, 1998). The panel comprises five microsatellite loci: two mononucleotide markers and three dinucleotide markers. MSI-high tumours are defined by instability at two or more of the five loci (or >30% of loci if a larger panel of markers is used), whereas MSI-low tumours show instability at one locus out of the five (or in 10–30% of loci in larger panels). Microsatellite stable (MSS) tumours are those without instability at any loci (or <10% of loci in larger panels) (Vilar and Gruber, 2010). MSI-high status has been demonstrated to be an indicator of poor prognosis in International Federation of Gynecology and Obstetrics (FIGO) stage 1, but not FIGO 2–4 endometrioid ECs (Steinbakk *et al.*, 2011).

dMMR within somatic ECs is commonly associated with endometrioid histology (Hecht and Mutter, 2006). In sporadic EC, dMMR is mainly caused by hypermethylation of the *MLH1* promoter, silencing its expression, thus leading to MSI. This is then responsible for a lack of immunohistochemically detectable MLH1 protein expression. (Simpkins *et al.*, 1999). Woo *et al* demonstrated the utility of MMR immunohistochemistry in their 2014 study of MMR proteins in women with EC (Woo *et al.*, 2014).

Berends *et al*, suggest that loss of MLH1 or MSH2 protein may be an early event in endometrial carcinogenesis. Their study of 62 cases was interesting in that they looked at patients with EC who had germline HNPCC (Hereditary non-polyposis colorectal cancer / Lynch syndrome) mutations, patients with HNPCC and no EC and patients with EC without HNPCC. In patients with EH both with and without a germline *MLH1* mutation, loss of the corresponding protein was detected using immunohistochemistry (Berends *et al.*, 2001). In 6 cases of EH and concurrent EC, loss of MLH1 or MSH2 proteins was seen in both hyperplastic and tumour areas within the tissue (Berends *et al.*, 2001).

Hamid *et al* analysed endometrial samples from 123 women (including 51 EH cases) for MSH2 expression. They noted that all simple hyperplasias showed a normal positive expression of MSH2, with some complex and atypical EHs demonstrating weak or no MSH2 expression at all (Hamid *et al.*, 2002). However, this was not significant enough to be able to infer utility as a diagnostic marker for distinguishing between EH categories (Hamid *et al.*, 2002). The authors also comment that loss of MSH2 expression is rarely observed in sporadic EC cases (Hamid *et al.*, 2002). Orbo *et al* looked at EC progression from EH and analysed

expression of MLH1, MSH2 and MSH6. They found loss of expression in these markers was higher in EH cases where there was either a concurrent EC or subsequent progression to EC (Orbo *et al.*, 2003).

Molecular evidence connecting an absence of expression of MLH1 with tumour-specific promoter hypermethylation in EH has previously been described, suggesting ECs with MSI may acquire this feature as pre-cancers (Jovanovic *et al.*, 1996). Esteller and colleagues share this view; they found that aberrant *MLH1* methylation is almost exclusively restricted to atypical EHs (Esteller *et al.*, 1999). In addition, the group noted that the atypical EHs methylated at *MLH1* which demonstrate a MSI phenotype are usually those also associated with a concurrent EC that also have MSI and *MLH1* methylation (Esteller *et al.*, 1999). These reports and the trends observed from the above literature imply a role for the detection and categorisation of deficiencies in the MMR system within EHs, with suggestions that deficiencies in the MMR system may be useful in predicting malignant progression.

1.7 General conclusions, hypothesis and aims of this study

Endometrial hyperplasia is an abnormal proliferative disorder of the uterus, most often caused by exposure of the endometrium to oestrogens unopposed by progesterone. Endometrial hyperplasia is not a homogenous entity, rather the condition represents a variety of morphologically and cytologically abnormal endometrial lesions, defined histologically by an increase in the endometrial gland-to-stroma ratio. When cytological atypia is present within EH lesions there is a substantial risk of progression to endometrioid EC However, not all hyperplastic lesions will progress to malignancy, some occur in response to an abnormal hormonal environment without an underlying neoplastic mechanism.

Making the correct distinction between benign hyperplasia and pre-malignant hyperplasia has significant implications, since their differing endometrial cancer risks must be matched with an appropriate clinical intervention to avoid detrimental undertreatment or unnecessary overtreatment. At present histopathological classification is the only method used to achieve this objective, and as discussed, reports of diagnostic reproducibility vary depending on the classification scheme used. With the reported rise in endometrial cancer incidence, the clinical need for improved patient risk stratification has received renewed interest, especially in the context of women who are either unable to undergo surgical treatment or who wish fertility preservation.

As such, the overarching aim of the studies described in this thesis was to improve our capacity for earlier diagnosis of EC through targeting and enhancing our understanding of EH. Specific chapter aims include:

1. **To develop a human EH tissue resource and utilise this to evaluate the current methods used to classify EH and predict its progression to EC.**

Hypothesis: The 2014 World Health Organisation (WHO2014) / Endometrioid Intraepithelial Neoplasia (EIN) system of endometrial hyperplasia classification improves diagnostic reproducibility and prediction of endometrial cancer progression when compared with its predecessor.

2. **To characterise key molecular changes within EH lesions so that they can be used to extend and enhance pathological classification of EH.**

Hypothesis: An immunohistochemical 'biomarker' panel can be used to improve the diagnosis of endometrial hyperplasia

3. **To explore *in vitro* models of the endometrium and investigate the role of PTEN and ARID1A in oestrogen driven cellular proliferation.**

Hypothesis: Reduced expression of the tumour suppressors PTEN *and* ARID1A *increase proliferation of endometrial epithelial cells and these effects are further enhanced by oestrogen.*

To achieve these aims, the studies described herein capitalised on access to an archival pathology resource of human endometrial hyperplasia tissues, in addition to informative endometrial cancer cell lines.

Chapter 2

2 General materials and methods

Unless otherwise specified all chemicals and standard laboratory reagents were purchased from Sigma-Aldrich (Sigma-Aldrich Ltd, Dorset, UK).

2.1 Human endometrial tissue samples

2.1.1 MRC-CIR archival human endometrial tissue

Archival human endometrial tissues held within the MRC Centre for Inflammation Research were utilised in the current study. These tissues were collected under Lothian Research Ethics number LREC/1999/6/4 held by Professor Richard Anderson. In brief, endometrial biopsies were obtained from women undergoing hysterectomy for a suspected endometrial cancer between March 1999 and October 2010. The tissues were fixed in 4 % neutral buffered formalin (NBF), prior to paraffin embedding and histological analysis by a gynaecological pathologist. Written informed consent was obtained from the patients. Endometrial tissues with a histological diagnosis of endometrial hyperplasia without evidence of malignancy were selected from this cohort (Appendix. 1).

2.1.2 Lothian NRS Human Annotated Bioresource endometrial tissue

The Lothian NRS Human Annotated Bioresource is a Tissue Bank based within NHS Lothian. The Tissue Bank supports a wide range of research involving disorders of the human body. The material collected is from living donors and consists of residual or waste tissues that are surplus to diagnostic requirements or have been removed for therapeutic reasons and would normally be disposed of. Under ethical approval REC/13/ES/0126 and REC/15/ES/0994 unconsented archival diagnostic tissue samples (including material from the histopathology diagnostic archive) can be utilised, provided all samples and data are anonymised.

An application was made to the Bioresource for the purposes of the current study (SR465, Appendix. 2). Formalin-fixed paraffin-embedded (FFPE) serial sections of human endometrial tissue (n=127 endometrial biopsies) pathologically reported and coded as having a diagnosis of endometrial hyperplasia between the years 2004-2009 were obtained, in

addition to their matched patient demographic data. The endometrial biopsies were either collected using a Pipelle® endometrial sampler or via a dilatation and curettage (D&C) procedure at the time of a hysteroscopy. All the samples obtained represent an index endometrial hyperplasia diagnosis, i.e. they were not follow-up biopsies and thus were obtained prior to the commencement of any form of treatment. In addition, anonymised vermiform appendix FFPE tissue sections were also obtained (n=2 samples) for use as positive control tissue. Specific sample details are provided in the relevant results chapter.

2.1.3 Human tissue collection and processing

Human endometrial tissues were obtained from women undergoing surgery for benign gynaecological conditions. Endometrial biopsies were performed using a Pipelle® endometrial sampler, divided equally and processed as follows: 1) DPBS (Dulbecco's Phosphate-Buffered Saline, without calcium and magnesium, Gibco 14040-091) for immediate *in vitro* culture, 2) 4 % NBF for processing into paraffin wax and histological analysis, 3) RNASave (Biological Industries, 01-891-1) for 24 hours at 4 ºC and then stored at -80 ºC for subsequent RNA extraction. Informed written consent was obtained prior to tissue collection by a member of the research team. Ethical approvals were held by Professor AW Horne (LREC/11/AL/0376) and Professor HOD Critchley (LREC/10/S1402/59, LREC/16/ES/007). Specific sample details are provided in the relevant results chapter.

2.2 *In vitro* cell culture

2.2.1 Isolation of primary human endometrial cells

Primary human endometrial cells were isolated from endometrial biopsy tissue (section 2.1.3) by a modified enzymatic digestion as previously described (Bombail, Gibson, *et al.*, 2010). In brief, endometrial tissue specimens were washed twice in 37 ºC DPBS, finely dissected using sterile scalpels and digested with type IV collagenase (1 mg/mL; Sigma-Aldrich, C5138) and DNase (0.1 mg/mL; Sigma-Aldrich, DN25) in 2 mL of DPBS for 90 minutes at 37 ºC. The digested tissue was then resuspended in RPMI 1640 medium (Gibco, 21875) to halt enzymatic digestion and passed through a syringe with 19-gauge needle to aid tissue dispersion. The digested tissue was then sequentially passed through a 70 μm and a 40 μm nylon mesh cell strainer (BD Falcon, 352350; 352340), to separate stromal (pass through mesh) from glandular (remain above mesh) cell components. The stromal follow-through was

used for other *in vitro* research projects within the laboratory. The cell strainers were backwashed with DPBS to obtain the glandular epithelial components and pelleted by centrifugation (115 g for 5 minutes, room temperature). An optional red cell lysis step was performed at this stage dependent on the amount of blood contamination of the digested tissue. If needed, 1 mL of red cell lysing buffer (Sigma-Aldrich, R7757) was added to the cell pellet and gently mixed for 1 minute. 15 mL of complete primary epithelial cell medium (Table. 2-1) was then added, the specimen again pelleted by centrifugation (115 g for 5 minutes, room temperature) and the supernatant decanted. The final cell pellet was resuspended in complete primary epithelial cell medium (Table. 2-1), transferred to a 25 cm^3 tissue culture flask (Corning, CLS430639) pre-coated with attachment factor (Gibco, S006100) and maintained in 37 ºC humidified conditions with 5 % CO_2 in air.

Table 2-1: Components of complete cell culture medium

	Gibco Catalogue Number
Complete primary epithelial cell medium	
DMEM/F12 GlutaMAX medium to 500 mL	31331028
5 mL 100x Insulin-Transferrin-Selenium (ITS)	51500056
50 ng/mL EGF Human Recombinant Protein	PHG0311
5 mL Penicillin/Streptomycin (10,000 U/mL, 10 mg/mL)	15140122
2.5 mL Amphotericin B (2.5 µg/mL)	15290026
5 mL L-Glutamine (2 mM)	25030081
5 mL 100x MEM Non-essential Amino Acid Solution	11140050
Complete epithelial cell line medium (Ishikawa / MFE-280 / KLE cells)	
DMEM/F12 GlutaMAX medium to 500 mL	31331028
10 % Heat inactivated fetal calf serum (FCS)	16140071
5 mL Penicillin/Streptomycin (10,000U/mL, 10mg/mL)	15140122
2.5 mL Amphotericin B (2.5 µg/mL)	15290026
5 mL L-Glutamine (2 mM)	25030081
5 mL 100x MEM Non-essential Amino Acid Solution	11140050
Complete SHT-290 cell medium	
RPMI 1640 medium to 500 mL	A1049101
10 % Heat inactivated fetal calf serum (FCS)	16140071
5 mL Penicillin/Streptomycin (10,000 U/mL, 10 mg/mL)	15140122
2.5 mL Amphotericin B (2.5 µg/mL)	15290026

2.2.2 Human endometrial cell lines

Cell line identity was authenticated by Eurofins Medigenomix Forensik GmbH. In brief, genomic DNA was provided from available cell lines for multiplex short tandem repeat (STR) loci analysis using the following profile markers: Amelogenin, D3S1358, D1S1656, D6S1043, D13S317, Penta E, D16S539, D18S51, D2S1338, CSF1PO, Penta D, TH01, vWA, D21S11, D7S820, D5S818, TPOX, D8S1179, D12S391, D19S433 and FGA.

Cell lines were routinely tested for mycoplasma contamination using the commercially available MycoAlert™ mycoplasma detection kit (Lonza, LT07-318).

2.2.2.1 Human Ishikawa endometrial epithelial cancer cell line

The human Ishikawa cell line was purchased from the European Collection of Authenticated Cell Cultures (ECACC, Wiltshire, UK; 99040201). The cell line is a well differentiated endometrial epithelial cancer cell line, derived in 1980 (Tsukuba University Hospital, Japan) from a 39-year-old parous patient diagnosed with a grade 2 endometrioid endometrial adenocarcinoma (Nishida, 2002). Ishikawa cells are well recognised to express functional ERs and progesterone receptors (PRs) (Lessey *et al.*, 1996; Nishida, 2002).

2.2.2.2 Human MFE-280 endometrial epithelial cancer cell line

The human MFE-280 cell line was purchased from the European Collection of Authenticated Cell Cultures (ECACC, Wiltshire, UK; 98050131). The cell line is a poorly differentiated endometrioid endometrial epithelial cancer cell line, derived from a recurrent grade 3 endometrial adenocarcinoma from a 77-year-old patient. MFE-280 cells have been documented not to have functional ERs or androgen receptor (AR) (Hackenberg *et al.*, 1997). Of note for the current study, MFE-280 cells do not possess mutations of the tumour suppressor genes *PTEN* or *ARID1A* (Liang *et al.*, 2012).

2.2.2.3 Human KLE cell line endometrial epithelial cancer cell line

The human KLE cell line was purchased from the American Type Culture Collection (ATCC, Manassas, USA; CRL-1622). The cell line is a poorly differentiated endometrioid endometrial epithelial cancer cell line, derived in 1982 (Vincent Memorial Hospital, Boston,

USA) from a 68-year-old parous patient diagnosed with a grade 3, locally invasive endometrioid endometrial adenocarcinoma (Richardson *et al.*, 1984). KLE cells have defective ERα, however express ERβ (Raam *et al.*, 1983; Richardson *et al.*, 1984; Zhang *et al.*, 2015). Of note for the current study, KLE cells do not possess mutations of the tumour suppressor genes *PTEN* or *ARID1A* (Liang *et al.*, 2012).

2.2.2.4 Human SHT-290 endometrial stromal fibroblast cell line

The human SHT-290 cell line was gifted from Dr. David Kaufman, Department of Pathology and Laboratory Medicine, University of North Carolina at Chapel Hill, NC, USA. This endometrial stromal fibroblast cell line is derived from a patient with normal endometrium and has been immortalised by expressing a transduced human telomerase reverse transcriptase (hTERT). SHT-290 cells are reported to retain steroid hormone receptor expression and responsiveness (Barbier *et al.*, 2005).

2.2.3 Routine culture of cell lines

Ishikawa, MFE-280, KLE and SHT-290 cell lines were routinely maintained in 162 cm^3 tissue culture flasks (Corning, CLS3151) with complete medium (Table. 2-1) in 37 ºC humidified conditions with 5 % CO_2 in air. Cell passage was performed twice weekly at a split ratio of 1:10 for Ishikawa cells and a ratio of 1:2-3 for MFE-280, KLE and SHT-290 cell lines. Experiments were carried out using the lowest possible passage number. Phenol-red containing culture medium was substituted for phenol-free variants (DMEM/F12 (Gibco, 21041025), RPMI 1640 (Gibco, 11835030)), in addition to charcoal stripped fetal calf serum (CSFCS, as per 2.3.3.4), 72 hours prior to experimentation. This was performed to reduce confounding effects; phenol-red can act as a weak ER agonist (Berthois *et al.*, 1986; Welshons *et al.*, 1988).

2.2.3.1 Cell harvesting

To harvest cells in routine culture, the 162 cm^3 plastic tissue culture flasks were first washed twice with DPBS to remove all traces of sera which inhibits trypsin. Cells were then detached from the plasticware by incubating with 5 mL of 0.05% phenol-red Trypsin-EDTA (Gibco, 25300054) for 5 minutes at 37 ºC. Trypsin was then inactivated by adding 10 mL of

complete medium. The resultant cell suspension was then pelleted by centrifugation at 115 g for 5 minutes at room temperature and the supernatant discarded.

2.2.3.2 Cryopreservation

Cells were harvested as per 2.2.3.1. The cell pellets were resuspended in 2-3 mL of complete medium containing 5 % DMSO (KLE cells) or 10 % DMSO (Ishikawa, MFE-280, SHT-290 cells). The cell suspension was then equally decanted into Nunc® 1.8ml CryoTubes (Sigma-Aldrich, V7884), labelled and frozen immediately at -80 ºC for 24 hours prior to transfer to liquid nitrogen storage units for long-term storage.

To recover cells from liquid nitrogen storage, CryoTubes containing cells were rapidly defrosted to 37 ºC, the contents transferred to 15 mL falcon tubes (BD Biosciences, 352096) with 10 mL of complete medium and pelleted by centrifugation at 115 g for 5 minutes. Cell pellets were resuspended in 5 mL of complete medium and seeded into 25 cm^3 tissue culture flasks (Corning, CLS3055). Cell viability was checked at 24 hours and complete medium exchanged. Cells were grown to confluence before harvesting and transferring into larger tissue culture flasks.

2.2.3.3 Cell counting

Cells were harvested as per 2.2.3.1 and the cell pellets resuspended in 5 mL of complete medium. 10 µL of the cell suspension was mixed with 10 µL of 0.4 % trypan blue solution (ThermoFisher Scientific, T10282). 10 µL of the cell mix was then loaded into each chamber of a Countess™ Cell Counting Chamber Slide (ThermoFisher Scientific, C10228) and read on the Countess™ II Automated Cell Counter (ThermoFisher Scientific, AMQAX1000). The total alive cell count was obtained for each chamber and the average of the two counts used to dilute the cell suspension to the correct cell number needed for each experiment.

2.2.3.4 Dextran charcoal stripping of fetal calf serum

Heat inactivated fetal calf serum (FCS) was substituted in complete medium (where required, see Table. 2-1) with charcoal stripped fetal calf serum (CSFCS) for all cell lines, 72 hours prior to experimentation. Charcoal treatment of FCS is used to deplete a number of peptides and small molecules ordinarily found in FCS, e.g. steroid hormones. Short-term maintenance of cells in complete medium lacking significant levels of steroid hormones (i.e.

with phenol-red free medium and CSFCS) permits more reliable phenotypic analysis after cell treatment with exogenous hormones (Sikora *et al.*, 2016). In brief, 500 mL of heat-inactivated FCS (Gibco, 1614007) was mixed with 5 g dextran coated charcoal (Sigma-Aldrich, C6241) overnight on a stirrer at 4 ºC. Excess charcoal was removed by centrifugation (10 minutes, 13,000 g, room temperature) and the supernatant passed through 0.2 μm filters, aliquoted and stored at -20 ºC.

2.2.4 Manipulation of gene expression within cell lines

2.2.4.1 Lentiviral miRNA knockdown

Lentiviral vectors (created by Dr. Pamela Brown and Ms. Linda Ferguson, Shared University Research Facility (SuRF), Bimolecular Core, see Evans *et al.*, 2009; McCloskey *et al.*, 2014 for detailed methods) were utilised in this study to manipulate gene expression within human endometrial cell lines (see 2.2.2) utilising the principles of RNA interference (RNAi). After screening of efficiency of gene knockdown, several stably transduced cell lines variants were created utilising these vectors as described below.

In brief, miRNA oligonucleotides of interest to this project were designed using a combination of published literature data (Ayhan *et al.*, 2015; Guan, Wang, *et al.*, 2011; Juric *et al.*, 2015), the Invitrogen BLOCK-iT™ RNAi designer web programme or were purchased directly from ThermoFisher Scientific (see corresponding results chapters for further details).

Each miRNA oligonucleotide construct was then cloned into a pcDNA6.2_GW_EmGFP_miR Gateway plasmid (ThermoFisher Scientific) using the BLOCK-iT™ Pol II miR RNAi Expression Vector Kit (ThermoFisher Scientific, K4935-00) according to the manufacturer's protocols and the inserts verified by DNA Sanger Sequencing. Human endometrial cell lines (MFE-280 and KLE, see 2.2.2) were transiently transfected with the plasmid vectors and the effect on protein expression analysed by Western Blotting (see 2.9). The two most favourable plasmids were then recombined into pLent6.2 vectors. HEK293T cells were transfected with the pLent6.2 vectors to produce the Lentivirus particles using the BLOCK-iT™ Lentiviral Pol II miR RNAi Expression System (ThermoFisher Scientific, K4937-00).

2.2.4.2 Transduction efficiency testing of cell lines

To determine the optimum lentiviral transduction conditions of cell lines a test lentivirus carrying emerald GFP (ThermoFisher Scientific) was used, Lv-cppt-CMV-emGFP-opre. This was previously generated in house by Biomolecular Core at the University of Edinburgh.

2.2.4.3 Cloning of oestrogen receptor alpha (ERα / ESR1).

ESR1 (NCBI Reference Sequence: NM_000125.3) was liberated from pDC315-ESR1 (as described in Bombail *et al.*, 2010) using an *Eco* RI/*Bam* HI digest, then inserted into digested pDONR221-attB1-IRES-mcherry-attB2 (IRES-mCherry (Clontech)) and finally Gateway cloned in pLenti6-cppt-DEST-opre (as described in McCloskey *et al.*, 2014) to generate pLenti6-cppt-CMV-ESR1-IRES-mCherry-opre. Unmodified pLenti6-cppt-CMV-IRES-mCherry-opre was used as a control. This was packaged (as described in McCloskey *et al.*, 2014) to generate high titre > 3 x 10^7 transduction units (TU) / ml lentivirus.

2.2.5 Ligands

17β-Oestradiol (E_2, C18H24O2) is a steroid ligand; it is the primary female sex hormone produced by the premenopausal ovary. E_2 (Sigma-Aldrich, E8875) powder was reconstituted in dimethyl sulfoxide (DMSO) to a stock concentration of 10^{-3} M and stored, protected from light, in a glass bijou at -20 ºC for a maximum of three months. Working stock dilutions were prepared, as required, in sterile Dulbecco's calcium and magnesium free phosphate buffered saline (DPBS; Gibco, 14190136) diluted to a final working concentration of 10^{-8} M.

4-Hydroxytamoxifen (4-OHT, $C_{26}H_{29}NO_2$) is the active metabolite of the antioestrogen, Tamoxifen. It is a cell permeable SERM, with a partial agonist action in the endometrium. 4-OHT (Sigma-Aldrich, H7904) powder was reconstituted in DMSO to a stock concentration of 10^{-3} M and stored, protected from light (to reduce a *cis-trans* interconversion), in a glass bijou at -20 ºC for a maximum of three months. Working stock dilutions were prepared, as required, in DPBS diluted to a final working concentration of 10^{-7} M.

Propyl pyrazole triol (PPT, $C_{24}H_{22}N_2O_3$) is a potent subtype-selective ER agonist, with a 410-fold selectivity for oestrogen receptor alpha (ERα) over oestrogen receptor beta (ERβ)

(Stauffer *et al.*, 2000). PPT (Tocris, 1426) powder was reconstituted in DMSO to a stock concentration of 10^{-3} M and stored, protected from light, in a glass bijou at -20 ºC for a maximum of three months. Working stock dilutions were prepared, as required, in DPBS diluted to a final working concentration of 10^{-8} M.

Fulvestrant (ICI 182,780, $C_{32}H_{47}F_5O_3S$) is a high affinity ER antagonist, demonstrated to block both ERα and ERβ activity (Wakeling *et al.*, 1991). ICI 182, 720 (Tocris, 1047) powder was reconstituted in DMSO to a stock concentration of 10^{-3} M and stored, protected from light, in a glass bijou at -20 ºC for a maximum of three months. Working stock dilutions were prepared, as required, in DPBS diluted to a final working concentration of 10^{-7} M.

2.3 Immunohistochemistry

Immunohistochemistry (IHC) is a widely used, multistep, histological technique which permits the detection and localisation of proteins of interest by exploiting the ability of an antibody to bind to specific antigenic sites on proteins against which they have been raised. Through the use of a detection system, either an enzyme mediated chromogenic reaction or a fluorescence-based system, visualisation of the antibody-antigen complex can be achieved. Generally speaking, immunohistochemistry refers to the detection of antigens in tissues and immunocytochemistry to the detection of antigens in individual cells. Unless otherwise stated, all wash steps were carried out twice for 5 minutes at room temperature on a rocker.

2.3.1 Tissue processing

Formalin-fixed paraffin-embedded (FFPE) blocks of human endometrial tissue (see 2.1.1 and 2.1.2) were cooled on ice blocks to facilitate tissue sectioning and increase the rigidity of the tissue. 5 µm sections were cut from the FFPE tissue blocks using a microtome (Leica Biosystems, RM2135), floated on a water bath set at 40 ºC (Thermo Shandon, 3120058) and mounted on charged glass slides (Leica, 3800084E). Cut tissue section slides were oven dried overnight at 55 ºC.

2.3.2 Dewaxing and tissue rehydration

Cut tissue sections of human endometrial tissue (see 2.2.2 and 2.4.1) were dewaxed by immersion in xylene (VWR Chemicals, 28975.325) twice for 5 minutes. Rehydration of the tissue sections was achieved by immersion in descending grades of ethanol (absolute to 70 %) for 20 seconds each followed by a tap water wash.

2.3.3 Heat-induced epitope retrieval

Formalin fixation of tissue causes protein crossing-linking, stabilising the architecture of the tissue for histological processing and increasing tissue longevity. However, this limits the ability of an antibody to bind to the antigenic determinant site (epitope) of the protein of interest. As a consequence, epitope retrieval, using sufficient heat and an acid or alkali pH to break the cross-linking without denaturing the protein of interest, must be performed.

After dewaxing and tissue rehydration, tissue sections were submersed in 0.01 M pH 6 citrate retrieval buffer (0.1 M stock: Citric acid 84.04 g, 3.5 L deionised H_2O, adjusted to pH 6 with NaOH). Heat-induced epitope retrieval (HIER) was performed in one of two ways: 1) Heating submersed tissue sections to 110 ^{o}C in a pressurised decloaking chamber (BioCare Medical, DC2012) and gradually cooling to 90 ^{o}C over the course of 1 hour, or 2) Microwave HIER; Boiling 0.01 M pH 6 citrate retrieval buffer - full power 4 ½ minutes, adding the tissue sections in a plastic rack, boiling on full power for 2 ½ minutes and then leaving for 30 minutes to cool. Microwave HIER was only used when a second HIER was required during dual immunofluorescence (see 2.5.1). Tissue sections were allowed to cool and then washed in tap water.

2.3.4 Peroxidase blocking

Endogenous peroxidase enzymes found within several tissues can interact with enzyme mediated chromogen detection systems and increase non-specific background staining during immunohistochemistry. In order to avoid this, a peroxidase block was performed by incubating the tissue sections with 3 % (v/v) hydrogen peroxide (H_2O_2; VWR Chemicals, 23614.360) in methanol (Fisher Chemical, M/4000/15) for 15 minutes, followed by a tap water wash and a 5 minute wash with tris-buffered saline (TBS; 0.05 M Tris-HCL, pH 7.4, 0.85 % NaCl).

All subsequent incubations after this point were performed in a humidity chamber (Sigma-Aldrich, H6644) to prevent drying of tissues.

2.3.5 ImmPRESS™ polymerised reporter enzyme staining system

Commercially available ImmPRESS™ detection kits (Vector Laboratories, Inc., Burlingame, USA) were used for the human endometrial tissue immunohistochemistry in this study. The kits contain a ready-to-use ImmPRESS™ reagent, which employs horseradish peroxidase (HRP) micropolymers conjugated to affinity-purified secondary antibodies. This permits a higher density of enzymes per antibody to bind to the target, increases binding specificity and reduces background staining.

2.3.5.1 Serum blocking

To reduce non-specific binding from the ImmPRESS™ reagent, a blocking step with serum from the same animal species used to produce the reagent, i.e. horse, was performed. The serum carries antibodies that bind to reactive sites in the tissue and thus prevents nonspecific binding. After peroxidase blocking (see 2.4.4), ready-to-use 2.5 % normal horse blocking serum (NHS; Vector Laboratories, Inc., S-2012) was applied to the tissue sections for 20 minutes. The excess serum was then blotted away using cleaning tissue.

2.3.5.2 Primary antibody incubation and controls

The primary antibody diluted in NHS at an optimised concentration (Figure. 2-1), was applied to the tissue sections and incubated overnight at 4 ºC in a humidity chamber. Lists of the antibodies used during this study can be found in the materials and methods sections of the corresponding results chapters.

Control tissues were included with each experimental run. Positive controls utilised either internal control regions within the tissue of interest or separate tissue sections known to express the antigen of interest. A no-primary antibody control was used to detect false-positive or background staining as a result of non-specific binding of the ImmPRESS™ regent.

2.3.5.3 ImmPRESS™ reagent incubation

After incubation overnight with the primary antibody, the tissue sections were washed in TBS and the ImmPRESS™ (peroxidase) polymer IgG reagent (horse raised) applied and incubated for 30 minutes (Figure. 2-1). The animal species of the ImmPRESS™ IgG reagent used was dependent on the animal species that the primary antibody was produced in, e.g. a mouse produced primary antibody would be used with the ImmPRESS™ (peroxidase) polymer anti-mouse IgG reagent. Two further washes in TBS were then performed.

2.3.6 Enzyme medicated chromogenic detection

Enzyme mediated chromogenic detection utilises an enzyme/substrate reaction to produce a detectable (normally coloured) precipitate, the signal from which can be easily visualised. Commonly used enzymes include HRP and alkaline phosphatase. An enzyme-labelled primary antibody can be used (direct method), however as this involves only one labelled antibody binding per epitope, little signal amplification is achieved. A more commonly used technique modifies a two-step indirect method, whereby a secondary antibody directed against the same animal species of the primary antibody is used. The secondary antibody can be directly conjugated to an enzyme (e.g. HRP, as is the case with the ImmPRESS™ polymer system, see Figure. 2-1) or the secondary antibody can be biotinylated, whereby biotin is covalently attached. In the latter method, the high affinity of streptavidin for biotin is exploited and a preformed streptavidin-biotin enzyme complex (ABC method) or an enzyme-labelled streptavidin substrate (LAB method) can then be used. By introducing a secondary antibody, signal amplification is enhanced since several secondary antibodies (and hence more enzyme molecules) are likely to react with different epitopes on the primary antibody.

In this study the 3, 3'-diaminobenzidine (DAB) chromogen system was used (Vector Laboratories, Ltd., SK-4105). DAB is oxidised by any antigen bound antibody HRP complexes resulting in the development of brown deposit at antigen sites, indicating a positive reaction (see Figure. 2-1). DAB chromogen was diluted in its own dilutant as per manufacturer's instructions and incubated on the tissue sections until brown colour developed (maximum 5 minutes). After which the reaction was terminated by immersing the tissue section in H_2O.

2.3.7 Nuclear counterstaining – immunohistochemical method

In order to achieve optimal contrast between positive (brown) and negative areas after the use of the DAB chromogen system, tissue sections were counterstained with haematoxylin. Haematoxylin is a dark blue stain which binds basophilic structures such as those found within cell nuclei. Slides were submersed in Harris' haematoxylin (CellPath, RBA-4213-000A) for 5 minutes followed by a tap water wash. Next, slides were submersed in acid-alcohol (CellPath, RHS-787-1L) for 10 seconds to remove excess haematoxylin, followed by a tap water wash. Finally, tissue sections were submersed in Scott's tap water (CellPath, EGW-0200-25A) for 30 seconds to 'blue-up' the nuclei, followed by a tap water wash.

Tissue sections were then dehydrated through ascending grades of ethanol (70 % to absolute) for 20 seconds each and then immersed in xylene twice for 5 minutes, before being mounted with glass coverslips (VWR, various) using Pertex solvent-based glue (CellPath, SEA-0100-00A).

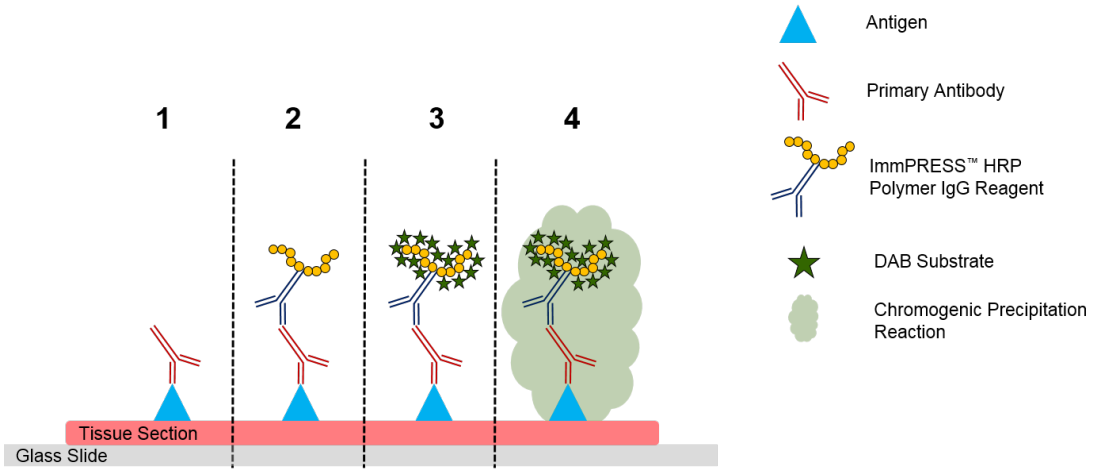

Figure 2-1: Schematic representation of DAB chromogen mediated immunohistochemistry using the ImmPRESS™ detection system. 1) Primary antibody binding to antigen of interest within tissue section. **2)** ImmPRESS™ reagent (secondary antibody conjugated to HRP polymer) binding to primary antibody. **3)** Incubation with DAB chromogen substrate. **4)** Enzyme/substrate reaction between HRP and DAB with production of a detectable brown precipitate.

2.3.8 Automated immunohistochemistry

The Leica BOND-MAX (Leica Biosystems) robotic staining platform was used to automate immunohistochemical staining of human endometrial hyperplasia tissue sections

(see 2.1.2) with the antibody PTEN. This work was undertaken by the Shared University Research Facility (SuRF, Edinburgh University). It is well known that the antigenicity of tissue sections can decline with time after sections are cut from FFPE blocks (Grillo *et al.*, 2017). A reduction in antigenicity can cause a reduction in signal intensity and increase non-specific background staining. This is especially true for the antibodies PTEN (Combs *et al.*, 2016; Gelb *et al.*, 2011). Therefore, the high-throughput ability of automated immunohistochemistry was utilised in order to stain endometrial hyperplasia tissues for these antibodies as soon as possible after tissues sections were generated. Table. 2-2 briefly summarises the optimised automated protocols and reagents used.

Table 2-2: Optimised IHC staining protocols using Leica BOND-MAX robotic system.

Antibody	HIER	Bond protocol & detection method	Notes
PTEN 6H2.1 (Dako, M3627) 1:300	10 minutes pH9 (Novocastra, RE7119-CE)	Bond polymer refine detection (Leica Biosystems, DS9800) Protocol 60/10/10 DAB enhancer (Leica Biosystems, AR9432) Haematoxylin counterstain	Protein block, serum free (Dako, X090930-2) used

2.3.9 Haematoxylin and eosin staining

Haematoxylin and eosin (H&E) staining is the principle stain used in histology, producing a spectrum of blue, violet and red colours within tissue sections that permits examination of the different compartments of the tissue. H&E staining was performed on all human endometrial tissue sections used in this study to facilitate tissue diagnosis and morphological assessment. As described in 2.3.7, haematoxylin binds basophilic structures, whilst eosin (a red/pink stain) binds acidophilic structures. After dewaxing and rehydration (see 2.4.2) tissue sections were stained with haematoxylin as per 2.3.7. After submersion in Scott's tap water, tissue sections were washed with tap water and submersed in 1 % aqueous eosin Y (CellPath, RBC-0100-00A) for 5-10 seconds followed by a final wash with tap water. Tissue sections were then dehydrated and mounted as described in 2.3.7.

2.4 Immunofluorescence

Immunofluorescence utilises the same principles as immunohistochemistry, only instead of an enzyme mediated chromogenic detection method, fluorochrome generated fluorescence is employed instead (summarised in Figure. 2-2). The tissue sections are subsequently imaged using confocal microscopy. Immunofluorescence permits the simultaneous detection of several target antigens and is useful for detecting co-localisation of different antigens within the same tissue section.

After dewaxing and tissue rehydration (see 2.3.2), HIER (see 2.3.3) and peroxidase blocking (see 2.3.4), tissue sections were blocked in normal animal serum buffer (50 mL stock: 20 % normal animal serum (10 mL), 5 % bovine serum albumin (2.5 g) (BSA; Sigma-Aldrich, 05470), made up to 50 mL with TBS) for 30 minutes at room temperature, followed by TBS washes. The species of the animal serum used was dependent upon the species that the secondary antibody was created in, i.e. a goat hosted secondary antibody against a mouse IgG (for use with a mouse created primary antibody) would require normal goat serum for blocking non-specific binding of the secondary antibody.

Following serum blocking, the primary antibody diluted to an optimised concentration in normal animal serum buffer (NAS), was applied to the tissue sections and incubated overnight in a humidity chamber at 4 ºC (Figure. 2-2). The next day, after TBS washes, a HRP-conjugated secondary antibody was diluted 1:500 in NAS and the tissue sections incubated for 30 minutes followed by further TBS washes (Figure. 2-2). Lists of the antibodies used during this study can be found in the materials and methods sections of the corresponding results chapters.

2.4.1 Tyramide™ signal amplification system

The Tyramide™ signal amplification system (TSA™; PerkinElmer, USA) was the principal fluorochrome system used in this study (Figure. 2-2). Tyramide induces signal amplification, permitting sub-cellular localisation of low abundance antigens. In addition, there are a large selection of fluorochromes that can be combined for multiple antigen detection. Following HRP-conjugated secondary antibody incubation, TSA™-fluorochrome was diluted 1:50 with its own diluent as per the manufacturer's instructions and incubated with tissue sections incubated for 10 minutes in the dark (all incubations and washes were conducted in the dark thereafter to prevent photo-bleaching of the fluorochromes), followed

by TBS washes (Figure. 2-2). Specific TSA™-fluorochromes used in this study can be found in the materials and methods sections of the corresponding results chapters.

2.4.2 Nuclear counterstain – immunofluorescence method

Tissue sections undergoing an immunofluorescent detection method were counterstained with the fluorescent dye, DAPI (4`, 6-diamidion-2-phenylindole; ThermoFisher Scientific, D1306). DAPI passes through the cell membrane and binds to A-T rich regions within DNA. It stains nuclei blue since its emission wavelength is 461 nm. DAPI was diluted 1:500 in TBS and tissue sections were incubated for 10 minutes at room temperature, followed by 3 TBS washes. Tissue sections were mounted with glass coverslips (VWR, various) using PermaFluor™ aqueous mounting medium (ThermoFisher Scientific, TA-030-FM) and allowed to dry protected from the light.

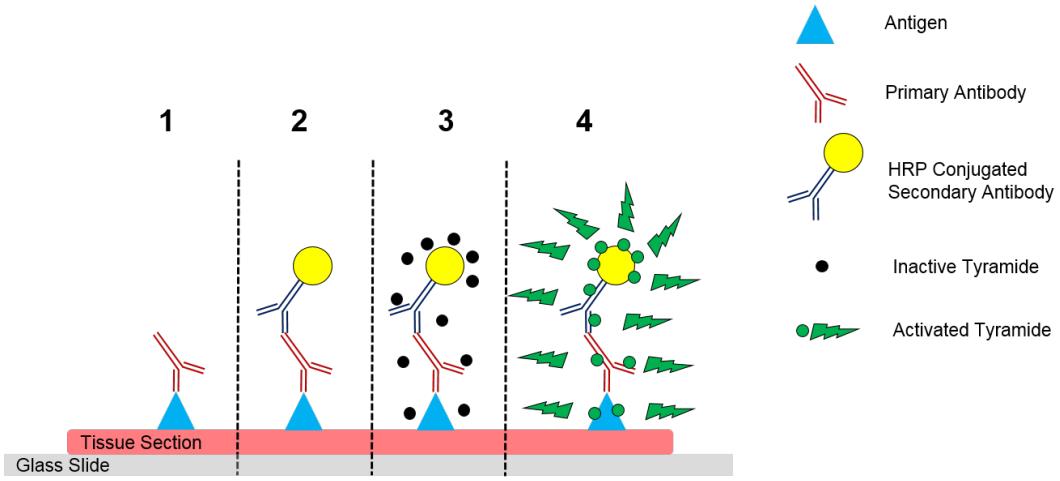

Figure 2-2: Schematic representation of immunofluorescence using TMA™ amplification system. 1) Primary antibody binding to antigen of interest within tissue section. **2)** Secondary antibody conjugated to HRP binding to primary antibody. **3)** Incubation with TMA™ reagent. **4)** TMA™ reagent activated by the enzyme HRP and converted into a short-lived, extremely reactive free radical intermediate. This free radical intermediate covalently binds to electron-rich regions of adjacent proteins (predominantly tyrosine residues). This binding occurs adjacently to the sites at which the HRP enzyme is bound. Fluorescence detected by excitation with the appropriate light wavelength.

2.4.3 Dual immunofluorescence

Detection of two antigens was performed using dual immunofluorescence. After incubation with the first TSA™ fluorochrome and TBS washes (see section 2.4.1), a second

round of HIER was performed using a microwave (see 2.3.3). This does not elute antibodies but prevents their reaction with subsequently applied regents (Tornehave *et al.*, 2000). It also inhibits reactions with endogenous immunoglobulins present in extracellular compartments (Tornehave *et al.*, 2000).

A second NAS buffer blocking step was then performed, again using serum from same animal species as the secondary antibody. A second primary antibody (for detection of the second antigen of interest) was then applied to the tissue sections and incubated overnight at 4 ^{o}C in a humidity chamber. The next day, after TBS washes, a HRP-conjugated secondary antibody was diluted 1:500 in NAS buffer and the tissue sections incubated for 30 minutes, followed by further TBS washes. A second TSA™ fluorochrome (different to the first; unless otherwise stated the green fluorochrome, fluorescein was normally added second since it is particular prone to photo-bleaching) was then applied (as per 2.5.1) and nuclear counterstaining and mounting performed (as per 2.5.3).

2.5 Fluorescent immunocytochemistry

Cells grown *in vitro* as part of this study underwent both single and dual fluorescent immunocytochemistry for detection of proteins/antigens of interest. For this method, phosphate buffered saline (PBS; VWR, E404) was used for all wash steps in place of TBS.

Primary human endometrial cells (see 2.2.1) and informative cell lines (see 2.2.2) were seeded into 4-well chamber slides (BD Falcon, 354104). Chamber slides were pre-treated with attachment factor (Gibco, S006100) prior to seeding with primary endometrial cells. Cells were counted (see 2.2.3.3) and 1 mL of cell suspension seeded into individual chambers at a density of 1 x 10^4 cells/mL. After appropriate incubation periods, cell medium was aspirated, and the chambers washed twice with PBS. Care was taken not to disturb cell monolayers throughout this method, i.e. chamber slides were tilted and a vacuum aspirator (Integra Biosciences, 158310) used to remove the liquid contents at each step.

Fixation was performed by adding 1 mL of ice-cold acetone (Acros Organic, 423240010) per chamber for 10 minutes at -20 ^{o}C, followed by PBS washes. Several fixation chemicals and methods were tested during optimisation, these included: methanol, acetone, 50:50 methanol/acetone, 4 % paraformaldehyde (PFA; Sigma-Aldrich, P6148) and 10% NBF. Acetone yielded the best imaging results. Acetone fixed cells do not require a permeabilisation step in order to permit antibody entry. Cell permeabilisation is required for intracellular

epitopes when the antibody requires access to the inside of the cell to detect a protein. It is also required for detection of transmembrane proteins if the epitope is in the cytoplasmic region.

A peroxidase block was performed (modified method from 2.3.4) with 0.15% H_2O_2 in PBS (1:200 dilution of 30 % H_2O_2) for 15 minutes, followed by PBS washes. NAS blocking was the performed (as per 2.4) for 30 minutes, followed by PBS washes. The primary antibody and secondary antibodies were applied (as per 2.4) with intermediate PBS washes. At this point the plastic inserts were removed from the chamber slides. A TSA™ fluorochrome was then applied (see 2.4.1) and nuclear counterstaining performed (see 2.4.2) prior to slide mounting with PermaFluor.

2.5.1 Dual fluorescent immunocytochemistry

Detection of two antigens in the same cell was performed using dual fluorescent immunocytochemistry using the same method as described in 2.4.3, modified to exclude the HIER step and to substitute TBS for PBS washes. The exception to this was where both primary antibodies were raised from the same animal species, i.e. both mouse. This would not ordinarily be a problem when performing dual immunofluorescence on tissue sections with the TMA™ system, since the second HIER step would prevent reaction of the first primary antibody complex with subsequently applied regents. However, HIER is not routinely performed for immunocytochemistry due to the damage and cell loss that it can cause. For this reason, an alternative fluorochrome detection method to the TSA™ system was employed for the second antibody/antigen complex detection for dual fluorescent immunocytochemistry.

After incubation with the first TSA™ fluorochrome and PBS washes (see section 2.4.1), a second NAS buffer blocking step was then performed, using serum from same animal species as the second, secondary antibody. This was again followed by PBS washes. A streptavidin (Vector, SP-2002) block was then performed for 15 minutes, followed by PBS washes and a 15-minute biotin block (Vector, SP-2002) and further PBS washes. A second primary antibody (for detection of the second antigen of interest) was then applied and incubated overnight at 4 ^{o}C in a humidity chamber. The next day, after PBS washes, a biotinylated secondary antibody was diluted 1:500 in NAS buffer and the tissue sections incubated for 30 minutes followed by further PBS washes. A streptavidin, Alexa Fluor™ 555 conjugate was then added, diluted 1:500 in PBS and incubated for 1 hour, followed by PBS washes. Counterstaining and mounted was then performed (see 2.4.2).

2.6 Image analysis

Tissue sections stained by immunohistochemistry and H&E were scanned using a NanoZoomer-XR (Hamamatsu, C12000-01) digital slide scanner in 40x mode. Digital images were stored electronically on a University of Edinburgh managed and backed-up server; NDP.view2 (Hamamatsu, U12388-01) imaging software was used to view the digital images. For quantitative image analysis, .ndpi (NanoZoomer Digital Pathology Image) files were imported and processed using StrataQuest analysis software (TissueGnostics GmbH, Vienna).

Tissue sections and fixed cells that were fluorescently stained were visualised using a Zeiss confocal laser scanning microscope 780, (Carl Zeiss Microscopy, Cambridge, UK) and analysed using Zen Black Edition 2.0 software (Carl Zeiss Microscopy).

2.7 RNA Extraction

Total RNA from endometrial cells (see 2.2.1 and 2.2.2) was extracted using the commercially available RNeasy Mini Kit (Qiagen, 74106) according to the manufacturer's instructions. This spin-column method enriches for mRNA by excluding sRNAs and rRNAs based upon their size. RNA extraction was performed in a dedicated region of the laboratory, with all surfaces and equipment cleaned with RNaseZAP (ThermoFisher Scientifc, AM9780) before commencing.

Endometrial cells were harvested using the method described in 2.2.3.1. Cell pellets were first lysed with a denaturing guanidine-thiocyanate containing buffer (RLT buffer) with 1 % (v/v) β-Mercaptoethanol (Sigma Aldrich, M6250) added. Individual cell lysates were then homogenised by centrifugation (12,000 g for 2 minutes, room temperature) using QIAshredder spin columns (Qiagen, 79654); an equal volume of 70 % ethanol was added to each sample to aid binding conditions. Each sample was subsequently transferred to a RNeasy mini spin column, where the total RNA was allowed to bind to the membrane and contaminants were washed away during progressive wash buffer steps. Finally, RNA was eluted in 30 μL RNase free H_2O. Genomic DNA contamination was removed using an intermediate DNase digestion step (Qiagen, 79654).

2.7.1 RNA quantification

RNA concentrations were measured using a Nanodrop® ND-1000 spectrophotometer (ThermoFisher Scientific). Spectrophotometric analysis is based on the principle that nucleic acids absorb ultraviolet light in a specific pattern. The ratio of the absorbance at 260 and 280 nm ($A_{260/280}$) was used to assess the purity of the RNA. A ratio of ~2.0 is generally accepted as "pure" for RNA. If the ratio is appreciably lower, it may indicate the presence of protein, phenol or other contaminants that absorb strongly at or near 280 nm. RNA samples were individually standardised to a concentration of 100 ng/µL using RNase free H_2O and stored at -80 ºC.

2.8 Two-step quantitative real-time reverse transcription polymerase chain reaction (qRT-PCR)

A two-step method was utilised to perform relative quantification of gene expression for this study. Complementary DNA (cDNA) molecules were first created from total RNA (extracted as per section 2.7) via a reverse transcription polymerase chain reaction (RT-PCR). A real-time quantitative polymerase chain reaction (qPCR) was then used to measure the amplification of targeted genes of interest (GOI) within the cDNA using fluorescent molecules (TaqMan® method). Target GOIs were normalised to an endogenous control 'house-keeping gene' and relative quantitation performed to analyse fold-change differences in the expression levels of individual GOIs between different samples.

2.8.1 Reverse transcription and synthesis of cDNA

A reverse transcription polymerase chain reaction (RT-PCR) using a template of total RNA to generate a pool of cDNA was performed using the SuperScript™ VILO™ cDNA synthesises kit (ThermoFisher Scientific 11754250), adapted from the manufacturer's instructions as follows. Each reaction contained a final concentration of 1x VILO™ reaction mix (random primers, dNTPs, and $MgCl_2$), 0.125x SuperScript™ enzyme (reverse transcriptase) and 100 ng/µL of RNA, made to a final volume of 20 µL with RNase free H_2O.

For each group of cDNA samples made, the following control samples were also added: 1) a no reverse transcriptase (RT) control with substitution of the SuperScript™ enzyme by using RNase free H_2O, 2) a positive control using 100 µg/µL Human Total RNA Control

(ThermoFisher Scientific, 4307281) and 3) a negative control substituting the RNA with 1 µL of RNase free H_2O. In addition, where qPCR primer validation was required a standard curve was created using 10-fold serial dilutions of pooled RNA from the cohort (1000ng, 100ng, 10ng, 1ng, 0.1ng) to adequately cover the 100 ng/µL starting concentration of RNA.

Samples were incubated in a thermal cycler (MJ Research PTC-200 Thermo Cycler, BC-MJPC200) under the following conditions: 25 ºC for 10 minutes (annealing), 42 ºC (extension) for 60 minutes, and 85 ºC for 5 minutes (termination and inactivation of RT).

2.8.2 Quantitative real-time PCR (TaqMan® method)

The TaqMan® method was used for qPCR in this study. The method utilises the ability of the thermostable DNA polymerase, *Taq* polymerase, to cleave fluorescently labelled probes from a template sequence of DNA. In brief, TaqMan® probes consist of a 'reporter' fluorophore covalently joined to the 5'-end of an oligonucleotide and a 'quencher' at the 3'-end. The quencher molecule, as the name suggests, quenches the fluorescent ability of the reporter, provided that the two remain in proximity to one another. This occurs via a process of fluorescence resonance energy transfer (FRET). TaqMan® probes are 8-9 nucleotides long and designed such that they will anneal within a DNA region amplified by a specific set of PCR primers. During the extension phase of the PCR cycle, *Taq* polymerase extends the primer templates (designed to bind to a specific GOI) along the nascent DNA strand to produce the complementary DNA strand (amplicon). On encountering a TaqMan® probe the 5' to 3' exonuclease activity of the *Taq* polymerase breaks down the probe, separating the reporter and quencher, with the resultant fluorescence detected by the qPCR machine. With each PCR cycle, more reporter molecules are released, resulting in an increase in fluorescence intensity which is proportional to the amount of DNA being synthesised (Figure 2-3).

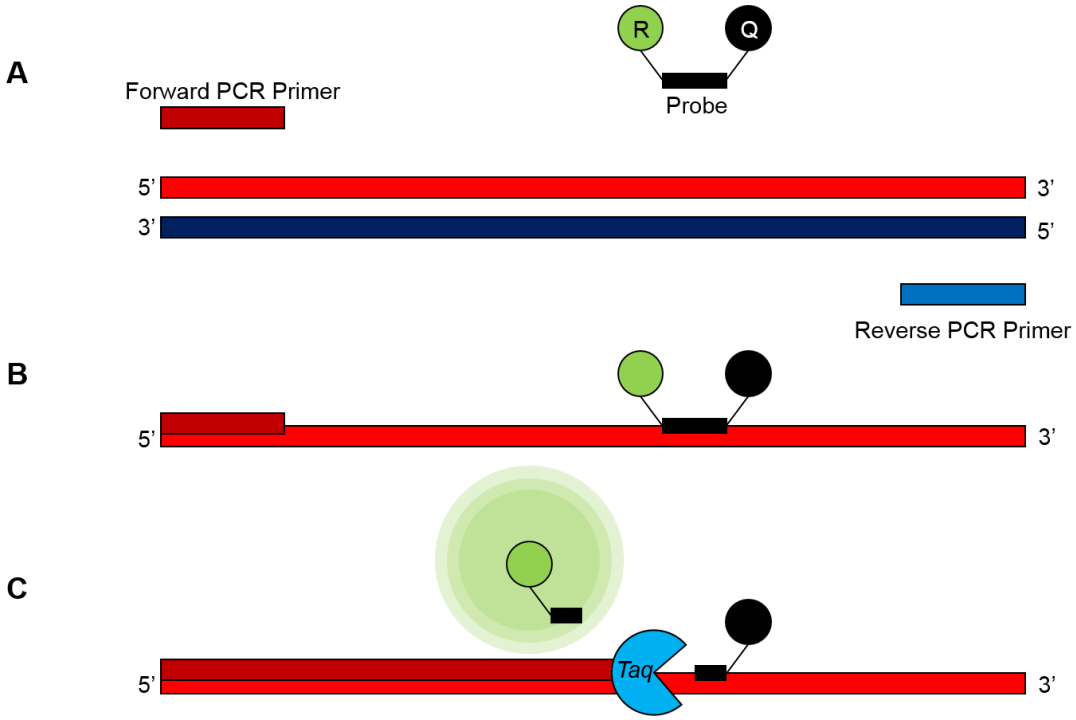

Figure 2-3 Schematic representation of TaqMan® qPCR. A) Denaturing of cDNA, B) Annealing of primers and probe to cDNA (only sense strand of cDNA shown), and C) The 5'-nuclease activity of *Taq* polymerase cleaves the probe during the amplicon extension step, which separates the detectable reporter fluorophore (R) from a quencher (Q). Adapted from Macmillan Publishers Ltd: Nature Reviews Drug Discovery. Koch W (Koch, 2004) copyright 2004.

2.8.3 TaqMan® qPCR reagents

TaqMan® probes used in this study utilised the Universal ProbeLibrary™ system (UPL™; Roche, West Sussex, UK) and were labelled at their 5' -end with a 6-carboxy-fluorescein (FAM) reporter and a dark quencher dye at their 3' -end. Primers were designed using the Roche online UPL assay design centre (Roche Molecular Systems, 2017) and primers purchased from Eurofins (Eurofins Genomics, Ebersberg, Germany). Lists of the primer/probe combinations used during this study can be found in the materials and methods sections of the corresponding results chapters. All primers were validated for efficiency of amplification prior to use. A TaqMan® master mix was created for qPCR experiments as per Table. 2-3 and mixed thoroughly with 1 µL of cDNA. 15 µL of samples were plated, in duplicate, into MicroAmp™ 96-well optical reaction plates (ThermoFisher Scientific, 403012). The plates were then sealed with clear adhesive film (ThermoFisher Scientific, 4306311) and briefly centrifuged at room temperature. qPCR was performed using an Applied Biosystems (ABI) 7900HT fast real-time qPCR machine (ABI, 4329001). The following programme was

used; 95 ºC for 10 minutes and 40x cycles of 95 ºC for 15 seconds, 60 ºC for 1 minute. Data were analysed and processed using Sequence Detector System version 2.4 (SDS; Applied Biosystems, California, USA).

Table 2-3: Constituent reagents for qPCR reaction mix

Reagent	Final Concentration	Volume / 15 µL reaction	Manufacturer
2x TaqMan™ Fast Advanced Reaction Mix	1x	7.5 µL	ThermoFisher Scientific, 4444963
Forward Primer 20µM	200nM	0.15 µL	EuroFins
Reverse Primer 20µM	200nM	0.15 µL	EuroFins
UPL™ Probe 10µM	100nM	0.15 µL	Roche Molecular Systems
20x Endogenous Control Gene, CYC (VIC® Conjugated)*	1x	0.75 µL	ThermoFisher Scientific, 4310883E
RNase-free H_2O		to 15 µL final	
cDNA		1.5 µL	

*Assay-On-Demand™; used in place of forward / reverse primers and probe

2.8.4 TaqMan® qPCR analysis

As described in 2.8.2, increasing levels of fluorescence are detectable with each PCR cycle as more and more reporter molecules are released. The fluorescence intensity at each PCR cycle can be graphically represented as an amplification plot using SDS analysis software (Figure. 2-4).

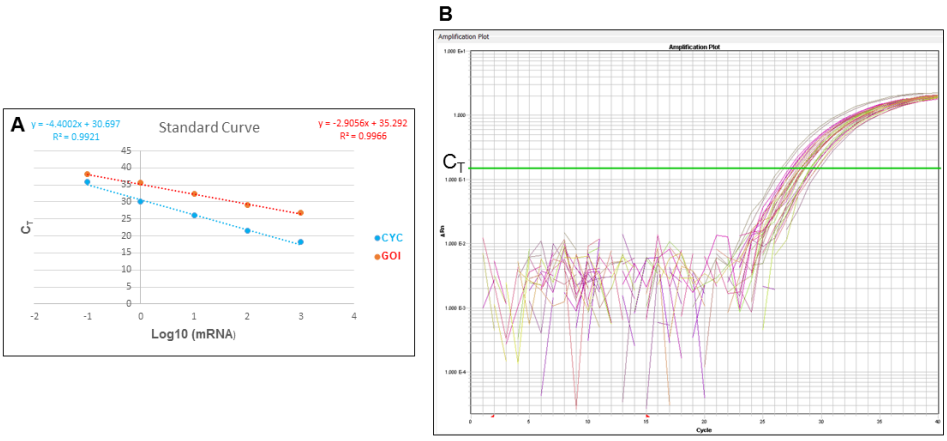

Figure 2-4: Real-Time PCR TaqMan® data. A) Standard curve for a gene of interest (GOI) and an endogenous control (CYC). The C_T value for each standard is plotted against the common logarithm of the mRNA concentrations. The equation of the linear trendline is used to analyse data by the relative standard curve method. **B)** An example of a typical qPCR amplification plot from a TaqMan® reaction, demonstrating the cycle threshold (C_T).

A threshold for the detection of fluorescence can be established as the point where the amount of fluorescent signal achieves statistical significance over the background / baseline fluorescent signal. The number of PCR cycles at which the fluorescence signal exceeds this threshold is called the cycle threshold (C_T) (Figure. 2-4). During the exponential phase of the PCR reaction, C_T values are directly proportional to the amount of targeted nucleic acid in the sample; assuming a 100 % reaction efficiency, an increase of 1-fold in C_T value corresponds to a 2-fold increase in cDNA concentration.

2.8.4.1 Determination of qPCR primer efficiency

As described above, qPCR analysis applies the premise of a 100 % reaction efficiency, whereby a doubling of PCR product occurs with each cycle during the exponential phase of the reaction. This however is not always the case. Suboptimal primer/probe design, reaction contaminants with PCR inhibitors and technical errors can all reduce the efficiency of the PCR. To establish primer efficiency, a standard curve was used to validate all primer/probe combinations used in this study (Figure. 2-4). The exception to this was when Assay-On-Demand™ (Applied Biosystems, California, USA) gene expression products were used. These are TaqMan® gene expression assays that have already been externally validated by the manufacturer for optimal reaction efficiency.

To establish primer efficiency a cDNA standard curve was created using 10-fold serial dilutions of RNA (as per 2.8.1). The common logarithm of the RNA concentrations was plotted against the C_T values using Excel® (Microsoft®, Redmond, WA, USA) and a linear regression trendline calculated using the least squares method (Figure. 2-4A). The slope of the trendline was then used in the following formula in order to calculate the percentage primer efficiency:

*% Efficiency (E) = (10^(-1/slope)-1)*100.*

Where primer efficiency was between 95-105 % the $2^{-\Delta\Delta CT}$ method was used for TaqMan® qPCR analysis, otherwise the relative standard curve method was used.

2.8.4.2 $2^{-\Delta\Delta CT}$ method for analysis of TaqMan® data

Utilising a standard curve as per 2.8.4.1 the efficiency of the target GOI amplification and the efficiency of the endogenous control gene amplification were first calculated. Where these were both between 95-105 % the $2^{-\Delta\Delta CT}$ method was used for relative quantification analysis as follows: ΔC_T was first calculated, whereby the C_T value of the endogenous control sample (CYC in this study) was subtracted from the C_T value of the target GOI sample, i.e. ΔC_T = target GOI C_T – CYC C_T. This normalises the target GOI to the endogenous control. ΔC_T was then expressed as a relative change to a reference sample (i.e. a no treatment or vehicle control sample) to give $\Delta\Delta C_T$, i.e. $\Delta\Delta C_T$ = ΔC_T sample - ΔC_T reference sample. Relative fold-change in gene expression was then calculated from this value using the formula $2^{-\Delta\Delta CT}$.

2.8.4.3 Relative standard curve method for analysis of TaqMan® data

The relative standard curve method for analysis of qPCR data first quantitates gene expression for each unknown experimental sample from a set of known standards. This quantity is then expressed relative to that of a reference sample (i.e. a no treatment or vehicle control samples). This method negates the need for extensive validation and optimisation of the qPCR reaction. However, it is more time consuming, uses more reagents and requires accurate serial dilutions of the template RNA to produce the standards.

Standard curves were prepared for both the target GOI and the endogenous control (CYC) as per 2.8.4.1 (Figure. 2-4A). For each experimental sample, the amount of target GOI and endogenous control was determined utilising the equation of the trendline from their corresponding standard curve. These values were then raised to the power 10, since the standard curves plot the common logarithm of the RNA concentrations. The target GOI values were then divided by the endogenous control values for each experimental sample to normalise. Each of the normalised target GOI values were then divided by the reference sample normalised target value to generate the relative gene expression levels.

2.9 Western Blotting

Western blotting is a long-established laboratory technique used to detect and quantify proteins of interest within a tissue lysate. In common with immunohistochemistry, the process is dependent on the interaction between an antibody and the antigen to which it was raised, to visualise proteins of interest. However, unlike immunohistochemistry proteins are not visualised *in-situ*, but they are extracted from the tissue and separated by size using electrophoresis, before being transferred to a membrane (in this study polyvinylidene difluoride, PVDF) where they can be detected and also quantified.

2.9.1 Whole protein extraction from human endometrial cell lines

Human endometrial cell lines (detailed in 2.2.2) were utilised for experiments in this study. Following experimental procedures (see relevant results chapters for further details), cell lines were harvested and pelleted (modified as per 2.2.3.1). After DPBS washes of the plastic tissue culture flasks, cells were detached from the plasticware by incubating with 5 mL of 0.05% phenol-red Trypsin-EDTA (Gibco, 25300054) for 20 seconds at room temperature.

Trypsin was aspirated, discarded and the flask incubated at 37 ºC for 5 minutes. 10 mL of ice-cold DPBS was used to wash the flask and in doing so, detach the cells. The resultant cell suspension was pelleted by centrifugation (115 g, 5 minutes, room temperature) and the supernatant discarded. 500 uL of ice-cold protein lysis buffer (Table. 2-4) was added to the cell pellet and pipetted up-and-down to mix, followed by a 20 second vortex. Samples were kept on ice from this point forward. After vortexing, the samples were placed on a rocker at 4 ºC for 10 minutes prior to transfer to 1.5 mL Eppendorf® microcentrifuge tubes (Sigma-Aldrich, T9661). The lysate was centrifuged (10 minutes, 13,000 g, 4 ºC) to pellet cellular debris and the supernatant was aliquoted into fresh microcentrifuge tubes, before immediately storing at -80 ºC. Whole protein lysates underwent a maximum of x3 freeze/thaw steps before being discarded.

Table 2-4: Composition of protein lysis buffer

Reagent	Final Concentration	Manufacturer
1 M Tris base pH 7.5	50 mM	Sigma-Aldrich, 252859
0.5 M EDTA pH 8.5	5 mM	Sigma -Aldrich, E5134
1 M NaCl	150 mM	Sigma-Aldrich, S3014
Triton-X	1 %	Sigma-Aldrich, T8787
Aprotinin	2 μg/mL	Sigma-Aldrich, A3428
100x Halt™ Protease Inhibitor Cocktail	1x	ThermoFisher Scientific, 78430

2.9.2 Measurement of whole protein lysate concentration

The commercially available Bio-Rad DC Protein Assay (Bio-Rad Laboratories, 5000111) was used to measure whole protein lysate concentration (extracted as per 2.9.1). This assay utilises a colorimetric technique for measuring protein concentration following detergent solubilisation. The assay is based on the reaction of protein with an alkaline copper tartrate solution and Folin reagent, leading to colour development which can be measured on a spectrophotometer.

In brief, a BSA standard curve of known protein concentrations (1.5, 1.0, 0.75, 0.5, 0.25, 0.125 and 0.0625 mg/mL respectively) made up in protein lysis buffer (Table. 2-4) was first created. 5 uL of each of the standard curve samples and protein lysates were added in duplicate to a clear, flat-bottomed 96-well plate (Sigma-Aldrich, CLS3628). Assay buffers were added as per the manufacturer's instructions and the plate incubated in the dark for 15 minutes. Blank wells (buffer only) were also included to control for any background signal. The plate was read on a spectrophotometer (Multiscan EX, Labsystems) at both 620 nm and 540 nm. The 540 nm reading was subtracted from the 620 nm reading to give the optical density (OD). A standard curve graph was created plotting the OD reading against the known BSA standard concentrations. The equation of the line was then used to calculate the protein concentration of the experimental lysates in mg/mL.

2.9.3 Denaturing gel electrophoresis

As part of the Western blotting procedure, protein lysate samples were first resolved by gel electrophoresis. Following protein extraction (as per 2.9.1), lysates were thawed on ice and protein concentration measured (as per 2.9.2). 40-60 ng of protein lysate was used from each sample and added to an electrophoresis sample mix (Table. 2-5). The mix contained lithium dodecyl sulphate (LDS), pH 8.4, which together with the reducing agent, breaks disulphide bonds between protein molecules and maintains them in a denatured state during the electrophoresis. Sample mixes were heated to 70 ^{o}C for 10 minutes and kept on ice prior to loading into a precast electrophoresis gel (10 well comb, 1.5mm thick, maximum load volume 37 μL). Positive control protein lysates were included as necessary.

Table 2-5: Protein electrophoresis sample mix preparation

Regents and samples	Amount per sample	Manufacturer
4x NuPage™ LDS Sample Buffer	1x (8.5 μL)	ThermoFisher Scientific, NP0007
10x NuPage™ Reducing Agent	1x (3.4 μL)	ThermoFisher Scientific, NP0004
Protein Lysate	40-60 ng (variable volume)	
Deionised H_2O	Made up to 34 μL total volume	

2.9.3.1 4-12 % Bis-Tris gel electrophoresis

For detection of proteins with an expected size of between 15-260 kDa, NuPAGE™ 4-12 % Bis-Tris Protein Gels (ThermoFisher Scientific, NP0322) were used. These precast gels cassettes were first washed with deionised H_2O and their combs removed. The gel cassettes were washed three times with 1x running buffer (50 mLs 20x NuPAGE™ MOPS SDS Running Buffer (ThermoFisher Scientific, NP000102) made up as 1x with 950 mL deionised H_2O). Cassettes were loaded into an XCell *SureLock*™ Mini-Cell (ThermoFisher, EI0001) and 1x running buffer added, ensuring an adequate seal between upper and lower chambers. 34 µL of each protein sample was added per gel well, in addition to a well containing 10 µL of Chameleon® Duo Pre-stained Protein Ladder (Li-Cor Biosciences, 928-60000). 500 µL of Novex™ NuPAGE™ Antioxidant (FisherScientific, 15744412) was added to the running buffer in the upper chamber prior to commencing electrophoresis to help maintain the samples in a reduced state during electrophoresis. The gel was run at 200 V constant for approximately 50 minutes.

2.9.3.2 3-8 % Tris-Acetate gel electrophoresis

For detection of proteins with an expected size of between 40-500 kDa, NuPAGE™ 3-8 % Tris-Acetate Protein Gels (ThermoFisher Scientific, NP0378) were used. The same protocol as per 2.9.3.1 was used, with the following modifications: 1) 1x running buffer (50 mLs NuPAGE™ Tris-Acetate SDS Running Buffer (ThermoFisher Scientific, LA0041) made up as 1x with 950 mL deionised H_2O) was used and 2) the gel was run at 150 V constant for 60 minutes.

2.9.4 Gel transfer to Immobilon® membrane

For proteins to be accessible to antibody detection they need to be transferred to a porous membrane. An electric current is used to 'pull' proteins from the gel into the membrane whilst maintaining the same layout that they had within the gel. After electrophoresis was completed, gel cassettes were removed from the XCell *SureLock*™ Mini-Cell and the stacking gels removed, cut as needed and equilibrated in 1x transfer buffer (Table. 2-6) for 15 minutes to remove salts and detergents. For most proteins separated on Bis-Tris gels, transfer used a semi-dry method, whereas larger proteins of interest were transferred from Tris-Acetate gels using an overnight wet transfer method.

2.9.4.1 Semi-dry electrophoretic transfer

An Immobilon®-FL PVDF (Millipore, IPFL00010) membrane was first cut to size (slightly larger than the gel being transferred) and pre-soaked in methanol for 15 seconds. The membrane was equilibrated in 1x transfer buffer (Table. 2-6) for 5 minutes, along with 6 sheets of Whatman™ 3 mm Chr chromatography paper (FisherScientific, 10211031) cut to a corresponding size. A Trans-Blot SD semi-dry electrophoretic transfer cell (Bio-Rad, 1703940) was then loaded, stacked as follows on to the anode plate: 1) three sheets of pre-soaked Whatman™ 3 mm Chr chromatography paper, 2) equilibrated PVDF membrane, 3) equilibrated electrophoresis gel, 4) three sheets of pre-soaked Whatman™ 3 mm Chr chromatography paper. A Corning® Costar® Stripette® serological pipette (Sigma-Aldrich, CLS4488) was used to 'roll' the final stack to remove any trapped air bubbles. The cathode plate and safety cover were then placed on top to 'sandwich' the stack. Semi-dry transfer was performed for 90 minutes, 14 V constant.

Table 2-6: Composition of Western blot transfer buffers

Reagent	Quantity	Concentration	Manufacturer
Tris base	30.28 g	250 mM	Sigma-Aldrich, 252859
Glycine	144 g	1.92 M	Sigma-Aldrich, G8898
Sodium dodecyl sulphate (SDS)	1 g	0.1 %	Sigma-Aldrich, L3771
Ultrapure deionised H_2O	To a make final volume of 1 L	10x	

Final transfer buffered used at a 1x concentration

Semi-dry Transfer: 100 mL 10x transfer buffer, 200 mL methanol (20 %), 700 mL ultrapure deionised H_2O

Wet transfer: 100 mL 10x transfer buffer, 100 mL methanol (10 %), 800 mL ultrapure deionised H_2O, 1 mL Novex™ NuPage™ Antioxidant

2.9.4.2 Wet electrophoretic transfer

For transfer of large molecular weight proteins from the Tris-Acetate gels an overnight wet transfer was favoured. Membrane, chromatography paper and Tris-Acetate gels were prepared and equilibrated as described in 2.9.4.1. 1x transfer buffer as per Table. 2-6 was used. Note, for transfer of larger proteins, methanol concentration was reduced, and antioxidant added (both following extensive optimisation), to enhance transfer success.

A Hoefer® Mighty Small Transfer Tank (Hoefer®, TE22) was used for the transfer. Cartridges were stacked as follows, grey side to the bottom: 1) sponge, 2) three sheets of pre-soaked Whatman™ 3 mm Chr chromatography paper, 3) equilibrated PVDF membrane, 4) equilibrated electrophoresis gel, 5) three sheets of pre-soaked Whatman™ 3 mm Chr chromatography paper, 5) sponge. A serological pipette was used to 'roll' the final sponge stack to remove any trapped air bubbles, before locking the transfer cartridge closed. The transfer cartridge was placed centrally within the transfer tank, black side of cartridge facing the cathode and grey side to the anode. 1x transfer buffer was added to the tank as per manufacturer recommendations, completely submerging the transfer cartridge. Wet transfer was performed for 16 hours (overnight) in a cold-room (4 ^{o}C) at 10 V constant.

2.9.5 Blocking and antibody incubation

Following transfer, PVDF membranes were placed in either PBS or TBS for 5 minutes (dependent on the protein of interest; PBS was used routinely unless phosphorylated proteins were being detected, in which case TBS was used). A blocking step was then performed to prevent non-specific antibody binding and reduce background signal. 5 mL of PBS or TBS (see previous comment) Odyssey® Blocking Buffer (Li-Cor Biosciences, 927-50000 / 927-40000) was used to cover the PVDF membrane and incubated for 1 hour at room temperature on a rocker.

Primary antibodies were diluted to optimised concentrations in 5 mL of blocking buffer with the addition of 0.1 % Tween®-20 (Sigma-Aldrich, P6416). The antibody directed against the protein of interest was multiplexed with an antibody directed against an endogenous 'loading' protein (the antibodies used were always raised in two different species, i.e. a mouse antibody to the protein of interest with a rabbit antibody directed against the loading protein). Lists of the antibodies used during this study can be found in the materials and methods

sections of the corresponding results chapters. Primary antibodies were incubated with the PVDF membrane for 16 hours (overnight) at 4 ºC on a rocker.

The following day, PVDF membranes underwent 4 washes with PBST or TBST (PBS or TBS with 0.1 % Tween®-20 added) for 5 minutes each. An IRDye® 640RD secondary antibody and an IRDye® 800CW secondary antibody (Li-Cor, Biosciences) were multiplexed in 5 mL of blocking buffer with 0.1 % Tween®-20 and incubated with the membrane for 1 hour on a rocker at room temperature. PVDF membranes were kept in the dark from this point. The secondary antibodies corresponded to the animal species of the primary antibodies and were all raised in donkey, i.e. a mouse primary antibody would be used with an IRDye® 680RD donkey anti-mouse IgG (H + L) secondary. Secondary antibodies to detect proteins of interest were all IRDye® 680RD, detected with a 700 nm channel. Whereas IRDye® 800CW secondaries were exclusively used for loading controls, detected with an 800 nm channel. Four further PBST or TBST washes were then performed followed by a final rinse in PBS or TBS.

2.9.6 Detection and analysis

Two-colour multiplex detection using near-infrared fluorescence was performed. PVDF membranes were scanned using an Odyssey® FC imaging system (Li-Cor Biosciences, 2800-03) using the 700 nm and 800 nm channels for 4 minutes each. Detectable protein bands were pseudo-colour labelled, red for the protein of interest and green for the loading control. Image Studio™ (Li-Cor Biosciences) software was used to view Western blots and perform densitometry for protein quantification. Each sample band was normalised to its own loading control and expressed as a fold-change over a reference/control sample.

2.10 Statistical Analysis

Statistical analysis was performed using GraphPad Prism version 8.0 (GraphPad Software, CA, USA) unless otherwise stated. Details of specific statistical tests can be found in the respective results chapters. For human samples, ‘n’ represents the number of individual patients. For *in vitro* cell experiments, ‘n’ denotes the number of times the experiment was repeated, with the number of technical replicates per experiment indicated in the figure legend. All graphs display mean ± standard error of the mean, unless otherwise stated in figure legends, $p < 0.05$ was considered statistically significant.

Chapter 3

3 Exploring the utility of pathological classification in the diagnosis of endometrial hyperplasia

3.1 Introduction

The endometrium is a complex, well organised, multicellular tissue that forms the inner lining layer of the uterus. As reviewed in chapter 1, the endometrium is comprised of luminal and glandular epithelia with a multicellular stromal compartment, it physiologically responds to changes in the steroid hormone environment, notably fluctuating concentrations of ovarian oestrogen and progesterone. Aberrant steroid hormone exposure and coexisting pathology can have profound effects on both the structure and function of the endometrium, leading to menstrual abnormalities and in some cases neoplasia.

Endometrial hyperplasia (EH) is an 'umbrella' term that incorporates a heterogeneous spectrum of abnormal endometrial lesions. EH is characterised by irregular proliferation of the glandular epithelial compartment, whereby the endometrial gland-to-stroma ratio becomes markedly increased when compared to endometrium from the normal proliferative phase of the menstrual cycle (Ellenson *et al.*, 2011; Kurman *et al.*, 1985). Hyperplastic endometrial glands can vary both in size and shape, with cytological atypia also seen in some cases. The clinical significance of a diagnosis of EH relates to an associated risk of progression to endometrioid endometrial cancer (EC). The presence of cytological atypia is generally accepted as the principal histological characteristic when assessing EH lesions for their malignant potential (Ellenson *et al.*, 2011). Risk factors for the development of EH are similar to those associated with EC (as discussed in chapter 1), with the majority of EHs developing within a background of chronic endometrial stimulation by oestrogens unopposed by progesterone (reviewed in Sanderson *et al.*, 2017).

Clinically, most women with EH will present with abnormal uterine bleeding (AUB). Two high-risk patient populations prone to the development of EH are (i) obese peri/postmenopausal women, due to peripheral aromatisation of androgens to oestrogens in adipose tissue, coupled with erratic anovulatory menstrual cycles, and (ii) premenopausal patients with polycystic ovarian syndrome (PCOS), due to hyperandrogenic anovulation.

Not all EHs will progress to malignancy; EHs occurring entirely due to unopposed oestrogen exposure, i.e. an 'endocrine effect' (as discussed in chapter 1), are capable of

regression back to normal endometrium through the withdrawal of the oestrogen source or through exogenous progesterone administration. Some patients with EH may be entirely asymptomatic and EH may even regress without being clinically detected. Argenta *et al*, investigated the prevalence of occult uterine pathology in asymptomatic, morbidly obese women before and after bariatric surgery-induced weight loss (Argenta *et al.*, 2013). In this cohort they demonstrated a baseline EH prevalence of 6.8 % (n=4/59) in pre-surgery obese (mean BMI 46.8 kg/m^2) women (Argenta *et al.*, 2013). Interestingly, the EH of all 4 women regressed following surgery-induced weight loss, albeit n=2 patients were potentially aided by the use of hormonal contraception. This raised the notion that weight loss may potentially reverse EH (Argenta *et al.*, 2013).

The difficulty for both gynaecologist and pathologist alike is in achieving reproducible stratification of women with EH attributable to purely endocrine factors (i.e. chronic unopposed oestrogen exposure), from those women with EH that also harbours significant malignant potential. Multiple pathological classification systems, stretching back to 1963, have attempted to do just this (reviewed in Chandra *et al.*, 2016). As discussed in chapter 1, the two prominent EH classification systems in current widespread use are: (i) The World Health Organisation (WHO) 1994 system and (ii) The endometrial intraepithelial neoplasia (EIN) system, which was recently endorsed in 2014 by the WHO (Zaino *et al.*, 2014).

Despite extensive use and popularity within modern gynaecological practice, the WHO94 system is widely reported to suffer from poor pathological reproducibility, in part due to the vast heterogeneity demonstrated by EH lesions (Bergeron *et al.*, 1999; Skov *et al.*, 1997). In contrast, the premise of the EIN system is based around the molecular assessment of the clonality of EH lesions, whereby premalignant EH lesions and their subsequent ECs have been demonstrated to have a shared lineage (Jovanovic *et al.*, 1996; Mutter *et al.*, 1996). The EIN classification system is based upon objective diagnostic criteria (Table. 3-1 reproduced from chapter 1) that can be determined from a H&E stained tissue section (Mutter, 2000) and is supported by evidence derived from computerised morphometric analysis (Baak, Mutter, *et al.*, 2005; Dunton *et al.*, 1996). EIN classification categories do not correspond directly to specific categories in the WHO94 system (Mutter, 2000) although, there is an element of recognisable overlap.

In 2014 the WHO published the 4th edition of Classification of Tumours of Female Reproductive Organs in which they endorse the EIN system (Zaino *et al.*, 2014) and revised the classification of EH. The EIN/WHO2014 system splits EHs into two groups based upon the presence or absence of cytological atypia, i.e. (i) hyperplasia without atypia (HwA) and

(ii) atypical hyperplasia/EIN. The complexity of the gland architecture is removed from this classification system. A diagnosis of EIN in this revised WHO classification is considered interchangeable with a diagnosis of atypical hyperplasia (Zaino *et al.*, 2014). This 'half-way house' approach to nomenclature integrates the two-tier subjective EIN system and its molecular foundations, with evidence that cytological atypia (rather than gland architecture) appears to be the main characteristic of EH that determines the risk of progression to malignancy (Lacey, Ioffe, *et al.*, 2008). The two-tier EIN/WHO2014 classification recognises that EHs fall into very different functional categories: i) polyclonal lesions diffusely responding to an abnormal hormonal milieu (i.e. HwA) and ii) intrinsically proliferative monoclonal lesions that arise focally and confer an elevated risk for endometrioid EC (i.e. EIN/atypical hyperplasia). The subjective EIN diagnostic criteria (Table. 3-1) permits the histological segregation of these two entities.

Table 3-1: Haematoxylin and eosin section diagnostic criteria for Endometrial Intraepithelial Neoplasia (EIN)

EIN Criterion	Comments
Architecture	Area of glands exceeds that of stroma (VPS <55 %).
Cytology	Cytology differs between architecturally crowded focus and background.
Diameter >1 mm	Maximum linear dimension of the lesion exceeds 1 mm.
Exclude mimics	Benign conditions with overlapping criteria: basalis, secretory, polyps, repair, etc.
Exclude Cancer	Carcinoma if maze-like meandering glands, solid areas, or appreciable cribriforming.

NB: All criteria must be met in order for a diagnosis of EIN to be made.
VPS = volume percentage stroma.
Reproduced with permission from Baak and Mutter, 2005.

Documented progression rates to endometrioid EC differ dependent on the EH classification system used. A 1985 study by Kurman *et al.* (Kurman *et al.*, 1985) performed a retrospective analysis of 170 'untreated' EH patients diagnosed on uterine curettage. These EH cases were classified using the same 4-tier system that would go on to become the WHO94 classification. The mean follow-up period for the women was 13.4 years, during which time a

hysterectomy was not performed <1 year following the index diagnosis. Of the 170 women in the study, 13 progressed to EC during the follow-up period (Kurman *et al.*, 1985). The authors published EC progression rates of 1 % (simple hyperplasia, SH, without atypia), 3 % (complex hyperplasia, CH, without atypia), 8 % (simple atypical hyperplasia, SAH) and 29 % (complex atypical hyperplasia, CAH), respectively, for the four categories (Kurman *et al.*, 1985). Lacey *et al*. conducted a nested case–control study in 2007. The authors analysed 138 cases of EH (and 241 matched controls) who progressed to EC at least 1 year following an index EH diagnosis. They demonstrated a 40 % probability of developing EC following a diagnosis of atypical hyperplasia (incorporating both simple and complex architectural variants), compared to only a 10 % probability when atypia was not present (Lacey, Ioffe, *et al.*, 2008).

Outcome data for a diagnosis of EIN suggests that approximately 40 % of women will have an EC diagnosed within 12 months of index biopsy (Baak and Mutter, 2005; Mutter, 2008). The mostly likely explanation for this is the presence of a concurrent EC that was not sampled on initial biopsy. Those women who do not develop EC within 12 months are 45-times more likely to develop a future EC (Baak and Mutter, 2005). Baak *et al.* also argued that the EIN classification system more accurately predicts progression to EC than the WHO94 system (Baak, Mutter, *et al.*, 2005). Although, a subsequent study reported that both EIN and atypical hyperplasia have similar risks of progression to EC when followed-up for 12 months after the index diagnosis (Lacey, Mutter, *et al.*, 2008).

The EIN system has been suggested to improve upon interobserver reproducibility and reduce the subjective bias inherent within the WHO94 classification system (Baak and Mutter, 2005; Semere *et al.*, 2011). However, the EIN system is not without its own set of challenges. A crucial feature of the EIN diagnostic criteria (Table. 3-1) is the ability to define cytological atypia in an architecturally crowded area of tissue and differentiate that from normal endometrial glands present within the same tissue section/sample. This is not always easy to achieve, especially in the context of fragmented endometrial biopsies, which are increasingly more common with the use of outpatient vacuum aspiration biopsies, e.g. the Pipelle® system. In addition, the light microscopic assessment of gland-to-stroma ratio to ascertain a volume percentage stroma (VPS) of <55 % still remains a subjective measure and its diagnostic reproducibility has not been comprehensively assessed (Ellenson *et al.*, 2011).

In summary, rates of EC are rising (Cancer Research UK, 2018) and establishment of robust methods for diagnosis and prognostication of EH have received renewed interest because of the association of some, but not all, of these endometrial lesions with progression to EC. The studies described in this chapter utilise retrospectively collected endometrial tissue

samples from 125 women who received a WHO94 diagnosis of EH between the years 2004 and 2009; all samples were reclassified according to the EIN/WHO2014 criteria and the diagnoses of two expert gynaecological pathologists investigated. We hypothesised that pathological reclassification of these tissue samples using the EIN/WHO2014 system would i) increase the diagnostic reproducibility of premalignant EH lesions and ii) confer a greater prediction of EC progression.

For the purposes of this study, when referring to the premalignant EH lesion diagnosed under the EIN/WHO2014 classification, the lesion will be referred to as EIN and it should be assumed that where a diagnosis of EIN has been made, the five diagnostic criteria (Table. 3-1) have all been met.

3.2 Aims of the chapter

1. To establish and retrospectively phenotype a human endometrial hyperplasia tissue resource.
2. To assess interobserver variability between the two most widely used endometrial hyperplasia pathological classification systems, WHO94 and EIN/WHO2014, using this tissue resource.
3. To explore the role of semi-automated computerised image analysis to objectively quantify endometrial tissue compartments as a diagnostic adjunct to pathological classification.
4. To evaluate the WHO94 and EIN/WHO2014 pathological classification systems with respect to subsequent endometrioid endometrial cancer progression using this tissue resource.

3.3 Materials and methods

3.3.1 Human endometrial hyperplasia tissue resource

A human EH tissue resource was established as summarised in the workflow diagram (Figure. 3-1). In brief, following a search of the NHS Lothian pathology 'Apex' clinical database, n=143 patient cases clinically coded with a diagnosis of EH were identified between January 2004 and December 2009. After exclusions and accounting for the availability of archival tissue, n=125 EH patients were finally identified (Figure. 3-1). Following an application to The Lothian NRS Human Annotated Bioresource (as described in 2.1.2), anonymised, serial sections of formalin-fixed, paraffin embedded (FFPE) tissue from these patients (n=125) was obtained along with matched medical history information (where available). In addition, the original diagnostic H&E stained section for each of these patients was also obtained.

3.3.2 Haematoxylin and eosin staining

In some cases, the original index H&E sample from the histopathology diagnostic archive was too badly degraded or bleached to assess the tissue morphology. For this reason, a freshly stained H&E sample was made available for pathological review. Human EH FFPE tissue, obtained as described in 3.3.1 underwent haematoxylin and eosin (H&E) staining as described in 2.3.9.

3.3.3 Histopathological assessment, reclassification and imaging

All human EH tissues used and described in this study underwent a dual, blinded review by two expert gynaecological pathologists, Professors Alistair Williams (Professor of Gynaecological Pathology, The University of Edinburgh 'AW') and Simon Herrington (Professor of Molecular Cancer Pathology, The University of Edinburgh 'SH'). The original diagnostic H&E stained tissue sections were reviewed by each pathologist (Professor Williams was accompanied by myself 'PS' for educational purposes) using standard light microscopy techniques.

Each pathologist was instructed to review each sample as they would a routine endometrial biopsy. No corresponding clinical information was provided at the time of the review to blind the pathologist and attempt to reduce bias. Where the original diagnostic slide

was unavailable or too badly degraded for complete assessment, a freshly stained H&E tissue section was provided, as described in section 3.3.2.

Diagnostic coding is a method of translating a written diagnosis into an alphanumeric value in order to group and identify disease types. The most commonly used coding system for classifying diseases is the International Statistical Classification of Diseases and Related Health Problems version 10 (ICD-10). Each expert pathologist was asked to independently assess every H&E stained tissue sample, originally ICD-10 coded by NHS Lothian pathologists as EH (n=125), utilising a standardised diagnostic proforma (Appendix 3). Each expert pathologist was instructed to diagnose all samples according to both the WHO94 and EIN/WHO2014 classification systems.

After data collation, where there was a diagnostic discrepancy between the two expert pathologists (AW and SH) using the EIN/WHO2014 system, both were asked to re-review the discrepant samples using a dual-headed microscope (if needed) in order to reach a final consensus diagnosis. A third independent pathologist was available to settle any unresolvable discrepancies. For the purposes of the consensus review, only those discrepancies that would hypothetically result in a change to clinical management (n=32) were subject to re-review, e.g. where one pathologist diagnosed a case as HwA and the other pathologist diagnosed the same case as EIN.

The threshold for making a benign diagnosis and 'drawing a line' between it and a diagnosis of an unopposed oestrogen effect is notoriously subjective and as such double-reporting and consensus diagnostic meetings are becoming more commonplace. A diagnosis of disordered proliferative endometrium (DPE) *versus* HwA often involves interpretation of varying degrees of difference along a subtle spectrum caused by prolonged oestrogen exposure (discussed in chapter 1). In addition, the Pipelle® endometrial sampler produces smaller and often fragmented tissue biopsy samples when compared to curettage samples, reducing the overall sense of tissue volume. Thus, where there were discrepancies between DPE and HwA, the cases were not subjected to consensus review and were instead upgraded into the HwA category. Furthermore, discrepancies between two benign diagnoses were upgraded to the more 'abnormal' of the two in order to form the final diagnosis, e.g. a discrepancy between proliferative endometrium and DPE was considered as DPE.

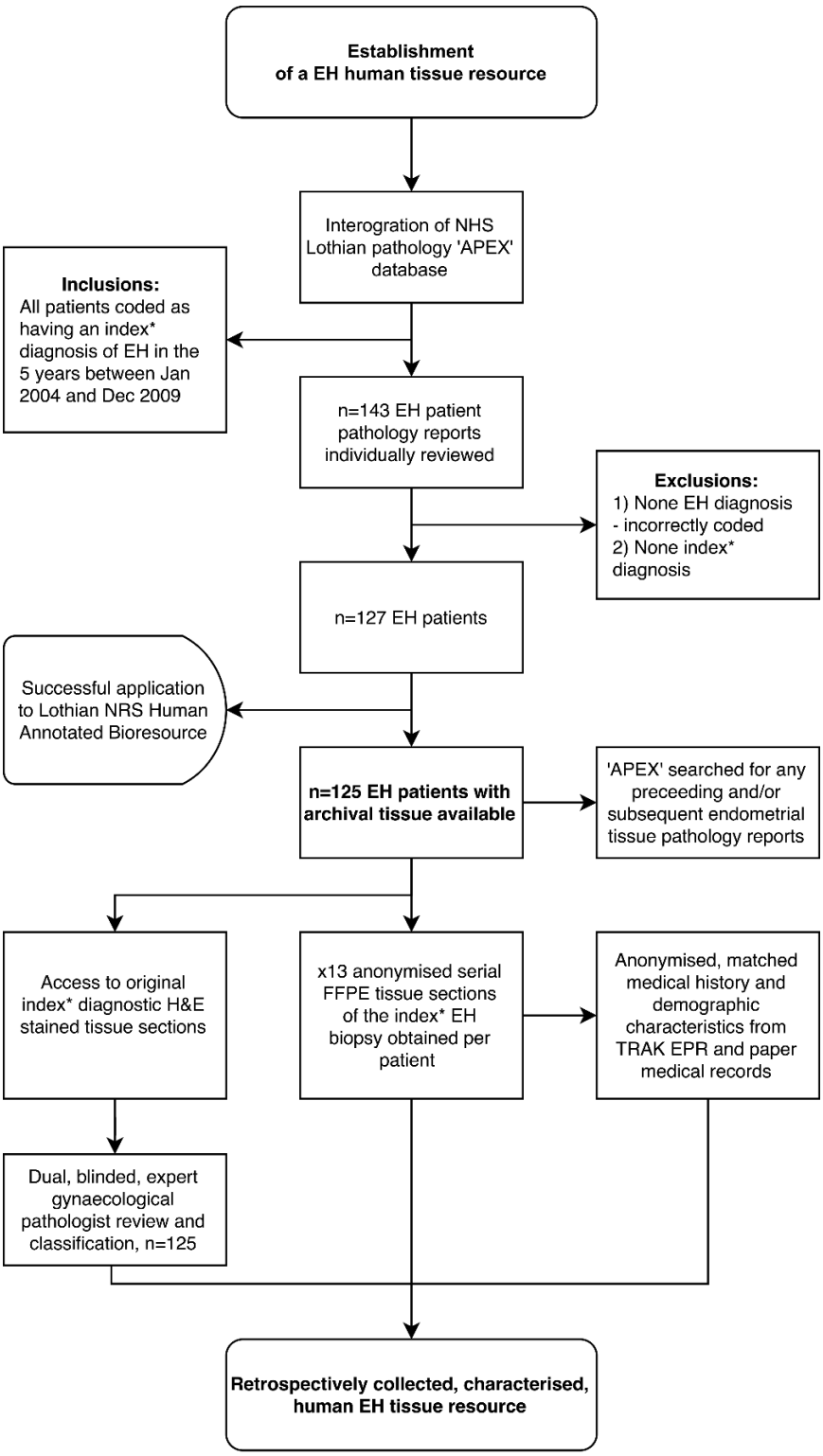

Figure 3-1: Workflow-diagram to summarise the establishment of a human endometrial hyperplasia (EH) tissue resource. *Index refers to the first documented EH biopsy, i.e. not a repeat or follow-up biopsy. TRAK EPR = NHS Lothian's electronic patient records system. APEX = NHS Lothian's pathology records system.

3.3.4 Whole-slide imaging and region of interest (ROI) selection

All original diagnostic H&E stained EH slides (n=125) were digitally slide-scanned (as per section 2.6). Using the NDP.view2 (Hamamatsu, U12388-01) imaging software, each whole-slide scanned image was then digitally marked with two separate regions of interest (ROIs) by AW and PS (Figure. 3-2).

One ROI corresponded to the pathologically 'most abnormal' appearing area of the sample. For example, in samples with a consensus expert pathologist diagnosis of EIN, the 'most abnormal' ROI corresponded to the entire clonal expansion of EIN (or where the entire tissue section contained only EIN / multiple foci, then the most abnormal focus of EIN was marked). The second ROI marked within the sample corresponded to the background endometrium or the 'least abnormal' area.

Where the sample had a non-EIN consensus diagnosis, the 'most abnormal' ROI corresponded to an area displaying the most representative pathological features of the non-EIN sample, whilst the 'least abnormal' ROI within the sample corresponded to the background endometrium.

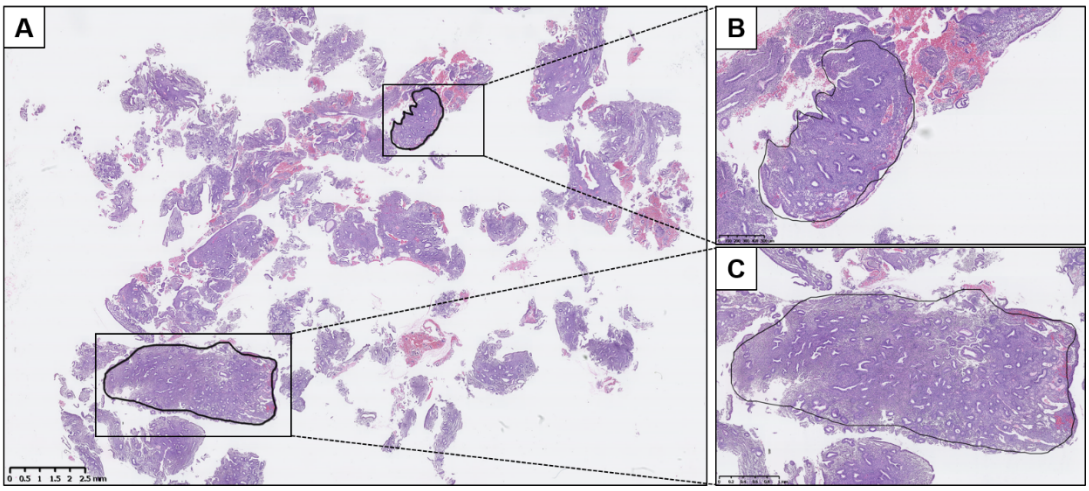

Figure 3-1: An example H&E stained tissue section containing two highlighted ROIs (exploded regions) digitally marked by AW and PS. In this example the consensus diagnosis of tissue section 'A' was HwA. ROI 1 (B) therefore represented the 'most abnormal' region within the tissue section i.e. the region contained the most representative features of HWA and ROI 2 (C) corresponded to the 'least abnormal' region or background endometrium. Where a tissue sample had a consensus diagnosis of EIN, one ROI would correspond to the entire clonal expansion of EIN and the other to the 'background endometrium' with the sample. Varying magnifications, see scale bars.

3.3.5 Digital computerised quantitative image analysis

Quantitative image analysis of the endometrial cellular compartments (i.e. epithelial area, stromal area, etc.) of EH tissues was performed. In brief, StrataQuest analysis software, v5.0 (TissueGnostics GmbH, Vienna) was utilised for cytometric analysis of H&E stained EH tissue sections. Whole slide-scanned H&E images (see section 2.6) were imported into the StrataQuest software. Pre-defined, bespoke analysis parameters for endometrial H&E image processing and pattern recognition algorithms were commercially designed, 'the H&E app' (TissueGnostics GmbH, Vienna) and applied to individual regions of interest (ROI – see 3.3.4) within the imported EH images. After manual optimisation and correction of analysis parameters (Ms Arantza Esnal-Zufiurre, Research Support, The University of Edinburgh), layered segmentation or 'masks' were applied. These were assigned colours (Figure. 3-3) by the software dependent on the tissue structure being detected (i.e. endometrial stromal cells = dark green). On final analysis the 'masks' were built up to give a final image (Figure. 3-3) and numerical data calculated for each tissue compartment, e.g. tissue area, number of nuclei, etc. Volume percentage stroma (VPS) was calculated as: VPS = total stromal area (dark green) / [total stromal area (dark green) + total epithelial area (blue + red) + total glandular lumen area (light green) + total vessel area (purple)] x 100.

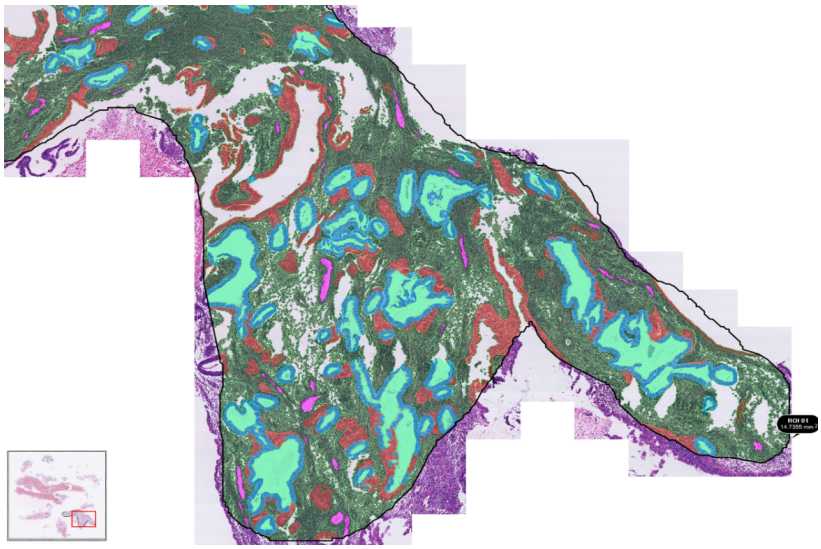

Figure 3-3: A representative example of layered segmentation analysis of an EH tissue sample using the TissueGnostics 'H&E app'. Individual regions of interest (ROI) within whole slide-scanned H&E stained EH tissues were analysed using the software to permit numerical area/volume analysis of the individual tissue components. Dark green = endometrial stromal, blue area = endometrial gland connecting with a lumen, red = endometrial gland without lumen / surface epithelium, light green = gland lumen, purple = bloods vessel.

3.4 Results

3.4.1 Endometrial hyperplasias represent a heterogeneous spectrum of endometrial lesions

Haematoxylin and eosin (H&E) stained tissue sections of n=125 pathologically diagnosed and coded, human endometrial hyperplasia lesions were obtained as described in 3.3.1 and 3.3.2. On baseline examination using light-microscopy, considerable heterogeneity was identified between the EH lesions. Compared to human endometrium from the normal proliferative phase of the menstrual cycle (Figure. 3-4A), EH lesions demonstrated a range of appearances, from large cystically dilated glands (Figures. 3-4B and C) surrounded by abundant cellular stroma, to glands demonstrating architectural complexity and arranged in a 'back-to-back' fashion with very little intervening stroma (Figure. 3-4D). On closer observation of the endometrial glands from certain EH lesions, features consistent with cytological atypia could be identified (Figures. 3-4E and F). High power magnifications confirmed that these glandular cells had enlarged and irregular nuclei, rounded in places, with coarse chromatin clumping towards the nuclear membrane and often prominent nucleoli (Figure. 3-5).

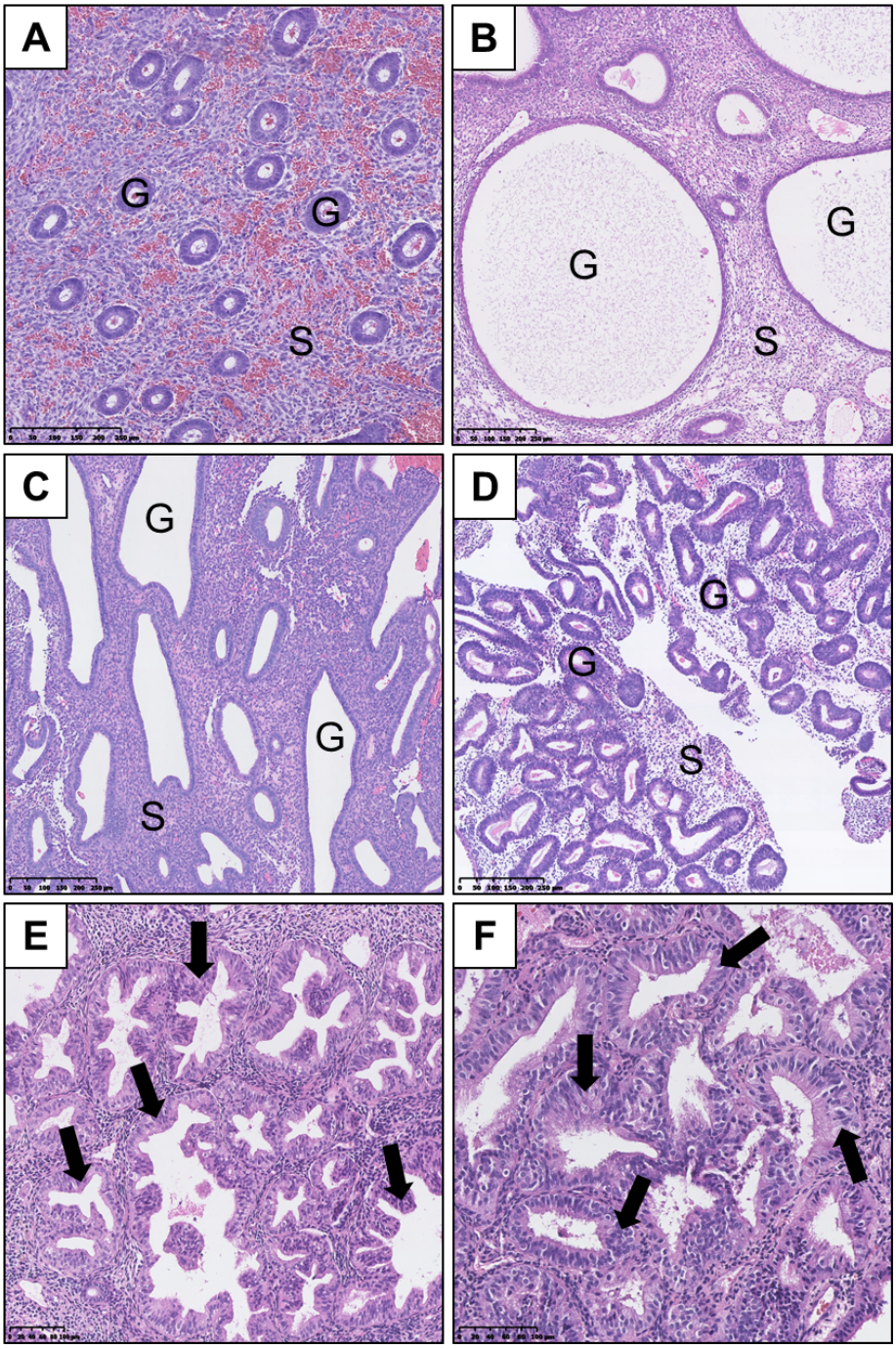

Figure 3-4: Haematoxylin and eosin (H&E) stained sections demonstrating variation in size and shape of endometrial glands within a spectrum of endometrial hyperplasia (EH) lesions compared to normal proliferative endometrium (PE). Glands marked by (G) in lumen and (S) to mark the stroma. A) Normal proliferative phase, B) and C) large, cystically dilated glands surrounded by ample stroma, D) EH sample exhibiting crowded, varied and irregular gland morphology with reduced areas of stroma, E & F) EH lesions with irregular gland architecture and cytological atypia (arrowed). Varying magnifications: see scale bars.

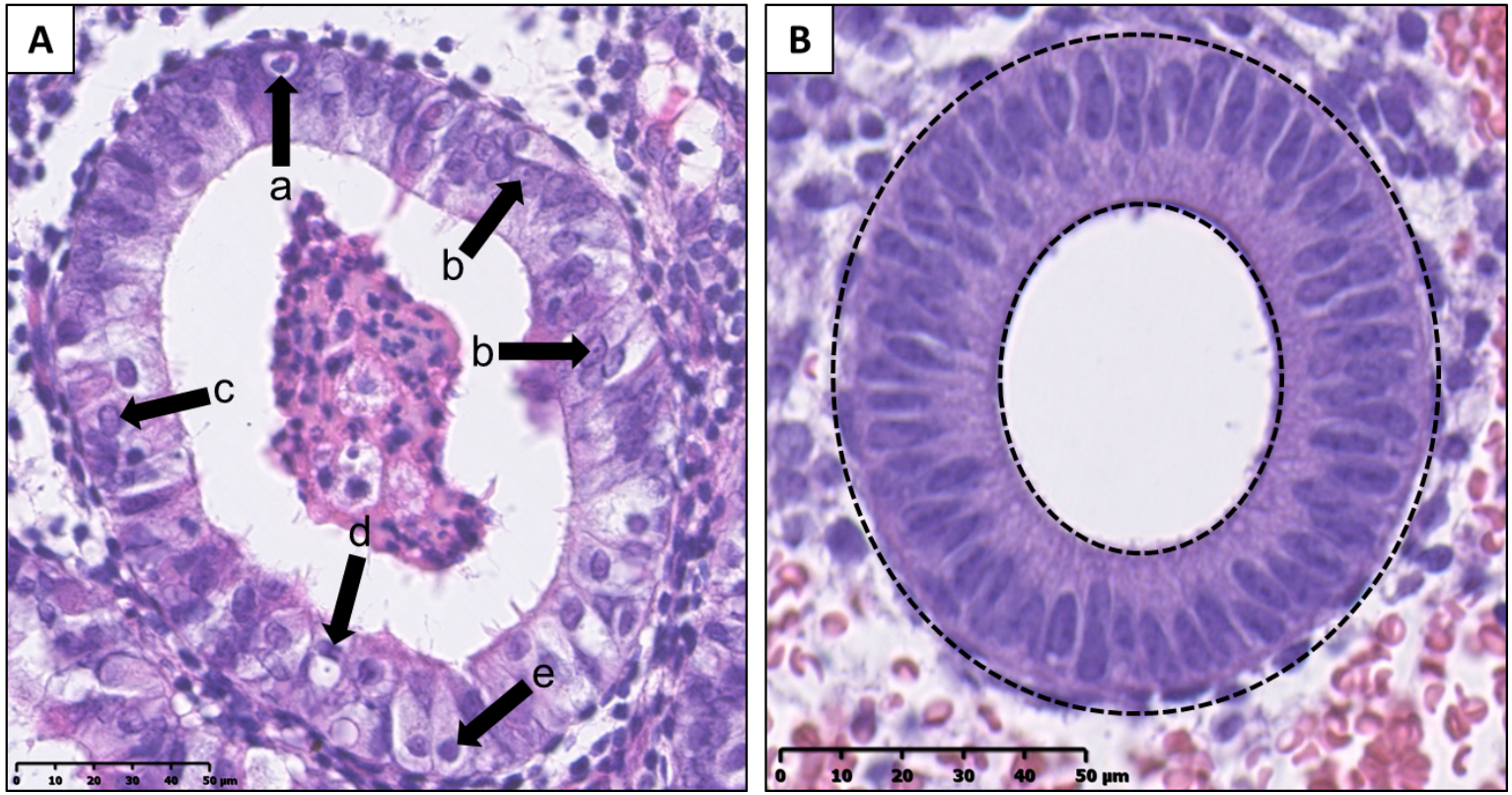

Figure 3-5: Cytological atypia within an H&E stained endometrial gland. A) High-power view of an endometrial gland exhibiting features of cytological atypia: Pseudostratified appearance of the glandular epithelial cells, with necrotic and apoptotic cells centrally within the glandular lumen. Evidence of a) apoptotic body, b) prominent nucleoli, c) chromatin clumping around the nuclear membrane, d) mitotic figure, e) rounded nuclei. B) For comparison, a high-power view of an endometrial gland from the normal proliferative phase, with uniform 'cigar' shaped nuclei and consistent nuclear: cytoplasmic ratios. Epithelial compartment highlighted by concentric dashed ovals on image B. Varying magnifications: see scale bars.

3.4.1.1 Effect of exogenous progesterone on the appearance of the hyperplastic endometrium

The effects of exogenous progesterone on the endometrium were noted in this study. Four of the n=125 patients reported hormonal contraceptive use at the time of their initial index biopsy, three of whom were using progesterone only preparations and one patient a combined oral contraceptive (both oestrogen and progesterone). Figure. 3-6 demonstrates the histological features seen with recent progesterone exposure to hyperplastic endometrium. The most common pattern of response seen was that of a pseudodecidualised stromal pattern (Figure. 3-6A), whereby the stromal cells were noted to be enlarged, with abundant more eosinophilic cytoplasm, prominent cell borders and occasional mitotic figures. Some affected glands displayed a secretory phenotype (Figure. 3-6B) with vacuolated cytoplasm and luminal secretions. The spiral arteries also demonstrated marked thickening (Figure. 3-6C) and leucocytes were visualised (Figure. 3-6D).

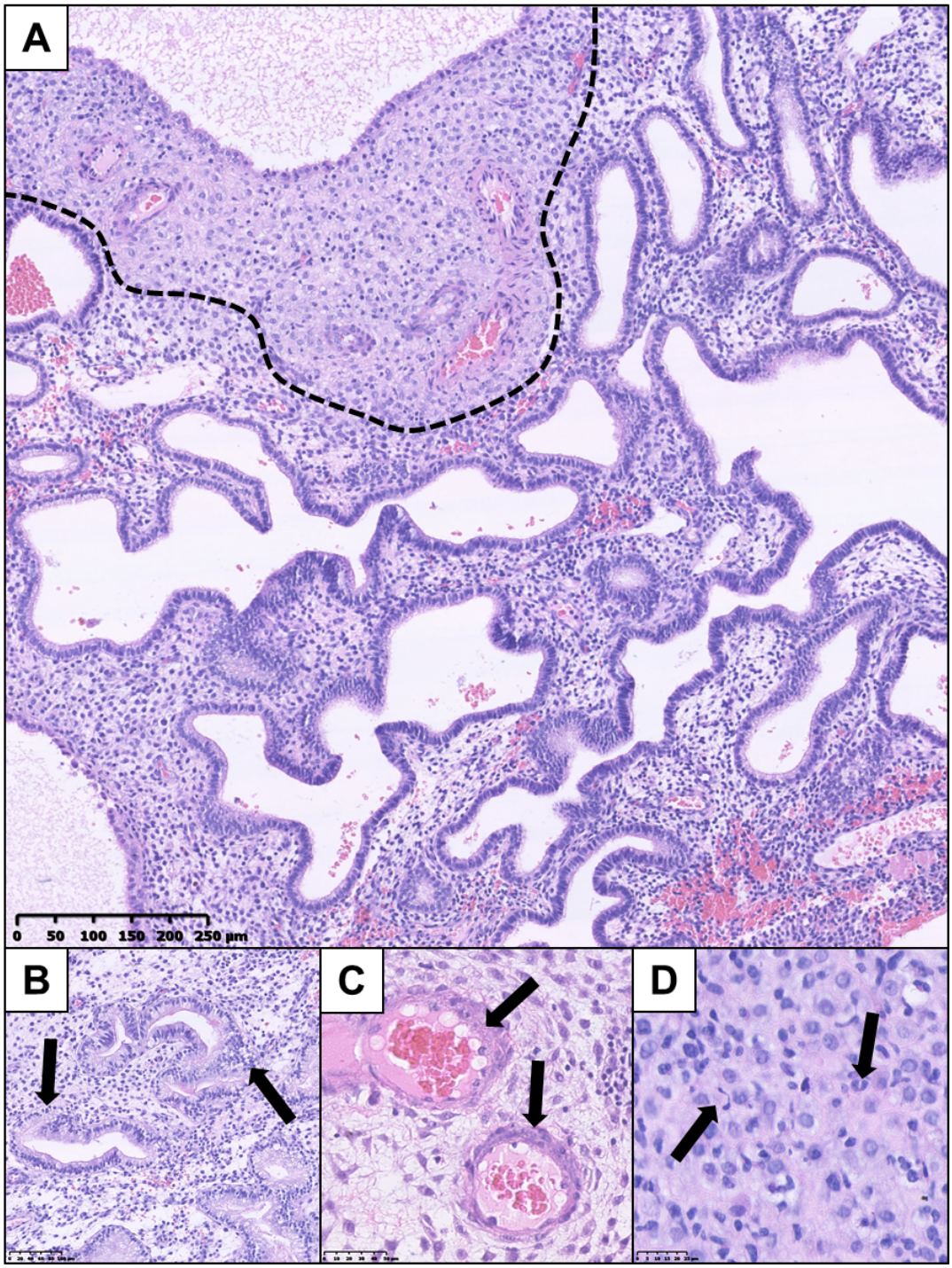

Figure 3-6: Evidence for the impact of progesterone in endometrial tissue sections containing areas of endometrial hyperplasia. A) H&E section of hyperplasia without atypia (HwA) demonstrating a pseudodecidualised stromal response (above dashed line), from within the same tissue section note, B) endometrial glands with a secretory phenotype (arrowed) with sub-nuclear vacuoles C) prominent coiled arterioles (arrowed) and D) an influx of leucocytes (arrowed). Varying magnifications: see scale bars.

3.4.2 Interobserver variability is apparent when diagnosing EH using the WHO94 classification

All n=125 EH lesions were originally diagnosed and coded by NHS pathologists (i.e. the 'index' diagnosis) utilising the WHO94 classification system (as described in chapter 1). Table. 3-2. displays the breakdown of these index diagnoses by each WHO94 diagnostic category. A dual, blinded, expert gynaecological pathologist review was carried out (as described in section 3.3.3) and the number of cases where each expert pathologist agreed with the index diagnosis are also displayed in Table. 3-2.

For all n=125 cases, percentage agreement between each expert pathologist and the original diagnosis was 56.0 % (n=70) and 48.8 % (n=61) respectively. This amounted to a Cohen's Kappa (*k*) interobserver agreement score of 0.385 (95 % CI 0.268-0.501) 'fair' for expert pathologist A and a score of 0.298 (95 % CI 0.210-0.387) 'fair' for expert pathologist B. Of note was the complex hyperplasia (CH) category which exhibited the lowest levels of agreement between that of the index diagnoses and the experts, with pathologist A agreeing with 12/29 (41.3 %) of the index diagnoses and pathologist B not agreeing with any. In addition, pathologist B upgraded n=2 diagnoses from EH to malignancy. Interobserver agreement was also assessed between the two expert pathologists utilising the WHO94 classification. Agreement did not improve upon that seen between the experts and the original index diagnoses, with total percentage agreement reaching 52.1 % (n=64), $k = 0.327$ (95 % CI 0.227-0.427) 'fair'.

Diagnostic inconstancy was noted within the complex atypical hyperplasia (CAH) category of the original index diagnoses, with six descriptive variants of the CAH category identified (Table. 3-3). A diagnosis of CAH would normally lead to a clinical recommendation of a hysterectomy, therefore atypia subgroupings within this category may create potential confusion over the urgency or indeed the necessity for a surgical intervention.

Table 3-2: Interobserver agreement when diagnosing endometrial hyperplasia samples using the WHO94 classification.

Diagnostic category	Index diagnosis	Path A diagnosis	Path B diagnosis	Agreement between Path A & index diagnosis	Agreement between Path B & index diagnosis	Agreement between Path A & Path B diagnoses
Complex atypical hyperplasia (CAH)	24	26	67	15	21	23
Simple atypical hyperplasia (SAH)	0	2	0	0	0	0
Complex hyperplasia (CH)	29	21	1	12	0	0
Simple hyperplasia (SH)	56	54	45	36	38	34
Malignant	0	0	2	0	0	0
Hyperplastic polyp (HP)	16	12	4	7	2	4
Other*	0	10	6	0	0	3
Combined total (%)	125	125	125	**70 (56.0)**	**61 (48.8)**	**64 (52.1)**
Kappa, *k* (95% CI)				**0.385 (0.268-0.501) 'Fair'**	**0.298 (0.210-0.387) 'Fair'**	**0.327 (0.227-0.427) 'Fair'**

Numbers in each column are based on classification of a single H&E stained section of endometrial tissue from n=125 women. *Incorporates functional endometrial polyps and normal / cycling endometrium. Cohens Kappa, *k*, is a measure of agreement among observers that attempts to correct for chance agreement and whose values are 1.00 or less, where 1.00 indicates perfect agreement and 0 indicates the level of agreement expected by chance alone. Interpret as follows: 0.00–0.20, slight; 0.21–0.40, fair; 0.41–0.60, moderate; 0.61–0.80, substantial; and 0.81–1.00, almost perfect agreement.

Table 3-3: Subgroup breakdown within the index WHO94 complex atypical hyperplasia category. Multiple variants of the diagnostic subgroup of complex atypical hyperplasia can create confusion when translating the diagnosis to clinical management.

Subgroup Variant	Patients, n (%)
Complex atypical hyperplasia	10 (41.6)
Complex hyperplasia with mild atypia	6 (24.0)
Complex hyperplasia with moderate atypia	4 (16.0)
Complex hyperplasia with severe atypia	2 (8.0)
Severe atypical hyperplasia	1 (4.0)
Complex hyperplasia with minor atypia	1 (4.0)
Total combined	**24**

3.4.3 Identification of EIN within the patient cohort

The premalignant lesion, EIN can be diagnosed on a routine H&E stained section of EH tissue by adhering to the prescribed criteria listed in Table. 3-1. To investigate whether this EH patient cohort contained cases of EIN, each H&E stained patient sample was reviewed as described in 3.3.3. Figure. 3-7 is a representative EH tissue example from the patient cohort containing a focal region of EIN. The diagnostic process firstly involved establishing the presence an architecturally crowded focus of endometrial glands, >1 mm in size and with a volume percentage of glands to stroma exceeding 55 % (indicated in Figure. 3-7A by a dashed oval). Within this architecturally crowded focus the glandular cells were required to differ cytologically from those of the background endometrium for an EIN diagnosis. Figure. 3-7B indicates a gland from within the area of glandular crowding and 3-7C displays a background endometrial gland, confirming cytological differences. In cases with no 'normal' background glands for internal reference, the freestanding cytology of relevant endometrial fragments was assessed in the context of their architectural features. EIN was ultimately identified in 52/125 patients and HwA in 54/125 patients following consensus diagnosis by 2 expert gynaecological pathologists (see 3.4.4). Demographic details for these two groups are displayed in Table. 3-4. Note the statistically significant differences between the two groups regarding parity, with a greater number of nulliparous patients diagnosed with EIN (a known risk factor for EIN development). In addition, a statistically significant difference between the groups was noted in terms of co-existing PCOS.

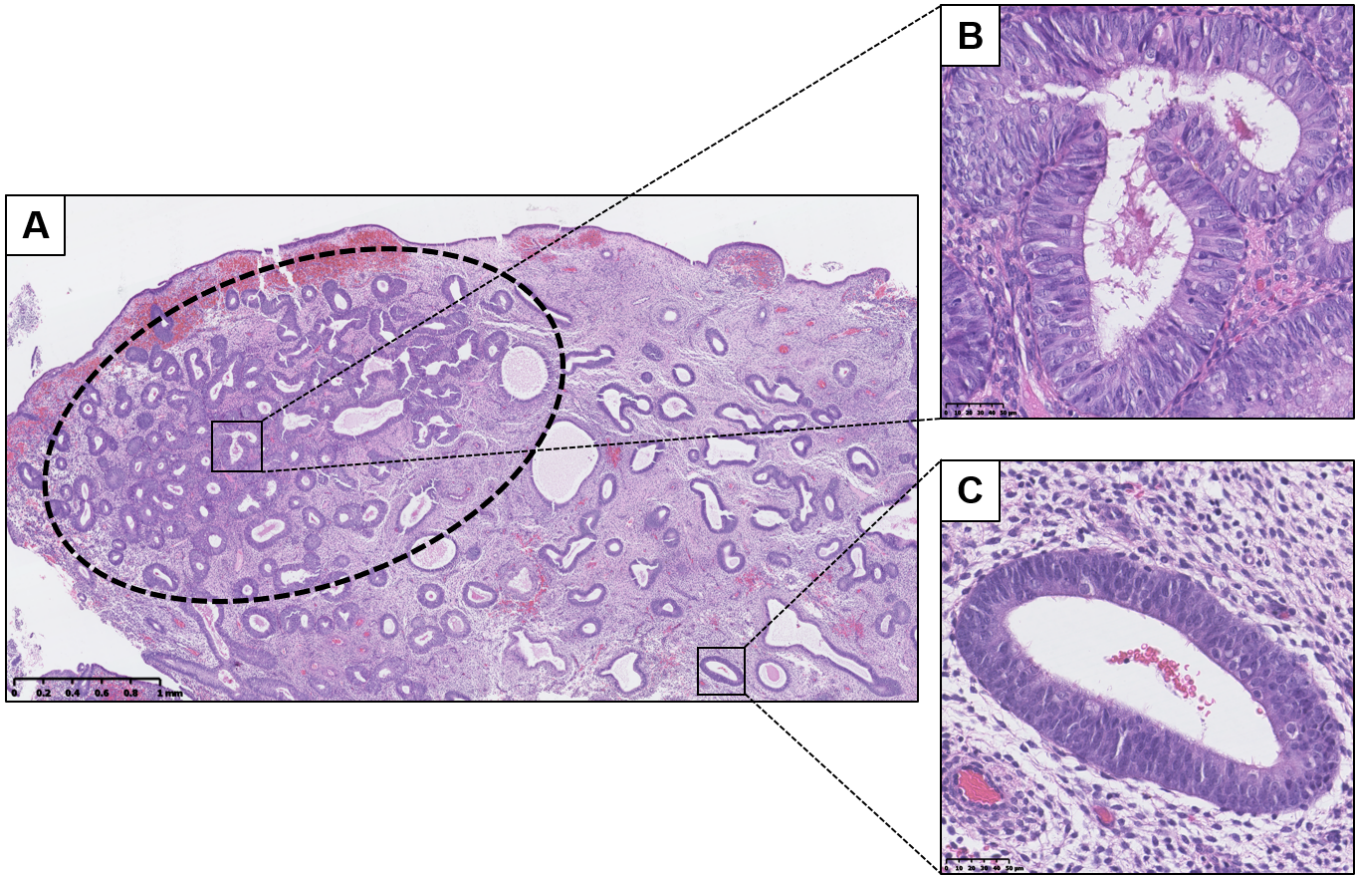

Figure 3-7: A clonal area of EIN within an endometrial biopsy. A) Low power view of a clonal area of EIN, with prominent gland crowding (marked in oval with bold dashes), in a background endometrium demonstrating HwA, B) high-power view of EIN lesion gland, C) high-power view of a gland from the background endometrium as a comparator. Sample stained with H&E, varying magnifications: see scale bars.

Table 3-4: Demographics and clinical features of patients with EIN and HwA following consensus diagnosis by two gynaecological pathologists.

	EIN n=52 (%)	HwA n=54 (%)	P Value
Age			
Mean	52.8	52.9	0.9898
≤40	6 (11.6)	4 (7.4)	0.7206
41-50	16 (30.8)	22 (40.8)	0.3419
51-60	18 (34.6)	19 (35.2)	0.7343
61-70	10 (19.2)	4 (7.4)	0.9585
>70	2 (3.9)	5 (9.3)	0.0718
Ethnicity			
White Scottish	26 (50.0)	21 (38.9)	0.3284
White English	6 (11.6)	8 (14.8)	0.7759
Other	1 (1.9)	0	0.4906
Not disclosed	19 (36.5)	25 (46.3)	0.3308
Menopausal status			
Premenopausal	14 (26.9)	15 (27.8)	>0.9999
Perimenopausal	6 (11.5)	7 (13.0)	>0.9999
Postmenopausal	30 (57.7)	30 (55.6)	0.8428
Unknown	2 (3.9)	2 (3.7)	
Presenting complaint			
PMB	28 (53.9)	26 (48.2)	0.5672
HMB	13 (25.0)	16 (29.6)	0.6657
IMB	6 (11.5)	8 (14.8)	0.7759
Subfertility	2 (3.9)	0	0.2383
Incidental finding	3 (5.8)	4 (7.4)	>0.9999
Parity			
Nulliparous	16 (30.8)	7 (13.0)	*0.0308
1-4	29 (55.8)	40 (74.1)	*0.0222
≥5	2 (3.9)	1 (1.9)	0.6170
Unknown	5 (9.6)	6 (11.1)	
BMI			
Mean	37.9	38.3	0.8661
21-25	5 (9.6)	2 (3.7)	0.4425
26-30	2 (3.8)	5 (9.3)	0.1964
31-35	8 (15.4)	2 (3.7)	0.1411
36-40	9 (17.3)	8 (14.8)	0.5687
>40	6 (11.5)	8 (14.8)	0.2149
Unknown	22 (42.3)	29 (53.7)	
Co-morbid factors^			
Diabetes mellitus	12	12	>0.9999
PCOS	7	1	*0.0264
HRT use	4	7	0.5283
Tamoxifen use	4	4	>0.9999
≥ 2 of above	2	1	0.6060

^Complete co-morbid factor information unavailable for n=5 EIN and n=3 HwA patients. Statistical analysis performed using the 2-sided Fisher's exact test to determine statistical differences between the categorical data and a two-tailed unpaired t-test used to compare the means of the continuous data, for those with EIN and those with HwA. *p<0.05.

3.4.3.1 Mimics and technical processing can influence an EIN diagnosis

Technical artefacts were noted when assessing the cohort (Figure. 3-8). These, if they remain unrecognised can lead to inaccuracies in diagnosis and contribute to poor levels of interobserver diagnostic agreement. Several architectural mimics of EIN were also identified and excluded before a final diagnosis of EIN was made. Figure. 3-9 displays a representative sample of the architectural mimics of EIN that were noted in this study.

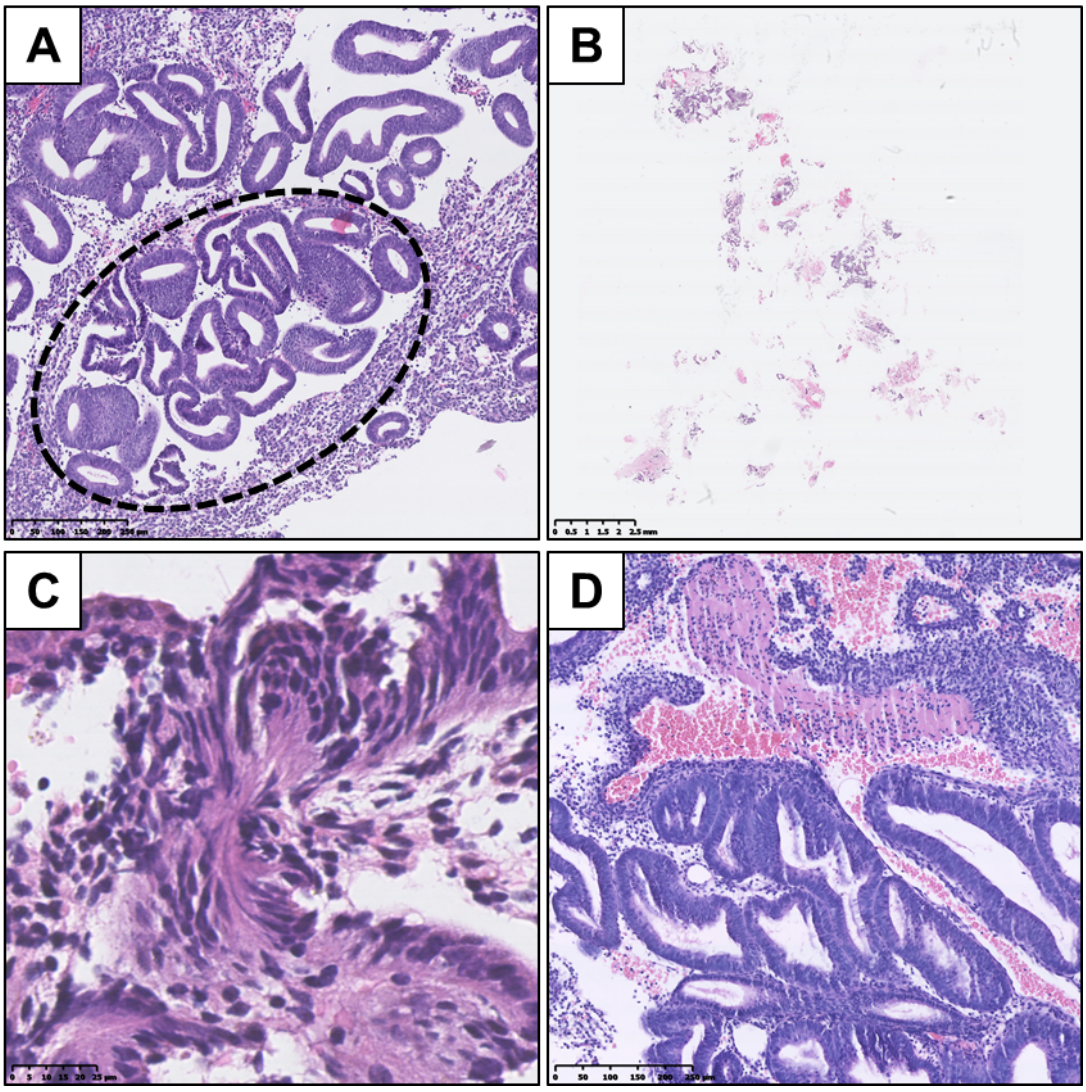

Figure 3-8: Encountered technical problems with H&E stained sections may lead to difficulties in making a reliable diagnosis. A) Specimen architectural compression, demonstrating pseudo gland-crowding (dashed oval) which may be mistaken for EIN – commonly seen with Pipelle® endometrial sampling due to the negative pressure created when the biopsy is taken, B) Small and scanty specimen, not permitting adequate architectural assessment, C) Tissue distortion from histological processing, D) microtome 'chatter' artefacts. Varying magnifications: see scale bars.

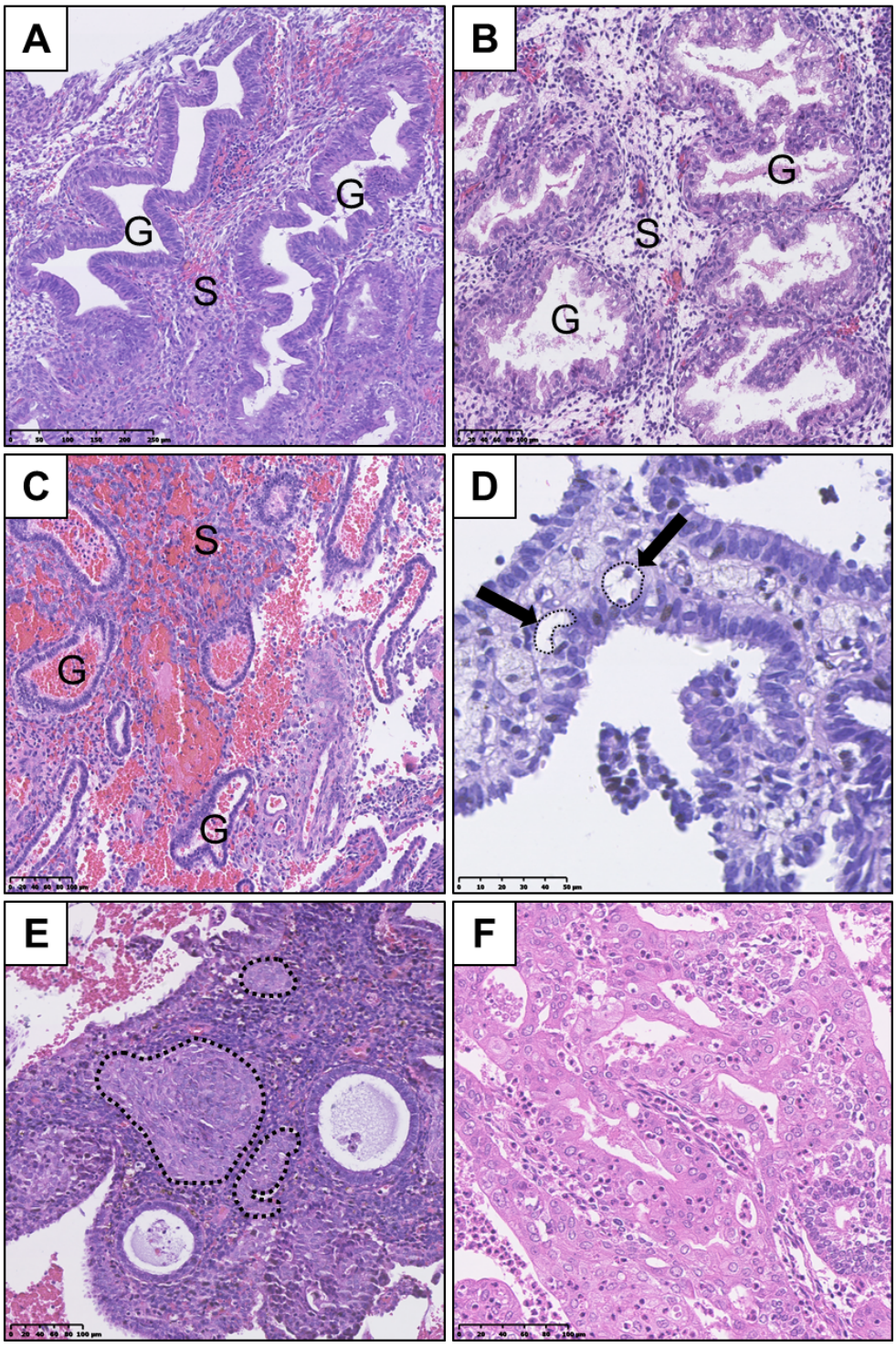

Figure 3-9: Representative samples of H&E stained images of the common mimics of EIN lesions seen within this study. A) and B) secretory endometrium, C) menstrual endometrium, D) Lipid-laden "foam-cells" within the stroma (examples marked / arrowed) that are commonly seen in cases of EH, E) Squamous metaplasia, with morules (encircled by dashed line) admixed amongst the glands, F) endometrioid endometrial carcinoma, note disorganised tissue architecture with prominent numbers of cells with condensed nuclear architecture and lack of a defined stromal/epithelial architecture. Varying magnifications: see scale bars.

3.4.4 Interobserver variability is improved upon when diagnosing EH using the EIN/WHO2014 classification

As already described, all n=125 EH lesions were retrospectively reclassified using the EIN/WHO2014 system. Total percentage agreement between the diagnoses for each expert pathologist was higher than that previously seen when utilising the WHO94 system, standing at 67.2 % (n=84) and amounting to an interobserver agreement score of k = 0.478 (95 % CI 0.356-0.600) 'moderate' (Table. 3-5). Interestingly and somewhat unexpectedly, pathologist A diagnosed n=46 cases of EIN and pathologist B diagnosed n=66 cases, both noticeably different and both higher than the number of cases originally given an index diagnosis of CAH (n=24), i.e. the highest risk category under the WHO94 criteria. A final consensus diagnosis was reached (as described in 3.3.3) and the results displayed in Table. 3-5. For the purpose of completeness, endometrial polyp diagnoses and "others" (incorporating benign/atrophic changes and DPE, etc.) are displayed.

3.4.5 Potential for disparity between clinical treatments dependent upon the EH classification system used

As previously discussed in chapter 1, patients diagnosed with a high risk EH, i.e. CAH (WHO94) and EIN (EIN/WHO2014) are usually recommended to have definitive surgical treatment in the form of a total hysterectomy, due to the risk of a concurrent un-biopsied EC or future malignant progression. Reclassification from WHO94 to EIN/WHO2014 criteria revealed a potential for disparity between clinical treatments.

Following consensus reclassification, n=52 patient samples were diagnosed as EIN, incorporating n=20 patients with an original index diagnosis of CAH (Table 3-6). For these n=20 patients, surgical treatment would have been recommended under both classification systems. The remaining n=32 EIN diagnoses had an original index WHO94 diagnosis less severe than CAH. Consequently, under the WHO94 system they may not have been recommended surgery as a 1st line treatment. Figure. 3-10 is a representative example of a case with an index WHO94 diagnosis of simply hyperplasia without atypia (SH) and upgraded to EIN following consensus reclassification using the EIN/WHO2014 system. Conversely, n=3 patients originally diagnosed as CAH and for whom hysterectomy would have been recommended, were downgraded to HwA under EIN/WHO2014. These patients may have been offered conservative observation and/or progestins as first-line treatment under the EIN/WH02014 system. Figure. 3-11 displays the histology from one of these cases.

Table 3-5: Interobserver agreement when diagnosing endometrial hyperplasia samples using the EIN/WHO2014 classification.

Diagnostic category	Path A diagnosis	Path B diagnosis	Agreement between Path A & Path B diagnosis	Final consensus diagnosis
Endometrial intraepithelial neoplasia (EIN)	46	66	40	52
Hyperplasia without atypia (HwA)	58	46	37	54
Malignant	0	2	0	2
Endometrial intraepithelial neoplasia in a polyp (EIN-EMP)	1	0	0	3
Hyperplastic polyp (HP)	10	4	3	6
Others*	10	7	4	8
Combined total (%)	125	125	**84 (67.2)**	125
Kappa, *k* (95% CI)			**0.478 (0.356-0.600)** **'Moderate'**	

Numbers in each column are based on classification of a single H&E stained section of endometrial tissue from n=125 women. *Incorporates atrophic/benign endometrium, DPE, etc. Cohens Kappa, *k*, is a measure of agreement among observers that attempts to correct for chance agreement and whose values are 1.00 or less, where 1.00 indicates perfect agreement and 0 indicates the level of agreement expected by chance alone. Interpret as follows: 0.00–0.20, slight; 0.21–0.40, fair; 0.41–0.60, moderate; 0.61–0.80, substantial; and 0.81–1.00, almost perfect agreement.

Table 3-6: Contributions of each hyperplasia type (index WHO94 classification) to the final consensus (EIN/WHO2014 classification) diagnostic classification

Index WHO94 classification	Patients	Consensus EIN/WHO2014 classification, patients					
		EIN	HwA	Malignant	EIN-EMP	HP	Others*
Complex atypical hyperplasia (CAH)	24 (19.2)	20 (16.0)	3 (2.4)	1 (0.8)	0	0	0
Complex hyperplasia (CH)	29 (23.3)	18 (14.4)	7 (5.6)	0	1 (0.8)	0	3 (2.4)
Simple hyperplasia (SH)	56 (44.8)	8 (6.4)	43 (34.4)	0	0	2 (1.6)	3 (2.4)
Hyperplastic polyp (HP)	16 (12.8)	6 (4.8)	1 (0.8)	1 (0.8)	2 (1.6)	4 (3.2)	2 (1.6)
		52 (41.6)	54 (43.2)	2 (1.6)	3 (2.4)	6 (4.8)	8 (6.4)
Total	**125**	**125**					

Numbers in each column are based on classification of a single H&E stained section of endometrial tissue from n=125 women. Percentages in brackets. *Incorporates atrophic/benign endometrium. Under the EIN/WHO2014 classification system, all patients with a diagnosis of EIN (red) should, where able, be offered surgical treatment in the form of a total hysterectomy, due to the high associated risk of concurrent or future endometrial cancer. Conversely, those patients with a diagnosis of HwA could be offered medial therapy with progestins or a conservative approach in the first instance. As a comparison, only those diagnosed with complex atypical hyperplasia (Green; CAH) should, where able, be offered surgical treatment under the WHO94 system. This highlights a potential for treatment disparity between the two classification systems.

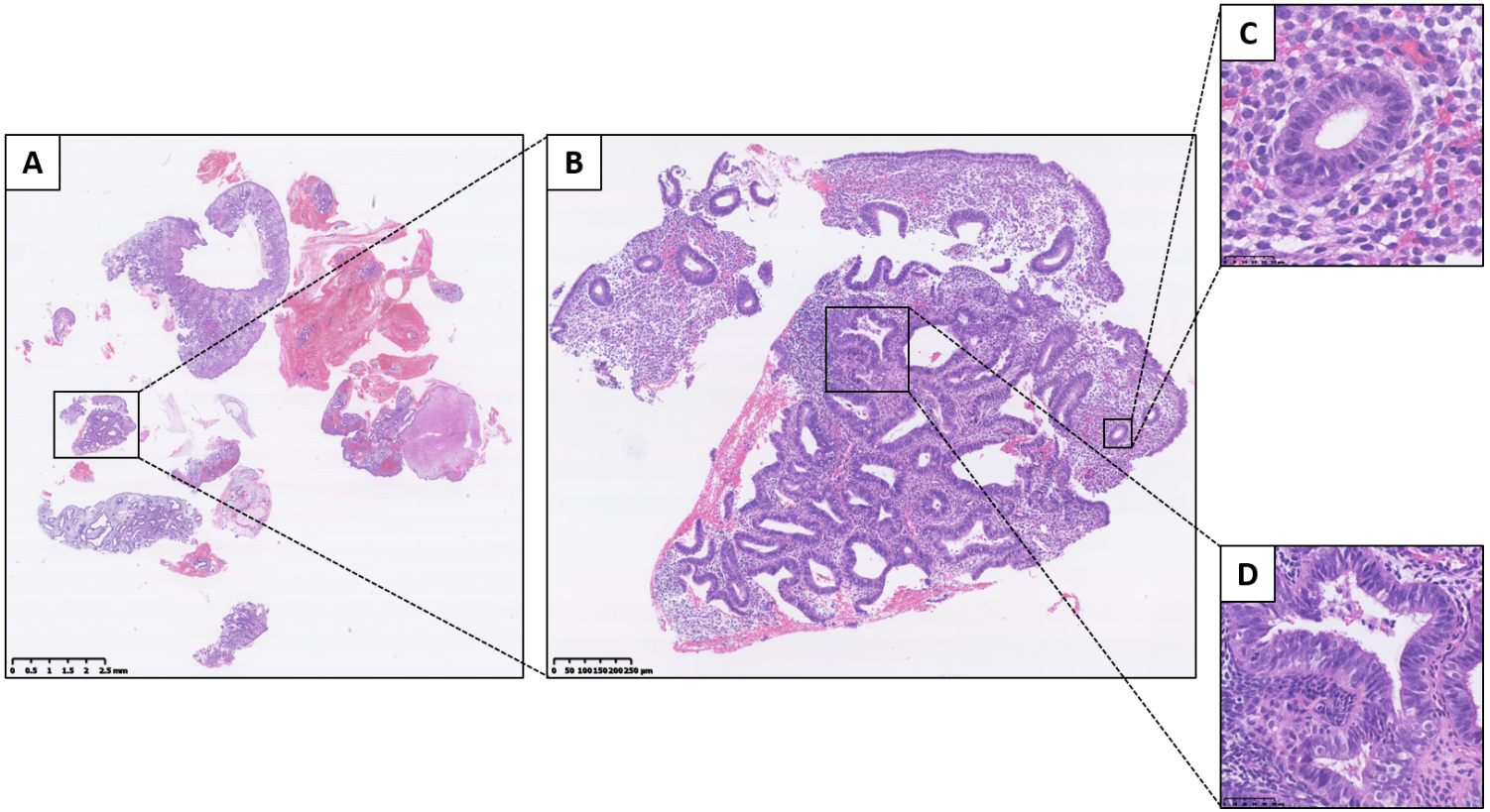

Figure 3-10: Reclassification to EIN using the EIN/WHO2014 classification system. H&E stained human EH tissue section, originally diagnosed as simple hyperplasia (SH), this tissue section underwent dual, blinded expert gynaecological pathologist review and a final consensus diagnosis of EIN was made. A) Low power view of entire tissue section, B) higher power view of a region with an architecturally crowded focus, note VPS >55 % and size >1 mm, C) background endometrial gland, D) gland from within the architecturally crowded focus, demonstrating cytological differences from the background gland in C. Varying magnifications: see scale bars.

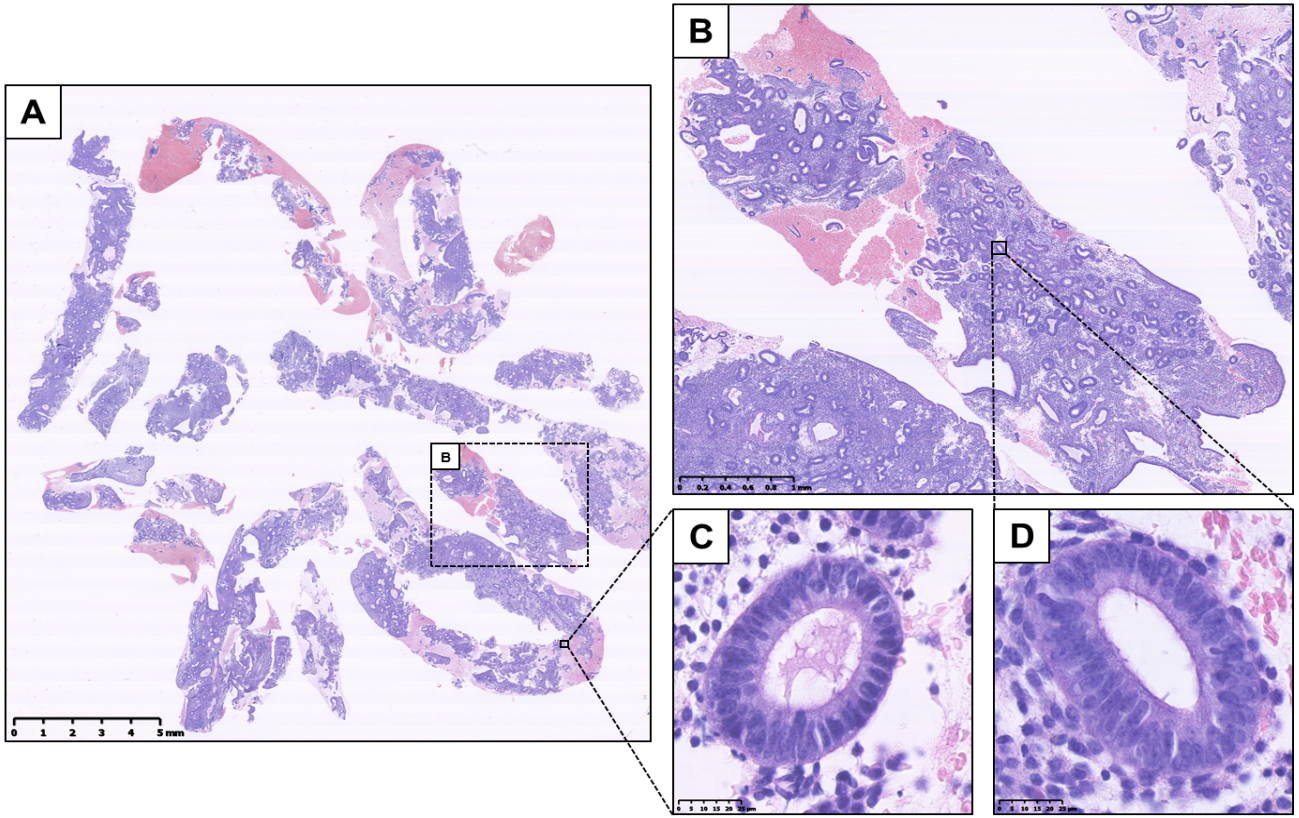

Figure 3-11: Reclassification to HwA using the EIN/WHO2014 classification system. H&E stained human EH tissue section, originally diagnosed as complex atypical hyperplasia (CAH), this tissue section underwent dual, blinded expert gynaecological pathologist review and a final consensus diagnosis of HwA was made. A) Low power view of entire tissue section, B) higher power view from a representative region of the tissue section with an architecturally crowded focus, note VPS <55 %, C) background endometrial gland, D) gland from within the architecturally crowded focus, demonstrating no significant cytological differences from the background gland in C. Varying magnifications: see scale bars.

3.4.6 Computerised quantification of EH tissue compartment architecture could assist pathologists with difficult to classify EH cases when utilising the EIN/WHO2014 classification system.

As previously discussed, the EIN/WHO2014 classification system relies on a subjective volume assessment of the endometrial stromal compartment by the diagnosing pathologist in order to estimate a volume percentage stroma (VPS) of <55 % (Table. 3-1). Following the initial dual pathological review, n=32 EH cases required re-review since the two expert pathologists failed to initially agree. After a consensus review of these cases, n=10 had a final diagnosis of EIN and n=11 a final diagnosis of HwA, and the remaining were deemed non-hyperplastic.

To assess the role of semi-automated computer image analysis as a diagnostic adjunct to pathological classification, these consensus EH cases (n=21) underwent digital image analysis (as per 3.3.5) to quantify objectively the volume percentages of the stromal and epithelial tissue compartments. The hypothesis was that the subjective nature of VPS architectural assessment was a factor which may have caused the pathologists to initially disagree regarding these samples. The ROIs deemed the 'most abnormal' within each tissue sample (as described in 3.3.4) were used for the analysis. Thus, for the EIN samples (n=10) the 'most abnormal' ROI corresponded to a clonal region of EIN and for the HwA samples (n=11), the 'most abnormal' ROI corresponded to the most representative region of HwA.

Computerised digital quantification of the stromal and glandular compartments demonstrated that the consensus EIN cases (n=10), which by definition should have a VPS of <55 %, were identified by computer-assisted image analysis as having a VPS of <55 % in 30 % (3/10) of cases (Figure. 3-12A) indicating that in the 'most abnormal' region of the tissue sections, 7/10 of the cases did not have glandular area which exceeded that of the stromal area by image analysis. Therefore, based on this image analysis evaluation of architecture alone these cases may not be considered as meeting the VPS criterion for EIN as per the classification system (Table. 3-1). All of the consensus cases of HwA (n=11) met the architectural requirements of the EIN/WHO2014 classification system and demonstrated a VPS of >55 % using this image analysis technique (Figure. 3-12B).

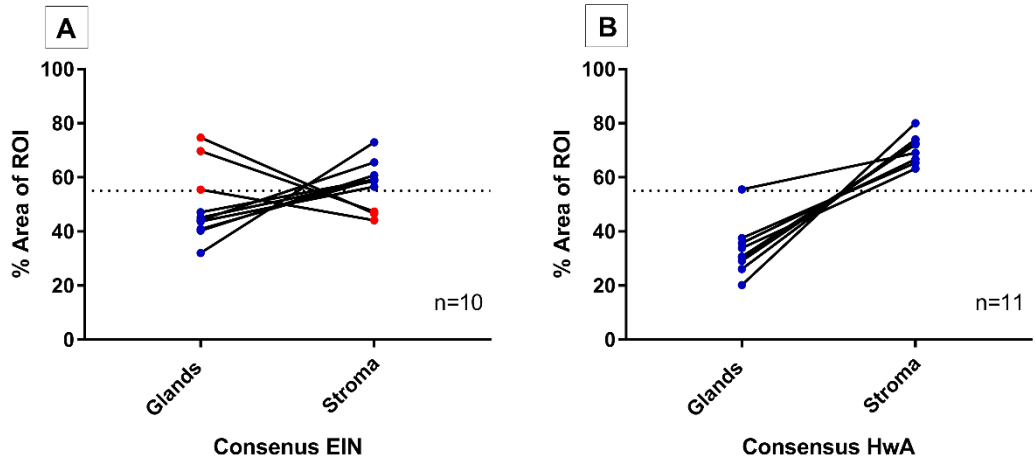

Figure 3-12: Semi-automated quantitative image analysis demonstrates discrepancies between the final consensus pathology diagnosis and the EIN diagnostic criteria. Dashed line represents the 55 % threshold for volume percentage stroma (VPS). A) 3/10 (red) cases with a final consensus diagnosis of EIN met the EIN diagnostic criteria for architecture with a VPS of <55 %, meaning that the glandular epithelial compartment exceeded that of the stromal compartment within the ROI. The remaining 7/10 cases (blue) do not show image analysis evidence of EIN using the architectural definition of a VPS <55 %. B) All final consensus diagnoses of HwA were correctly found to have stromal areas that exceeded that of the glands by image analysis.

3.4.7 Computerised image analysis quantification of difficult to classify EIN cases using a comparison of the most and least abnormal regions of interest

The EIN classification system requires a comparison between the cytology within an architecturally crowded glandular focus and the cytology within the background endometrial glands (Table. 3-1.). As described in 3.4.6, objective quantification of the volume percentage stroma (VPS) demonstrated that for 7/10 re-reviewed consensus cases the EIN diagnostic threshold of a VPS <55 % was not met using this image analysis technique. These n=10 cases are likely to be difficult to diagnose cases since the two expert pathologists were unable to agree upon their initial assessments.

To investigate why a final consensus diagnosis of EIN may have been reached, further quantitative architectural analysis of these n=10 cases was undertaken (Figure 3-13). The hypothesis was that the background endometrial architecture within these cases may display less gland crowding than the presumed clonal EIN region, contributing to the reporting pathologist subjectively judging the clonal region as showing a VPS of <55 %. A direct comparison was made between the 'most-abnormal' ROI (deemed to be the clonal expansion of EIN, as described in 3.3.4) and the 'least-abnormal' ROI (deemed to be the background endometrial tissue) for each of these n=10 cases.

The VPS values of the 'most abnormal' ROIs were significantly less than those of the 'least abnormal' ROIs (Figure. 3-13A.) within these n=10 cases. There also appears to be clustering of the 'most abnormal' ROIs closer to the 55 % VPS definition threshold when compared to the 'least abnormal' ROIs, which demonstrated a trend well above this threshold line (Figure. 3-13A). In addition, the epithelial compartment demonstrates significantly increased percentage volumes within the 'most abnormal' ROIs compared with the 'least abnormal' ROIs (Figure. 3-12B.), with a non-significant trend towards an increased overall glandular volume suggested (Figure. 3-13C.).

Taken together this implies a potential increase in glandular crowding within the 'most abnormal' ROIs when compared with the 'least abnormal' ROIs. The luminal volume remains largely unchanged (Figure. 3-13D.) suggesting no differences in cystic dilatation of the endometrial glands between the two ROIs.

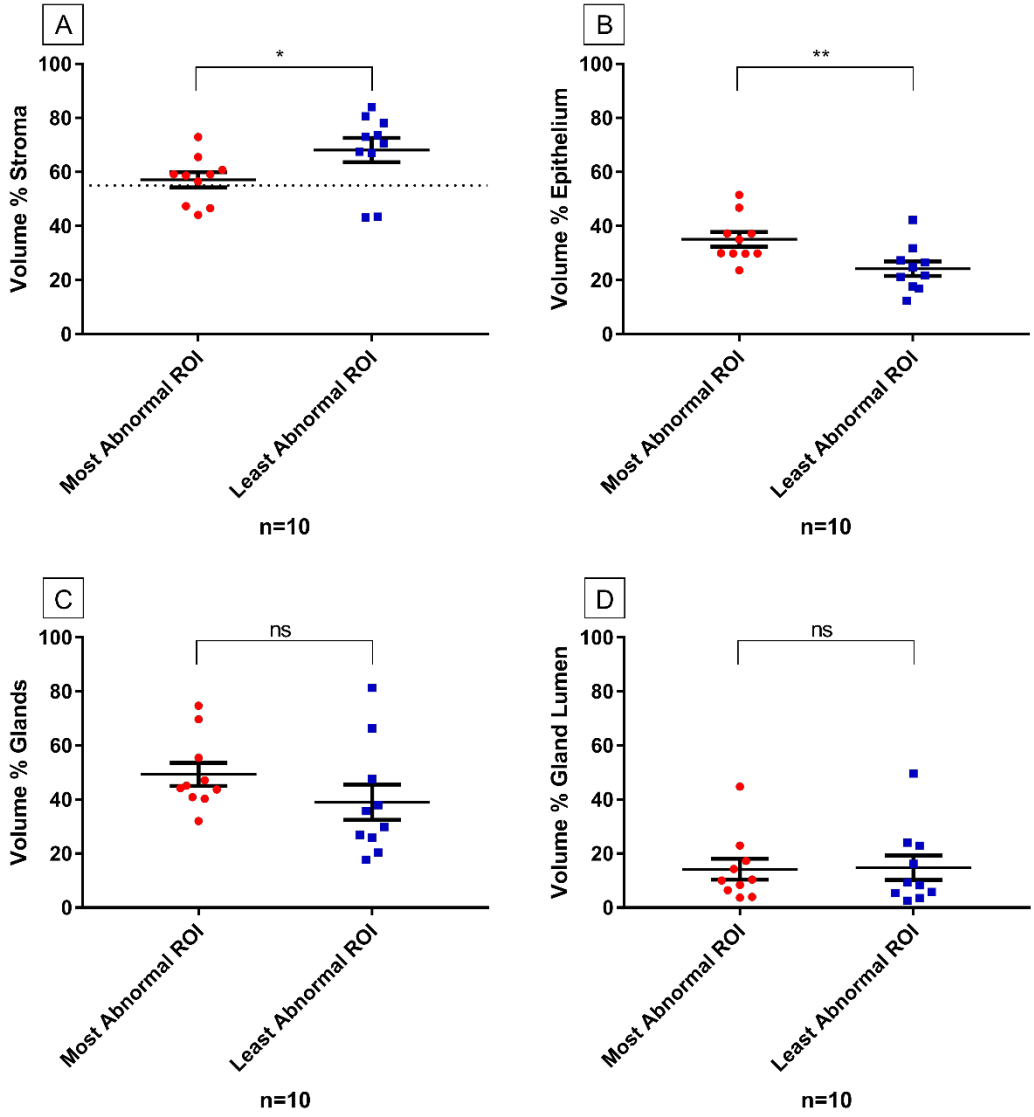

Figure 3-13: Semi-automated quantitative image analysis of individual tissue compartments in difficult to diagnose cases of EIN. A) Volume percentage stroma within the 'most' and 'least abnormal' ROIs within a tissue section diagnosed as EIN. Dashed line represents the 55 % VPS defined diagnostic threshold for EIN, B) Volume percentage epithelium within the 'most' and the 'least abnormal' ROIs within a tissue section diagnosed as EIN, C) Volume percentage of total glands (epithelium and lumen) within the 'most' and 'least abnormal' ROIs within a tissue section diagnosed as EIN, D) Volume percentage of glandular lumen within the 'most' and 'least abnormal' ROIs within a tissue section diagnosed as EIN. Statistical analysis performed using a two-tailed paired t-test. *$p<0.05$, **$p<0.01$.

3.4.8 Progression of EH to endometrioid endometrial cancer

12 (10.17 %) from 118 (n=7 lost to follow-up from the original n=125 cohort) patients for whom the index endometrial biopsy demonstrated an EH were later diagnosed with endometrioid EC. Table. 3-7 displays the demographics and clinical details for these 12 patients, along with the detail of the patients who did not progress to cancer for comparison. Median time from index EH diagnosis to EC diagnosis was 146.5 days (range 36 – 3481 days, standard deviation, SD 1081.46 days). Ten of the ECs were diagnosed within 12 months of the index EH diagnosis and are therefore considered to be concurrent cancers not sampled by the initial index endometrial biopsy. The remaining 2 ECs were diagnosed 1571 and 3481 days respectively after the initial index EH diagnosis and therefore developed subsequently. Of note, n=5 (41.7 %) patients who developed EC were premenopausal and n=2 (16.7 %) were under 40 years of age.

Table 3-1: Demographics and clinical features of patients who did and who did not develop an endometrial cancer following an initial biopsy diagnosis of endometrial hyperplasia.

	Cancer n=12 (%)	No cancer n=106 (%)	P Value
Age			
Mean	55.4	53.8	
≤40	2 (16.7)	8 (7.6)	0.7619
41-50	4 (33.3)	36 (34.0)	0.3259
51-60	1 (8.3)	37 (35.0)	>0.9999
61-70	4 (33.3)	16 (15.1)	0.1844
>70	1 (8.3)	9 (8.5)	>0.9999
Menopausal status			
Premenopausal	5 (41.7)	26 (24.5)	0.7642
Perimenopausal	2 (16.7)	13 (12.3)	0.6493
Postmenopausal	5 (41.7)	67 (63.2)	0.2114
Presenting complaint			
PMB	4 (33.3)	59 (55.7)	0.2115
HMB	4 (33.3)	28 (26.4)	0.7327
IMB	1 (8.3)	12 (11.3)	>0.9999
Subfertility	2 (16.7)	1 (0.9)	*0.0270
Incidental Finding	1 (8.3)	6 (5.7)	0.5378
Parity			
Nulliparous	4 (33.3)	22 (20.8)	0.2968
1-4	8(66.7)	71 (67.0)	>0.9999
≥5	0	3 (2.8)	>0.9999
Unknown	0	10 (9.4)	

Continued.

BMI			
Mean	30.9	39.0	
≤20	0	1 (0.9)	>0.9999
21-25	3 (25.0)	5 (4.7)	0.9183
26-30	0	5 (4.7)	>0.9999
31-35	3 (25.0)	7 (6.6)	0.2073
36-40	2 (16.7)	17 (16.0)	0.9822
>40	0	16 (15.1)	>0.9999
Unknown	4 (33.3)	55 (52.0)	
Co-morbid factors			
Diabetes Mellitus	1 (8.3)	20 (18.8)	0.6904
PCOS	1 (8.3)	7 (6.6)	0.5877
HRT Use	1 (8.3)	8 (7.5)	>0.9999
≥ 2 of above	1 (8.3)	2 (1.9)	0.2772
Index EH biopsy sample (WHO94)			
Complex atypical hyperplasia (CAH)	4 (33.3)	18 (17.0)	0.2332
Complex hyperplasia (CH)	5 (41.7)	23 (21.7)	0.2962
Simple hyperplasia (SH)	1 (8.3)	51 (48.1)	*0.0166
Hyperplastic polyp (HP)	2 (16.7)	14 (13.2)	0.6659
Index EH biopsy sample (EIN/WHO2014) *			
Endometrial intraepithelial neoplasia (EIN)	10 (83.3)	41 (38.7)	**0.0044
EIN-EMP	0	3 (2.8)	>0.9999
Hyperplasia without atypia (HwA)	0	50 (47.2)	**0.0011
Hyperplastic polyp (HP)	0	6 (5.7)	>0.9999
Malignant^	1 (8.3)	0	0.7327
Benign	1 (8.3)	6 (5.7)	0.5378
Endometrial cancer subtype	All endometrioid	-	
FIGO Stage (Pre-2009)			
1A	5 (41.7)	-	
2A	2 (16.7)	-	
1B	3 (25.0)	-	
2B	2 (16.7)	-	
Clinical outcome			
Alive without disease	10 (83.3)	-	
Dead from disease	1 (8.3)	-	
Dead from other cause	1 (8.3)	-	
Median follow-up (mean, SD), days	3485 (3180, 1383)	3673 (3744, 522)	

*Consensus review by two gynaecological pathologists using EIN/WHO2014 criteria. ^Upgraded to a malignant index biopsy sample, despite an original index diagnosis of CAH using WHO94. EIN-EMP = endometrial intraepithelial neoplasia in a polyp. Statistical analysis performed using the 2-sided Fisher's exact test to determine statistical differences between the categorical data and a two-tailed unpaired t-test used to compare the means of the continuous data, for those with EIN and those with HwA. *$p<0.05$, **$p<0.01$

3.4.8.1 Malignant outcome by hyperplasia classification system

Table. 3-8 details the progression of EH to EC in this study, broken down according to the classification system used. Using the initial WHO94 index diagnosis, the progression rate to EC was 17.40 % (4/23) for CAH and 8.42 % (8/95) when atypia was not present. Using the EIN/WHO2014 classification system, 19.23 % (10/52) of patients with EIN were later diagnosed with EC, contrasting with 1.56% (1/64) for a non-EIN diagnosis. n=2 of the index EHs biopsies reclassified using EIN/WHO2014 were deemed to be malignant specimens, only n=1 of these was found to have an EC at hysterectomy during the follow-up period.

Table 3-8: Disease progression of endometrial hyperplasias by World Health Organization (WHO94) and Endometrial Intraepithelial Neoplasia (EIN/WHO2014) classification schemes.

Index WHO94 Classification	Patients	Consensus EIN/WHO2014 Classification, patients					
		Progression to malignancy					
		Yes			No		
		EIN[$]	Non-EIN[#]	Malignant	EIN[$]	Non-EIN[#]	Malignant
Complex atypical hyperplasia (CAH)	23 (20.0)	3 (25.0)	0	1 (8.3)	16 (15.1)	3 (2.8)	0
Complex hyperplasia (CH)	29 (24.8)	5 (41.6)	0	0	12 (11.3)	10 (9.4)	0
Simple hyperplasia (SH)	51 (43.2)	1 (8.3)	0	0	6 (5.7)	44 (41.5)	0
Hyperplastic Polyp (HP)	15 (11.2)	1 (8.3)	1 (8.3)	0	8 (7.6)	6 (5.7)	1 (0.9)
Total		10 (83.3)	1 (8.3)	1 (8.3)	42 (38.7)	63 (59.4)	1 (0.9)
Overall Totals	**118***	**12 (10.2)**			**106 (89.8)**		

Numbers in each column are based on classification of a single H&E stained section of endometrial tissue from n=118 women. Percentages in brackets. *Less than the overall n=125 original EH patients; n=7 patients excluded as they were lost to follow-up immediately after their initial index biopsy (moved NHS health board or to the private sector for treatment/follow-up). [$]EIN represents all EIN and EIN-EMP. [#]Non-EIN represents all HwA, HP without EIN and atrophic/benign endometrium.

3.4.8.2 Sensitivity and specificity of a malignant outcome by EH classification system

When comparing the WHO94 classification system with the EIN/WHO2014 system, a diagnosis of EIN more often correctly predicted a malignant outcome (EIN sensitivity 91.0 %) than a diagnosis of complex atypical hyperplasia (CAH sensitivity 33.3 %) (Table. 3-9). The specificity of both classification systems to correctly predict a non-malignant outcome favoured the WHO94 system (specificity 82.1 %), since the EIN/WHO2014 system demonstrated a higher rate of 'false positives', i.e. those diagnosed as EIN who did not develop a malignancy during the follow-up period (n=42, Table. 3.8).

The EIN/WHO2014 system was excellent in predicting the absence of malignant progression (negative predictive value, of 98.4 %), i.e. a non-EIN diagnosis demonstrated a higher probability of being associated with a non-malignant outcome than a non-CAH diagnosis. Both systems displayed similarly low positive predictive values, i.e. a premalignant diagnosis (EIN or CAH) associated with a subsequent malignant outcome, reflecting the overall low prevalence of subsequent malignancy within the cohort.

Table 3-9: Prediction of a malignant outcome following a biopsy diagnosis of endometrial hyperplasia. Comparing WHO94 CAH WHO2014 EIN, in terms of progression to malignancy in this study.

	WHO94	**EIN/WHO2014**
	CAH	EIN
% Sensitivity (95% CI)	33.3 (13.8-61.0)	91.0 (62.3-99.5)
% Specificity (95% CI)	82.1 (73.7-88.2)	60.0 (50.4-68.7)
% Positive predictive value (95% CI)	17.4 (7.0-37.1)	19.2 (10.8-31.9)
% Negative predictive value (95% CI)	91.6 (84.3-95.7)	98.4 (91.7-99.9)

NB/ EIN incorporates EIN (n=49) and EIN-EMP (n=3).

3.4.8.3 An EIN/WHO2014 diagnosis of EIN improves the prediction of a malignant outcome compared with a WHO94 diagnosis of Complex Atypical Hyperplasia.

As already stated, EC occurrences in this study were most often seen within the first 12-months of an initial EH biopsy diagnosis (10/12). Figure 3-14 demonstrates Kaplan-Meier 'survival-curves' detailing the percentage (y-axis) of patients with EH remaining cancer-free during the follow-up period (x-axis), subdivided into, Figure 3-14A: those with CAH (highest risk category for EC progression in WHO94) vs. non-CAH and Figure 3-14B: EIN (highest risk category for EC progression in WHO14/EIN) vs. non-EIN. The median (mean, SD) follow-up period was 3485 days (3180 days, 1383 days). Statistical analysis of the curves using a Log-rank (Mantel-Cox) test demonstrated a statistically significant difference between the curves for EIN vs. non-EIN (10.41, p=0.0013**), compared with CAH vs. non-CAH (2.115, p=0.145 ns). This suggests that in this study an EIN diagnosis, as part of the WHO2014/EIN classification system, better identifies those at risk of future EC than the CAH category in the WHO94 classification system. In this study an EIN diagnosis carried a 13x higher chance of a subsequent or concurrent EC than a non-EIN diagnosis (Hazard ratio (HR) 13.37, 95 % CI 4.05-44.13) over the follow-up period, compared to a CAH diagnosis which had a 3x higher chance of a subsequent or concurrent EC than a non-CAH diagnosis (Hazard ratio, (HR) 3.029, 95 % CI 0.68-13.49).

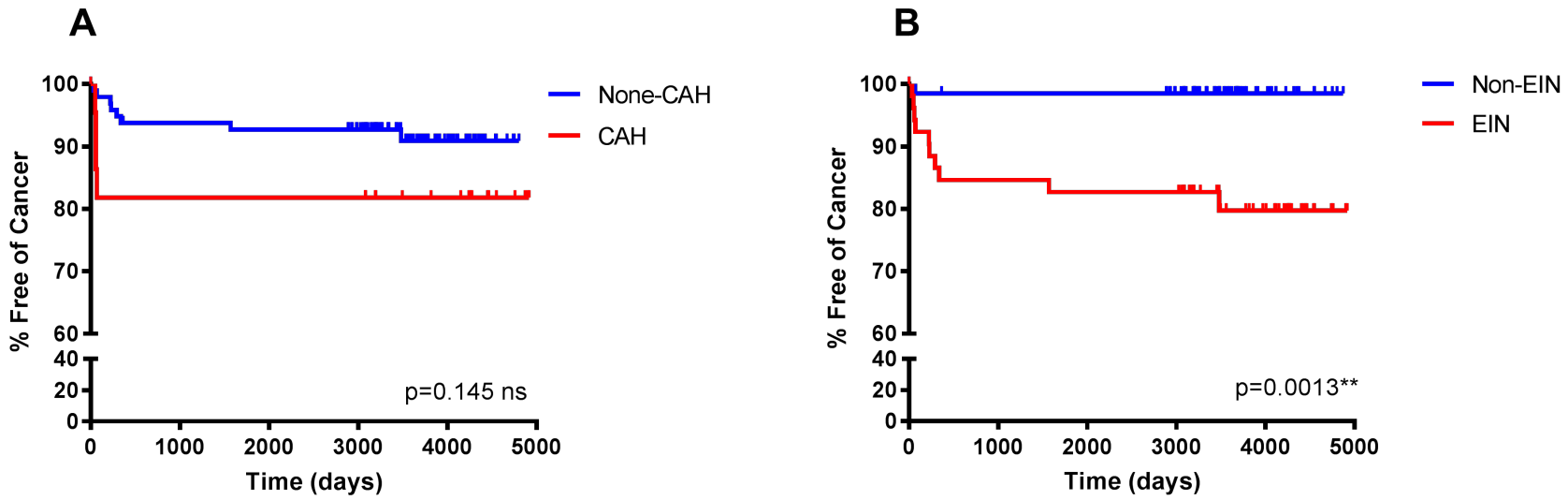

Figure 3-14: Kaplan-Meier curves to demonstrate the percentage of endometrial hyperplasia patients free of cancer during follow-up when classified using the WHO94 compared with the EIN/WHO2014 classification systems. Median follow-up period (mean, SD) 3485 days (3180 days, 1383 days). A) The original diagnostic classification of the patients in this study utilised WHO94 criteria. Percentage cancer-free time was not statistically significantly different between those with a WHO94 diagnosis of CAH vs those with a non-CAH diagnosis, Log-Rank (Mantel-Cox) 2.115, p=0.145 ns, HR 3.029 (95% CI 0.68-13.49). B) Consensus reclassification of the same EH cohort of patients utilising EIN/WHO2014, revealed a statistically significant difference in the percentage cancer-free time between those reclassified to an EIN diagnosis vs those reclassified to a non-EIN diagnosis, Log-Rank (Mantel-Cox) 10.41, p=0.0013**, HR 13.37 (95% CI 4.05-44.13). NB/ Non-CAH incorporates patients with CH (n=29), SH (n=51) and HP (n=15). EIN incorporates EIN (n=49) and EIN-EMP (n=3). Non-EIN incorporates patients with HwA (n=50) HP without EIN (n=6) and atrophic/benign endometrium (n=8).

3.5 Discussion

The incidence of EC within the United Kingdom has increased across all adult female age ranges since the early 1990s (Cancer Research UK, 2018). Having previously been considered a predominantly postmenopausal disease, a notable increase in EC incidence is now seen within younger age groups. A 36 % increase in incidence rate was observed in 25-49-year-old women during the period 1993-2015 within the UK (Cancer Research UK, 2018). A driving factor for this increase is the current unprecedented level of obesity, with an estimated 34 % of all UK ECs linked with being overweight or obese (Parkin and Boyd, 2011). Meta-analysis data suggests that the risk of EC is 81 % higher per 5-unit BMI gained during adulthood (Stevens *et al.*, 2014). Longer menstrual lifespans, diabetes mellitus and polycystic ovarian syndrome (PCOS) have also been demonstrated to be significant EC risk factors (Dossus *et al.*, 2010; Komm and Mirkin, 2014; Luo *et al.*, 2014). All these factors are creating unique challenges both diagnostically and therapeutically. In addition, with the 'gold-standard' treatment for EC being hysterectomy and younger women potentially wishing to preserve fertility, there exists an unmet need for personalised EC risk prediction (Wan *et al.*, 2016).

Advancing understanding of the hyperplastic endometrium and the pre-malignant stages of EC development are essential if we are to devise strategies to improve earlier EC diagnosis, enable appropriate risk stratification of women and allow for timely therapeutic interventions. Diagnostic classification of endometrial hyperplasia (EH) is currently in a state of transition from the legacy four-class WHO94 system to the newer two-class EIN/WHO2014 system. The current study sought to establish and retrospectively phenotype a human EH tissue resource to; i) investigate interobserver variability between the WHO94 and EIN/WHO2014 classification systems and ii) evaluate within this cohort, the ability of each system to predict subsequent endometrioid EC progression.

In preparing the samples for the EH tissue resource described herein it became immediately apparent that EH tissues are very heterogeneous by nature, since a significant spectrum of endometrial architectural and cytological variants were observed during the initial light-microscopy assessment. At one end of the spectrum were tissues with regions of slight glandular crowding and large cystically dilated endometrial glands, whilst at the other end were tissues with nearly 'back-to-back' glands and markedly abnormal nuclei, almost bordering on the appearances of carcinoma. In the past, several terms have been utilised in an attempt to define these observed features and capture the differences in morphological severity across the spectrum, for example, 'adenomatous hyperplasia,' and 'carcinoma *in situ*'

(Chandra *et al.*, 2016; Ellenson *et al.*, 2011). The overall aim being to pathologically classify EH lesions and to correlate the microscopic features with patient outcomes and clinical treatments.

The endometrium is a dynamic, multicellular tissue structure that undergoes hormonally driven cyclical proliferation, shedding and rapid healing (reviewed in Jabbour *et al.*, 2006). This renders a consistently 'normal' or 'control' reference state difficult to establish (Ellenson *et al.*, 2011). This is especially true for perimenopausal women (a high-risk group for EH development) who will often have erratic menstrual cycles. As described herein, several morphological mimics of EH are commonly observed and the diagnosing pathologist needs to be aware of the confounding effect that the cycling endometrium can have on the appearances of EH, especially in pre/peri-menopausal women e.g. the mimic effects of secretory endometrium. In addition, the effect of both endogenous and exogenous steroid hormones, e.g. progesterone, also need to be considered. Progesterone is used either as a single agent or combined with oestrogen as part of medical contraceptives, in addition to itself being a medical therapy for EH treatment (Gallos *et al.*, 2016). Within this study the effect of progesterone on the hyperplastic endometrium was noted to cause a pseudodecidualised pattern and the affected endometrial glands displayed a secretory phenotype. These features are predominantly seen following recent commencement of progesterone, i.e. when the endometrium is still 'oestrogen-primed' (Rex and Bentley, 2009). After prolonged use of progesterone an atrophic glandular appearance would typically be expected, due to downregulation of both the oestrogen and progesterone receptors (Critchley *et al.*, 1998; Rex and Bentley, 2009).

As discussed above the aim of the pathological classification of EHs is to permit correlation with patient outcomes and facilitate appropriate clinical treatments. However, how does one go about categorising a lesion so heterogeneous by its very nature? This is a question with which pathologists have grappled for decades (Beutler *et al.*, 1963). The WHO94 classification was one of the first systems to assess both architectural and cytological changes within EH lesions and link these categories to clinical outcome data for their risk of EC progression (Kurman *et al.*, 1985; Scully *et al.*, 1994). A striking feature of the data generated during the course of this chapter was the finding of poor interobserver variability within the WHO94 system, not only between the original index diagnoses and the expert review, but also between the diagnoses of the two expert pathologists. This was surprising given that they are both highly experienced in the evaluation of endometrial tissues. These data support the findings of others who have previously assessed interobserver variability with the WHO94

classification system (Kendall *et al.*, 1998; Skov *et al.*, 1997). Although the WHO94 classification contains four separate EH categories (simple or complex hyperplasia, with or without atypia), very few researchers analyse all four categories as originally described (Usubutun *et al.*, 2012). Simple atypical hyperplasia (SAH) is very rarely reported and has such low interobserver reproducibility scores (Kappa (*k*), 0.06–0.08), that some question its clinical relevance as a diagnostic category (Bergeron *et al.*, 1999; Kendall *et al.*, 1998; Skov *et al.*, 1997). Furthermore, assessment of cytological atypia is often problematic. As described herein, the presence of atypia is not always uniform across an EH lesion and subcategories of atypia grading are frequently applied to the WHO94 system. This becomes challenging for the treating gynaecologist, for example, should 'mild atypia' be treated the same as 'severe atypia'? Whilst the finding of both should warrant consideration of hysterectomy (dependent on patient wishes, comorbid status and fertility desires), the adjective 'severe' evokes a greater sense of urgency than 'mild'. Whilst higher atypia grades may be a subliminal tactic of the reporting pathologist to infer urgency, "I highly suspect that there may be an EC within this uterus that is not evident to me in the biopsy," it nevertheless creates added confusion within a classification system that already does not straightforwardly correlate with available treatments, i.e. medical, surgical or conservative. Subjective atypia grading may also contribute to a tendency for surgical overtreatment due to the fear of malignant progression for lesions with no underlying sinister mechanism (Baak *et al.*, 2001). For example, nuclear rounding, enlargement and vesicular change as seen in metaplasia, can suggest cytological atypia, but this metaplastic change should not be construed as true atypia since it has not been shown to affect clinical outcome (Hendrickson and Kempson, 1980).

The endometrial collaborative group (an informal affiliation of pathologists) published recommendations in 2000, advocating a move away from the WHO94 system of EH classification (Mutter, 2000). Summarising pertinent advances in the understanding of the evolution of premalignant disease, they introduced the concept of Endometrial Intraepithelial Neoplasia (EIN) as a monoclonally derived premalignant endometrial lesion, distinguishable as a separate entity from both endometrioid EC and from hormonally reactive hyperplastic endometrial tissue (Baak and Mutter, 2005; Mutter, 2000; Mutter *et al.*, 2001). The concept of EIN signalled a paradigm shift from the previously held notion that unopposed oestrogenic stimulation (discussed in chapter 1) causes ever-increasing hyperplastic endometrial proliferation, with accumulating cytological atypia leading to the development of endometrioid EC (reviewed in Sanderson *et al.*, 2017). The EIN concept recognises the importance of unopposed oestrogenic stimulation but distinguishes this from the separate

event of a mutationally activated clone developing within an oestrogenic background (Mutter, 2000; Mutter *et al.*, 2007; Owings and Quick, 2014). Moreover, a diagnosis of EIN is made upon observation and confirmation of defined diagnostic criteria (Table. 3-1) which can be determined from a H&E stained tissue section. Several studies have published findings suggesting that use of EIN improves diagnostic reproducibility (Hecht and Mutter, 2006; Usubutun *et al.*, 2012).

Certainly, within this study we have demonstrated that interobserver variability is improved following the application of EIN diagnostic criteria (Table. 3-1) when compared with the WHO94 system within the same set of EH samples. However, we did not see the large increases in reproducibility scoring that have been proposed by others. For example, Usubutun and colleagues investigated 62 EH samples concordantly diagnosed by three experts using EIN criteria (Usubutun *et al.*, 2012). They proceeded to use a panel of 20 reviewing pathologists (self-taught the EIN criteria) to compare to the experts and reported a Cohen's Kappa (k) score of 0.72 between the reviewers and the experts (Usubutun *et al.*, 2012). Interestingly, Usubutun and colleagues conducted hierarchical clustering of their results and suggest that pathologists will fall into one of three groups when diagnosing EH using EIN criteria; i) those offering a balanced approach to EIN *versus* non-EIN, ii) those favoring a benign diagnosis over pre-malignant/malignant and iii) those who favor EIN (Usubutun *et al.*, 2012). The authors refer to the phenomenon of 'splitters *versus* lumpers' when describing the diagnostic 'personality' of a pathologist. A 'lumper' being a pathologist who groups into broad categories, which are more often exaggerated. Whereas a 'splitter' favors precision and prefers to divide into smaller categories that differ in key ways.

Although, the concept of a diagnostic 'personality' may partly offer an explanation as to the smaller increase in reproducibly found within this current study, other factors including place of postgraduate training, departmental practice and years active as a clinician may also contribute. Cofounding histological factors should also not be overlooked, which may influence interobserver variability. An interesting feature noted in the data generated for this chapter was the way in which each expert pathologist approached endometrial polyps. Expert pathologist A classified 12/125 cases as a hyperplastic polyp using WHO94 criteria, whilst 10/125 using EIN criteria. Whereas pathologist B reached the diagnosis of a HP in 4/125 cases in both instances. Endometrial polyp diagnoses can be problematic since polyps themselves have variable gland density and somewhat altered gland cytology (Carlson and Mutter, 2008; Ellenson *et al.*, 2011).

Ordi and colleagues argue that all systems of EH classification suffer from marked interobserver variability, including both the WHO94 and EIN systems (Ordi *et al.*, 2014). The authors unsurprisingly noted that a reduction in the number of categories within a classification system is the only way to increase interobserver reproducibility / Cohen's Kappa (*k*) rating (Ordi *et al.*, 2014). The authors reasoned that EC risk is considerably greater when atypia is present and therefore in order to increase reproducibility a 'dichotomous' classification should be used, segregating 'atypical' hyperplasias from less severe lesions (Ordi *et al.*, 2014). In 2014, the WHO revised their classification of EHs (see chapter 1) and recommended classification of EHs into two groups based upon the presence or absence of cytological atypia, i.e. (i) hyperplasia without atypia (HwA) and (ii) atypical hyperplasia/EIN (Zaino *et al.*, 2014).

As discussed above the data herein describes a modest improvement in interobserver reproducibility with the application of EIN diagnostic criteria. An EIN diagnosis relies on an internal comparison within the tissue in question for cytological assessment. As suggested herein, cases demonstrating interobserver variability are more likely to contain equivocal or ambiguous diagnostic features. We and others recognise that use of the EIN criteria requires a subjective estimate of 'volume percentage stroma' (VPS), with the previously suggested definition of <55% VPS required to diagnose EIN (Table. 3-1) (Baak and Mutter, 2005). This threshold of 55% VPS was determined using a particular technique of computer-assisted morphometry (D-score) (Baak et al, 1988; Baak and Mutter, 2005) that is not in widespread use by gynaecological pathologists across the world. Other image analysis techniques may involve use of different thresholds for the VPS criterion, to be determined by large studies and validation studies using the new technique, such as the TissueGnostics app used in the work described in this chapter, which may require a higher VPS threshold. Subjective estimation of VPS is restricted by the reporting pathologist's judgement of whether the tissue section contains a focus of gland crowding where VPS should be assessed, and then providing an estimate of the extent of that crowding. In practice, most gynaecological pathologists do not use a computer-assisted image analysis technique and can only compare the crowded focus with background appearances (equivalent to comparing the most and least abnormal regions of interest) and judge whether the glands are more crowded in the most abnormal region of interest, but pathologists are not able to accurately quantify such gland crowding with respect to a pre-defined threshold without using an image analysis technique.

We utilised novel quantitative image analysis techniques (TissueGnostics app) to objectively measure intact foci of endometrial glands together with their surrounding stroma, within defined regions of interest (ROI). The data from this study indicate that the process of

searching within an EH tissue sample for a comparator 'background' region to act as a cytological control, whilst creating a 'mental-image' of the clonal focus of concern, does not allow accurate quantitation of VPS levels by the pathologist without computer assistance. This can lead to variability in the estimation of the VPS levels within the clonal focus and may contribute to the differences in levels of interobserver variability seen when using EIN diagnostic criteria.

Ultimately the purpose of EH pathological classification is to identify women who are at a higher risk of progression to EC. Several researchers have attempted to assess the risk of progression from EH to EC, with many of the studies unfortunately lacking robust methodology to permit comparison and ensure validity (Feldman *et al.*, 1995; Sherman and Brown, 1979; Weber *et al.*, 1999). As described in the introduction to this chapter, the 1985 study by Kurman *et al.* is frequently cited for the author's estimation of progression from EH to EC and formed the basis for the widely held opinion that approximately one third of patients with complex atypical hyperplasia (CAH) will eventually develop EC if they do not undergo hysterectomy (Kurman *et al.*, 1985; Lacey and Chia, 2009). As previously discussed, Lacey and colleagues demonstrated that women with both simple and complex EH without atypia, had a 10 % probability of developing EC in comparison to a 40% probability for those with atypical hyperplasia (Lacey, Ioffe, *et al.*, 2008). Researchers utilising the EIN diagnostic criteria have published clinical outcome data to suggest that approximately 40 % of women diagnosed with EIN will have an EC diagnosed within 12 months of index biopsy (Baak, Mutter, *et al.*, 2005; Mutter *et al.*, 2008). Those women who do not develop EC within 12 months are 45x more likely to develop a future EC (Baak, Mutter, *et al.*, 2005).

Baak *et al.* claim that the EIN classification system more accurately predicts progression to EC than the WHO94 system (Baak, Mutter, *et al.*, 2005). However, others report that both EIN and atypical hyperplasia have similar risks of progression to EC when followed-up for 12 months after the index diagnosis (Lacey, Mutter, *et al.*, 2008). Data described herein suggests that within our cohort of women (n=118, less than the original n=125 owing to losses to follow-up) an EIN diagnosis carried a 13x higher chance of subsequent EC than a non-EIN diagnosis, compared to a CAH diagnosis which had a 3x higher chance of a subsequent EC than a non-CAH diagnosis, over a median follow-up period of 9.5 years. Within our cohort 80 % (8/10) cases of EC were diagnosed within 12 months of an index biopsy of EIN. We chose to consider a 12-month cut off for distinguishing between a concurrent EC, 'mis-sampled' on initial biopsy and a genuine progression to a subsequent malignancy. This reflects published data to suggest that approximately 50 % of women who

have a hysterectomy for atypical hyperplasia in the subsequent weeks to months after an endometrial biopsy will be found to have an endometrial carcinoma, reflected a concurrent 'mis-sampled' initial biopsy (Lacey and Chia, 2009). Furthermore, from observational studies the natural progression of EIN/atypical hyperplasia to endometrioid EC is reportedly 4 - 7 years (Ellenson *et al.*, 2011).

Sensitivity and specificity data from this study are in keeping with that described by others (Baak, Mutter, *et al.*, 2005), although we found that the WHO94 system was not as good at predicting the absence of subsequent EC (Negative predictive value, NPV, of 91.6 %) when compared to the EIN/WHO2014 system (NPV 98.4 %).

Another striking feature of the data presented within this chapter is the discord between the numbers of patients diagnosed with a 'high-risk' EH, i.e. those originally diagnosed as CAH, n=23 (WHO94) and those reclassified to EIN, n=52 (EIN/WHO2014). A diagnosis of CAH or EIN should warrant clinical consideration of hysterectomy (Ellenson *et al.*, 2011; Gallos *et al.*, 2016). We have demonstrated that within our cohort, the EIN/WHO2014 classification system improves the prediction of a malignant outcome. However, within this cohort, n=29 additional women would have been offered surgical management under the EIN/WHO2014 system, a question of the potential for surgical over-treatment is therefore raised, especially when considering the lower percentage specificity rate which we found when assessing the EIN/WHO2014 system as a predictor of an EC outcome (60.0 % EIN/WHO2014 *versus* 82.1 % WHO94).

In conclusion, endometrial hyperplasia is an 'umbrella term' representing a uniquely heterogeneous spectrum of morphologically abnormal endometrial lesions. The significance of a diagnosis of EH lies with its associated risk of progression to EC, especially when cytological atypia is evident. Pathological classification of EHs aims to correlate morphological differences with patient outcomes and in so doing, enable appropriate and timely clinical treatments to be actioned. However, translating pathological classification of EHs into clinical management is challenging, since the desire to definitively treat those at high risk of EC needs to be balanced against potential fertility-limiting factors and the morbidity associated with EH treatments.

The data presented herein provide further insight into the diagnostic reproducibility of two EH pathological classification systems; i) the well-known and widely used WHO94 classification and ii) the more recent EIN/WHO2014 iteration, which draws upon molecular data suggesting a monoclonal pattern of development between EHs and ECs. Our findings add

support to the argument that the EIN/WHO2014 classification system increases the level of interobserver reproducibility between pathologists. We suggest however, that this increase may not be as marked as proposed by some researchers and suggest that a potential reason for this rests with the subjective non-quantitative estimates of the volume percentage stromal tissue compartment. This could be improved by the use of computer-assisted image analysis, such as the TissueGnostics app used here, but this would require further larger scale research studies and validation studies. In addition, our findings would suggest that the EIN/WHO2014 system of classification improves upon the WHO94 system when predicting progression to EC. However, we remain cautious, since the potential for surgical overtreatment when utilising the EIN/WHO2014 system of classification requires further investigation in larger prospective studies. In future studies we would wish to add some 'normal' and EC samples to our dataset when undertaking dual, blinded pathological re-classification in order to 'confuse' the assessors to try to further reduce any inherent bias during the reclassification process.

In subsequent studies, we have utilised the retrospectively phenotyped human EH tissue resource developed within this chapter to investigate the potential for diagnostic and prognostic adjuncts to pathological classification and these are described in chapter 4.

Chapter 4

4 Identification of potential diagnostic and prognostic immunohistochemical markers for endometrial hyperplasia

4.1 Introduction

Recent advances in our understanding of the genetic changes detectable within endometrial cancers (EC) are paving the way for a greater understanding of the aetiology of the disease. In a landmark study, The Cancer Genome Atlas (TCGA) Research Network used array and sequencing technologies to provide new insight into the genomic changes found in different EC subtypes, marking an important step forward from the traditional 'type 1' and 'type 2' dichotomous EC classification (discussed in chapter 1). Notably, the TCGA study reported that most endometrioid endometrial cancers (EEC) (the most common histological EC subtype, and strongly associated with a background of endometrial hyperplasia, (EH)) frequently harbour mutations in *PTEN, CTNNB1, PIK3CA, ARID1A* and *KRAS* (Kandoth *et al.*, 2013).

Despite these exciting developments in genomic profiling of EEC, only marginal advances have been made in establishing the molecular changes that might occur in EHs which predispose them to develop as premalignant EC lesions. There are several reasons why this may be the case. Firstly, as discussed previously, when studying the endometrium, the dynamic cyclical changes that take place in cell constituents and hormone-dependent changes in gene expression can make it difficult to characterise a consistently 'normal' or 'control' state against which to measure premalignant change. (Allison *et al.*, 2008; Ellenson *et al.*, 2011). This can be especially challenging in peri-menopausal women (a higher risk EH population) who will often have erratic menstrual cycles. Secondly, as demonstrated in chapter 3, EHs can be very heterogeneous; they may present as focal or diffuse lesions and often exhibit multifaceted architectural and cytological features. An EH lesion may be shed with menses or may regress with progestin treatment or even spontaneously without intervention (Trimble *et al.*, 2012). Furthermore, because of their aforementioned heterogeneity, and the blind manner in which endometrial biopsies are usually obtained (i.e. the Pipelle® endometrial sampler), EH lesions may be grossly under-sampled or missed entirely in a diagnostic specimen (Allison *et al.*, 2008).

Diagnostic reproducibility between EH pathological classification systems also varies, further hampering attempts to evaluate molecular changes within these lesions. As documented in chapter 3, the current study showed that the WHO94 classification suffers from poor reproducibility, a finding also echoed by other research groups (Bergeron *et al.*, 1999; Kendall *et al.*, 1998; Mutter, Baak, *et al.*, 2000). The introduction of the EIN system of EH classification, has been suggested to improve diagnostic reproducibility (reviewed in Sanderson *et al.*, 2017). However, as demonstrated in chapter 3, whilst this system does appear to improve upon the poor reproducibility inherent with the WHO94 classification, it is far from perfect and contains its own limitations, i.e. the subjective assessment of the volume percentage stroma (% VPS).

A number of studies have reported evidence that genomic changes in candidate genes and/or expression of key regulatory proteins may be involved in the development of EH and play a role in its progression to EC (reviewed in Sanderson *et al.*, 2017). Notably, changes in the tumour suppressor gene *PTEN*, a negative regulator of the PI3K/AKT/MTOR pathway, has been investigated by several groups. Loss of function mutations of *PTEN* have been reported in ~80 % of EECs (Daikoku *et al.*, 2008; Hayes *et al.*, 2006; Stambolic *et al.*, 2000). These mutations can lead to the development of a truncated PTEN protein which is detectable using immunohistochemical techniques. PTEN protein regulates cellular proliferation and apoptosis, acting as an antagonist to growth factor-induced intracellular signalling pathways (Kimura, Watanabe, *et al.*, 2004; Upson *et al.*, 2012). PTEN protein expression has been evaluated across the normal menstrual cycle with changes in concentrations occurring in response to changes in the hormonal environment across the different phases (Mutter, Lin, *et al.,* 2000). Evidence for an association with EH and EEC has been inferred from the results obtained using heterozygous *Pten* knockout mice, where all females developed evidence of EH by 6 months of age (Stambolic *et al.*, 2000). In addition, several researchers have investigated immunohistochemical loss of glandular PTEN protein expression within EHs, exhibiting a spectrum of findings and suggesting 38-55 % of EIN lesions contain PTEN protein-deficient glands (Mutter, Lin, *et al.*, 2000; Xiong *et al.*, 2010). Most surprising perhaps, was the discovery that very small foci of PTEN protein–deficient glands are frequently demonstrated within the endometrium of healthy pre-menopausal women (Mutter *et al.*, 2001). These PTEN-null glands appear phenotypically normal upon routine haematoxylin and eosin (H&E) staining and examination using light-microscopy, leading some to designate them as ‘latent-precancers’ and suggest that with further (not fully elucidated) genetic alterations, these glands could develop into pre-malignant lesions (Monte *et al.*, 2010; Mutter *et al.*, 2001, 2014).

Another prominent molecular candidate investigated for a role in progression of EH to EEC is Paired Box 2 Protein (PAX2). PAX2 is a transcription factor involved in embryogenesis and cell proliferation (Shang, 2007). High levels of PAX2 protein expression have been reported in endometrial glands throughout the menstrual cycle (Monte *et al.*, 2010). A role for the *PAX2* gene in the development of EC was suggested by Wu *et al*, who found that *PAX2* is activated by oestrogen and tamoxifen in ECs but not in normal endometrium, and that this activation is associated with cancer-linked hypomethylation of the *PAX2* promoter (Wu *et al.*, 2005). Several immunohistochemical studies have suggested a role for PAX2 in the development of EH, both in isolation and with loss of PTEN (reviewed in Sanderson *et al.*, 2017).

The data from the TCGA EC study identified a group of hypermutated ECs with microsatellite instability (MSI), highlighting the role for deficient DNA mismatch repair (dMMR) in endometrial carcinogenesis. MSI is characterised by defects in the DNA mismatch repair (MMR) system and represents phenotypic evidence that MMR is not functioning normally. Inactivation of any of the MMR genes (including *MLH1, MSH2, MSH6* and *PMS2*) can cause MSI (Poulogiannis *et al.*, 2010). In somatic EC, dMMR is mainly caused by hypermethylation of the *MLH1* promoter, silencing its expression, thus leading to MSI (Simpkins *et al.*, 1999; Woo *et al.*, 2014). Overall, MSI has been suggested to occur in ~25-30 % of somatic EECs (Hecht and Mutter, 2006). Inherited germline MMR gene mutations and subsequent development of dMMR with MSI in tumours are associated with Lynch Syndrome (hereditary non-polyposis colorectal cancer (HNPCC) syndrome). Lynch Syndrome confers an approximately 60 % lifetime risk of developing EC (Bonadona *et al.*, 2011; ten Broeke *et al.*, 2015). Lucas *et al* suggest that the prevalence of abnormal MMR expression in EIN adjacent to a concurrent EC and in patients with isolated EIN is similar to the reported prevalence of Lynch syndrome in EC (Lucas *et al.*, 2018). The group go as far as to suggest screening for Lynch syndrome by testing for abnormal MMR expression in EIN (Lucas *et al.*, 2018).

A further, novel candidate implicated in EH development and progression is Heart and neural crest derivatives expressed transcript 2 protein (HAND2). This transcription factor plays crucial roles during embryological cardiac morphogenesis (VanDusen *et al.*, 2014). In mice, *Hand2* has been shown to be a progesterone receptor-regulated gene and its expression in endometrial stromal cells inhibits epithelial cell proliferation via suppression of several fibroblast growth factors (FGFs) (Li *et al.*, 2011). Minimal data exist describing the expression pattern of HAND2 protein across the menstrual cycle. A comprehensive epigenome-

transcriptome-interactome analysis by Jones *et al*, found HAND2 at the centre of the most highly ranked differential hotspot in EC (Jones *et al.*, 2013), leading them to propose that epigenetic deregulation of HAND2 was a crucial step in endometrial carcinogenesis. They reported that methylation of *HAND2* was increased in pre-malignant endometrial lesions when compared to normal endometrium and that this was associated with a reduction in HAND2 protein expression (Jones *et al.*, 2013).

AT-Rich Interactive Domain-Containing Protein 1A (ARID1A) has emerged from molecular and genomic studies as an important candidate and tumour suppressor in gynaecological malignancies, especially EEC (Mao and Shih, 2013; Wiegand *et al.*, 2010, 2011). ARID1A is a component of the SWItch/Sucrose Non-Fermentable (SWI/SNF) nucleosome remodelling complex (Ayhan *et al.*, 2015). It is required for SWI/SNF complexes to suppress DNA synthesis, and as such *ARID1A* is considered a tumour suppressor gene since it regulates cell proliferation and functions to prevent genomic instability. Mutations of *ARID1A* have been described in 29–40 % of cases of EC (Mao *et al.*, 2013). *ARID1A* mutations are normally insertions or deletions that lead to the formation of a truncated protein detectable by immunohistochemistry.

Tumour Protein p53 is a protein encoded by the *TP53* gene. When cellular DNA is damaged, the p53 protein regulates cell-cycle inhibition and apoptosis which helps in determining whether or not the damaged DNA should be repaired, or the cell destroyed. It is fittingly called 'The Guardian of the Genome'(Lane, 1992). Loss of expression of wild-type p53 due to mutation or gene inactivation leads to malignant transformation (Sherman *et al.*, 1995). In ECs, most *TP53* mutations are missense mutations, generally detected in serous, 'Type 2' ECs, however, they have also been reported in in 2-20 % of EECs (Alkushi *et al.*, 2004; Sherman *et al.*, 1995). *TP53* mutations are associated with formation of a functionally defective p53 protein that is more stable and has a longer half-life than the wild-type p53 protein (Sherman *et al.*, 1995; Soong *et al.*, 1996). The missense mutated p53 protein product usually accumulates and is detected as overexpression in cell nuclei using immunohistochemistry. Typically, wild-type p53 in cells cannot be detected by immunohistochemistry; however, if p53 is stabilised, due to overexpression in normal cells in response to DNA damage, a positive immunohistochemistry reaction (usually focal, weak and heterogeneous) can be detected in the absence of any mutation (Soong *et al.*, 1996). To further complicate matters, deletions or frame-shift mutations of *TP53* can lead to a truncated/altered protein that lacks epitopes recognized by specific antibodies so a completely negative p53 immunohistochemistry reaction may also indicate a gene abnormality (Garg *et al.*, 2010).

In summary, current histological classification alone is unable to accurately predict which EH cases will progress to EEC and therefore accurate prognosticators are required. Having surveyed the available literature, some of which is summarised above, we would hypothesize that moving forwards, a collective 'panel' approach of multiple candidates may provide greater diagnostic and prognostic value than can currently be achieved by any single candidate in isolation. With this in mind, we have selected several prominent immunohistochemical markers from the current available literature (reviewed in Sanderson *et al,* 2017), spanning several facets of EEC carcinogenesis for investigation within the retrospective human endometrial hyperplasia tissue resource established in chapter 3.

4.2 Aims of the chapter

1) To establish the immunohistochemical expression pattern of the proteins PTEN, PAX2, ARID1A, MMR (MLH1, MSH2, MSH6, and PMS2), HAND2 and p53 within a retrospective human EH tissue resource classified using the EIN/WHO2014 diagnostic system.
2) To evaluate the above putative immunohistochemical markers with respect to their:
    i. Utility as diagnostic markers for EH
    ii. Association with progression of EH to endometrioid endometrial cancer.

4.3 Materials and methods

4.3.1 Human endometrial hyperplasia tissue resource

A human EH tissue resource was created as detailed in 2.1.2 This EH resource was pathologically classified according to the EIN/WHO2014 diagnostic system (Table. 3-1) and as detailed in 3.3.3. A total of 105 EH tissue samples were utilised. Endometrial Intraepithelial Neoplasia (EIN) was diagnosed in 51/105 cases and hyperplasia without atypia (HwA) in 54/105 cases. Serial sections of FFPE tissue were obtained (2.1.2).

4.3.2 MRC-CIR archival human endometrial tissue

Experimental control and optimisation tissues were obtained as described in 2.1.1.

4.3.3 Immunohistochemistry

Chromogenic Immunohistochemistry using detection with 3, 3 -diaminobenzidine (DAB) was performed as described in section 2.3 employing the ImmPRESS™ polymerised reporter enzyme staining system (described in 2.3.5): positive staining resulted in a brown colour reaction. A list of the primary antibodies used within this chapter can be found in Table 4-1 along with details of the corresponding ImmPRESS™ polymer detection system.

Antibody dilutions factors were optimised using archival human endometrial hyperplasia tissue, obtained as per 2.1.1. A no-primary antibody control was used to detect false-positive or background staining as a result of non-specific binding of the ImmPRESS™ regent. Appropriate positive control tissue was used as necessary and as recommended by the antibody manufacturer (antibodies marked with a * in Table 4-1 did not require a separate positive control tissue as the endometrial stromal cells were used as a positive internal control).

4.3.3.1 Automated immunohistochemistry

As described in 2.3.8, a reduction in antigenicity can cause a reduction in signal intensity and increase non-specific background staining. High-throughput automated immunohistochemistry was therefore performed to detected PTEN protein expression in this study (described in 2.3.8). Antibody concentrations were first optimised using the method described in 4.3.3 and validated literature protocols, prior to being performed on the Leica BOND-MAX (Leica Biosystems) robotic staining platform.

4.3.3.2 Image analysis

All immunohistochemical stained tissue sections were whole-slide scanned as described in 2.6 to create digital reference library.

Table 4-1: Primary antibodies and detection systems used for chromogenic immunohistochemistry

Antigen	Species	Supplier	Cat. No	Dilution	ImmPRESS™ polymer
Anti-PTEN (clone 6H2.1)*	Mouse (Monoclonal)	Agilent Dako	M362729-2	1:300	ImmPRESS™ Anti-Mouse (Vector MP 7402) - DAB
Anti-PAX2 (clone Z-RX2)	Rabbit (Polyclonal)	Invitrogen	71-6000	1:900	ImmPRESS™ Anti-Rabbit (Vector MP 7401) - DAB
Anti-ARID1A*	Rabbit (Polyclonal)	Sigma-Aldrich	HPA005456	1:2000	ImmPRESS™ Anti-Rabbit (Vector MP 7401) - DAB
dHAND (clone M-19)	Goat (Polyclonal)	Santa-Cruz	sc-9409	1:250	ImmPRESS™ Anti-Goat (Vector MP 7405) – DAB
p53 (clone DO7)	Mouse (Monoclonal)	Santa-Cruz	sc-126	1:500	ImmPRESS™ Anti-Mouse (Vector MP 7402) - DAB
MLH1 (clone C-20)	Rabbit (Polyclonal)	Santa-Cruz	sc-582	1:100	ImmPRESS™ Anti-Rabbit (Vector MP 7401) - DAB
MSH2 (clone FE11)	Mouse (Monoclonal)	Millipore Merck	MABE284	1:500	ImmPRESS™ Anti-Mouse (Vector MP 7402) - DAB
MSH6 (clone 44)	Mouse (Monoclonal)	BD Biosciences	610919	1:250	ImmPRESS™ Anti-Mouse (Vector MP 7402) - DAB
PMS2 (clone A16-4)	Mouse (Monoclonal)	BD Pharmingen	556417	1:300	ImmPRESS™ Anti-Mouse (Vector MP 7402) - DAB

*Internal positive control present within endometrial tissues.

4.3.4 Scoring of immunohistochemical staining

Scoring of immunohistochemical staining patterns for all tissue was performed as follows. Unless otherwise stated scoring was performed on the stained tissue section slides by Professor Alistair Williams (Professor of Gynaecological Pathology, The University of Edinburgh 'AW') with myself ('PS').

4.3.4.1 Scoring of Phosphatase and Tensin Homolog (PTEN) staining in endometrial hyperplasia tissues

Endometrial hyperplasia samples stained for PTEN protein were scored using a modified method based upon that described by Mutter *et al* (Mutter, Lin, *et al.*, 2000). In brief, PTEN immunoreactivity was evaluated within the endometrial glandular and stromal cells of an entire EH tissue section. A result of PTEN 'positive' was recorded if the entire tissue section contained endometrial glands and stromal cells which demonstrated a brown (3, 3 – diaminobenzidine (DAB)) nuclear and cytoplasmic staining pattern. The stromal cells served as a positive internal control. A result of 'isolated null glands' was recorded if ≤ 2 endometrial glands in close proximity within the tissue section demonstrated loss of both glandular nuclear and cytoplasmic brown DAB staining, resulting in a blue appearance of the nuclei (due to the haematoxylin counterstain), in addition to positive brown DAB nuclear staining within the stromal cells. A result of a PTEN 'null region' was recorded if a focal region of endometrial glands (>2 glands) within the tissue section demonstrated loss of glandular nuclear and cytoplasmic brown DAB staining, in addition to positive brown DAB nuclear staining within the stromal cells. The scoring descriptors were translated into a plain numerical value as per table 4-2 for the purposes of hierarchical agglomerative clustering (HAC) analysis.

4.3.4.2 Scoring of Paired Box 2 Protein (PAX2) staining in endometrial hyperplasia tissues

Endometrial hyperplasia samples stained for PAX2 protein were scored using a modified method based upon that described by the Mutter group (Monte *et al.*, 2010; Quick *et al.*, 2012). In brief, PAX2 immunoreactivity was evaluated within the endometrial glandular cells of an entire EH tissue section. A result of PAX2 'positive' was recorded if the entire tissue section contained endometrial glands which demonstrated a brown nuclear (3, 3 – diaminobenzidine (DAB)) staining pattern. A result of 'null glands' was recorded if small

isolated clusters of endometrial glands in close proximity within the tissue section demonstrated loss of glandular nuclear brown DAB staining, resulting in a blue appearance of the nuclei (due to the haematoxylin counterstain). A result of a PAX2 'altered expression' was reported if large foci of endometrial glands or the entire population of glands within the tissue section, demonstrated loss of glandular nuclear brown DAB staining. The scoring descriptors were translated into a plain numerical value as per table 4-2 for the purpose of HAC analysis.

4.3.4.3 Scoring of Heart and Neural Crest Derivatives-expressed 2 (HAND2) protein staining in endometrial hyperplasia tissues

Firstly, in order to reduce inherent scoring bias, whole-slide scanned H&E stained sections of EH tissue were digitally annotated with two regions of interest (ROI) as described in 3.3.4. Each ROI corresponded to either the 'most abnormal' or the 'least abnormal' region within the EH tissue section as described in 3.3.4. Utilising the NDP.view2 (Hamamatsu, U12388-01) imaging software, each ROI was exactly digitally copied from the H&E scanned image on to a corresponding serial section that had been stained for HAND2 and subsequently slide-scanned. Each ROI was then 'blinded' by randomly assigning a designation of either 'Area 1' or 'Area 2'. The pathological classification / diagnosis of each 'Area' was known to only 'PS' and 'AW'.

Endometrial hyperplasia samples stained for HAND2 protein were scored using a modified method based upon that described by Buell-Gutbriod *et al* (Buell-Gutbrod *et al.*, 2015). Briefly, three members of the Saunders laboratory group (Ioannis Simitsidellis ('IS'), Phoebe Kirkwood ('PK') and Olympia Kelepouri ('OK') - each member is familiar with normal endometrial morphology but not with EH) were asked to independently score the percentage number of stromal cells demonstrating HAND2 expression for both 'Area 1' and 'Area 2' in each tissue section. The scoring was based solely on the appearances of the endometrial stroma within each area. Any degree of brown (3, 3 –diaminobenzidine (DAB)) staining intensity was deemed as demonstrating HAND2 expression. A score of 0 (absent expression) was given if 0 % of stromal nuclei in the designated area stained brown, 1 (reduced expression) if 1-50 % of the stromal nuclei in the designated area stained brown and 2 (positive) if >50 % of stromal nuclei in the designated area stained brown. The scoring results of 'PK' and 'OK' were compared for consensus agreement. Where a consensus was not reached, the score from 'IS' was used to achieve a 2/3 majority consensus. The scores were then unblinded by 'PS' and compared to their pathological classification / diagnosis for

analysis. The 'most abnormal' ROI score was used for further analysis and the scoring descriptors were translated into a plain numerical value as per table 4-2 for the purposes of HAC analysis.

4.3.4.4 Scoring of mismatch repair (MMR) protein expression in endometrial hyperplasia tissues

Immunohistochemistry for the DNA Mismatch repair proteins (MLH1, MSH2, MSH6 and PMS2) were scored in EH tissues as described by Woo, *et al* (Woo *et al.*, 2014) and in keeping with UK NEQAS recommendations (Arends *et al.*, 2008). All scoring was performed on the stained tissue section slides by Professor Mark Arends (Professor of Pathology and Head of the Division of Pathology, The University of Edinburgh 'MA') with myself ('PS'). Any tissue areas demonstrating evidence of poor fixation were not taken into consideration. Normal human vermiform appendix tissue was used as a positive control as described by Arends, *et al* (Arends *et al.*, 2008).

Table 4-2: Plain numerical scoring of observed immunohistochemical staining patterns.

	Score 0	Score 1	Score 2
PTEN	Positive	Isolated Null Glands	Null Region
PAX2	Positive	Null Glands	Altered Expression
HAND2	Positive (>50 %)	Reduced Expression (1-50 %)	Absent Expression (0 %)

PTEN - Phosphatase and Tensin Homolog, PAX2 - Paired Box 2 Protein, HAND2 - Heart and Neural Crest Derivatives-expressed 2.

4.3.4.5 Scoring of AT-rich interactive domain-containing protein 1A (ARID1A) within human endometrial hyperplasia tissues.

Endometrial hyperplasia samples stained for ARID1A protein were scored using a modified method based upon that described by Ayhan *et al* (Ayhan *et al.*, 2015). In brief,

ARID1A immunoreactivity was evaluated within the endometrial glandular and stromal cells of an entire EH tissue section. A result of ARID1A 'positive' was recorded if the entire tissue section contained endometrial glands and stromal cells which demonstrated a brown nuclear (3, 3 –diaminobenzidine (DAB)) staining pattern. The stromal nuclear cells served as a positive internal control. A result of 'isolated null glands' was recorded if $\leq$ 2 endometrial glands in close proximity within the tissue section demonstrated loss of glandular nuclear brown DAB staining, resulting in a blue appearance of the nuclei (due to the haematoxylin counterstain), in addition to positive brown DAB nuclear staining within the stromal cell nuclei. A result of 'confluent null glands' was recorded if a focal region of endometrial glands (>2 glands) within the tissue section demonstrated loss of glandular nuclear brown DAB staining, in addition to positive brown DAB nuclear staining within the stromal cell nuclei. A result of 'complete expression loss' was recorded if the entire tissue section demonstrated loss of glandular nuclear brown DAB staining, in addition to positive brown DAB nuclear staining within the stromal cell nuclei.

4.3.4.6 Scoring of Tumour protein 53 (p53) within human endometrial hyperplasia tissues.

Endometrial hyperplasia samples stained for p53 protein were scored using the method described by Alkushi, *et al* (Alkushi *et al.*, 2004). In summary, diffuse brown (3, 3 –diaminobenzidine (DAB)) nuclear staining was deemed as demonstrating p53 'overexpression'. Weak, patchy and heterogenous nuclear expression was interpreted as 'Wild-Type' p53 expression. Completely absent nuclear brown DAB staining was regarded as 'aberrant' p53 expression.

4.3.5 RNA extraction

RNA was extracted and quantified as described in section 2.7.

4.3.6 Two-step quantitative real-time reverse transcription polymerase chain reaction (qRT-PCR)

Reverse transcription, quantitative real-time PCR (TaqMan® method) and qPCR analysis was performed as described in section 2.8. *CYC* was used as the housekeeping gene. Primer/probe use for this chapter is listed below (Table. 4-3).

Table 4-3: Primer pair sequences and probes used for qRT-PCR

Gene Name	Accession Code	Primer Sequences	Primer Position / Probe	
HAND2	NM_021973.2	ggtagctttgcagtgagcagt	391-411	19
		gaatccaggggcgagtct	463-480	

4.3.7 Statistical analysis

Statistical analysis was performed using GraphPad Prism 8.0. The two-sided Fisher's Exact test was used to compare between groups for the immunostaining data. For qRT-PCR samples, data were tested for normality (Gaussian distribution) using the D'Agostino & Pearson normality test. If they passed the normality test an ordinary one-way ANOVA with Holm-Sidak's multiple comparison post-test used to compare between groups. If they failed the normality test the nonparametric Kruskal-Wallis test with Dunn's multiple comparison post-test was used to compare between groups.

4.3.7.1 Unsupervised hierarchical clustering analysis

Unsupervised hierarchical agglomerative clustering (HAC) was used to evaluate the correlation of immunohistochemical scoring data with EH diagnosis and also with subsequent malignant progression. Clustering analysis organises the data according to the similarity/dissimilarity of immunostaining profiles, arranging the cases with similar immunoprofiles together in rows in a heatmap. The relationship between EH cases and immunomarkers is displayed graphically as a dendrogram, where the branch length is determined by correlation between immunostaining scores.

Immunohistochemical score data was firstly formatted as described by Liu *et al* (Liu *et al.*, 2002) further to analysis and visualisation using the Cluster and TreeView software platforms respectively, as described by Eisen, *et al* (Eisen *et al.*, 1998). The clustering of the immunohistochemical data was performed using the complete linkage method and the Euclidean distance. Comparison was performed to the average linkage clustering method to assess reproducibility of the cluster groups described. This demonstrated a 75.2 % agreement with a Kappa, *k* score of 0.629 "Substantial". Cohens Kappa, *k*, is a measure of agreement among observers that attempts to correct for chance agreement and whose values are 1.00 or less, where 1.00 indicates perfect agreement and 0 indicates the level of agreement expected by chance alone. Interpret as follows: 0.00–0.20, slight; 0.21–0.40, fair; 0.41–0.60, moderate; 0.61–0.80, substantial; and 0.81–1.00, almost perfect agreement. Chi-squared and Fisher's exact tests were used to determine which EH diagnosis and immunohistochemical markers contributed to the formation of individual clusters.

4.4 Results

4.4.1 Immunohistochemical expression pattern of Phosphatase and Tensin Homologue (PTEN) protein within a human endometrial hyperplasia (EH) tissue resource

Positive PTEN protein expression was visualised as brown DAB staining within the nuclear and cytoplasmic compartments of both the endometrial glandular and stromal cells. A total of 104/105 (99.0 %) EH samples were successfully stained and interpreted. The appearance of the glandular compartment was the primary site of interest for PTEN protein expression. In all cases, stromal cells and blood vessels had intensely positive immunoexpression for PTEN and thus served as positive internal controls. EH samples demonstrating a loss of PTEN glandular protein expression could be readily identified in this study; glands with no PTEN staining were distinct from glands with strong PTEN staining and surrounding stroma (Figure. 4-1). Loss of PTEN protein expression was observed in two distinct patterns: 1) A PTEN null region, where a confluent region of >2 endometrial glands demonstrated widespread loss of nuclear and cytoplasmic brown DAB staining (Figure. 4-1B). The endometrial glands displayed a blue appearance due to haematoxylin counterstaining. 2) Isolated PTEN null glands (Figure. 4-1D & E), where $\leq$ 2 endometrial glands in close proximity demonstrated a loss of both nuclear and cytoplasmic brown DAB staining.

4.4.1.1 Confluent regional loss of PTEN protein expression in endometrial glands is significantly associated with Endometrial Intraepithelial Neoplasia (EIN)

Loss of PTEN protein expression was observed in 61/104 (58.7 %) of the total EH cases examined in this study, with 24/104 (23.1 %) demonstrating a PTEN null region (Figure. 4-1B) and 37/104 (35.6 %) demonstrating isolated PTEN null glands (Figure. 4-1D & E). The finding of a PTEN null region was significantly associated with an EH diagnosis of EIN, with 23/51 (45.1 %) of EIN cases demonstrating a PTEN null region compared to 1/53 (1.9 %) of HwA cases ($p<0.0001$, 2-sided Fisher's exact test), with the abnormal glands demonstrating either features of EIN or HwA showing loss of PTEN immunostaining. The finding of isolated PTEN null glands also significantly differed between the two groups, with EIN cases being significantly less likely to demonstrate isolated null glands 11/51 (21.6 %), compared to HwA cases 26/53 (49.1 %) ($p=0.042$, 2-sided Fisher's exact test). Overall, loss of PTEN protein

expression was not significantly associated with either EH diagnosis, with 34/51 (66.7 %) of EIN cases and 27/53 (50.1 %) of HwA cases demonstrating some degree of loss of PTEN protein expression (p=0.1155, 2-sided Fisher's exact test).

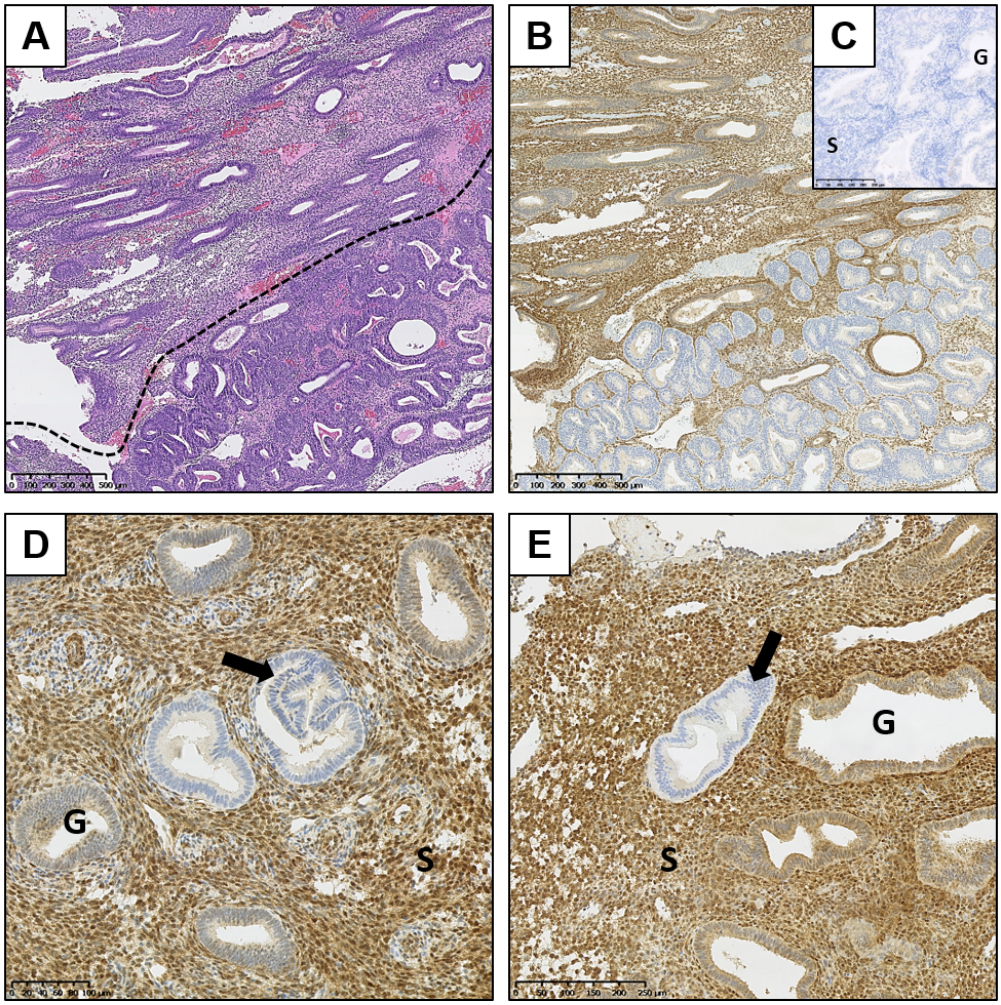

Figure 4-1: **Immunohistochemical expression of PTEN protein within human endometrial hyperplasia (EH) tissue.** A) Haematoxylin and Eosin (H&E) staining of human endometrial tissue containing an area of Endometrial Intraepithelial Neoplasia (EIN) below the dashed line. B) PTEN immunohistochemical staining of a serial tissue section from the same patient as in A. PTEN null glandular region demonstrated by a loss of brown (DAB) nuclear and cytoplasmic staining in the same region corresponding to the EIN lesion as seen in image A. C) Negative control. D&E) Isolated PTEN null glands (arrowed; highlighting glands with loss of brown (DAB) staining) seen within two separate tissue sections diagnosed as hyperplasia without Atypia (HwA). G = representative endometrial gland. S = endometrial stromal; used as a positive internal control for PTEN immunohistochemistry. Varying magnifications – see scale bars.

4.4.2 Immunohistochemical expression pattern of Paired Box 2 Protein (PAX2) within a human endometrial hyperplasia (EH) tissue resource

Positive PAX2 protein expression was detected as any degree of brown DAB staining within the nuclei of the endometrial glands (Figure. 4-2A). All samples (n=105) were successfully stained and interpreted. The endometrial stromal compartment was not used for interpretation. Loss of PAX2 protein expression was observed in two distinct patterns in this cohort of EH samples: 1) PAX2 null glands, where small isolated clusters of endometrial glands demonstrated widespread loss of nuclear brown DAB staining (Figure. 4-2C & D). The null endometrial glands displayed a blue appearance due to haematoxylin counterstaining (Figure. 4-2C). 2) Altered PAX2 expression (Figure. 4-2E), where large foci or the entire tissue section demonstrated a loss of glandular nuclear brown DAB staining. Of note, whilst staining for PTEN allowed for distinct definition of PTEN glands, the positive nuclear staining pattern of PAX2 was observed to have a variable intensity pattern across individual EH lesions which may relate to variation in fixation efficiency.

4.4.2.1 Loss of PAX2 protein expression is significantly associated with a diagnosis of Endometrial Intraepithelial Neoplasia (EIN)

Loss of PAX2 protein expression was observed in 21/105 (20.0 %) of the total EH cases examined in this study, with 15/105 (14.3 %) demonstrating PAX2 altered expression (Figure. 4-2E) and 6/105 (5.7 %) demonstrating PAX2 null glands (Figure. 4-2C & D). The finding of a PAX2 altered expression pattern was significantly associated with an EH diagnosis of EIN, with 15/51 (29.4 %) of EIN cases demonstrating PAX2 altered expression compared to 0/54 of HwA cases ($p<0.0001$, 2-sided Fisher's exact test). The finding of PAX2 null glands was not significantly different between the two groups. Both EIN and HwA cases, n=3/51 and n=3/54 respectively, demonstrated very few regions of PAX2 null glands ($p>0.9999$, 2-sided Fisher's exact test). Overall loss of PAX2 protein expression was significantly associated with an EIN diagnosis, with 18/51 (35.3 %) of EIN cases and only 3/54 (5.6 %) of HwA cases demonstrating some degree of loss of PAX2 protein expression ($p=0.0002$, 2-sided Fisher's exact test), with loss seen in the abnormal glands.

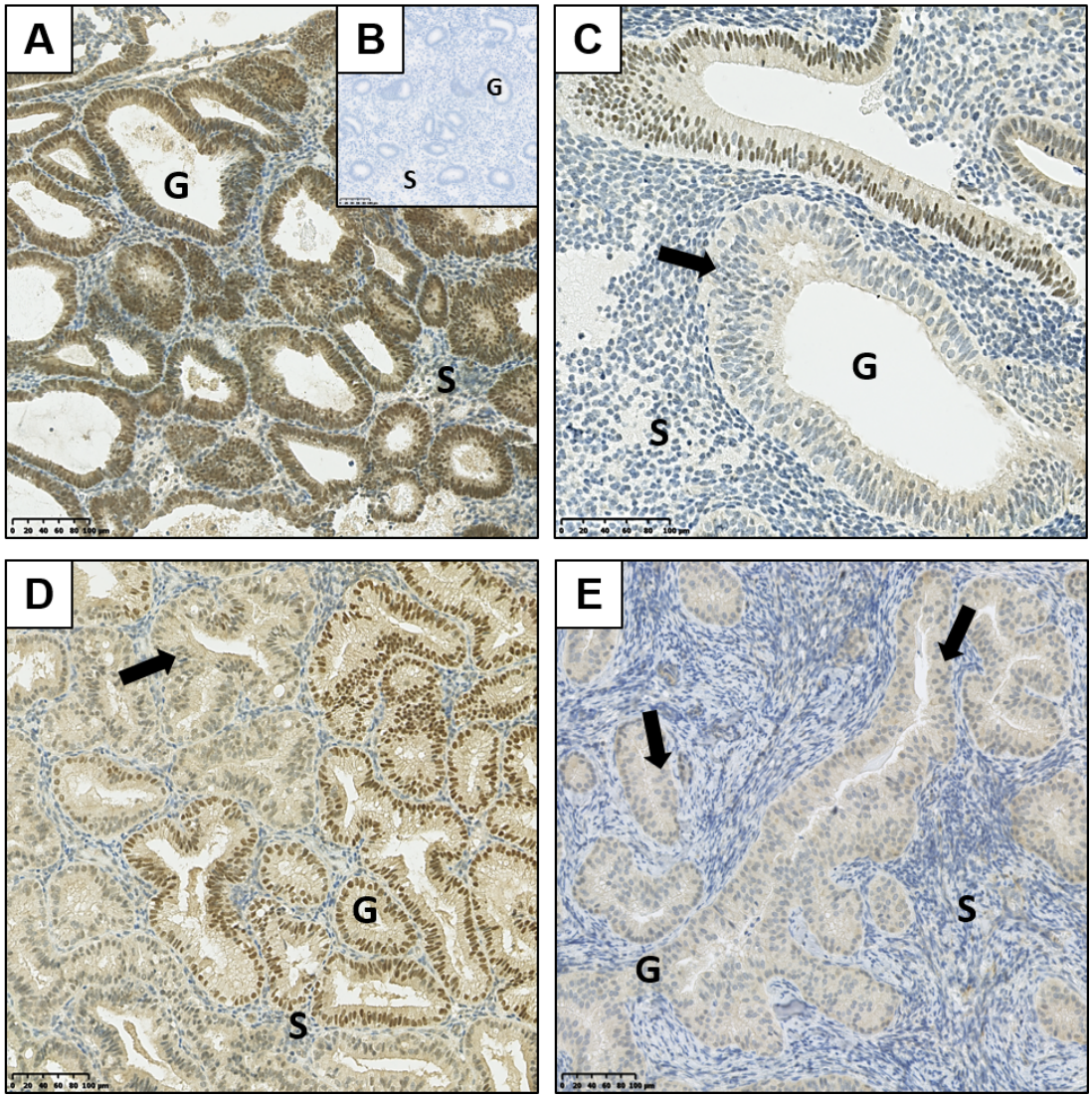

Figure 4-2: Immunohistochemical expression of PAX2 protein within human endometrial hyperplasia (EH) tissue. A) PAX2 immunohistochemical staining of a tissue section demonstrating hyperplasia without atypia (HwA). Positive PAX2 endometrial glands (G = representative endometrial gland) demonstrated by brown (DAB) glandular nuclear staining. B) PAX2 negative control. C) PAX2 null gland (arrow indicating loss of brown DAB glandular nuclear staining) within a tissue section demonstrating HwA. D) PAX2 null glands (arrow indicating loss of brown DAB glandular nuclear staining) within a tissue section demonstrating Endometrial Intraepithelial Neoplasia (EIN). Comparative PAX2 positive glandular area seen to the right side of figure 4-2D with a representative positively stained gland marked as G. E) PAX2 altered expression (arrow indicating loss of brown DAB glandular nuclear staining) within a tissue section demonstrating EIN. S = endometrial stroma, expression of PAX2 in the stromal compartment was not used for PAX2 immunohistochemical interpretation. Varying magnifications – see scale bars.

4.4.3 Expression pattern of Heart and Neural Crest Derivatives-expressed 2 (HAND2) within the normal human endometrium.

In order to establish the expression pattern of HAND2 within the normal human endometrium, *HAND2* mRNA expression was investigated within cycling and non-cycling endometrial tissues by qRT-PCR. In addition, immunohistochemistry was performed on representative samples from across the menstrual cycle to investigate HAND2 protein expression.

4.4.3.1 *HAND2* mRNA expression within the normal human endometrium.

HAND2 mRNA was detected in all samples of normal postmenopausal, proliferative and secretory endometrium. An apparent increase in *HAND2* mRNA expression was demonstrated within the secretory phase, however overall expression was not significantly different between the groups in this small sample set (Figure. 4-3).

4.4.3.2 HAND2 protein expression within the normal human endometrium

HAND2 protein expression was detected by immunohistochemistry within representative tissues from all phases of the menstrual cycle (Figure. 4-4). HAND2 protein expression was detected as any degree of brown DAB staining within the nuclei of the endometrial stromal cells (Figure. 4-4). All representative samples of normal cycling endometrium demonstrated a positive staining pattern with >50 % of the endometrial stromal cells exhibiting HAND2 staining. Of note, endometrial epithelial cells (endometrial glands and luminal surfaces) do not express HAND2 protein and thus HAND2 is a purely stromal cell marker within the human endometrium.

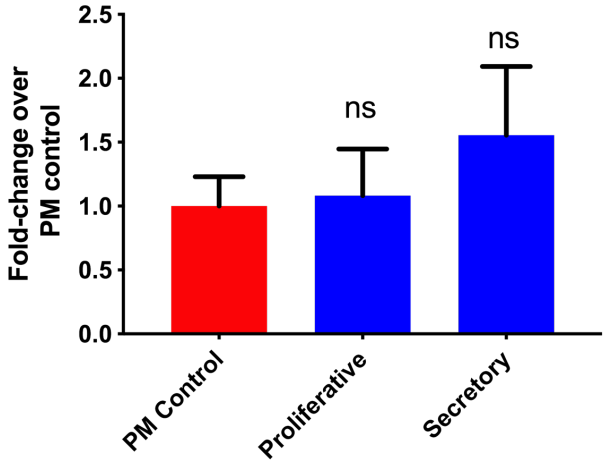

Figure 4-3: Expression of *HAND2* mRNA is not significantly different between normal postmenopausal, proliferative and secretory endometrium. 1) Whole tissue homogenates from hysterectomy specimens of postmenopausal endometrium (n=9), proliferative endometrium (n=5) and secretory endometrium (n=8) underwent qRT-PCR analysis for *HAND2* gene expression. NB/ Early, mid and late secretory endometrial data were pooled for comparison due to the small numbers of samples available. No menstrual endometrial samples were available for comparison. The data are presented as a relative fold-change over postmenopausal endometrium and all data were normalised to the housekeeping gene *CYC*. Kruskal Wallis statistical test. ns=non-significant.

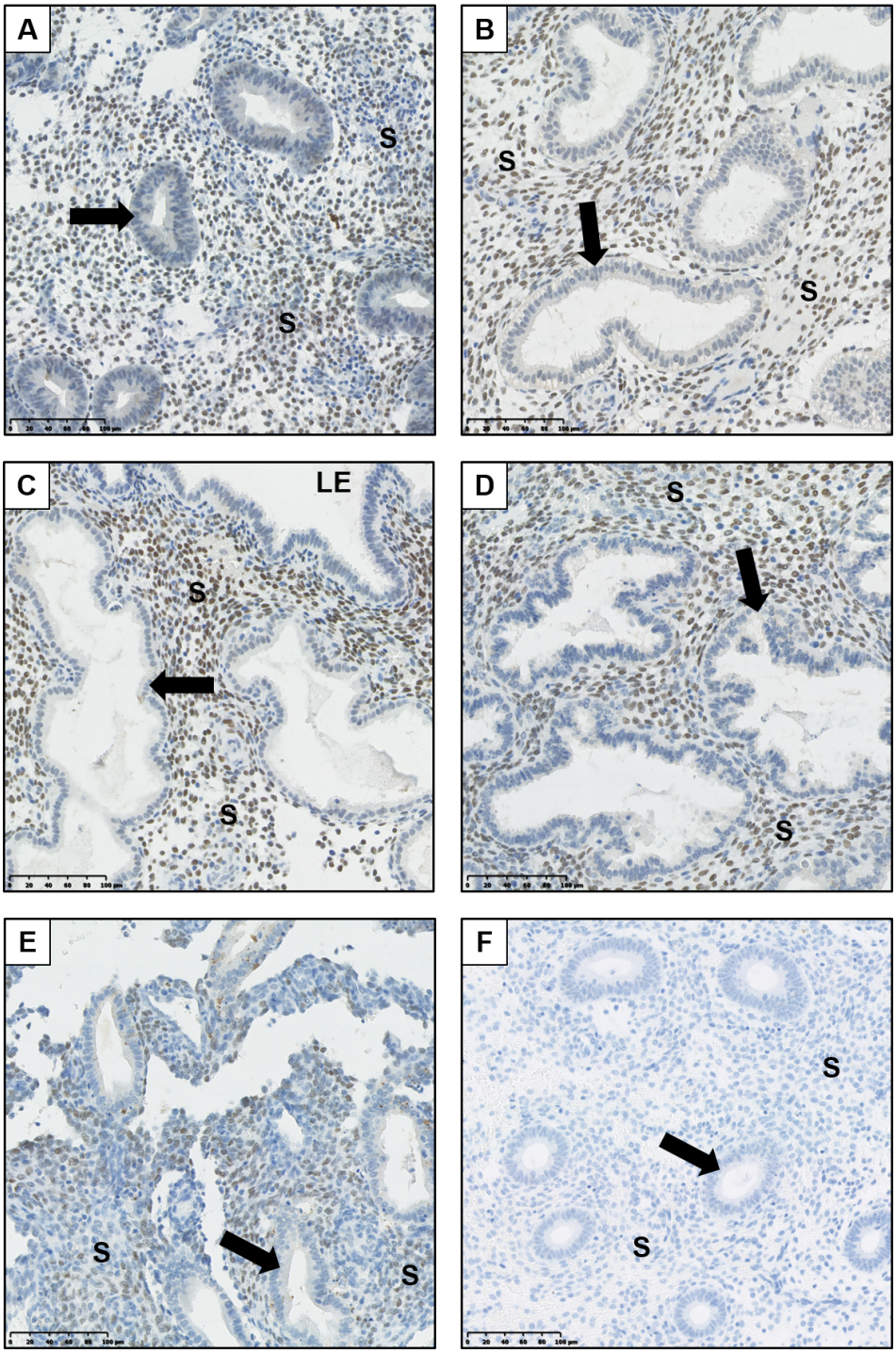

Figure 4-4: Immunohistochemical expression of HAND2 protein within the normal cycling human endometrium. Endometrial Pipelle® biopsy specimens from all phases of the menstrual cycle demonstrate positive stromal nuclear immunohistochemical expression of HAND2 protein. A) Proliferative endometrium, B) Early secretory endometrium, C) Mid-secretory endometrium, D) Late secretory endometrium, E) Menstrual endometrium, F) Negative control (proliferative endometrium). S = endometrial stroma. LE = Luminal epithelium. Arrows highlight representative endometrial glands which do not express HAND2 protein. Varying magnifications – see scale bars.

4.4.4 Heart and Nuclear Crest Derivatives-expressed 2 (HAND2) mRNA and protein expression is reduced in all grades of endometrioid endometrial cancer (EEC).

In order to establish the expression pattern of HAND2 within the malignant endometrium, samples from a human data resource of endometrioid endometrial cancer (EEC) (see 2.1.1) were utilised. *HAND2* mRNA expression was investigated using tissue homogenates from postmenopausal endometrial tissues and samples of EEC previously classified (Collins *et al.*, 2009) as well, moderately or poorly differentiated, (i.e. grades 1-3 EEC respectively) by qRT-PCR. In addition, immunohistochemistry was performed on representative samples from both the postmenopausal endometrium and G1-3 EEC data resource to investigate HAND2 protein expression.

HAND2 mRNA expression was significantly reduced across all grades of EEC when compared to normal postmenopausal endometrium (Figure. 4-5-1). There were no significant differences in *HAND2* mRNA expression between the individual grades of EEC. Normal postmenopausal endometrium demonstrated strong positive (>50 %) HAND2 staining by immunohistochemistry (Figure. 4-5-2A) in keeping with the pattern of staining previously described within normal cycling endometrial tissues (Figure. 4-4). All representative tissue samples spanning grades 1-3 of EEC were immunonegative for HAND2 protein (Figure. 4-5 2C, 2E and 2F), with no stromal nuclear staining demonstrated (0 %).

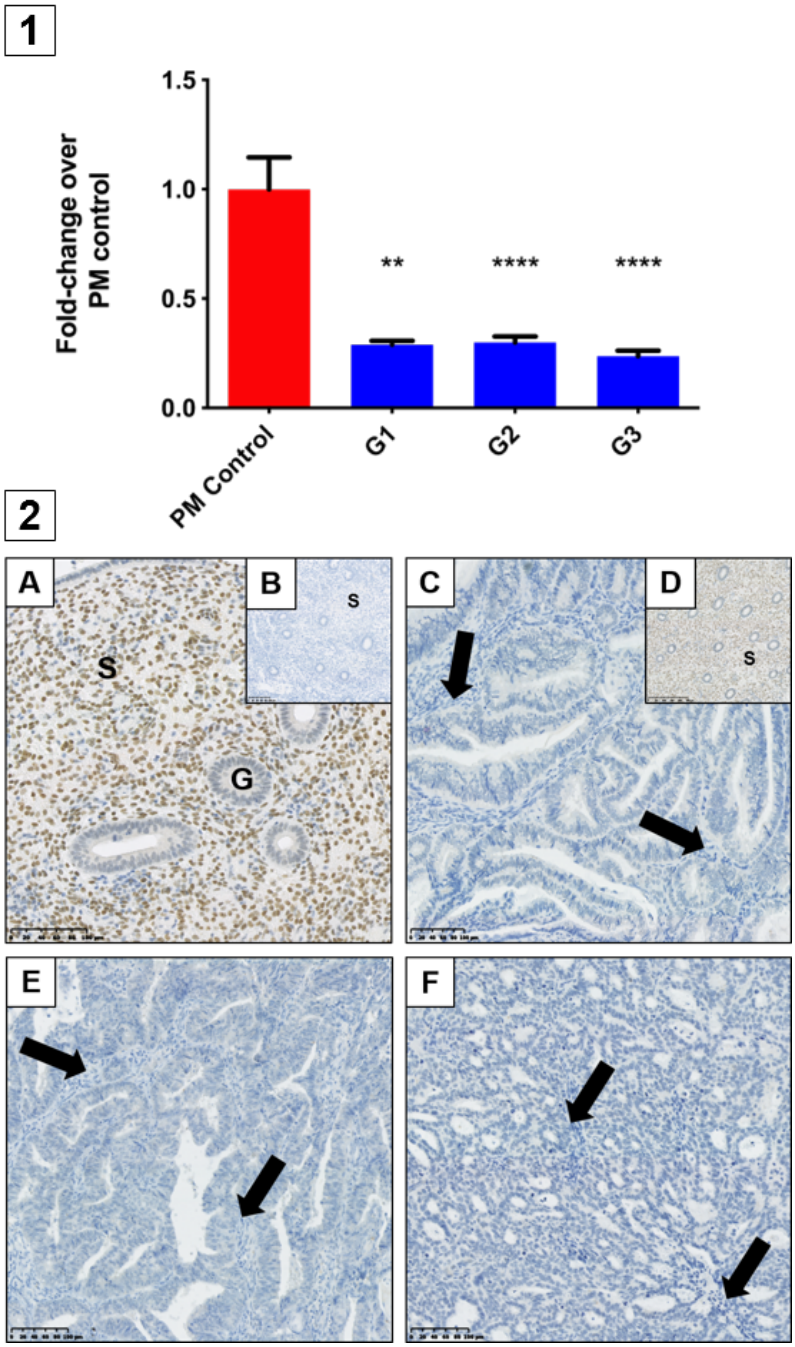

Figure 4-5: Expression of HAND2 mRNA and protein is reduced in human endometrioid endometrial cancers (EEC). 1) Whole tissue homogenates from hysterectomy specimens of postmenopausal endometrium (n=9) and grade 1 (n=32), grade 2 (n=65) and grade 3 (n=36) EEC underwent qRT-PCR analysis for *HAND2* gene expression. The data are presented as a relative fold-change over postmenopausal endometrium and all data were normalised to the housekeeping gene *CYC*. Kruskal Wallis statistical test. **p<0.01, ****p<0.0001. 2) Representative immunohistochemistry for HAND2 protein expression. 2A) Postmenopausal endometrium demonstrating HAND2 positive stromal nuclear staining. 2B) Negative control. 2C) Grade 1 EEC. 2D) Positive Control. 2E) Grade 2 EEC. 2F) Grade 3 EEC. All EEC specimens demonstrate loss of HAND2 stromal nuclear staining (arrowed). S = Stroma. G = Gland. Varying magnifications – see scale bars.

4.4.5 Immunohistochemical expression of Heart and Nuclear Crest Derivatives-expressed 2 (HAND2) within a human endometrial hyperplasia (EH) tissue resource

Having established the pattern of HAND2 expression within both normal and malignant endometrial tissues, HAND2 protein expression was evaluated within the cohort of EH tissue samples developed as part of this study. A total of 103/105 (98.1 %) EH samples were successfully stained and interpreted. HAND2 protein expression was visualised as any degree of brown DAB staining within the nuclei of the endometrial stromal cells as previously described. Three distinct patterns of staining were observed: 1) Positive HAND2 protein expression was noted if >50 % of the stromal cells demonstrated brown DAB staining (Figure. 4-6A). 2) Reduced HAND2 protein expression was noted where 1-50 % of the stromal cells demonstrated brown DAB staining (Figure. 4-6C&D). 3) Some samples were immunonegative for HAND2 (0 % of the stromal cells DAB+, Figure. 4-6E).

The pattern of HAND2 protein expression was scored within digitally marked regions of interest (ROIs) on slide scanned images (as described in 4.3.4.3). Absent or reduced HAND2 protein expression was noted to occur in two distribution patterns, either focally around the EH lesion with normal positive HAND2 expression within the background tissue (unique to cases of EIN and demonstrated in Figure. 4-7) or diffusely across the entire ROI and further beyond into the tissue section.

4.4.5.1 Altered HAND2 protein expression is significantly associated with a diagnosis of Endometrial Intraepithelial Neoplasia (EIN)

Altered HAND2 protein expression (either reduced or absent) was observed in 45/103 (43.7 %) of the total EH cases examined in this study, with 11/103 (10.7 %) demonstrating absent HAND2 expression (Figure. 4-6E) and 34/103 (33.0 %) demonstrating reduced HAND2 expression (Figure. 4-6C&D). The finding of a HAND2 altered immunoexpression pattern was significantly associated with an EH diagnosis of EIN, with 38/49 (77.6 %) of EIN cases demonstrating reduced or absent HAND2 expression compared to 7/54 (13.0 %) of HwA cases ($p<0.0001$, 2-sided Fisher's exact test). The finding of absent HAND2 protein expression alone (Figure. 4-6E and Figure. 4-7) was also significantly associated with an EH diagnosis of EIN. 9/49 (18.4 %) of EIN cases demonstrated absent HAND2 expression compared to 2/54 (3.7 %) of HwA cases ($p=0.0235$, 2-sided Fisher's exact test).

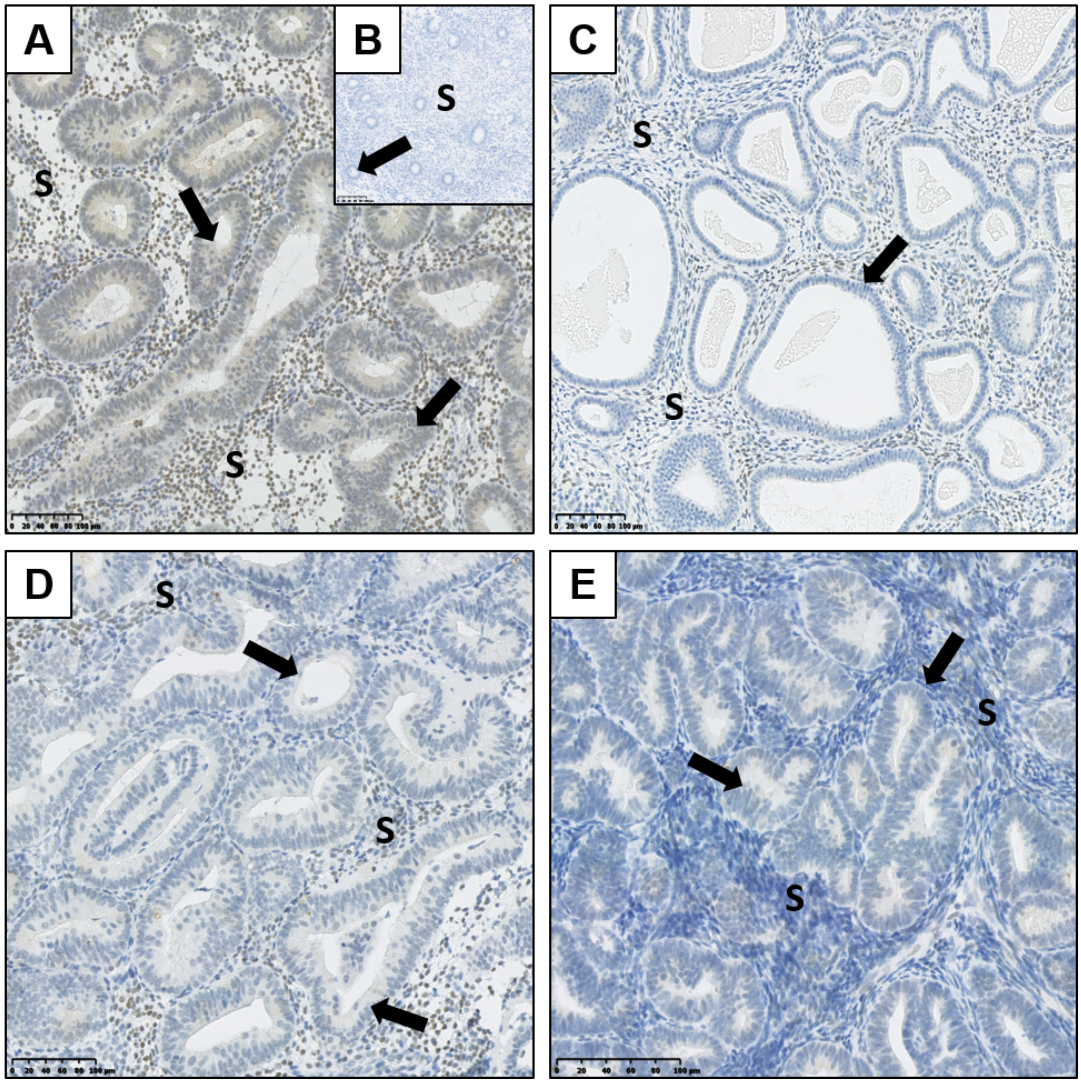

Figure 4-6: Immunohistochemical expression of HAND2 protein within human endometrial hyperplasia (EH) tissue. A) HAND2 immunohistochemical staining of a tissue section demonstrating hyperplasia without atypia (HwA). Positive (scored as >50 %) HAND2 endometrial stromal cell nuclear staining (S = endometrial stroma) demonstrated by brown (DAB) nuclear staining. B) HAND2 negative control. C) Reduced (scored as 1-50 %) HAND2 stromal cell nuclear staining within a tissue section demonstrating HwA. D) Reduced (scored as 1-50 %) HAND2 stromal cell nuclear staining within a tissue section demonstrating Endometrial Intraepithelial Neoplasia (EIN). E) Absent (scored as 0 %) HAND2 stromal cell nuclear staining within a tissue section demonstrating EIN. Arrows highlighting representative endometrial glands not do not demonstrate HAND2 protein expression and were not used for immunohistochemical interpretation of HAND2 staining. Varying magnifications – see scale bars.

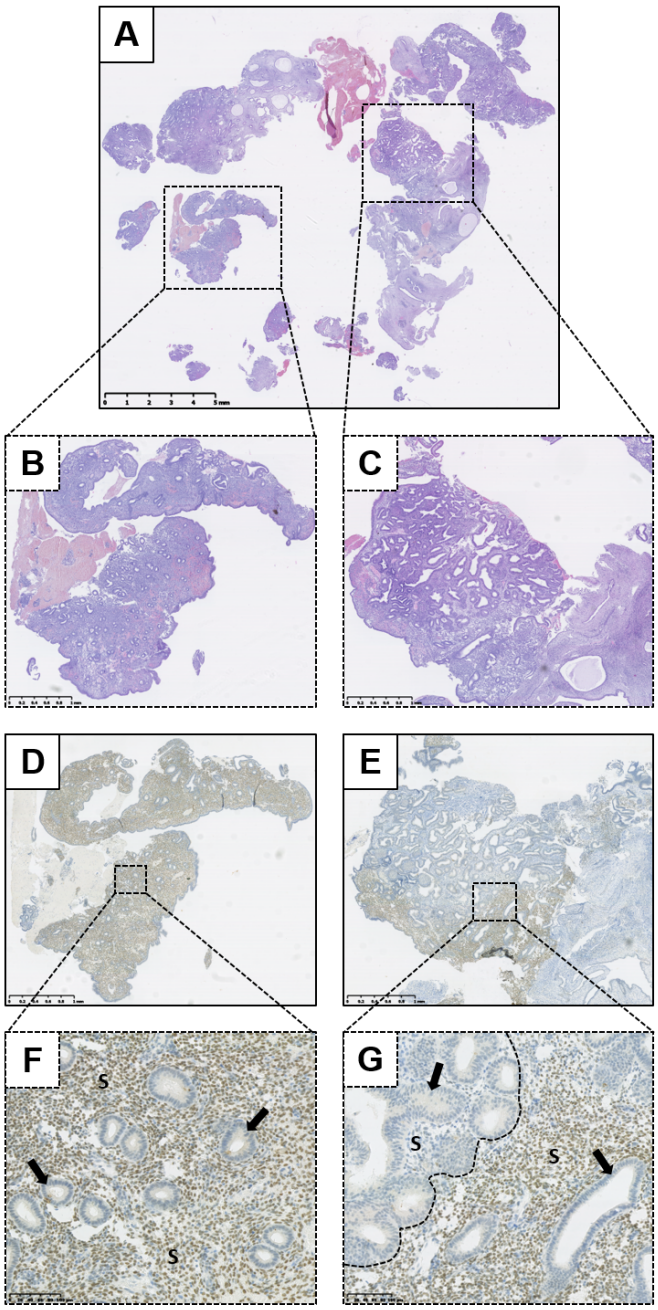

Figure 4-7: Immunohistochemical expression of HAND2 protein within a tissue biopsy specimen demonstrating Endometrial Intraepithelial Neoplasia (EIN). A) Haematoxylin and Eosin (H&E) stained biopsy specimen containing EIN. B) Higher power representative background endometrium from A. C) Higher power EIN lesion from A. D) HAND2 immunohistochemical staining of B. E) HAND2 immunohistochemical staining of C. F) Higher power image of D demonstrating positive (scored as >50 %) HAND2 stromal nuclear staining within the background endometrium. G) Higher power image of E demonstrating absent (scored as 0 %) HAND2 stromal nuclear staining within an EIN lesion (left of dashed line). Junctional region marked with dashed line. Positive HAND2 (>50 %) staining of background endometrium to right of dashed line. Arrows highlight representative endometrial glands. S= Stroma. Varying magnifications – see scale bars.

4.4.6 Immunohistochemical expression of AT-rich interactive domain-containing protein 1A (ARID1A) within a human endometrial hyperplasia (EH) tissue resource

ARID1A protein expression was visualised as brown DAB staining within the nuclear compartments of both the endometrial glandular and stromal cells. All samples (n=105) were successfully stained and interpreted. The appearance of the glandular compartment was the primary site of interest for ARID1A protein expression. In all cases, stromal cells and blood vessels had intensely positive expression for ARID1A and thus served as positive internal controls. EH samples demonstrating a loss of ARID1A glandular protein expression could be readily identified; glands with no ARID1A nuclear staining were distinct from glands with strong ARID1A staining and surrounding stroma (Figure. 4-8). Loss of ARID1A protein expression was observed in three distinct patterns: 1) ARID1A isolated null glands, where $\leq$ 2 endometrial glands demonstrated complete loss of glandular nuclear brown DAB staining (Figure. 4-8C). The endometrial glands displayed a blue nuclear appearance due to haematoxylin counterstaining. 2) ARID1A confluent null glands, where there was a focal loss of ARID1A in >2 glands (Figure. 4-8D). 3) ARID1A complete expression loss, where the entire tissue section demonstrated loss of brown glandular nuclear staining (Figure. 4-8E).

4.4.6.1 Loss of ARID1A protein expression is significantly associated with a diagnosis of Endometrial Intraepithelial Neoplasia (EIN)

Loss of ARID1A protein expression was observed in 6/105 (5.7 %) of the total EH cases examined in this study, with 1/105 (1.0 %) demonstrating ARID1A isolated null glands (Figure. 4-8C), 4/105 (3.8 %) demonstrating ARID1A confluent null glands (Figure. 4-8D) and 1/105 (1.0 %) demonstrating ARID1A complete expression loss (Figure. 4-8E). Overall loss of ARID1A protein expression was significantly associated with an EIN diagnosis, with 6/51 (11.8 %) of EIN cases and 0/54 of HwA cases demonstrating some degree of loss of ARID1A protein expression (Table 4-4, p=0.0112, 2-sided Fisher's exact test). There were no significant differences between individual ARID1A protein expression patterns for either EIN or HwA (Table. 4-4).

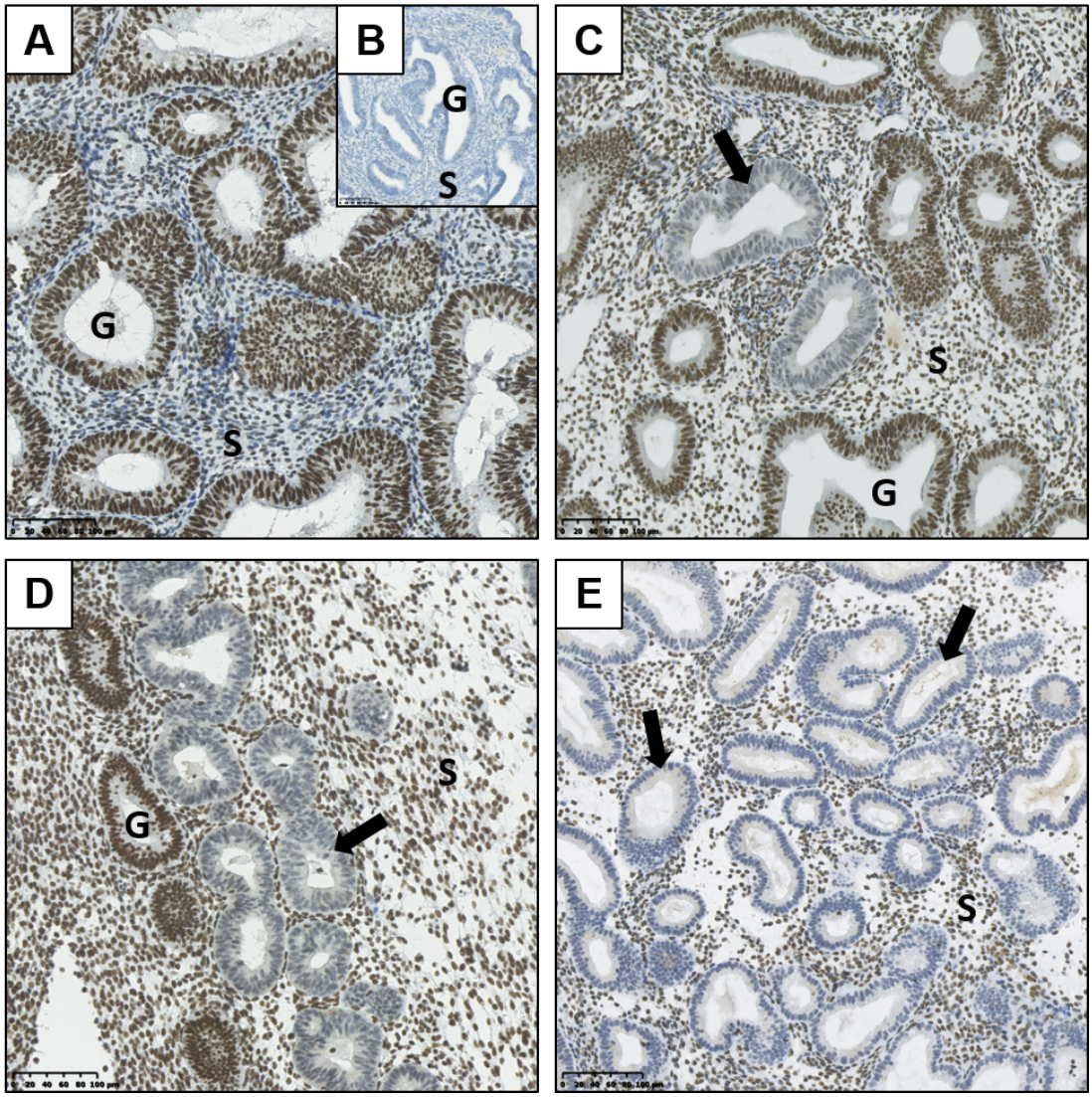

Figure 4-8: Immunohistochemical expression of ARID1A protein within human endometrial hyperplasia (EH) tissue. A) ARID1A immunohistochemical staining of a tissue section demonstrating hyperplasia without atypia (HwA). Positive ARID1A endometrial glands (G = representative endometrial gland) demonstrated by brown DAB glandular nuclear staining. B) ARID1A negative control. C) Isolated ARID1A null glands (arrow indicating loss of brown DAB glandular nuclear staining) within a tissue section demonstrating Endometrial Intraepithelial Neoplasia (EIN). D) ARID1A confluent null glands (arrow indicating loss of brown DAB glandular nuclear staining) within a tissue section demonstrating Endometrial Intraepithelial Neoplasia (EIN). E) ARID1A complete glandular expression loss (arrow indicating loss of brown DAB glandular nuclear staining) within a tissue section demonstrating Endometrial Intraepithelial Neoplasia (EIN). S = endometrial stromal; used as a positive internal control for ARID1A immunohistochemistry. Varying magnifications – see scale bars.

Table 4-4: Correlation between ARID1A immunoreactivity and endometrial hyperplasia diagnosis.

ARID1A	EIN, n=51	HwA, n=54	P Value
Positive	45 (88.2)	54 (100.0)	0.0112*
Null	6 (11.8)	0	
^Isolated Null Glands	1 (2.0)	0	0.4857
^Confluent Null Glands	4 (7.8)	0	0.0523
^Complete Expression Loss	1 (2.0)	0	0.4857

^Subgroups of Null ARID1A immunoreactivity included for comparison. HwA = Hyperplasia without Atypia, EIN = Endometrial Intraepithelial Neoplasia. Percentages in brackets. Statistical analysis performed using a Fisher's exact test, 2-sided. *p<0.05.

4.4.7 Immunohistochemical signature of mismatch repair (MMR) within a human endometrial hyperplasia (EH) tissue resource

The mismatch repair (MMR) proteins, MutL homologues (MLH1 and PMS2) and MutS homologues (MSH2 and MSH6) were evaluated in endometrial hyperplasia (EH) tissues by immunohistochemistry as part of this study. All samples (n=105) were successfully stained for all four MMR protein markers and interpreted. EH samples were considered to show abnormal protein expression (and thus deficient mismatch repair (dMMR) status) where there was clear absence of brown DAB staining within the nuclei of the glandular epithelial cells and positive brown DAB staining of lymphocytes or stromal cell nuclei in the adjacent stroma. Appropriate control tissue was included in all immunostaining runs (Figure. 4-9 demonstrates a representative positive control example for MSH2).

A single patient (1/105, 1 %) within the EH tissue resource demonstrated dMMR, with absence of MLH1 and PMS2 proteins within a focal region of EIN (Figure. 4-10 D1 and D4, respectively). This patient was 51-years-old at the time of endometrial biopsy, she was perimenopausal and presented with heavy menstrual bleeding. The patient had no family history of note. The patient was treated surgically with a total abdominal hysterotomy, bilateral salpingo-oophorectomy and peritoneal washings, the final surgical specimens demonstrated a small focus of residual EIN with no evidence of malignancy.

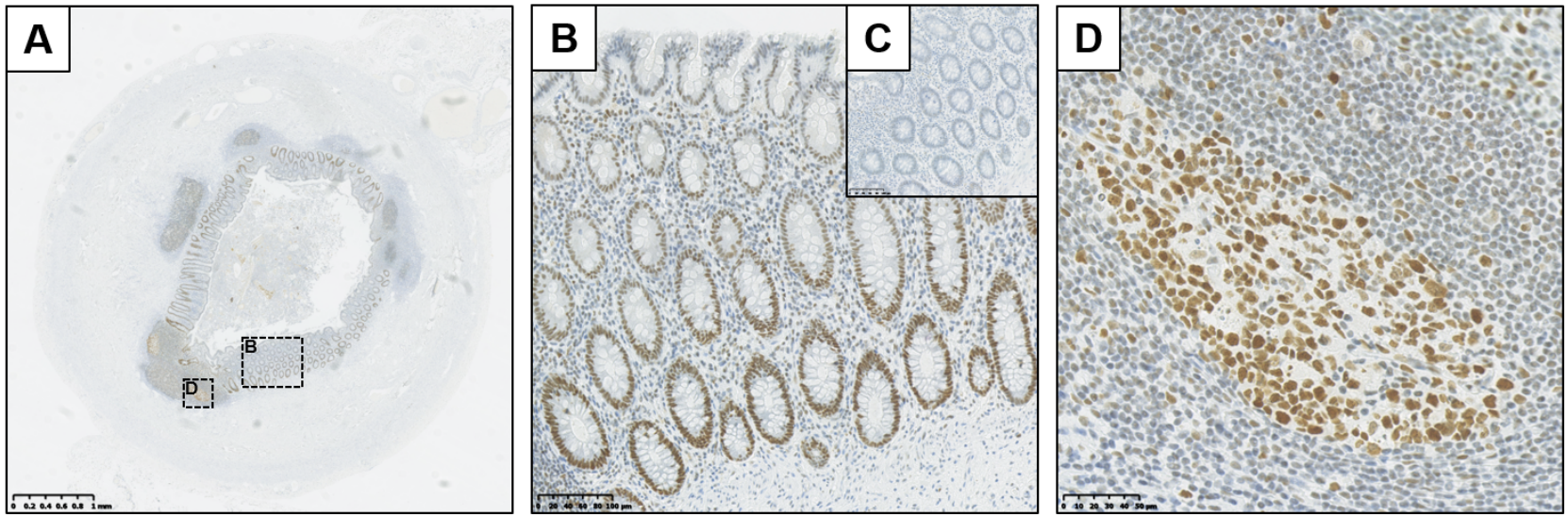

Figure 4-9: Representative example of positive control tissue (human vermiform appendix) immunohistochemistry for mismatch repair (MMR) function. Representative example of MSH2 positive control tissue immunohistochemistry demonstrating the expected positive expression pattern of immunostaining. A) Low-power view of a cross-section of normal human vermiform appendix tissue stained for MSH2 protein. B) Strong nuclear staining of the epithelium at the base of the crypts, with fading of nuclear intensity in the middle and upper third of the crypts, to negative / weak staining at the luminal surface. C) Negative control. D) Strong staining of the lymphoid follicles. Varying magnifications – see scale bars.

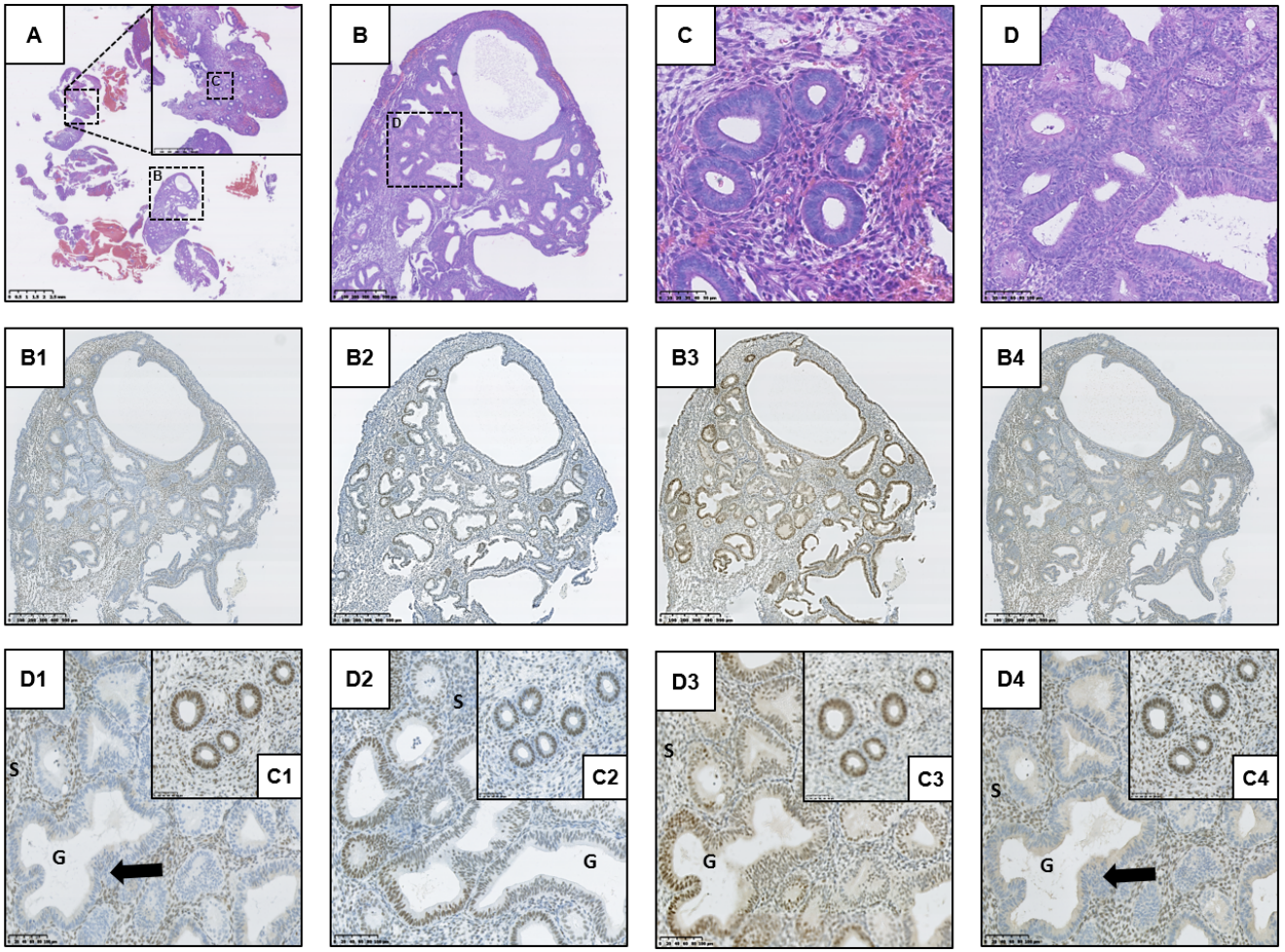

Figure 4-10: Deficient mismatch repair (dMMR) within endometrial hyperplasia tissue. A case of endometrial intraepithelial neoplasia (EIN) showing loss of MLH1 expression, together with loss of its binding partner PMS2.

Figure 4-10 continued.

A) Low power haematoxylin and eosin (H&E) image of an EH lesion containing a focus of EIN (B). C) Background endometrial glands for comparison. D) Higher power view of the EIN lesion from B. B1) Loss of MLH1 expression in the glandular nuclei of the EIN lesion (loss of nuclear brown DAB staining within the glandular nuclei). B2) Normal expression of MSH2 in the same sample. B3) Normal expression of MSH6 in the same sample. B4) Loss of binding partner PMS2 expression in the glandular nuclei of the same sample (loss of nuclear brown (3, 3 –diaminobenzidine (DAB)) staining within the glandular nuclei). D1 & D4) High power views demonstrating loss of MLH1 and PMS2 expression respectively (arrowed), background endometrium positively stained and included in C1 & C4 for comparison. D2 & D3) High power views demonstrating MSH2 and MSH6 positive expression, background endometrium positively stained and included in C2 & C3 for comparison. G = Representative endometrial gland, S = Endometrial Stroma. Varying magnifications – see scale bars.

4.4.8 Immunohistochemical expression of Tumour Protein p53 (p53) within a human endometrial hyperplasia (EH) tissue resource

All samples (n=105) were successfully stained for p53. Positive p53 protein expression (i.e. p53 'overexpression' occurring due to p53 mutation or gene inactivation) was anticipated to result in intense (strong) DAB staining within the nuclear compartments of both the endometrial glandular epithelial cells. 'Wild-type' p53 expression (occurring in the absence of mutant / inactivated p53) was anticipated to be focal, weak and heterogeneous glandular epithelial nuclear DAB staining. 'Aberrant' p53 expression (due to a nonsense or frameshift p53 mutation, known to be undetectable with immunohistochemistry) was anticipated to be complete absence of DAB staining with glandular epithelial cells, with only the haematoxylin blue counterstain evident. Serous endometrial carcinoma was used as a control tissue for analysis (Figure. 4-11A&B).

4.4.8.1 All EH tissues express 'Wild-type' p53 regardless of diagnosis

In our current dataset all EH tissues (n=105) regardless of diagnosis (EIN or HwA) demonstrated heterogenous, weak and patchy p53 staining in this study (Figure. 4-11 C&D) considered consistent with the presence of a functional 'wild-type' p53 protein in these tissues.

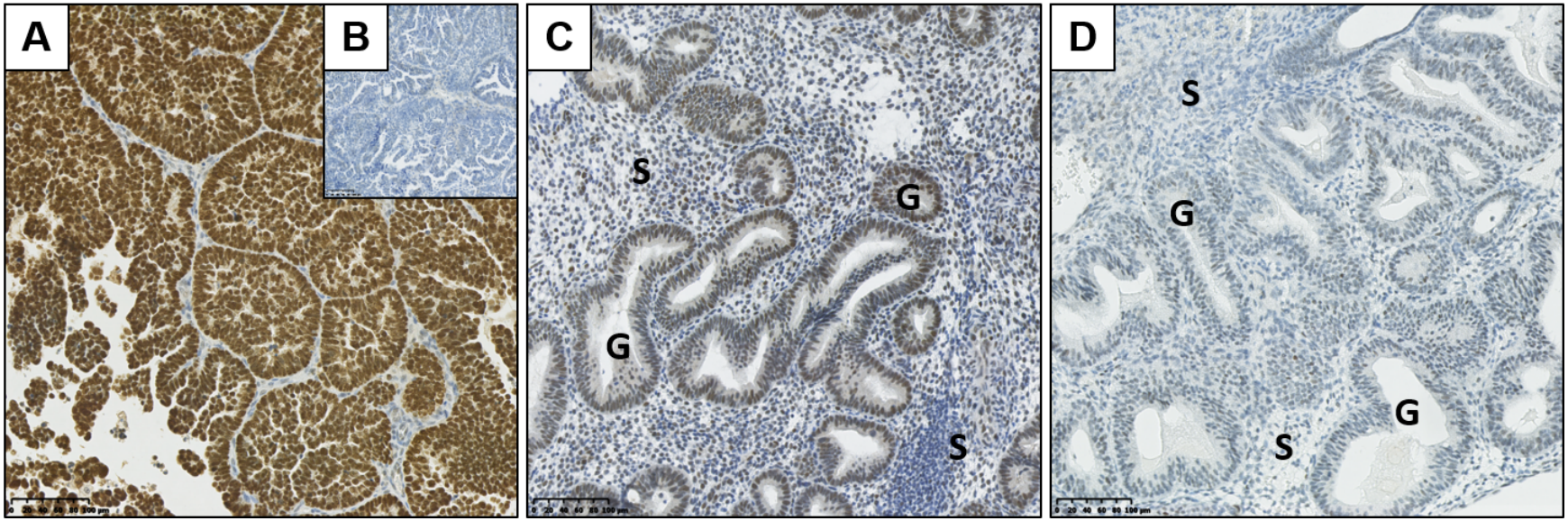

Figure 4-11: Immunohistochemical expression of Tumour protein p53 within endometrial hyperplasia (EH) tissue. A) Positive control tissue (serous endometrial cancer) p53 positive overexpression demonstrated by strong brown (DAB) glandular nuclear staining. B) Negative control. C) High 'Wild-type' heterogenous, weak/patchy p53 staining pattern within a tissue section demonstrating hyperplasia without atypia (HwA). D) Low 'Wild-type' heterogenous, weak/patchy p53 staining pattern within a tissue section demonstrating Endometrial Intraepithelial Neoplasia (EIN). G = Representative endometrial glands. S = Endometrial stroma. Varying magnifications – see scale bars.

4.4.9 Unsupervised hierarchical cluster analysis of PTEN, PAX2 and HAND2 protein expression within EH tissues

Further analysis of the relationship between EH diagnosis, EH progression to malignancy and the immunohistochemical expression of the proteins PTEN, PAX2 and HAND2 was undertaken utilising a method of unsupervised hierarchical agglomerate clustering (HAC). In order to undertake this method of analysis each immunostaining result was expressed as a plain score (0, 1 or 2) as described in Table 4-2. Table 4-5 summarises the plain score results for these three protein markers alongside the corresponding EH tissue diagnosis. ARID1A, the MMR proteins and p53 immunostaining results were not taken forward for further analysis due to the minimal changes noted in their expression patterns across the EH tissue resource as detailed above.

Table 4-5: Immunohistochemical scoring results of PTEN, PAX2 and HAND2 protein expression within a human endometrial hyperplasia tissue resource.

	EIN, n=51			HwA, n=54		
	Score 0	Score 1	Score 2	Score 0	Score 1	Score 2
PTEN^	17 (33.3)	11 (21.6)	23 (45.1)	26 (49.1)	26 (49.1)	1 (1.9)
PAX2	33 (64.7)	3 (5.9)	15 (29.4)	51 (94.4)	3 (5.5)	0
HAND2*	11 (21.5)	29 (59.2)	9 (18.4)	47 (87.0)	5 (9.3)	2 (3.7)

Scoring system as described in chapter 4 materials and methods (Table 4-2). ^x1 HwA sample stained for PTEN protein was not interpretable. *x2 EIN samples stained for HAND2 protein were not interpretable. Percentages in brackets. PTEN - Phosphatase and Tensin Homolog, PAX2 - Paired Box 2 Protein, HAND2 - Heart and Neural Crest Derivatives-expressed 2.

4.4.9.1 Unsupervised hierarchical cluster analysis reveals four distinct EH clusters, demonstrating potential clinical usefulness as a 'rule out test'

HAC analysis segregated the immunoscoring results of PTEN, PAX2 and HAND2 for the n=105 EH samples into four novel clusters based on their immunohistochemical staining patterns. The clusters were divided into cluster 1 (n=12), cluster 2 - which was further sub-classified into cluster 2a (n=4) and 2b (n=54) and cluster 3 (n=35) according to dendrogram branch length, which represents the correlation of the scoring data (Figure. 4-12).

Clusters 1, 2a and 3 largely contain cases of EIN i.e. the 'premalignant clusters' (44/51, 86.3 %), with cluster 2b containing the majority of HwA cases i.e. the 'benign cluster' (47/54, 87.0 %). Table 4-6 demonstrates the breakdown of each cluster by EH diagnosis and the statistical difference between EH diagnosis for each individual cluster. The patient demographics for each cluster group are displayed in Table 4-7, demonstrating no significant differences in clinical features between any of the four clusters. HAC analysis of immunostaining patterns may help in everyday pathological classification as a 'rule out test', i.e. it has a useful negative predicative value, whereby the majority of 'benign' HwA fall into cluster 2b.

Table 4-6: Summary of endometrial hyperplasia (EH) classification between cluster groups

	EIN, n=51	HwA, n=54	P Value
Cluster 1	12 (23.5)	0	0.0001***
Cluster 2a	4 (7.8)	0	0.0565 ns
Cluster 2b	7 (13.7)	47 (87.0)	<0.0001****
Cluster 3	28 (54.9)	7 (11.3)	<0.0001****

EIN = Endometrial Intraepithelial Neoplasia. HwA = Hyperplasia without atypia. Percentages in brackets. Statistical analysis using a Fisher's exact test, 2 sided. ***p<0.001, ****p<0.0001, ns = non-significant.

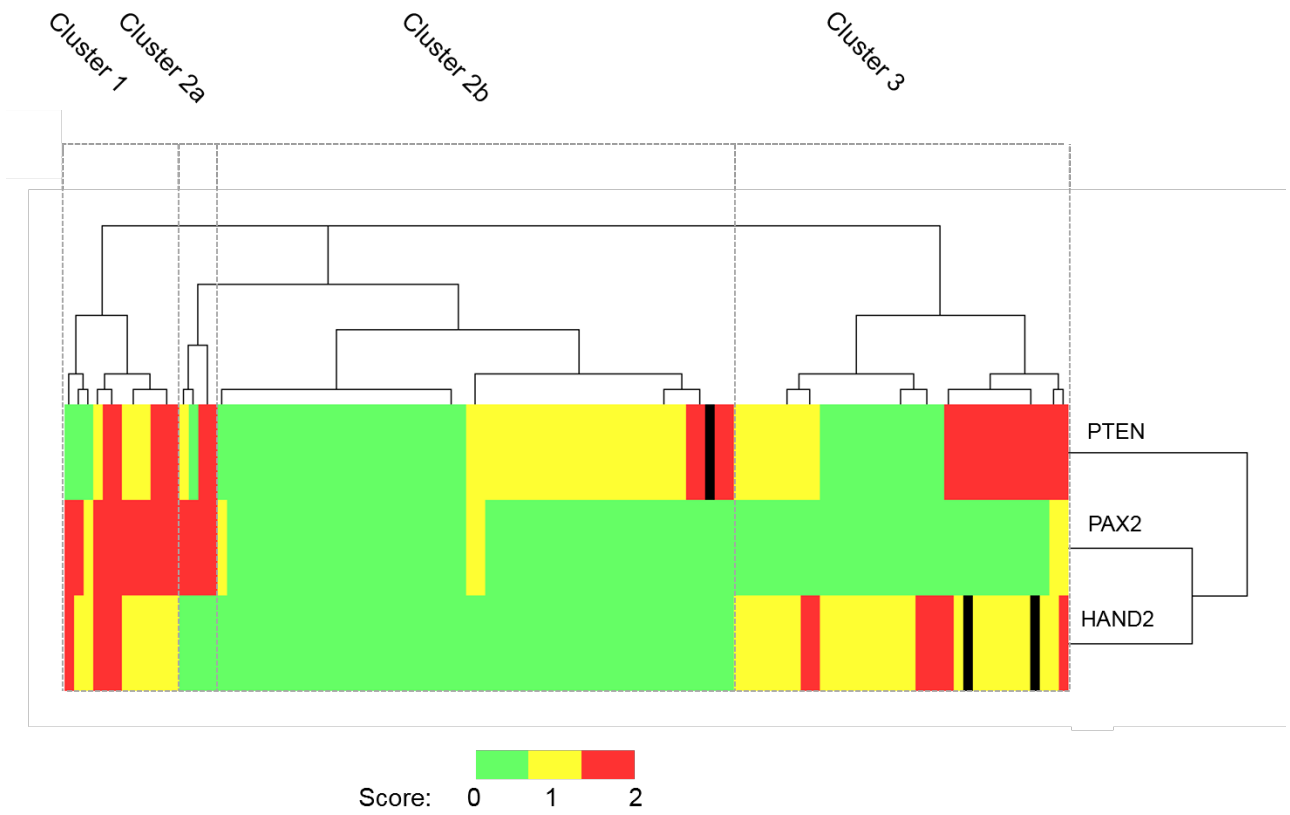

Figure 4-12: Dendrogram and heat map. Summary of unsupervised hierarchical cluster analysis of PTEN, PAX2 and HAND2 immunohistochemical staining data. Patient cases orientated along the horizontal axis (n=105). Immunohistochemical markers orientated along the vertical axis. Dendrogram branch length represents the similarity between the results obtained. Heat map colours represent outcome of immunohistochemical scoring (as described in Table 4-2) Endometrial hyperplasia cases were classified into 4 distinct cluster groups according to the dendrogram: Cluster 1 (n=12), Cluster 2a (n=4), Cluster 2b (n=54) and Cluster 3 (n=35). PTEN - Phosphatase and Tensin Homolog, PAX2 - Paired Box 2 Protein, HAND2 - Heart and Neural Crest Derivatives-expressed 2. Black lines in the heatmap represent cases where the immunoscore was not available.

Table 4-7: Demographics and clinical features of endometrial hyperplasia patients broken down by cluster group.

	Cluster 1 n=12 (%)	Cluster 2a n=4 (%)	Cluster 2b n=54 (%)	Cluster 3 n=35 (%)	P Value
Age^					
Mean	51.4	51.3	53.2	52.5	0.9329
≤40	3 (25.0)	0	3 (5.6)	4 (11.4)	0.5634
41-50	2 (16.7)	2 (50.0)	22 (40.7)	12 (34.3)	0.5297
51-60	5 (41.7)	1(25.0)	20 (37.0)	11(31.4)	0.4701
61-70	1 (8.3)	1 (25.0)	4 (7.4)	8 (22.6)	0.3461
>70	1 (8.3)	0	5 (9.3)	0	NS
BMI^					
Mean	35.33	34.50	38.7	39.1	0.8105
Normal (18.5 – 25)	1 (8.3)	0	2 (3.7)	2 (5.7)	0.9470
Overweight (26 – 30)	0	0	5 (9.3)	0	NS
Obese (> 30)	5 (41.7)	2 (50.0)	18 (33.3)	16 (45.7)	0.4602
Unknown	6 (50.0)	2 (50.0)	29 (53.7)	17 (48.6)	
Postmenopausal[$]					
Yes	5 (41.7)	2 (50.0)	31 (57.4)	21 (60.0)	0.7222
No	7 (58.3)	2 (50.0)	23 (42.6)	14 (40.0)	
Presenting complaint[$]					
PMB	5 (41.7)	2 (50.0)	29 (53.7)	17 (48.6)	0.9125
HMB	4 (33.3)	1 (25.0)	14 (25.9)	10 (28.6)	
IMB	2 (16.7)	1 (25.0)	8 (14.8)	3 (8.6)	
Others	1 (8.3)	0	3 (5.6)	5 (14.3)	
Parity[$]					
Nulliparous	3 (25.0)	2 (50.0)	8 (14.8)	11 (31.4)	0.2700
1-4	7 (58.3)	1 (25.0)	39 (72.2)	20 (57.1)	
≥5	0	0	1 (1.9)	2 (5.7)	
Unknown	2 (16.7)	1 (25.0)	6 (11.1)	2 (5.7)	

Body max Index (BMI) categorised according to the World Health Organisation (WHO) categories. PMB = Postmenopausal bleeding, HMB = Heavy menstrual bleeding, IMB = Intermenstrual Bleeding, Others = Incidental and subfertility. Statistical analysis performed using a Chi-Squared test to determine statistical differences between the categorical data ([$]) and a one-way ANOVA was used to compare the means of the continuous data (^). Percentages in brackets. NS = Non-significant.

4.4.9.2 Three distinct immunohistochemical phenotypes for EIN are evident following cluster analysis and are defined by PAX2 and HAND2 protein expression

Three distinct immunohistochemical phenotypes are evident for EIN based on the clustering analysis (Table 4-8). Cluster 1 contains exclusively cases of EIN (Table 4-6, n=12). The predominant immunohistochemical phenotype of this cluster is that of PAX2 altered expression (a PAX2 score of 2) and HAND2 altered expression (a HAND2 score of 1-2, i.e. absent or reduced HAND2 expression) (Figure. 4-12). Cluster 2a which is the smallest cluster, also contains exclusively EIN cases (Table. 4-6, n=4). Although more similar (as indicated by dendrogram branch length) to cluster 2b, i.e. the 'benign cluster' due to all its cases being HAND2 positive, cluster 2a has an exclusively PAX2 altered immunohistochemical phenotype (PAX2 score of 2) which defines it as a separate sub-cluster. Cluster 3, which contains the largest number of EIN cases (Table. 4-6, n=28) has a largely PAX2 positive (score of 0) and HAND2 altered expression (score of 1-2) immunohistochemical phenotype. Cluster 2b ('the benign cluster' with the largest number of cases of HwA, n=47), has the greatest number of cases which expressed positivity (i.e. a score of 0) for both PAX2 and HAND2.

Further analysis of the immunoscoring between each cluster group was undertaken (Table. 4-9). As described previously, an immunoscore of 0 used for the HAC analysis, equates to the descriptive finding of positive expression of the protein of interest within the EH tissue (Table. 4-2). Combining groups with an immunoscore score of 1 and 2 therefore equates to the descriptive finding of any degree of protein expression loss. A score of 0, vs a score of 1-2 were compared across the clusters. Results demonstrated statistically significant differences between the clusters for PAX2 and HAND2 expression (Table. 4-9).

Table 4-8: Predominant immunohistochemical phenotype of each cluster group

	Immunohistochemical phenotype
Cluster 1	PAX2 and HAND 2 altered expression
Cluster 2a	PAX2 altered expression, HAND2 positive expression
Cluster 2b	PAX2 and HAND2 positive expression
Cluster 3	PAX2 positive expression, HAND2 altered expression

PAX2 - Paired Box 2 Protein, HAND2 - Heart and Neural Crest Derivatives-expressed 2.

Table 4-9: Scoring of immunohistochemistry data between clusters

	Cluster 1 n=12	Cluster 2a n=4	Cluster 2b n=54	Cluster 3 n=35	P Value
PTEN					
Score 0, vs 1-2	3	1	26^	13	0.3453
PAX2					
Score 0, vs 1-2	0	0	51	33	<0.0001****
HAND2					
Score 0, vs 1-2	0	4	54	0[$]	<0.0001****

Scoring system as described in chapter 4 materials and methods (Table 4-2). ^x1 sample stained for PTEN protein was not interpretable. [$]x2 samples stained for HAND2 protein were not interpretable. PTEN - Phosphatase and Tensin Homolog, PAX2 - Paired Box 2 Protein, HAND2 - Heart and Neural Crest Derivatives-expressed 2. Statistical analysis performed using Chi-Squared test., ****p<0.0001.

4.4.9.3 PTEN protein is ubiquitously expressed across all EH cluster groups

There does not appear to be a well-defined pattern of PTEN protein expression unique to any of the individual EH cluster groups (Figure. 4-12). Indeed, loss of PTEN protein expression was not significantly different between cluster groups (Table. 4-9). This appears to be in keeping with the data described in section 4.4.1.1, whereby overall loss of PTEN protein expression (incorporating both the findings of PTEN isolated null glands and PTEN null regions) was found not to be significantly associated with either an EH diagnosis of EIN or HwA. Furthermore, as indicated by the vertical axis dendrogram (Figure. 4-12), PTEN stands very much on its own, unlike PAX2 and HAND2 which are more closely related (indicated by dendrogram branch length).

4.4.10 Progression of endometrial hyperplasia (EH) cases to endometroid endometrial cancer (EEC)

Of the 105 EH cases within the EH tissue resource used for immunohistochemical analysis, n=10 (9.5 %) went on to have a diagnosis of EEC. 8 of these were diagnosed within the first 12 months after an initial endometrial biopsy and were therefore considered likely to have a concurrent EEC which was not sampled on the initial biopsy. The remained 2 were diagnosed with cancer following hysterotomy, 9.5 and 4.3 years respectively after the initial EH biopsy. Notably, all ten of these subsequent EEC cases had a reclassified biopsy diagnosis of EIN following retrospective, dual gynaepathology review (as per 3.3.3).

4.4.10.1 Relationship of EEC cases to EH cluster group

Table 4-10 summarises the EH cluster groups from where each EEC originated. As demonstrated, clusters 1 and 3 contained most of the subsequent EECs, with cluster 1 containing n=3 (25.0 %) of cases that subsequently progressed and cluster 3 containing n=6 (17.1 %). There was a statistically significant difference in the occurrence of EEC cases between the cluster groups (p=0.0231).

Table 4-10: Summary of malignant outcome by cluster group.

	Cluster 1 n=12 (%)	Cluster 2a n=4 (%)	Cluster 2b n=54 (%)	Cluster3 n=35 (%)	P Value
Endometrioid Endometrial Cancer	3 (25.0)	0	1 (1.9)	6 (17.1)	0.0231*
Concurrent (<12months)	2 (16.7)	0	1 (1.9)	5 (14.3)	
Subsequent (>12 months)	1 (8.3)	0	0	1 (2.9)	

Malignancy was defined as concurrent if diagnosed <12 months from the index EH biopsy. Subsequent malignancy was defined as being diagnosed >12 months after the index EH biopsy. Percentages in brackets. Statistical analysis performed using Chi-Squared test. *p<0.05.

4.4.11 Immunohistochemical phenotype of EH cases that subsequently progressed to EEC demonstrates a tendency for altered HAND2 and PTEN protein expression

The immunohistochemical phenotype as determined using detection of PTEN, PAX2 and HAND2 proteins, for each case of EH that subsequently progressed to EEC is displayed in Figures. 4-13, 4-14, 4-15A and 4-15B. These were divided by the EH cluster groups from which the EEC originated. Importantly, n=9 (90 %) of the EH that progressed to EEC demonstrated reduced expression of HAND2 protein. PAX2 protein expression varied dependent on cluster grouping (altered PAX2 expression was exclusive to cluster 1 EH cases), with n=3 (30 %) of the overall EH cases that progressed to EEC demonstrating a change in PAX2 protein. PTEN protein loss was found in n=7 (70 %) of the EH cases which progressed to EEC, incorporating n = 2 (20 %) cases which exhibited isolated PTEN null glands, and n=5 (50 %) which exhibited a PTEN null region. Figure. 4-16 demonstrates two 'benign' HwA cases that did not progress to malignancy for comparison and to demonstrate the clinical usefulness of the HAC cluster analysis as a 'rule-out test'.

Regarding the additional protein markers investigated as part of this study, p53 expression and MMR status was not altered in any of the cases that subsequently progressed to EEC. Interestingly, ARID1A protein expression was lost in n=2 (20 %) of the EH cases that progressed to EEC. The loss of ARID1A immunostaining was confined to a single case demonstrating confluent null glands (Figure. 4-8D) and another case with complete loss of ARID1A glandular protein expression (Figure. 4-8E). Both cases of ARID1A loss in EH were associated with an EEC that was likely concurrent (i.e. diagnosed within 12 months of initial EH biopsy).

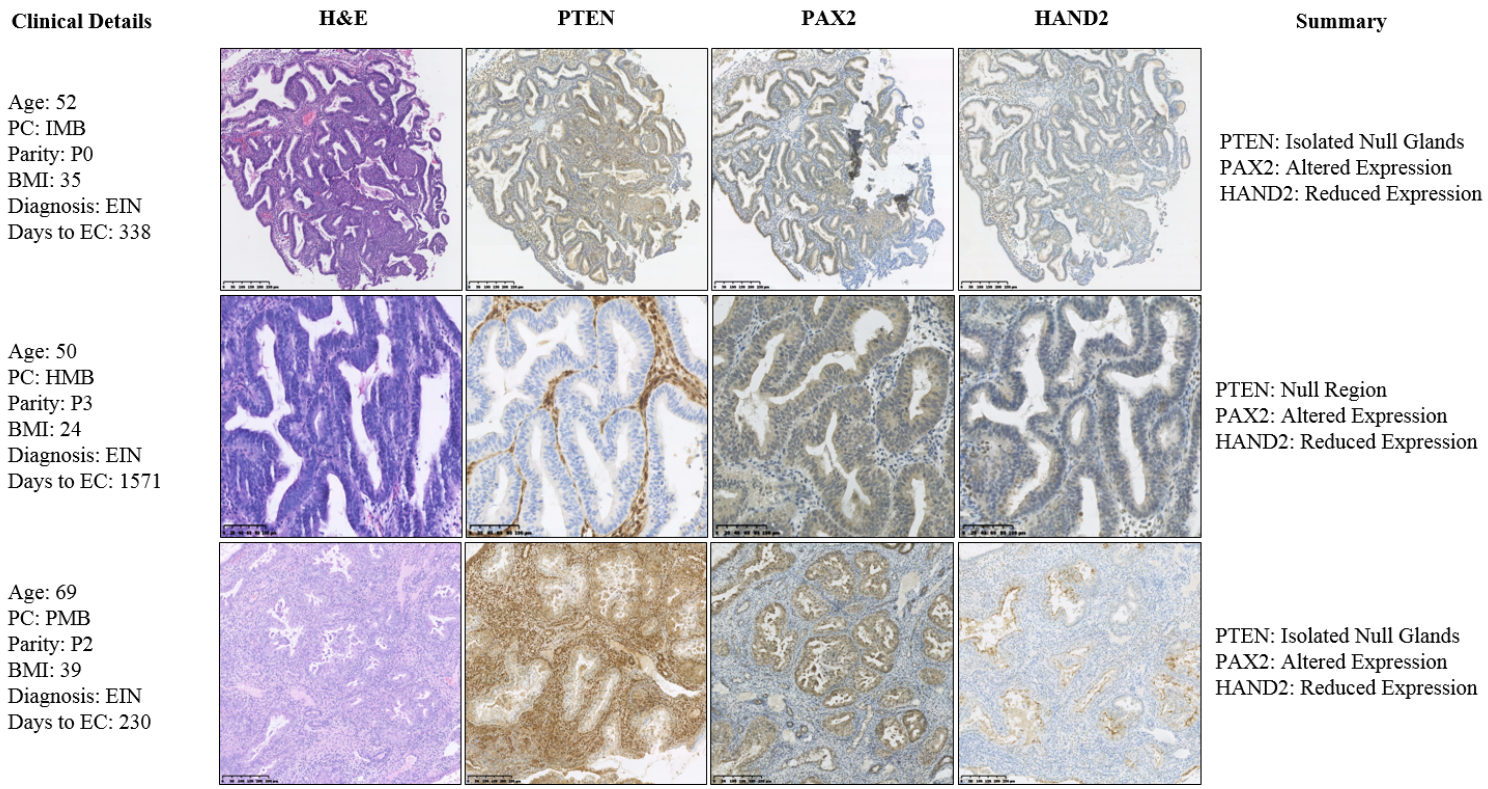

Figure 4-13: Immunohistochemical phenotype of Cluster 1 EH cases that progressed to malignancy. n=3 patients from cluster 1 had a subsequent endometrioid endometrial cancer diagnosis. Figure 4-13 summarises the expression pattern of the PTEN, PAX2 and HAND2 immunohistochemical staining profile for each EH case that progressed, along with pertinent clinical details. The selected images for each case represent serial tissue sections of the most abnormal hyperplastic region. H&E - Haematoxylin and Eosin, PTEN - Phosphatase and Tensin Homolog, PAX2 - Paired Box 2 Protein, HAND2 - Heart and Neural Crest Derivatives-expressed 2, EC - Endometrial cancer, PMB - Postmenopausal bleeding, HMB - Heavy menstrual bleeding, IMB - Intermenstrual bleeding. Varying magnifications – see scale bars.

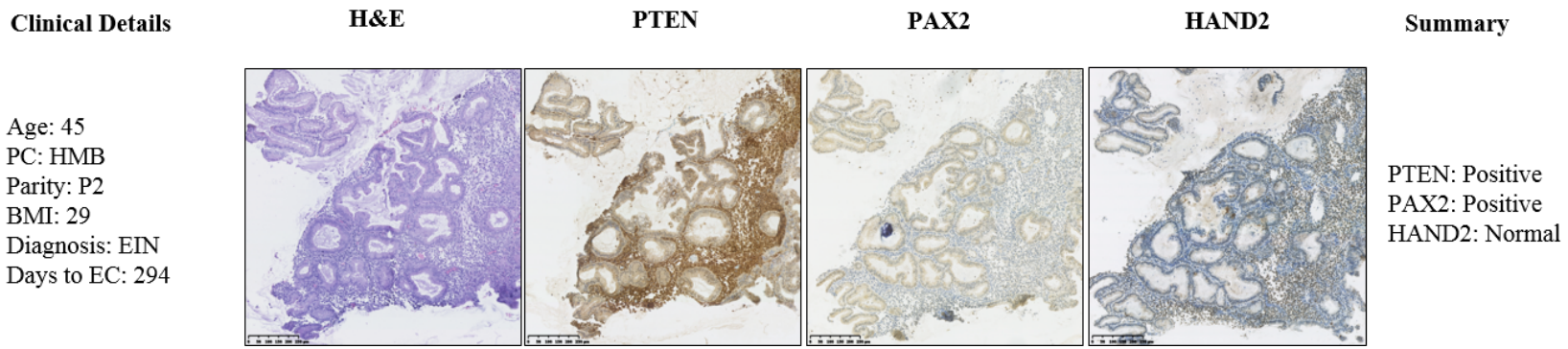

Figure 4-14: Immunohistochemical phenotype of the Cluster 2b EH case that progressed to malignancy. n=1 patient from cluster 2b had a subsequent endometrioid endometrial cancer diagnosis. Figure 4-14 summarises the expression pattern of the PTEN, PAX2 and HAND2 immunohistochemical staining profile for the case, along with pertinent clinical details. The selected images for each case represent serial tissue sections of the most abnormal hyperplastic region. H&E - Haematoxylin and Eosin, PTEN - Phosphatase and Tensin Homolog, PAX2 - Paired Box 2 Protein, HAND2 - Heart and Neural Crest Derivatives-expressed 2, EC - Endometrial cancer, HMB - Heavy menstrual bleeding. Varying magnifications – see scale bars.

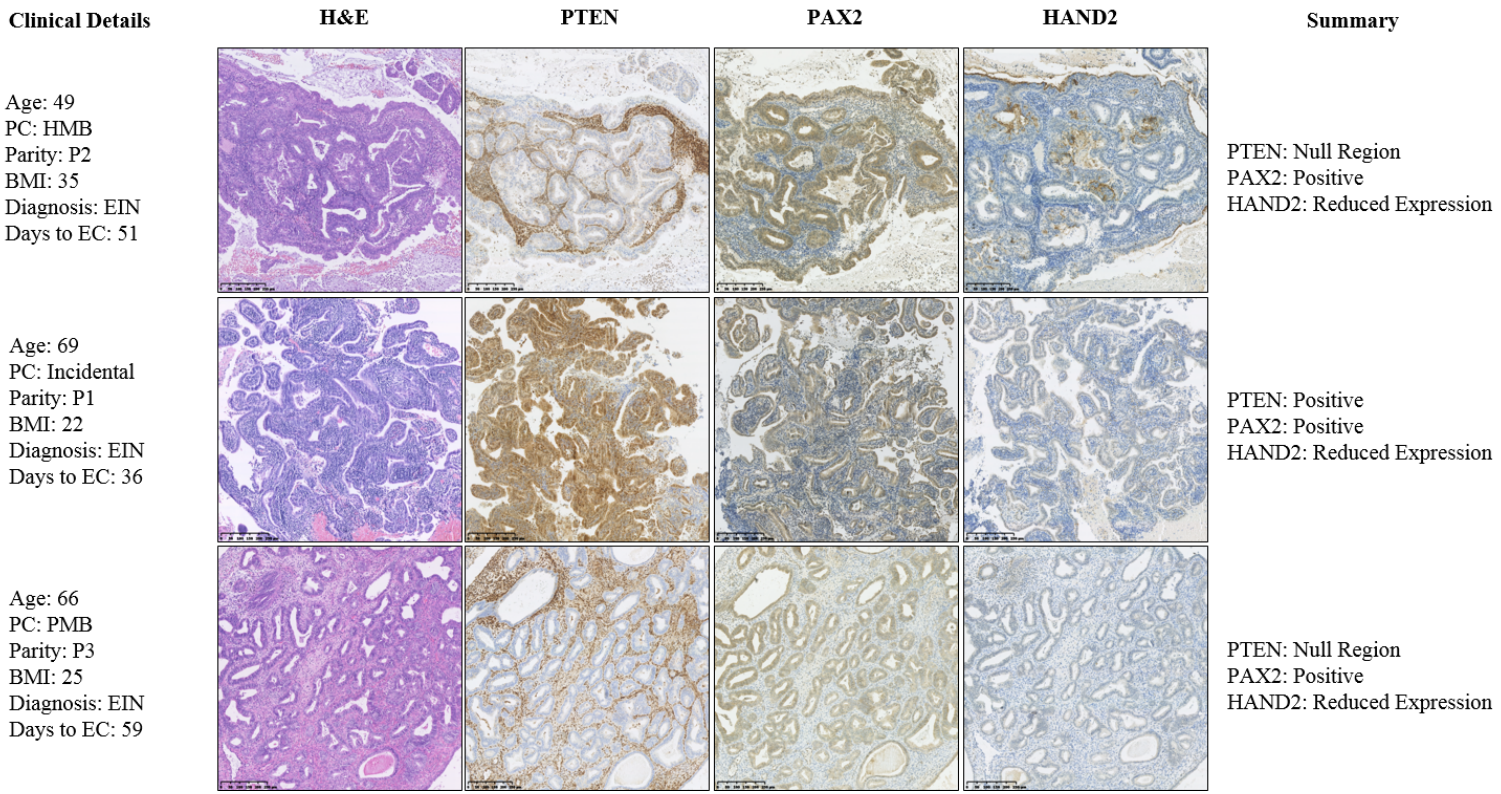

Figure 4-15A: Immunohistochemical phenotype of Cluster 3 EH cases that progressed to malignancy. n=6 patients from cluster 1 had a subsequent endometrioid endometrial cancer diagnosis. Figure 4-15A summarises the expression pattern of the PTEN, PAX2 and HAND2 immunohistochemical staining profile for each EH case that progressed, along with pertinent clinical details. The selected images for each case represent serial tissue sections of the most abnormal hyperplastic region. H&E - Haematoxylin and Eosin, PTEN - Phosphatase and Tensin Homolog, PAX2 - Paired Box 2 Protein, HAND2 - Heart and Neural Crest Derivatives-expressed 2, EC - Endometrial cancer, PMB - Postmenopausal bleeding, HMB - Heavy menstrual bleeding. Varying magnifications – see scale bars.

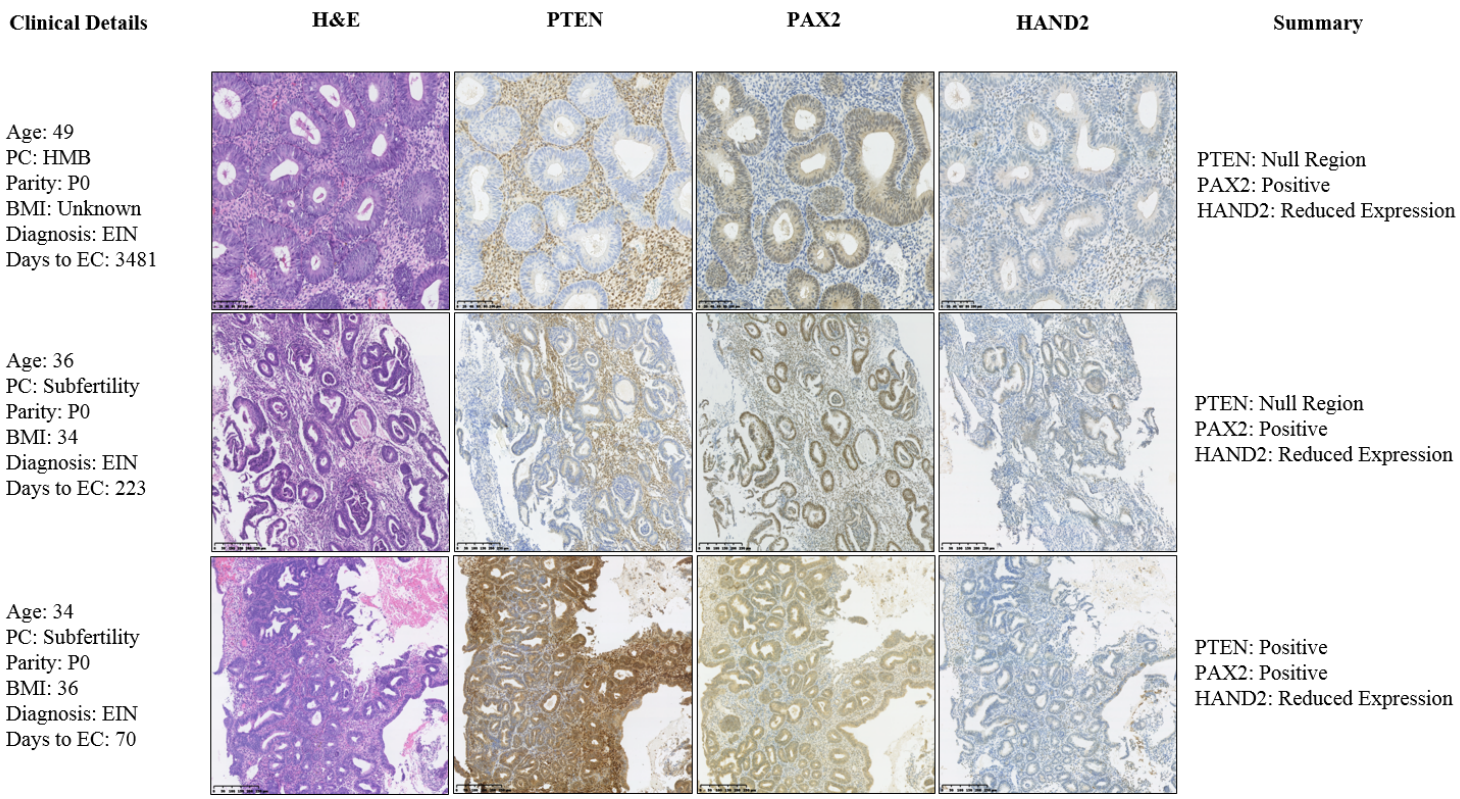

Figure 4-15B: Immunohistochemical phenotype of Cluster 3 EH cases that progressed to malignancy. n=6 patients from cluster 1 had a subsequent endometrioid endometrial cancer diagnosis. Figure. 4-15B summaries the expression pattern of the PTEN, PAX2 and HAND2 immunohistochemical staining profile for each EH case that progressed, along with pertinent clinical details. The selected images for each case represent serial tissue sections of the most abnormal hyperplastic region. H&E - Haematoxylin and Eosin, PTEN - Phosphatase and Tensin Homolog, PAX2 - Paired Box 2 Protein, HAND2 - Heart and Neural Crest Derivatives-expressed 2, EC - Endometrial cancer, HMB - Heavy menstrual bleeding. Varying magnifications – see scale bars.

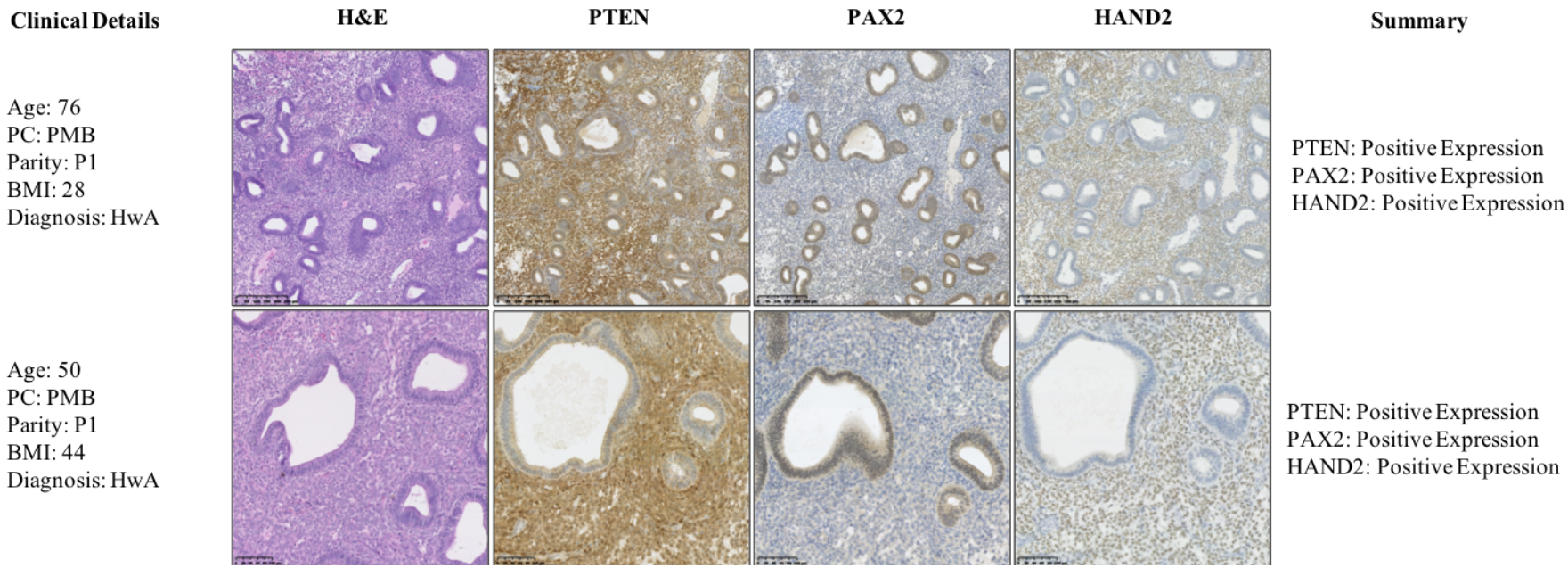

Figure 4-16: Representative immunohistochemical phenotype of Cluster 2b EH cases. n=2 patients from cluster 2b had a benign EH diagnosis. Figure. 4-16 demonstrates representative examples of the expression pattern of PTEN, PAX2 and HAND2 profile for two hyperplasia without atypia cases (HwA), along with pertinent clinical details. The selected images for each case represent serial tissue sections. H&E - Haematoxylin and Eosin, PTEN - Phosphatase and Tensin Homolog, PAX2 - Paired Box 2 Protein, HAND2 - Heart and Neural Crest Derivatives-expressed 2, EC - Endometrial cancer, HMB - Heavy menstrual bleeding. HwA - Hyperplasia without atypia. Varying magnifications – see scale bars.

4.5 Discussion

We used optimised immunohistochemistry techniques to evaluate the expression patterns of the proteins PTEN, PAX2, HAND2, MLH1, MSH2, MSH6, PMS2, ARID1A and p53 across a well characterised endometrial hyperplasia (EH) tissue resource. These proteins were selected for investigation following a review of the literature relating to changes in their expression pattern in EECs (Sanderson *et al.*, 2017). Our study benefitted from access to an EH tissue resource, the details of which are described in Chapter 3, as well as control samples from postmenopausal women without a diagnosis of EH or EEC. The overarching objective of our study was to see if we could elucidate any patterns of protein expression using these putative markers and we assumed that we might need to combine the results from several proteins to investigate the potential for a robust diagnostic marker panel for EH.

PTEN protein expression has been widely reported to be altered across EH tissues, with a propensity for expression loss in premalignant EH lesions (reviewed in Sanderson *et al.*, 2017). Moreover, during the 2014 joint consensus conference on EC by the triad of: The European Society for Medical Oncology (ESMO), The European Society for Radiotherapy & Oncology (ESTRO) and The European Society of Gynaecological Oncology (ESGO), it was recommended that PTEN immunohistochemistry could be used to distinguish atypical hyperplasia/EIN from benign mimics (Colombo *et al.*, 2016). In our current study, loss of PTEN protein in EH tissues with a diagnosis of EIN was 45.1 %, which is in keeping with previously published data (Monte *et al.*, 2010; Mutter *et al.*, 2001). However, we did not find any significant association between PTEN protein expression and a diagnosis of EIN or hyperplasia without atypia (HwA), concluding that PTEN is not a diagnostic marker for EIN, nor is it able to distinguish between high-risk EH (i.e. EIN) *versus* low-risk EH (i.e. HwA). Our data are supported by a recent meta-analysis of PTEN expression in EH tissues from Raffone *et al* (Raffone, *et al.*, 2018a). The authors reviewed 27 observational studies incorporating 1736 cases of EH, reporting low pooled diagnostic accuracy: sensitivity 54 % and specificity 66 % and concluding that immunohistochemical evaluation of PTEN expression has low usefulness in the differential diagnosis between benign and premalignant EH (Raffone, *et al.*, 2018a). Furthermore, when we analysed PTEN immunoexpression alongside the proteins PAX2 and HAND2 by hierarchical cluster analysis, PTEN protein was ubiquitously expressed across all cluster groups, with no significant difference in its expression pattern between the groups. This suggests that even as part of this potential diagnostic immunomarker panel, PTEN protein expression is not a helpful contributor. In terms of an association with progression of EH to EEC, 70 % of EH cases that progressed to

EEC in this study cohort exhibited some form of PTEN protein expression loss. This mirrors what is already known, that PTEN expression loss is associated with approximately 60 % of endometrioid endometrial cancers (EEC) (Garg *et al.*, 2012)

Loss of PAX2 protein was noted to exhibit two distinct expression patterns in our current study, either the presence of null glands (Figure. 4-2C) or complete altered expression across EH tissues (Figure. 4-2E). Immunostaining of PAX2 has been reported in the literature to be technically robust, with a distinct glandular nuclear staining pattern that is not difficult to interpret and is seemingly highly reproducible (Quick *et al.*, 2012; Rewcastle *et al.*, 2018). Previous studies have reported a PAX2 immunoexpression loss rate at 71 % within EIN cases (Monte *et al.*, 2010) and 74 % within atypical hyperplasia cases (Allison *et al.*, 2012). PAX2 immunohistochemistry was also recommended by the ESMO-ESGO-ESTRO Consensus Conference on EC to be used to distinguish atypical hyperplasia/EIN from benign mimics along with PTEN immunohistochemistry (Colombo *et al.*, 2016).

Contrary to published literature, we did not find similar rates of PAX2 protein expression loss within EIN cases from our human tissue resource, with 29.4 % of EIN cases demonstrating PAX2 altered expression in our hands. This is despite using the same antibody clone and immunohistochemical methodology as described by others (Jeffus *et al.*, 2014; Monte *et al.*, 2010; Quick *et al.*, 2012; Rewcastle *et al.*, 2018). Anecdotally, we did find that on reviewing our PAX2 stained tissues, a cytoplasmic 'flare' in the endometrial glands could sometimes be fairly significant and could distract from the evaluation of the pattern of nuclear immunostaining. This may reflect artefact from the age of the tissue specimens used in this study or the method of tissue fixation used, which could not be standardised. Our rate of PAX2 loss may therefore be higher than described. Moving forwards, this creates a potential role for automated image analysis in the assessment of PAX2 stained tissue sections, to improve assessment of a nuclear staining pattern whilst excluding any confounding influence from the background glandular cytoplasm.

Despite our overall lower rates of PAX2 expression loss, we did find that loss of PAX2 expression was significantly associated with a diagnosis of EIN in our study, although in isolation it was not a diagnostic marker. This is in keeping with a recent meta-analysis of PAX2 expression and EH by Raffone, *et al* who reviewed 6 studies, incorporating 266 normal endometrium, 586 EHs and 114 ECs. The authors observed that both decreased and complete loss of PAX2 expression were significantly more common in EC and precancerous EH than benign EH (Raffone, *et al.*, 2018b). When we analysed PAX2 expression alongside PTEN and HAND2 by hierarchical cluster analysis, we found that the immunoscores of both PAX2 and

HAND2 defined the individual clusters groups, achieving statistical significance. Indeed, positive expression of PAX2 and HAND2 was highly associated with a benign EH diagnosis, as indicated by cluster 2b in the heatmap (Figure. 4-12).

In murine models *hand2* has been shown to be a progesterone receptor-regulated gene and its expression in endometrial stromal cells inhibits epithelial cell proliferation via suppression of fibroblast growth factors (FGFs) (Li et al., 2011). In addition, epigenetic modification of *HAND2* has been suggested to play a role in endometrial carcinogenesis, whereby it is hypothesised that in the absence of *HAND2*, oestrogen signalling pathways become dominant and this may lead to increased endometrial proliferation (Bagcchi, 2013). Novel data generated by our study has demonstrated the stable expression of HAND2 protein across the normal cycling endometrium and the postmenopausal endometrium, which is exclusively located within the endometrial stromal compartment. We had considered that we might detect an increase in HAND2 protein expression in sections recovered during the secretory phase in keeping with higher expected levels of progesterone, and although there appeared to be a trend towards an increase in *HAND2* mRNA expression, the changes were not statistically significant. We did not detect a change in the intensity of immunoexpression in samples from tissues recovered across the menstrual cycle. In keeping with published literature (Buell-Gutbrod *et al.*, 2015; Jones *et al.*, 2013), we demonstrated loss of HAND2 protein immunoexpression across all grades of EEC utilising a representative sample set, with the novel finding of significant reductions in mRNA expression of *HAND2* irrespective of EEC grade.

Altered (absent and/or reduced) HAND2 immunoexpression was significantly associated with a diagnosis of EIN in our study, with 77.6 % of all EIN cases demonstrating altered HAND2 immunoexpression. Our data represents the first investigation of HAND2 protein expression applying the EIN classification system and we have utilised one of the largest sample sets of premalignant lesions (n=51 EIN cases) to date. These data corroborate findings from other groups who have investigated HAND2 protein expression within EH tissues and who found reduced protein expression, albeit using the WHO94 classification system and much smaller sample sets (complex atypical hyperplasia samples of n=10 and n=7 respectively) (Buell-Gutbrod *et al.*, 2015; Jones *et al.*, 2013).

Contrary to expectations based on genomic profiling of EEC, in our dataset of EHs we did not find evidence that changes in expression of ARID1A were common in benign EHs or, pre-malignant EH lesions. We demonstrated that changes in ARID1A expression were exclusive to EIN lesions, with 5/51 (9.8 %) of EIN lesions demonstrating focal glandular loss

(either isolated or confluent ARID1A null endometrial glands) or complete ARID1A expression loss 1/51 (2.0 %). This was surprising given that ARID1A expression has been reported to be lost in 26-29 % of low grade and 39 % of high-grade EEC respectively (Takeda *et al.*, 2016). Other groups have described similar rates of ARID1A expression loss in EH tissues. Mao *et al* reported clonal loss (focal regions of loss of ARID1A expression) at rates of 16 % in atypical endometrial hyperplasia, 24 % in uterine low-grade endometrioid carcinomas and 9 % in uterine high-grade endometrioid carcinomas, with respective rates of complete loss of 0, 25 and 44 % in these conditions (Mao *et al.*, 2013). The lower rates of ARID1A expression loss that we describe may reflect the lower rate of EEC progression in our cohort. We found that 10/105 (9.5 %) EH cases in our cohort progressed to EEC, of these cases, n=2 (20 %) had altered ARID1A expression. Both of the EH samples with altered ARID1A expression were deemed to have concurrent EECs. We would speculate therefore that alteration in ARID1A expression may be a late step in the precancer-cancer transition and would advocate for further studies of this protein to investigate its role as: 1) a predictor of higher-risk EIN lesions with significant malignant potential and 2) an indicator of a possible concurrent malignancy that has not been sampled on biopsy.

A further unexpected finding from our study was the low frequency of deficient mismatch repair (dMMR) within our tissue cohort, with a single patient sample exhibiting loss of MLH1 and PMS2 protein expression. dMMR is reported in ~25-30 % of somatic EEC (Hecht and Mutter, 2006) and in Lynch associated EEC, adjacent areas of atypical hyperplasia/EIN have been demonstrated to be highly concordant in their loss of expression of MMR proteins (Lucas *et al.*, 2018). Larger scale investigation of dMMR detection by immunohistochemistry may therefore be warranted on more diverse EH sample sets in order to establish firm conclusions, however based on our current data we would not advocate the use of MMR proteins in an EH diagnostic panel. Staining for p53 was also not informative in this study, which is probably unsurprising since *TP53* mutations are more usually associated with serous than endometrioid cancers for which EH is the major precursor (Alkushi *et al.*, 2004; Sherman *et al.*, 1995; Soong *et al.*, 1996).

We subjected the results of the immunohistochemical staining for PTEN, PAX2 and HAND2 to hierarchical agglomerative clustering analysis (HAC). This analysis is one of the multivariate statistical methods that identifies groups of samples that behave similarly or show similar characteristics (Eisen *et al.*, 1998). In the agglomerative approach used in our study, each immunohistochemical observation starts in its own cluster, and pairs of clusters are merged as one moves up the hierarchy (Szekely and Rizzo, 2005). Results of the present study

revealed that in utilising these three immunomarkers (PTEN, PAX2 and HAND2), EH samples could be classified into four distinct cluster groups. The immunohistochemical phenotype of each cluster was largely dependent on the pattern of HAND2 and PAX2 expression. The most striking feature from the cluster analysis was that in cluster 2b i.e. the 'benign cluster' containing 87.0 % of all the HwA cases, the immunohistochemical phenotype was that of PAX2 and HAND2 positivity. This suggests a potential role for these two protein markers as a diagnostic aid to differentiate between benign EH and premalignant EH. Certainly, this data warrants further prospective investigation in larger and more diverse sample cohorts. The largest number of EIN cases was located in cluster 3 (n=28, 54.9 %). This cluster group demonstrated predominantly HAND2 altered expression and interestingly also contained the largest number of cases which progressed to EEC (n=6, 60.0%). This finding raises further questions surrounding the role played by HAND2 in the premalignant-malignant transition of the endometrium. Further investigation is therefore needed into regulatory interactions between the stromal and epithelial cellular compartments in this context.

We acknowledge that there will be limitations to the data presented in this study due to the retrospective nature of the tissue resource, in particular the variables which could not be standardised, e.g. the age of the tissue samples and discrepancies in tissue fixation. Moving forward, we would wish to verify the results obtained on larger and prospectively collected tissue resources. Further potential limitations of the studies described herein include the use of manual over automated immunohistochemistry techniques, the use of biopsy material over whole tissue / hysterotomy specimens and the evaluation of an endometrial stromal marker (HAND2) for conditions where stromal to epithelial ratios are decreased.

Firstly, manual techniques were employed for immunohistochemical staining due to the heterogenous nature and the variable size of the tissue of interest. PTEN immunohistochemistry was performed using a Leica BOND-MAX (Leica Biosystems) robotic staining platform. This was due to known reports of a reduction in PTEN antigenicity within tissue sections with time after sections are cut from tissue blocks (Grillo *et al.*, 2017). An observation from the automated PTEN staining was that larger tissue sections (which would often cover the entirety of the glass slide), often exhibited an 'edge effect' due to incomplete reagent coverage because of the automated covertile. Taking all of the above factors into consideration, manual techniques were employed for the remaining proteins of interest to maximise the information gained from each tissue sample. Likewise, tissue microarrays were not utilised, since we wanted to evaluate protein expression across the entire biopsy specimen rather than run the risk of sampling a tissue area which underrepresented a particular staining

pattern. Each manual staining batch used relevant control tissues, with meticulous adherence to standard operating procedures and quality checks.

Secondly, biopsy materials were used in the current study over whole tissue or hysterectomy samples since the practical application of the protein markers would be on smaller biopsy samples, although we acknowledge that whole tissue wedge samples would permit localisation of protein expression patterns more accurately. Furthermore, tissue fixation is always superior in endometrial biopsy material, as there is no delay in formalin diffusing into the tissue, unlike hysterectomy specimens. Finally, with the use of a stromal immunomarker, a potential concern was that adequate volumes of stromal tissue would not be present in the EH and EEC samples to permit analysis. We did not find this to be the case and even in cases with limited amounts of stroma there was still sufficient material for analysis.

In conclusion, data presented in this chapter confirm and extend existing literature on the expression patterns of the proteins PTEN, PAX2, ARID1A, MMR (MLH1, MSH2, MSH6, and PMS2), HAND2 and p53 within EH tissues. Importantly, this observational study of well characterised human EH samples utilises the EIN/WHO2014 diagnostic system, which as previously demonstrated offers improved diagnostic reproducibility over its predecessors. In line with our expectations we did not find any single protein marker which was singularly able to act as a diagnostic aid to pathological classification of EH or predict progression from EH to EEC. However, novel data generated using hierarchical cluster analysis suggests that the combined use of PAX2 and HAND2 immunohistochemistry may prove useful in delineating benign from premalignant EH and that this warrants further prospective investigation, potentially also as part of a larger panel of immunomarkers.

Chapter 5

5 Investigation of the role of the tumour suppressors PTEN and ARID1A in endometrial epithelial cell proliferation

5.1 Introduction

The pre-menopausal endometrium undergoes cyclical changes in response to fluctuating levels of sex-steroid hormones produced by the ovaries (Critchley and Saunders, 2009). In post-menopausal life, ovarian follicles no longer form, and ovulation ceases so that progesterone is no longer produced by corpora lutea. Any exposure to oestrogens (either natural or synthetic) in the absence progesterone can result in chronic stimulation of the endometrium, increased cell proliferation and an increased risk of endometrial hyperplasia (EH) and endometrial cancer (EC) (Key and Pike, 1988).

Oestrogens occur naturally in several structurally related forms including, oestrone (E_1), oestradiol (E_2) and oestriol (E_3). Members of 7β-Hydroxysteroid dehydrogenase family of enzymes (17β-HSDs) can reduce E_1 to E_2 and conversely can oxidise E_2 to E_1. Although E_1 is the most abundant serum oestrogen during postmenopausal life, due to local biosynthesis within tissues (i.e. peripheral adipose tissue), the predominant intracellular oestrogen within the postmenopausal endometrium is reportedly E_2 (Whitehead *et al.*, 1981). Oestrogens bind to one of two nuclear receptors (oestrogen receptors (ERs) alpha and beta, ERα and ERβ), which are both encoded by independent genes (reviewed in Gibson and Saunders, 2012). The full-length receptors classically operate as ligand-dependent transcription factors, which in turn modulate gene expression.

The typical endogenous ligands for both ERα and ERβ are E_1 and E_2, both of which exhibit agonist activity (Gruber *et al.*, 2002). Classically, ligand-activated ERs form homo- or hetero-dimers which interact with consensus sequences, termed oestrogen response elements (EREs), within the promoter regions of genes (reviewed in Nilsson *et al.*, 2001). However, ERs can also bind imperfect EREs or ERE half sites, eliciting transcriptional responses (reviewed in Klinge, 2001) and genomic investigation has suggested that several oestrogen-response genes can also be regulated through indirect association of ERs with other DNA binding proteins (reviewed in Heldring *et al.*, 2007).

Molecular modelling of ER ligand binding domains has facilitated development of synthetic agonists and antagonists. For example, the compound Fulvestrant (ICI 182,780

marketed as Faslodex®) acts as an antagonist of both ERα and ERβ and is used for treatment of hormone-responsive breast cancer. An ERα-specific agonist, widely used in cell and animal studies is propyl-pyrazole-triol (PPT) (Sun, Huang, *et al.*, 2002). The selective oestrogen receptor modulator (SERM), Tamoxifen, is capable of mixed agonist and antagonist activities at ERs which is dependent on tissue type; acting as an antagonist in breast tissue, with mixed agonist/antagonist activity in endometrial tissues (Dutertre and Smith, 2000). As such, Tamoxifen treatment for breast cancer can increase the risk of developing of both EH and EC, and there should be a low threshold for investigation of women with abnormal uterine bleeding (AUB) who are taking this medication.

The *PTEN* tumour suppressor gene is reported to be the most commonly mutated and/or deleted gene within endometrioid ECs (Ayhan *et al.*, 2015). In the landmark genomic profiling study undertaken by The Cancer Genome Atlas, which characterised ECs into four groups (i) 'ultramutated', (ii) 'hypermutated', (iii) 'copy-number low' and (iv) 'copy-number high, *PTEN* mutations were found in 94 %, 88 %, 77 % and 15 % of cases respectively (Kandoth *et al.*). In addition, the endometrial premalignant lesion, atypical hyperplasia / endometrioid intraepithelial neoplasia (EIN), has been reported to harbour *PTEN* mutations in ~55 % of cases (Mutter, Lin, *et al.*, 2000).

PTEN mutations can lead to the development of a truncated protein product (Ali *et al.*, 1999), alterations in which can be detected by immunohistochemistry, providing a surrogate marker for mutational status. As reported in chapter 4, we noted a loss of PTEN protein expression in 23/51 (45.1 %) cases of EIN (4.4.1.1). Furthermore, loss of PTEN protein expression has also been described in morphologically normal endometrial tissues, leading some to speculate that PTEN abnormalities may be an early event in the development of sporadic EC (Mutter, Lin, *et al.*, 2000). On the contrary, a subsequent longitudinal study by the same group, analysed clone-specific PTEN mutations over time in the endometrium of women with a high- or low-reported risk for developing endometrial neoplasia (Mutter *et al.*, 2014). The group described that in only a small proportion (6.7%, 1/15) of cases, the PTEN-null glands seen within historic benign biopsies were the direct progenitors of the ensuing neoplasia (EIN or EC) in high-risk women (Mutter *et al.*, 2014). The authors therefore surmised that the temporal dynamics of PTEN clonal emergence, persistence, and involution are so sufficiently complex, that the presence of PTEN-null glands in otherwise histologically benign endometrium has an unknown contribution to long-term EC risk (Mutter *et al.*, 2014).

As discussed previously, PTEN expression is increased in both the glandular epithelium and stromal compartments during the oestrogen dominant proliferative phase, plausibly

influencing proliferation (Mutter, Lin, Fitzgerald, *et al.* 2000). Moreover, alterations in the endometrial hormonal milieu, both pharmacological (i.e. progestin therapy) (Zheng *et al.*, 2004) and physiological (i.e. bariatric weight loss surgery) (MacKintosh *et al.*, 2019) have been demonstrated to promote reversal of PTEN expression loss.

A suggested role for PTEN expression as a marker for EC progression stems from several lines of evidence showing that the protein regulates cell proliferation, tissue growth, and apoptosis via the PI3K/Akt/mTOR pathway (reviewed in Sansal and Sellers, 2004). PTEN catalyses degradation of Phosphatidylinositol (3,4,5)-trisphosphate (PIP_3) generated by the PI3K pathway, and as such it exerts its role as a tumour suppressor by inhibiting downstream functions, including; the activation of Akt, cell proliferation and cell survival (Stambolic *et al.*, 1998). *PTEN* overexpression in cancer cells carrying mutant- or deletion-type protein has been demonstrated to inhibit cell proliferation and tumorigenicity by instigating cell-cycle arrest at the G1 phase and also apoptosis (reviewed in Downward, 1998; Saito *et al.*, 2003).

Several *in vitro* and *in vivo* studies have suggested cross-talk between PI3K/Akt and oestrogen receptor signalling (Joshi *et al.*, 2012). In breast cancer epithelial cells, ERα can reportedly bind to the p85α regulatory subunit of PI3K, in the absence or presence of E_2, and as a consequence it can activate PI3K/Akt2 (Sun, Paciga, *et al.*, 2001). Furthermore, in human and bovine endothelial cells, Simoncini and colleagues demonstrated that ERα binds in a ligand-dependent manner to the p85α regulatory subunit of PI3K and that stimulation with oestrogen increases ERα-associated PI3K activity, leading to the activation of Akt (Simoncini *et al.*, 2000). It has also been suggested that PI3K and Akt can phosphorylate and directly activate ERα in the absence of a ligand, leading to an increased capacity to transcriptionally activate several target genes (Campbell *et al*., 2001). Moreover, in the endometrium of *Pten*$^{+/-}$ mice (which develop endometrial neoplastic lesions, both EH and EC), loss of *Pten* has been suggested to activate Akt leading to increased phosphorylation of ERα, and in turn activate the receptor *in vivo* and *in vitro* without the presence of a ligand (Vilgelm *et al.*, 2006). The same group also reported that a reduction in endometrial ERα activity dramatically reduces the neoplastic effect of *Pten* loss in the murine endometrium, in contrast to complete oestrogen depletion (Vilgelm *et al.*, 2006). These discoveries have led to some researchers to suggest that loss of *PTEN* may result in changes in tissue function through activation of ERα (Joshi *et al.*, 2012). In addition, nongenomic actions of oestrogen via a surface receptor have been studied (Coleman and Smith, 2001; Levin, 2000), providing an alternative mechanism via which *PTEN* and oestrogen signalling may overlap.

The chromatin remodelling gene, *ARID1A* has been reported to be frequently mutated in a number of human cancers, including renal, breast and prostate malignancies (reviewed in Mao and Shih, 2013). An interestingly link with endometriosis associated ovarian cancers has also been suggested (Wiegand *et al.*, 2010). *ARID1A* is described as a tumour suppressor (Huang *et al.*, 2007) with reports that it can influence cell proliferation in both *in vitro* and *in vivo* tumorigenesis models (reviewed in Guan *et al.*, 2011). Within the endometrium, *ARID1A* mutations have been demonstrated in ~40-50 % of low-grade endometrioid ECs (Guan, Mao, *et al.*, 2011; McConechy *et al.*, 2012). *ARID1A* mutations have been reported to frequently coexist with mutations of *PIK3CA* (Yamamoto *et al.*, 2012) and/or loss of PTEN expression (Bosse *et al.*, 2013), which both lead to a downstream activation of the PI3K/Akt pathway. Additionally, it has also been shown that loss of ARID1A expression in EC leads to an increased phosphorylation of Akt (Liang *et al.*, 2012).

Most mutations in *ARID1A* are insertions or deletions, bringing about the formation of a truncated protein that is susceptible to rapid degradation (as seen with PTEN). Thus, *ARID1A* gene mutations are highly correlated with loss of protein expression as assessed by immunohistochemistry, even in the absence of mutation in the other allele (i.e. haploinsufficiency) (Bosse *et al.*, 2013). Endometrial ARID1A protein expression has been investigated, with reports of 'clonal loss' within glandular regions in 16 % (6/38) of complex atypical hyperplasia's (WHO94 classified), rising to 'complete-loss' loss in 24 % (21/88) of low-grade endometrioid ECs (Mao *et al.*, 2013). This has led to the suggestion that ARID1A expression correlates with tumour progression in the endometrium (Mao *et al.*, 2013). In our own studies, we have noted loss of ARID1A protein expression in 6/51 (11.8 %) of EIN cases (4.4.6.1).

In summary, the proliferative endometrial environment created by exogenous or endogenous 'unopposed' oestrogen exposure (be that iatrogenic, pathological, obesity-related, or as a consequence of chronic anovulatory states) is generally regarded as one of the major risk factors for the development of both EH and EC. In addition, mutations of the tumour suppressors *PTEN* and *ARID1A* have been extensively described in endometrial neoplasia, with immunohistochemical evidence for loss of their protein expression within pre-malignant EH lesions (as reported in chapter 4). The potential for overlap of these two factors is apparent, especially in the context of driving the proliferation of a neoplastic endometrial environment. To that end, we hypothesised that manipulation of *PTEN* and *ARID1A* within endometrial epithelial cells would increase cellular proliferation and postulated that the effect may be further enhanced by an oestrogenic environment.

5.2 Aims of this chapter

1. To establish an *in vitro* endometrial epithelial cell model and use it to investigate cell proliferation in the context of:
    a. Knockdown of PTEN expression
    b. Knockdown of ARID1A expression
    c. Overexpression of oestrogen receptor alpha (ERα)

2. To explore the effect that knockdown of PTEN expression with overexpression of oestrogen receptor alpha (ERα) has on cell proliferation in an oestrogen stimulated environment

5.3 Materials and methods

5.3.1 *In vitro* cell culture

All cell culture work was carried out in class II biological safety cabinets designated specifically for either primary cell culture, secondary cell culture or for viral work. Local standard operating procedures for tissue culture were strictly adhered to.

5.3.1.1 Isolation of primary human endometrial cells

Primary human endometrial cells were isolated from human endometrial biopsy material as described previously (section 2.1.3 and 2.2.1) and following established literature protocols (Chan *et al.*, 2004; Gargett *et al.*, 2009; Valentijn *et al.*, 2013). All patient endometrial biopsy samples utilised for the isolation of primary endometrial cells in this study are listed in Table. 5-1, together with anonymised clinical information. All patients were within an 18-49-year age range and had menstrual cycles ranging between 24-35 days. Stage of the cycle was confirmed by histopathology. In addition to routine cell culture for propagation, a 4-chamber glass slide (Thermo Scientific Nunc 154526) pre-coated with attachment factor (Gibco, S006100) was seeded immediately after isolation (Day 0) at $1x10^5$ cells/mL (cells counted as per 2.2.3.3) for imaging and immunocytochemical analysis of each sample.

5.3.1.2 Human endometrial cell lines

Ishikawa, MFE-280, KLE and SHT-290 human cell lines were utilised as part of this study, as detailed in 2.2.2. Experiments were carried out using the lowest possible cell passage number. Routine cell culture was performed as per 2.2.3. As previously described, 72 hours prior to any experimentation, cells were moved to phenol-free media variants (DMEM/F12 (Gibco 21041025) and RPMI 1640 (Gibco, 11835030)), in addition to a switch to charcoal stripped fetal calf serum (CCFCS, as per 2.3.3.4), in order to reduce potential cofounding stimulatory effects.

5.3.1.3 Cell line doubling time

Experimental procedures were carried out with cell lines in the exponential growth phase, i.e. with all the cells dividing regularly and growing by geometric progression. Cell doubling time was calculated for all secondary cell lines (Table. 5-2). Cell lines were first seeded into 24-well plates (Corning, CLS3527) at $1x10^5$ cells/mL per well. Cell counts were performed every 24 hours for a period of 10 days (see 2.2.3.3). An online cell doubling time calculator (http://www.doubling-time.com/compute_more.php) was utilised to analyse the data. Cell doubling times were used to inform the initial seeding concentrations of cell lines within this study.

Table 5-1: Anonymised clinical information and histological cycle stage of endometrial biopsy material utilised for isolation of primary endometrial cells.

Ref	Ethics approval	Lab code	Age	BMI	Parity	Exogenous hormones	H&E stage
1	16/ES/007	CT1691	48	22	2	No	Proliferative
2	16/ES/007	CU1725	39	25	3	Yes	Proliferative
3	16/ES/007	CT1924	52	35	3	No	Proliferative
4	11/AL/0376	3526	40	19	1	UN	Early secretory
5	11/AL/0376	3520	29	24	1	UN	Proliferative
6	11/AL/0376	3519	UN	UN	0	No	Early secretory
7	11/AL/0376	3516	20	23	1	UN	Proliferative
8	11/AL/0376	3537	UN	UN	1	Yes	Early secretory
9	11/AL/0376	3540	22	26	0	No	Proliferative
10	11/AL/0376	3541	22	25	0	UN	Proliferative

BMI = body mass index (kg/m^2), H&E = haematoxylin and eosin stain, UN = Unknown

Table 5-2: Cell line doubling times.

Cell line	Cell doubling time (hours)
Ishikawa	22.4
MFE-280	52.0
KLE	96.2
SHT-290	48.7

5.3.1.4 3D cell co-culture

3D cell co-culture was performed utilising the Ishikawa and SHT-290 cell lines. In brief, highly porous polystyrene scaffolds engineered into a 200 µm thick membrane mounted on a 6-well insert (Alvetex®, Amsbio AMS.AVP004-32) were purchased. After washing the scaffold membrane in 70 % ethanol, followed by x2 sterile DPBS (Dulbecco's Phosphate-Buffered Saline, without calcium and magnesium (Gibco 14040-091)), washes, Matrigel® extracellular matrix (Corning, 734-110) was added to the centre of the scaffold at a 1:10 dilution in complete cell medium to a total volume of 300 µl and allowed to stand for 90 minutes at room temperature over a 6-well plate (Corning, CLS3516-50EA).

SHT-290 cells were added to the required number of scaffolds at $1x10^6$ cells per scaffold in 300 µl of media. Scaffolds were then incubated for 120 minutes at 37 ºC humidified conditions with 5 % CO_2 in air. 5 mL of complete cell medium was then added to the bottom of the well contained the scaffold using a pipette and allowed to slowly rise and submerse the scaffold membrane, prior to returning to the incubator. 24 hours later, cell culture medium was aspirated, and Ishikawa cells were added to the top of the scaffold membrane at $0.5x10^6$ cells per scaffold in 300 µl of media. Scaffolds were incubated for 30 minutes prior to the addition of 5 mL cell culture medium as above. Scaffolds were cultured for 10 days with complete cell medium changes every 2 days.

After 10 days of culture, scaffolds were removed from their inserts with sterile forceps and washed twice in sterile 37ºC DPBS. Scaffolds were bisected using a sterile scalpel with one half fixed for 24 hours in Bouins fixative (for future haematoxylin and eosin staining) and the other half for 24 hours in 4 % Paraformaldehyde (for future immunofluorescence). After 24 hours the bisected scaffolds were removed from their respective fixatives and carefully washed twice in sterile DPBS, prior to dehydration in various ethanol concentrations (50 %, 70 %, 80 %, 90 % and then 95 % ethanol). Bisected scaffolds were stored in 95 % ethanol prior to paraffin wax embedding, sectioning and histology (see 2.3.1).

5.3.2 Lentiviral manipulation of gene expression within cell lines

Lentiviral vectors (see Table. 5-3) were designed and created as described in 2.2.4 (by Dr. Pamela Brown and Ms. Linda Ferguson, Shared University Research Facility (SuRF), Biomolecular core, The University of Edinburgh). Viral transduction efficiency was determined for the MFE-280 and KLE cell lines using a test lentiviral construct, Lv-cppt-CMV-emGFP-opre (previously generated in-house by the Biomolecular core, The University of Edinburgh). This established the optimum lentiviral multiplicity of infection (MOI) number as 5 for both MFE-280 and KLE cell lines. The pLenti6-cppt-CMV-IRES-mCherry-opre control lentivirus (previously generated in-house by the Biomolecular core, The University of Edinburgh) was also used in this study.

5.3.2.1 Creation of stably transduced cell lines

In brief, MFE-280 and KLE cell lines were harvested and counted as per 2.2.3.1 and 2.2.3.3. MFE-280 and KLE cells lines were seeded into 6-well cell culture plates (Corning, CLS3516-50EA) at $5x10^5$ cells/well in 2 mL complete cell medium. After 24 hours incubation, the cells were visualised using an inverted phase contrast microscope to ensure their health and 40 – 80 % confluence. From this point forward, all experimentation took place in a designated viral cell culture room. The cells were infected with the desired lentivirus at a MOI of 5 in 1 mL of complete cell medium and incubated for 24 hours. Polybrene (Hexadimethrine Bromide, Sigma-Aldrich, 107689) was used as necessary (at 8 µg/mL) (see Table. 5-3) in order to increase transduction efficiency by neutralising any repulsion charge between viral particles and the cell surface. After 24 hours, cell medium was exchanged, and cells incubated for a further 48 hours.

At 72 hours post infection, cells were imaged using an epifluorescence microscope with relevant light filter cubes (EVOS™ FL Imaging System, Thermofisher Scientific FLAMF4300). Once expression of the expected fluorescent tag was confirmed (either EmGFP, Figure. 5-1 or mCherry, Figure. 5-2) the cells were incubated with 10 µg/mL of blasticidin (Thermofisher Scientific, A1113903) in 2 mL of cell medium. Resistant cells were selected by culture over a period of ~10-14 days with medium changes twice weekly. After ~10-14 days the cells were re-imaged with the epifluorescence microscope to confirm that all surviving cells were expressing the fluorescent tag. Cells were then propagated as per 2.2.3 in complete cell medium containing a maintenance dose of blasticidin (1 µg/mL) and protein expression was determined by Western blot prior to experimentation.

Table 5-3: Details of lentiviral vectors created specifically for use in this study

Lentiviral vector	Construct	Construct sequence	Titre (TU / mL)	Polybrene	Fluorescent tag
pLenti6-cppt-CMV-emGFP-hPTEN-1093	miR-1093	TGC TGT ATA GGT CAA GTC TAA GTC GAG TTT TGG CCA CTG ACT GAC TCG ACT TAC TTG ACC TAT A	1.3×10^8	No	EmGFP
pLenti6-cppt-CMV-emGFP-hPTEN-1672	miR-1672	TGC TGT TAG CTG GCA GAC CAC AAA CTG TTT TGG CCA CTG ACT GAC AGT TTG TGC TGC CAG CTA A	1.2×10^8	No	EmGFP
pLenti6-cppt-CMV-emGFP-hARID1A-1776	miR-1776	TGC TGT TTG CTG GTT GTA ATA TGG AGG TTT TGG CCA CTG ACT GAC CTC CAT ATC AAC CAG CAA A	1.4×10^8	No	EmGFP
pLenti6-cppt-CMV-emGFP-hARID1A-2233	mir-2233	TGC TGT CTT CTT GCC CTC CCT TAC TGG TTT TGG CCA CTG ACT GAC CAG TAA GGG GGC AAG AAG A	1.3×10^8	No	EmGFP
pLent6-cppt-CMV-emGFP-miR-NEG-control	Scr-miR	TGC TGA AAT GTA CTG CGC GTG GAG ACG TTT TGG CCA CTG ACT GAC GTC TCC ACG CAG TAC ATT T	$8x10^7$	No	EmGFP
pLenti6-cppt-CMV-ESR1-IRES-mCherry-opre	*ESR1*	GAT CCC AGA TTG GCC AGT ACC AAT GTT CAA GAG ACA TTG GTA CTG GCC AAT CTT TTT TTG GAA	3.2×10^7	Yes	mCherry

miR = micro-ribonucleic acid, IRES = internal ribosomal entry site, CMV = cytomegalovirus promotor, opre = optimised post-translational response element, emGFP = emerald green fluorescent protein, mCherry = member of red fluorescent protein family, cppt = central polypurine tract, Scr-miR = scrambled micro-ribonucleic acid, PTEN = phosphatase and tensin homolog, ARID1A = AT-rich interactive domain-containing protein 1A. TU = transduction unit.

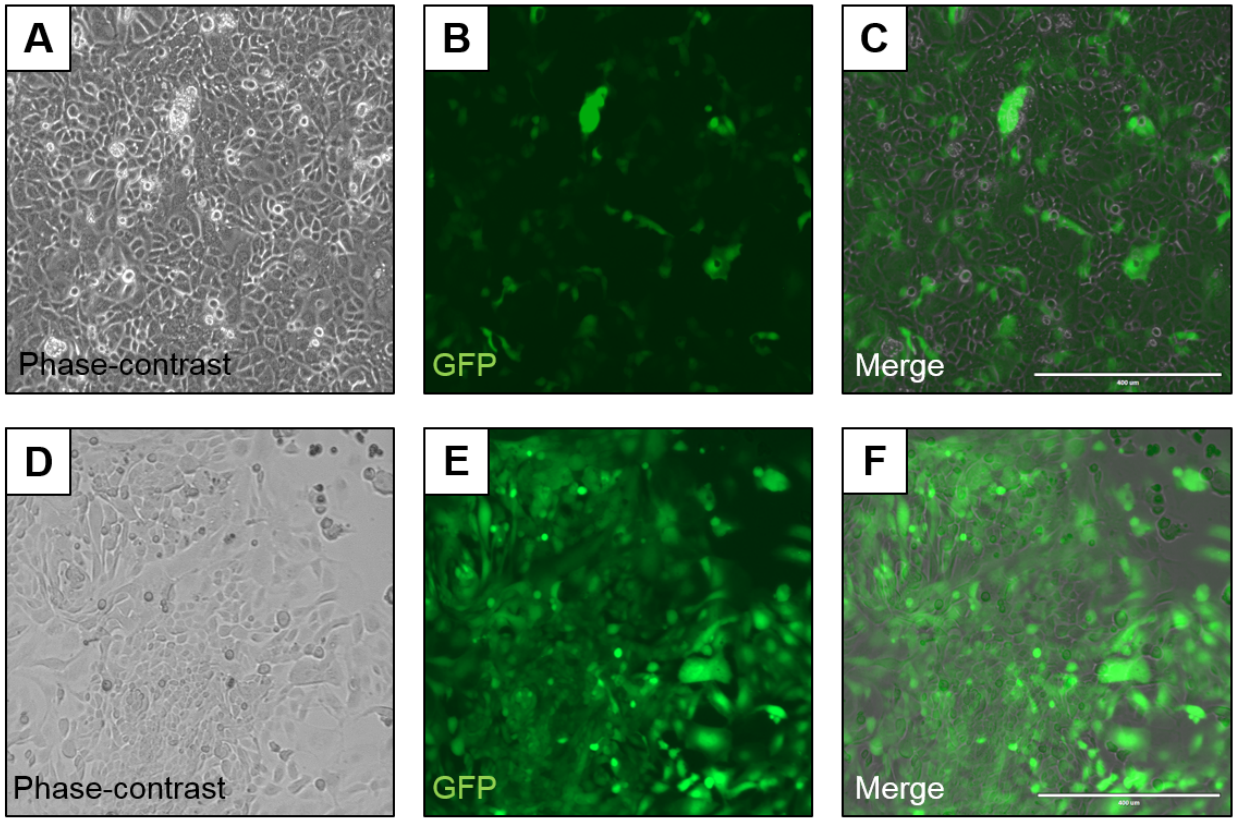

Figure 5-1:Representative images demonstrating lentiviral transduction of endometrial cell lines ('Knock-down'). Representative images of the KLE endometrial adenocarcinoma cell line following lentiviral transduction with Lv-cppt-CMV-EmGFP-ARID1A-1776-miR. A) KLE cells 72 hours after lentiviral transduction, phase-contrast image. B) As in image A, epifluorescent image with GFP light cube. Several cells demonstrate expression of emerald green fluorescent protein (EmGFP) indicating integration of the lentiviral vector into the host cell genome. C) Merged image A and B. D) KLE cells after 14 days of Blasticidin selection, phase-contrast image. E) As in image D, epifluorescent image with GFP light cube. All cells demonstrate expression of EmGFP, indicating integration of the lentiviral vector. Cells without lentiviral integration lack the resistance gene to blasticidin and have been killed by the selection agent. F) Merged image D and E. Magnification – see scale bar.

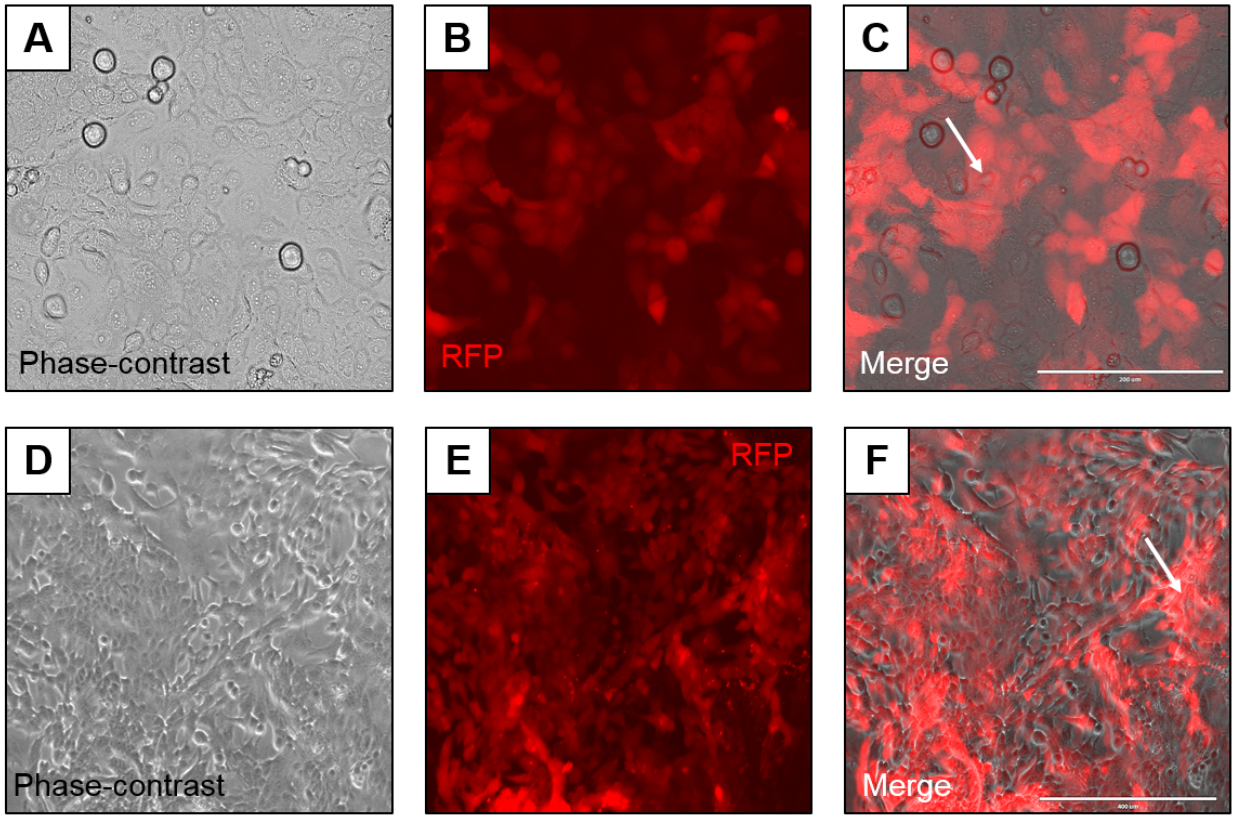

Figure 5-2: Representative images demonstrating lentiviral transduction of endometrial cell lines ('Overexpression'). Representative images of the MFE-280 endometrial adenocarcinoma cell line following lentiviral transduction with pLenti6-cppt-CMV-ESR1-IRES-mCherry-opre. A) MFE-280 cells 72 hours after lentiviral transduction, phase-contrast image. B) As in image A, epifluorescent image with RFP (red fluorescent protein) light cube. Several cells demonstrate expression of mCherry (member of the RFP family) indicating integration of the lentiviral vector into the host cell genome. C) Merged image A and B. D) MFE-280 cells after 14 days of Blasticidin selection, phase-contrast image. E) As in image D, epifluorescent image with RFP light cube. All cells demonstrate expression of mCherry, indicating integration of the lentiviral vector. Cells without lentiviral integration lack the resistance gene to Blasticidin and have been killed by the selection agent. F) Merged image D and E. Magnification – see scale bar.

5.3.2.2 Fluorescence activated cell sorting (FACS) of co-transduced cell lines

Cell lines co-transduced with two lentiviral vectors in order to alter the expression of two proteins of interest were created as per 5.3.1.6, with the following modifications. The cells were co-infected with two lentiviral vectors simultaneously at a MOI of 5 for each virus in a total of 1 mL of culture medium (+/- polybrene). In order to select for double positive cells expressing both EmGFP and mCherry the cells underwent FACS at 72 hours instead of blasticidin selection.

In brief, following detachment from plasticware as per 2.2.3.1, cells were washed with 3 mL filtered FACS buffer (sterile Dulbecco's Phosphate-Buffered Saline, without calcium and magnesium (Gibco 14040-091), with 2 % bovine serum albumin added). Samples were centrifuged for 5 minutes (115g at room temperature) prior to resuspension in 5 mL of FACS buffer and filtered to remove clumps using a 40 μm nylon mesh cell strainer (BD Falcon, 352340). Cell suspensions were counted, and viability assessed as per 2.2.3. FACS was performed by the Centre for Inflammation Research (CIR) Flow Cytometry Facility team, using a BD Aria Fusion FACS sorter (BD, UK). Sorted cells (Figure. 5-3) were then propagated as per 2.2.3 in cell medium containing a maintenance dose of blasticidin (1 μg/mL) and protein expression was determined by Western blot prior to experimentation.

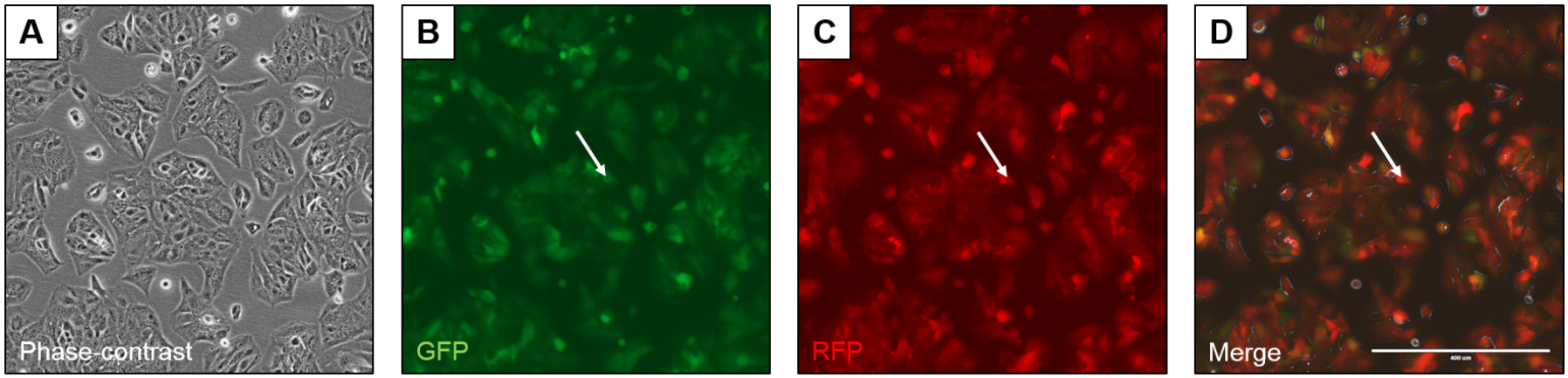

Figure 5-3: Representative images demonstrating lentiviral co-transduction of endometrial cell lines ('Knockdown and 'Overexpression') post FACS. Representative images of the MFE-280 endometrial adenocarcinoma cell line following lentiviral co-transduction with pLenti6-cppt-emGFP-hPTEN-1093 and pLenti6-cppt-CMV-ESR1-IRES-mCherry-opre. 72 hours post lentiviral co-transduction cells were detached from plasticware and underwent fluorescence-activated cell sorting (FACS) in order to produce a population of EmGFP and mCherry double positive cells. After sorting, double positive cells were returned to culture in maintenance Blasticidin cell media and imaged 24 hours later. A) MFE-280 co-transduced cells 24 hours after FACS sorting, phase-contrast image. B) As in image A, epifluorescent image with GFP (green fluorescent protein) light cube. All cells demonstrate expression of EmGFP (example with white arrow) indicating integration of the pLenti6-cppt-emGFP-hPTEN-1093 vector into the cell genome. C) As in image A, epifluorescent image with RFP light cube. All cells demonstrate expression of mCherry (example with white arrow), indicating integration of the pLenti6-cppt-CMV-ESR1-IRES-mCherry-opre vector into the cell genome. D) Merged image of A, B and C demonstrating co-localisation of EmGFP and mCherry expression in all cells (example with white arrow). Magnification – see scale bar.

5.3.3 Cell proliferation assay

The impact of both manipulation of gene expression and ligand treatment on cell proliferation was assessed using CyQUANT® Direct Cell Proliferation Assay (Thermo Fisher, C35011) according to manufacturer's instructions and nuclear fluorescence measured using a Novostar Microplate Reader (BMG labtech). The CyQUANT® assay consists of two components: a green fluorescent nucleic acid stain and a background suppression dye. The nucleic acid dye is a live cell-permeable reagent that mainly concentrates in the nucleus of mammalian cells. The suppression dye is impermeable in live cells and suppresses "green" fluorescence. The combination of these two components results in an assay based on both DNA content and membrane integrity.

In brief, cell lines were harvested and counted as previously described (2.3.3.1 and 2.2.3.3), before being seeding into black 96-well optical bottom plates (Thermofisher Scientific 165305) at 5000 cells per well in 200 µL of phenol-free, CSFCS containing cell medium – numbers of wells guided by individual experimental design. Each plate was centrifuged (Sorvall ST 16R, Thermofisher Scientific) (1 minute at 30g, room temperature) in order promote even spread of the cells within each well and cell adherence. The CyQUANT® assay was then utilised at desired time points.

Firstly, a 2x cell detection regent was made (12 mL required for x1 96-well plate; 11.7 mL of phenol-red free, CSFCS complete cell medium was added to 48 µL of CyQUANT® Direct nucleic acid stain and 240 µL of CyQUANT® Direct background suppressor I, prior to mixing at room temperature). 200 µL of the 2x detection reagent was added to the desired wells, followed by a 60-minute incubation at 37 ºC humidified conditions with 5 % CO_2 in air. Fluorescence was then measured using a Novostar Microplate Reader (BMG labtech) at 480/535 nm, 1500 gain. Cell free control wells were used to exclude background 'noise'. For each cell line variant investigated, cell number was first quantified using a standard curve of known cell numbers.

5.3.3.1 Treatments with ligand

The CyQUANT® Direct Cell Proliferation Assay was used to assess the effect of ligand treatment of cell lines and their variants. Ligands were prepared to final working concentrations as per 2.2.5. Cell lines were prepared as per 5.3.3. 24 hours after seeding, complete cell medium was removed from each well by gentle vacuum aspiration, taking care

not to dislodge the cells. 200 µL of phenol-free, serum free complete cell medium or phenol-free, serum free complete cell medium with 10^{-7}M Fulvestrant (ICI, 182,780) was added and incubated at 37 ºC in humidified conditions with 5 % CO_2 in air for 1 hour, thereafter the medium was removed by gentle aspiration and 200 µL of phenol-free, serum free complete cell medium containing the desired ligand was added. Plates were then incubated for 72 hours and the CyQUANT® assay performed as per 5.3.3. Using standard curves of known cell numbers for each transduced cell line, fold-change in cell number was calculated relative to vehicle control for each ligand treatment group.

5.3.4 Reporter assays

An adenoviral vector containing a 3× ERE-tk-luciferase reporter gene was generated as described in Collins *et al.*, 2009. Cells lines of interest were cultured in 6 well-plates (Corning, CLS3516-50EA) at $1x10^5$ cells/ well in 4 mL phenol-red free complete medium with the addition of CSFCS (complete medium for each cell line as per Table. 2-1). 24 hours later they were infected with Ad-ERE-Luc adenovirus at a MOI of 25 (MOI already established from previous adenoviral transfections performed by the Saunders group utilising MFE-280 and KLE cells). After a further 24 hours, cells were incubated with phenol-free, serum free, complete cell medium or phenol-free, serum free, complete cell medium with 10^{-7}M Fulvestrant (ICI, 182,780) for 1 hour (as described in 5.3.3.1, modified to account for the larger volume of complete cell medium required for a 6-well plate, i.e. 4 mL per well). Following this, medium was removed by gentle aspiration and 4 mL of phenol-free, serum free, complete cell medium containing the desired ligand (as described in 2.2.5) was added. Cells were treated for 24 hours, following which luciferase activity was determined using the Bright-Glo™ Luciferase Assay System (Promega, TM052). Luminescence was measured using Fluostar Microplate Reader (BMG labtech) and the change in luciferase activity was calculated relative to vehicle control for each treatment. All treatments were carried out in duplicate to permit measurement of whole protein lysate concentration (as per 2.9.2) in order to normalise the reporter assay for cell number.

5.3.5 Immunohistochemistry and immunofluorescence

Immunohistochemistry, immunofluorescence and fluorescent immunocytochemistry were carried out as described in section 2.3 using the antibodies and detection systems outlined in Tables. 5-4 and 5-5.

Table 5-4: Primary antibodies used for immunohistochemistry and immunofluorescence.

Primary antibody	Species	Supplier	Cat. No	Dilution IHC	Dilution IF
CD10	Mouse	ThermoScientific	MS-728-S	1:250	1:400
pan-Cytokeratin	Mouse	Sigma-Aldrich	C2562	1:4000	1:15000
pan-Cytokeratin*	Rabbit	Abcam	ab9377		1:100

IHC = immunohistochemistry, IF = immunofluorescence
*For dual fluorescent immunocytochemistry utilising both CD10 and pan-cytokeratin, where the antibodies need to be raised in different animal species (as discussed in 2.5.1) a rabbit raised pan-cytokeratin antibody was used.

Table 5-5: Detection systems used for immunohistochemistry and immunofluorescence.

Primary antibody	Detection			
	IHC		**IF**	
CD10	ImmPRESS™ Anti-Mouse	DAB	Goat anti-Mouse HRP	Tyramide (Fluoresin)
pan-Cytokeratin	ImmPRESS™ Anti-Mouse	DAB	Goat anti-Mouse HRP	Tyramide (Cyanine-3)
pan-Cytokeratin*			Goat anti-rabbit biotinylated IgG H&L	Streptavidin Alexa Fluor 555

IHC = immunohistochemistry, IF = immunofluorescence, DAB = 3, 3 –diaminobenzidine, HRP = horseradish peroxidase, H&L = heavy and light chains.
*For dual fluorescent immunocytochemistry a biotin and streptavidin method was used

5.3.6 Western Blot

Western blots were performed as described in Section 2.11. The antibodies used are listed in Table. 5-6. Semi-quantitative densitometry was performed using the Image Studio Lite software (Licor, UK).

Table 5-6: Antibodies used for the detection of proteins of interest in this study by Western blot.

Protein target	Species	Supplier	Cat. No	Dilution	IR Secondary antibody	Dilution
PTEN	Mouse	Agilent Dako	M362729-2	1:1000	DAM 680RD	1:10000
ARID1A	Rabbit	Sigma-Aldrich	HPA005456	1:500	DAR 680RD	1:10000
ERα	Mouse	Vector	ER6F11	1:800	DAM 680RD	1:10000
Actin	Goat	Santa-Cruz	SC-1616	1:500	DAG 800CW	1:10000
β-Tubulin	Mouse	Sigma-Aldrich	T8328	1:1000	DAM 800CW	1:10000

IR secondary antibody = IRDye® secondary antibody by Licor. DAM = Donkey anti-Mouse, DAR = Donkey anti-Rabbit, DAG = Donkey anti-Goat.

5.3.7 RNA extraction

RNA was extracted and quantified as described in section 2.7.

5.3.8 Two-step quantitative real-time reverse transcription polymerase chain reaction (qRT-PCR)

Reverse transcription, quantitative real-time PCR (TaqMan® method) and qPCR analysis was performed as described in section 2.8. *CYC* was used as the housekeeping gene. Primer/probe use for this chapter is listed below (Table. 5-7).

Table 5-7: Primer pair sequences and probes used for qRT-PCR

Gene Name	Accession Code	Primer Sequences	Primer Position / Probe	
MME	NM_000902.3	gcgaagcttgaccgagag	41-58	19
		tgcccatcacctaaaatcgt	108-127	

5.3.9 Statistical analysis

Statistical analysis was performed using GraphPad Prism 8.0. A one-way ANOVA was used to determine significance between variables that were normally distributed, with Tukey's multiple comparison test. A two-way ANOVA was used to determine significance between variables and time for data that were normally distributed, with Sidak's multiple comparisons test. Non-parametric testing was utilised where sample sizes were insufficient to confirm normality of data distribution or data was not normally distributed; Kruskal–Wallis test was used. For data analysed as fold-change, significance was tested using a one sample *t* test and a theoretical mean of 1. Criterion for significance was $p < 0.05$. All data are presented as mean ± s.e.m.

5.4 Results

5.4.1 Human endometrial epithelial tissue and the immortalised Ishikawa adenocarcinoma epithelial cells are both pan-Cytokeratin positive

Cytokeratins are keratin proteins found within the cytoskeleton of epithelial tissues. It is widely accepted that the pan-Cytokeratin (PCK) antibody provides a broad spectrum of reactivity and recognises epitopes in low-molecular weight and high-molecular weight cytokeratins in virtually all human epithelia. Expression of PCK was investigated in order to confirm or exclude the presence of endometrial epithelial cells within cell isolates from primary human endometrial tissue in this study. Within normal endometrial tissue, PCK was detected by immunohistochemistry, demonstrating a strong brown (DAB) cytoplasmic staining pattern within the endometrial glandular epithelial compartment; in line with expectations the endometrial stromal compartment was immunonegative (Figure. 5-4A).

A 'normal' human endometrial epithelial cell line is not widely available, since anecdotally the phenotype of such cells tends to vary, and there have been reports that some cultures that claim to be endometrial cells have become contaminated with other cell lines, e.g. MCF7 (Korch *et al.*, 2012). The Ishikawa cell line (see 2.2.2.1) is therefore commonly used as a surrogate for primary cells, as it was originally derived from a well-differentiated tumour (Nishida *et al.*, 1985) and shares several phenotypic characteristics with epithelial cells *in situ,* including expression of oestrogen and progesterone receptors (Lessey *et al.*, 1996b). Expression of PCK was confirmed within the Ishikawa cells grown in our laboratory (ECACC 99040201) by means of single fluorescent immunocytochemistry, showing intense strong cytoplasmic staining in keeping with epithelial cell lineage (Figure. 5-4C).

5.4.2 Human endometrial stromal tissue and human immortalised SHT-290 stromal cells are both CD10 positive

Expression of the cell surface enzyme CD10 was investigated in order to confirm or exclude the presence of endometrial stromal fibroblasts within cell isolates from primary human endometrial tissue samples. It has been reported that CD10 is exclusively expressed within the cytoplasm of stromal cells in normal cycling human endometrium (McCluggage *et al.*, 2001; Toki *et al.*, 2002). This was confirmed in house using immunohistochemistry to interrogate sections of normal human endometrial tissue (Figure. 5-4B, courtesy of Dr Douglas

Gibson, The University of Edinburgh). Expression of CD10 was investigated within immortalised SHT-290 cells (see 2.2.2.4) by means of single fluorescent immunocytochemistry, confirming strong cytoplasmic staining pattern and indicating that the SHT-290 cell line remains phenotypically similar to human endometrial stromal cells even after repeated passage *in vitro* (Figure. 5-4D).

5.4.3 Immuno-phenotyping of human immortalised SHT-290 stromal cells and the Ishikawa adenocarcinoma cell in a 3D co-culture system

The purpose of immuno-phenotyping endometrial epithelial and stromal cell lines was to provide positive controls for characterisation of primary cells isolated cells from human primary endometrial tissues. For this reason, Ishikawa and SHT-290 cells were grown in a 3D co-culture system and investigated for their dual expression of CD10 and PCK. Figure. 5-4E demonstrates that Ishikawa cells express PCK but not CD10 and SHT-290 cells express CD10 but not PCK, confirming that different cell types can readily be identified in 3D scaffolds, providing a platform for the future investigating of primary endometrial stromal and epithelial cells obtained from human tissue biopsy material.

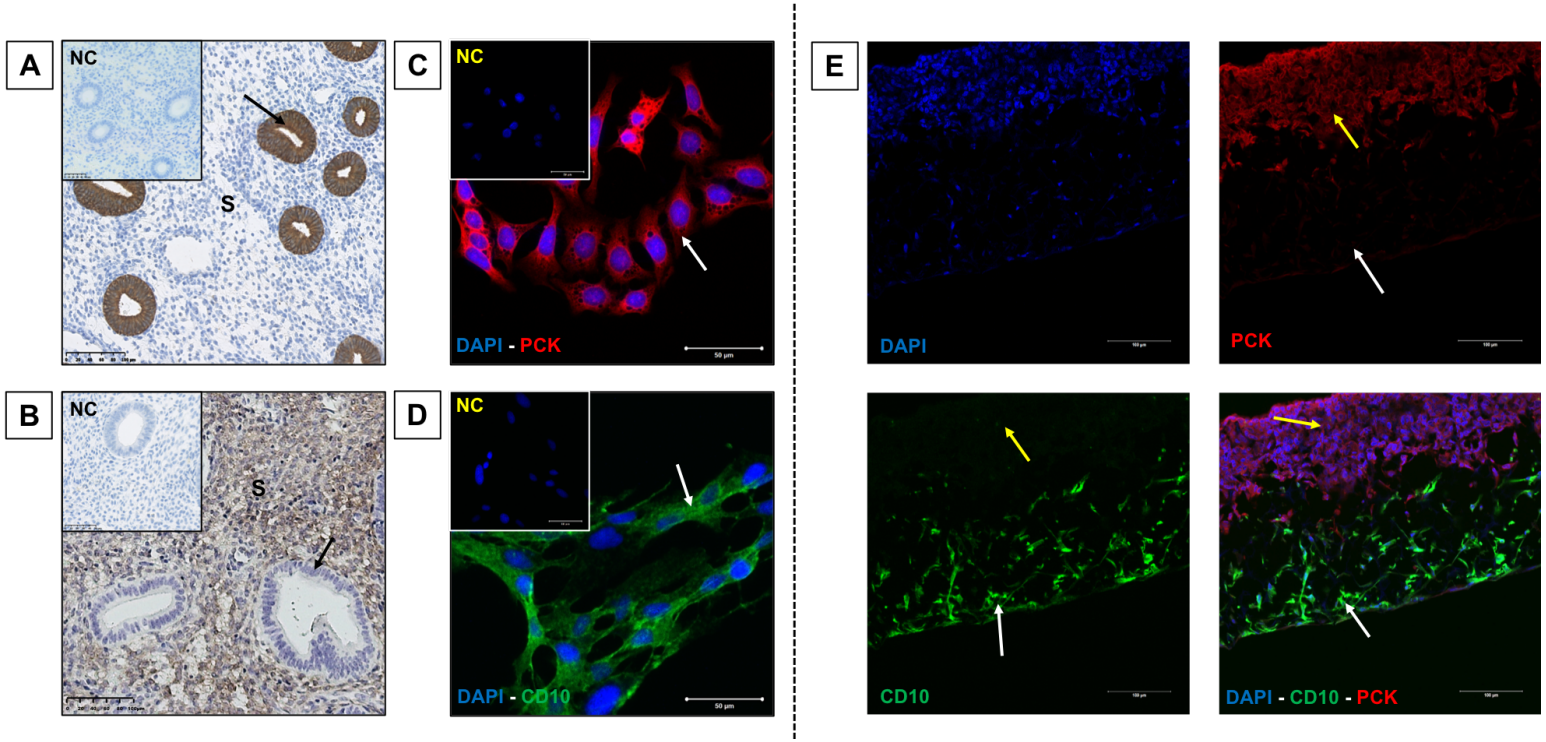

Figure 5-4: Immuno-characterisation of endometrial epithelial and stromal cells. A, B) Within FFPE tissue sections of normal human cycling endometrium, endometrial epithelial cells (black arrow) express strong cytoplasmic brown (DAB) staining of pan-Cytokeratin (PCK) (A) but are negative for CD10 (B). Conversely, endometrial stromal fibroblast cells (S) demonstrate strong brown (DAB) cytoplasmic staining of CD10 (B) but are negative for PCK (A). C) The human endometrial adenocarcinoma (epithelial cell malignancy) immortalised cell line, Ishikawa, demonstrates strong cytoplasmic staining of PCK (red - Cyanine3) by single fluorescent immunocytochemistry (white arrow). D) The human telomerase reverse transcriptase (hTERT) immortalised endometrial stromal cell line, SHT-290, demonstrates strong cytoplasmic staining of CD10 (green - fluorescein) by single fluorescent immunocytochemistry (white arrow). E) Dual fluorescent immunocytochemistry of both Ishikawa cells and SHT-290 cells grown in 3D co-culture, demonstrates that Ishikawa cells (yellow arrow) stain positively for PCK (red) and are negative for CD10 (green), whilst SHT-290 cells (white arrow) stain positively for CD10 (green) and are negative for PCK (red). NC = Negative control, DAPI (4', 6-diamidino-2-phenylindole) = blue nuclear fluorescent counterstain. Image B courtesy of Dr Douglas Gibson, The University of Edinburgh. Various magnifications – see scale bars.

5.4.5 Morphological characteristics of primary human endometrial cells isolated from Pipelle® human endometrial biopsy material

Human primary endometrial cells (PECs) were isolated as described (5.3.1.1) with the aim of obtaining a pure population of primary endometrial epithelial cells with which gene manipulation could be performed in order to address the objectives of this chapter. Figure. 5-5 shows phase-contrast microscopy images of a representative isolate of primary endometrial cells (sample 3526, Table. 5-1). In this representative example, the morphology of cells on day 2 post isolation was consistent with an epithelial cell phenotype (Figure. 5-5 C&D), with discernible isolated groups of adherent cells with a polygonal shape and regular dimensions. By day 4, the presence of cells with fibroblastic morphology (multipolar and elongated cells) was detected, suggestive of contamination with more rapidly dividing stromal cells. By day 10 of culture, significant cell death appeared to have occurred (less cells), those that remained adherent to the plastic had a morphology suggestive of senescence (Figure. 5-5 G&H) with flat, enlarged and irregular appearances.

5.4.6 Dual fluorescent immunocytochemistry for CD10 and pan-Cytokeratin on isolated primary endometrial cells suggests a mixed population of epithelial and stromal cells

As described in 5.3.1.1 four-chamber glass slides were seeded with isolated human PECs on day 0 for the purpose of immuno-phenotyping the isolated cells. Consistent with morphology observed under the phase-contrast microscope, on day 2 post isolation populations of cells that were immunopositive for PCK but not CD10 were present consistent with an epithelial cell phenotype (Figure. 5-6). By day 4 post isolation, the cultures contained some CD10 positive cells, PCK negative cells was more apparent, suggesting potential stromal cell contamination / overgrowth within the population of isolated primary cells (Figure. 5-7. NB/ this image is from the same culture as in Figure. 5.6).

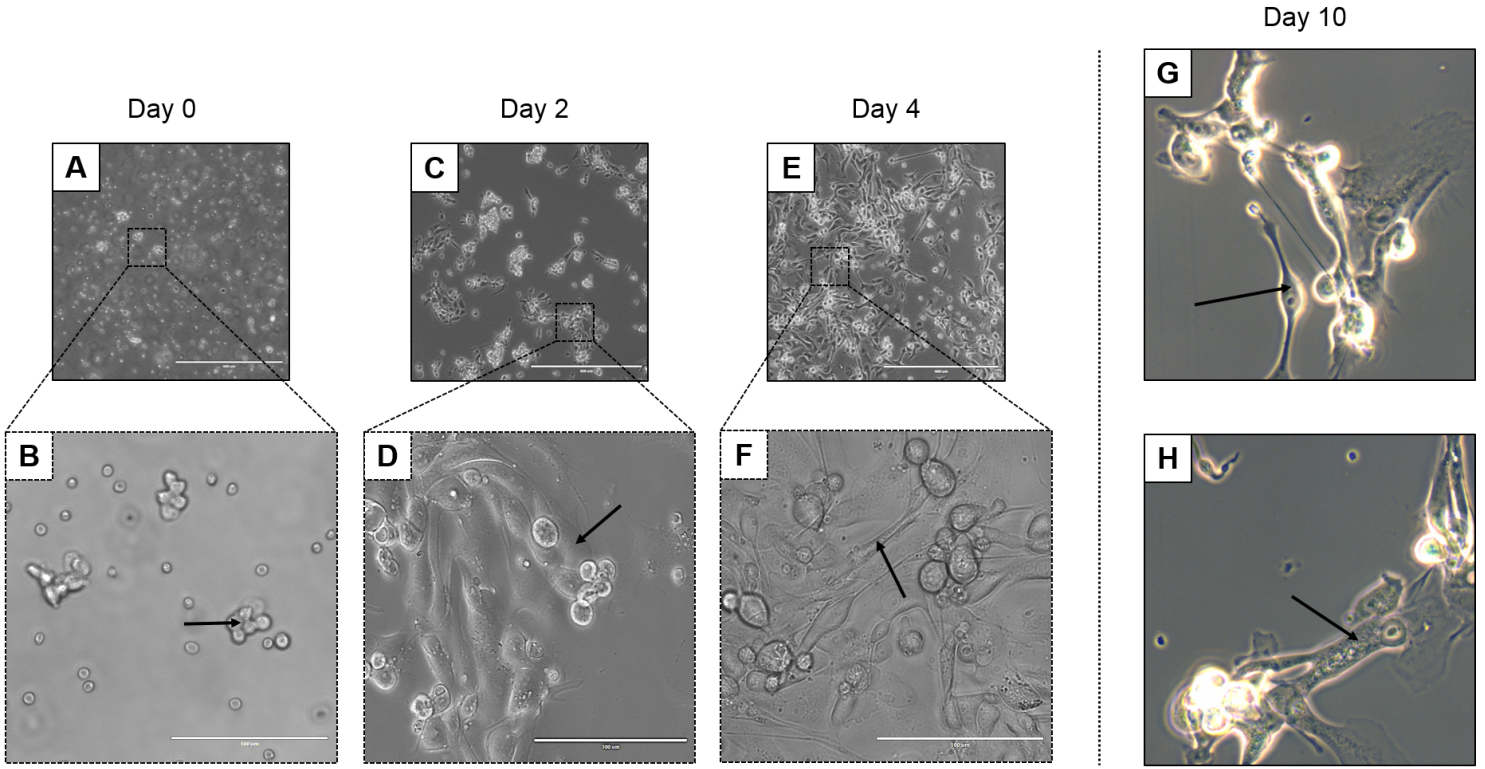

Figure 5-5: Representative inverted phase-contrast microscopy images of primary endometrial cells isolated from human endometrial Pipelle® biopsy material. A, B) Day 0 immediately post cell isolation. Several small clusters of presumed endometrial epithelial cells are noted in suspension (B – arrow). C, D) Day 2 post cell isolation. Cell attachment has occurred. Discrete patches of adherent cells (presumed endometrial epithelial cells) can be visualised demonstrating a polygonal shape with regular dimensions (D – arrow). E, F) Day 4 post cell isolation. Expansion of some of polygonal cells has occurred. The presence of multipolar, elongated cells is apparent (F – arrow), suggestive of stromal fibroblast contamination. G, H) Day 10 post cell isolation. Large numbers of cells appear dead and those that remain have a predominantly fibroblastic morphology (G – arrow). Cells appear enlarged, flattened and irregular (H – arrow) with morphology suggestive of senescence. Various magnifications – see scale bars.

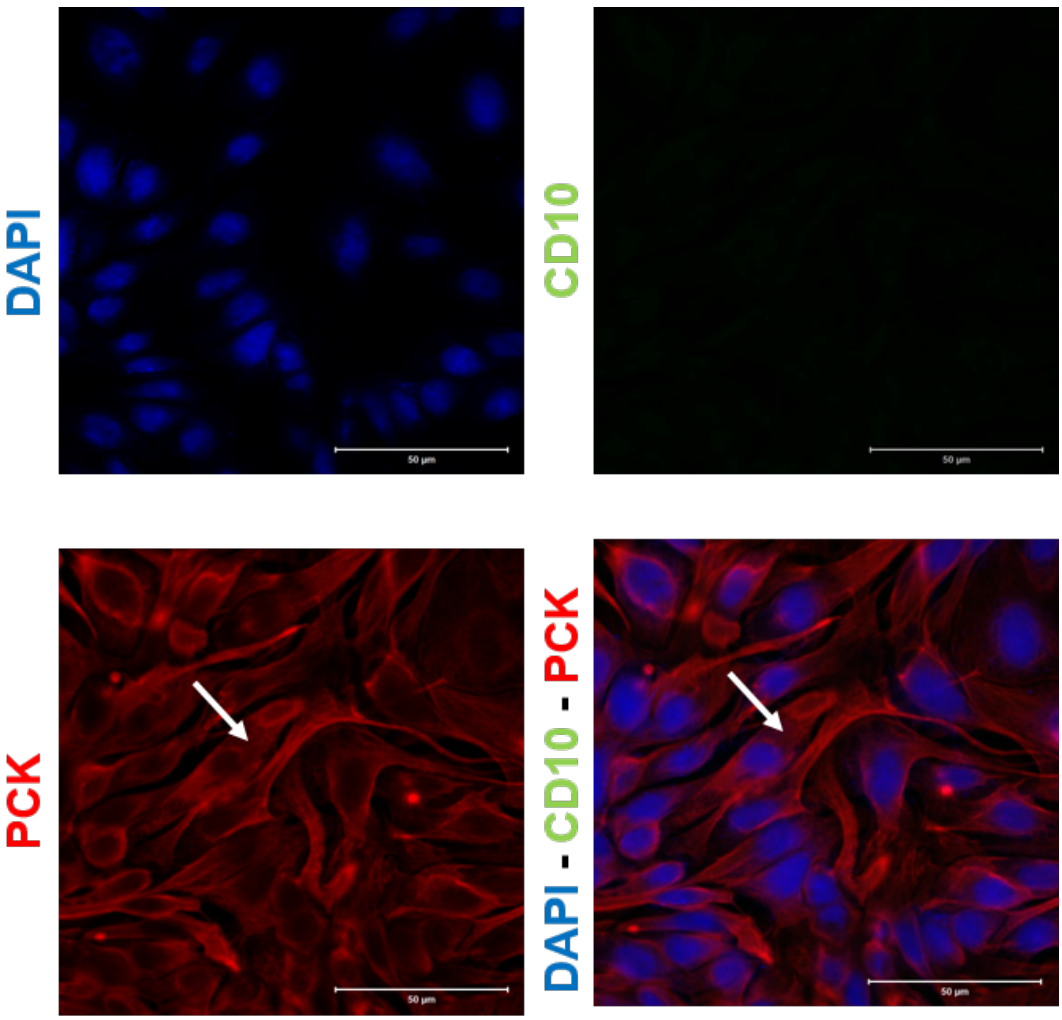

Figure 5-6: Representative dual fluorescent immunocytochemistry for pan-Cytokeratin (PCK) and CD10 expression in primary human endometrial cells day 2 after isolation. Isolated primary endometrial cells were grown in 4-well glass chamber slides alongside the standard cell culture flasks. The above figure utilises day 2 primary endometrial cells and suggests a predominantly epithelial cell population, with cells demonstrating positive expression of PCK (red - Cyanine3) and negative expression of CD10 (green-fluorescein). DAPI = blue nuclear counterstain. Magnification – see scale bar.

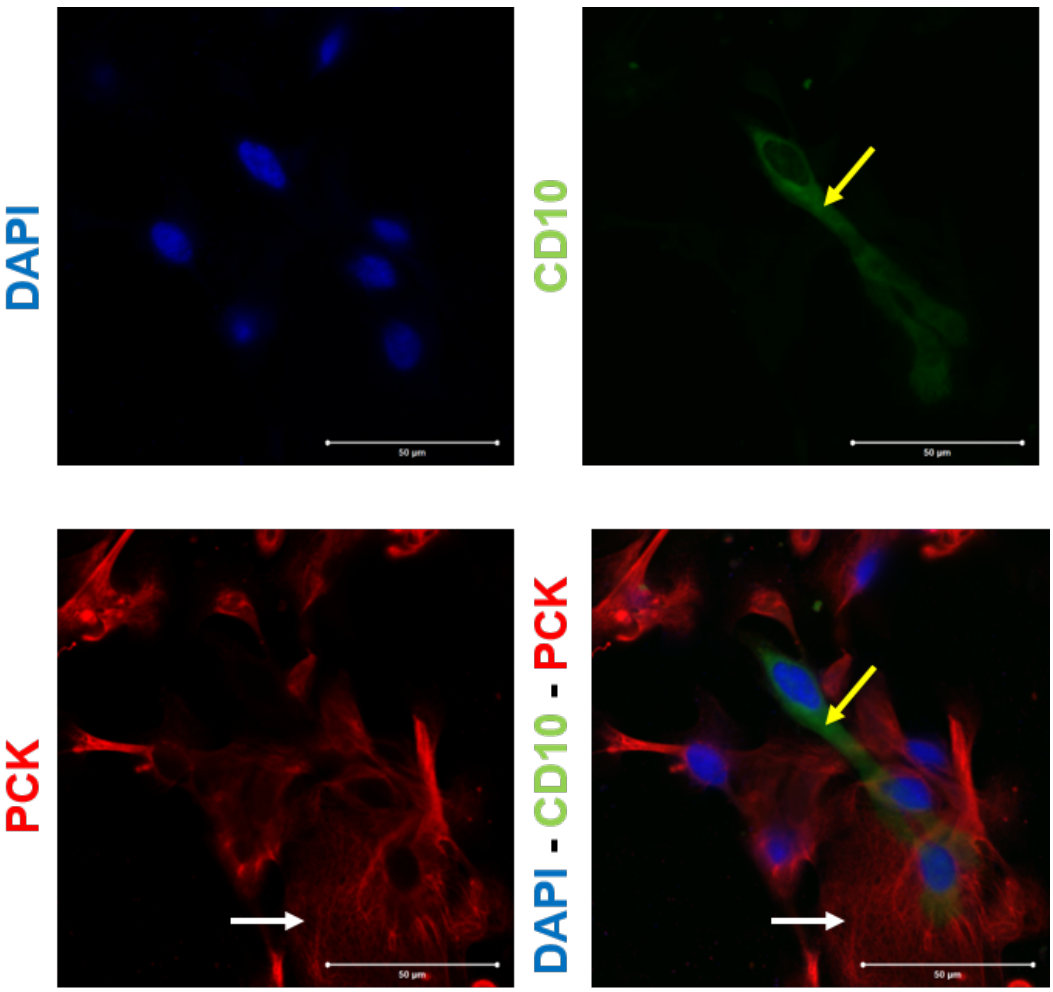

Figure 5-7: Representative dual fluorescent immunocytochemistry for pan-Cytokeratin (PCK) and CD10 expression in primary human endometrial cells day 4 after isolation. Isolated primary endometrial cells were grown in 4-well glass chamber slides alongside the standard cell culture flasks. The above figure utilises day 4 primary endometrial cells and suggests a mixed epithelial and stromal cell population. A CD10 positive (green - fluorescein), PCK negative (red - Cyanine3) endometrial cell can be seen in this field of view, suggestive of an endometrial stromal fibroblast (yellow arrow). In addition, a population of PCK positive, CD10 negative cells, suggestive of endometrial epithelial cells can also be seen (white arrow representative). DAPI = blue nuclear counterstain. Magnification – see scale bar.

5.4.7 qRT-PCR for membrane metallo-endopeptidase (*MME*) gene expression suggests the presence of stromal cells in primary endometrial cell isolates

In addition to immuno-phenotyping the human PEC isolates for their CD10 and PCK expression, day 4 isolates also underwent RNA extraction and qRT-PCR in order to quantify expression of the membrane metallo-endopeptidase (*MME)* gene. The *MME* gene encodes the CD10 protein and so SHT-290 mRNA lysates (positive control, n=3), Ishikawa cell mRNA lysates (negative control, n=3) and day 4 human PEC mRNA lysates (n=10) were analysed. In line with expectations, data shown in Figure. 5-8 confirm that Ishikawa cells have significantly lower levels of *MME* gene expression when analysed compared to SHT-290 cells. Notably, the PEC isolates expressed a range of *MME* expression levels compared to both SHT-290 cells and Ishikawa cells, suggestive of significant cell heterogeneity within this group, with some cultures having similar concentrations to Ishikawa (n=5), whilst others had variable amounts of *MME* mRNA. These results support and extend the immuno-phenotyping data and suggest a proportion of the cultures were predominantly made up of epithelial cells, whilst others were significantly contaminated with stromal fibroblasts.

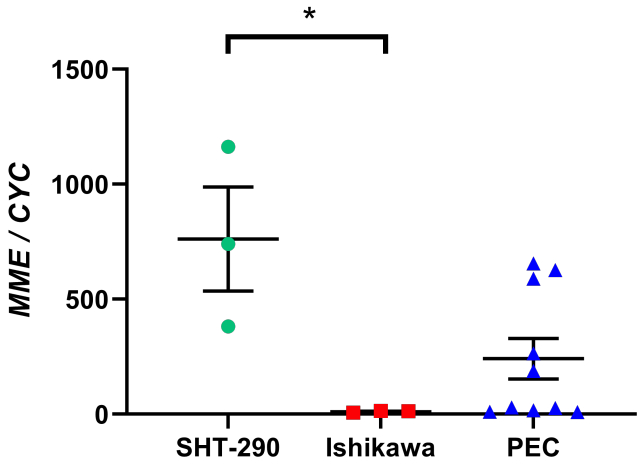

Figure 5-8: Analysis of *MME* gene expression is suggestive of stromal cell contamination of primary endometrial cell isolates. The expression of the *MME* gene relative to the internal control gene *CYC* was assessed by qRT-PCR within mRNA extracted from whole-cell lysates of SHT-290 (n=3 cell passages), Ishikawa (n=3 cell passages) and day 4 isolated primary endometrial cells (PEC) (n=10). The endometrial epithelial cancer cell line, Ishikawa, demonstrates significantly lower expression levels of *MME* gene expression compared to the endometrial stromal fibroblast cell line, SHT-290. In contrast, mRNA extracted from PEC demonstrates varying levels of *MME* gene expression, suggesting the presence of stromal fibroblast contamination in some cultures. Kruskal-Wallis, $p<0.05$.

5.4.8 Use of a cell line endometrial epithelial model and creation of MFE-280 and KLE stable cells line

Given the difficulties in reliably isolating and maintaining a population of pure primary human endometrial epithelial cells, experiments were refocused with the use of endometrial epithelial cancer cell lines in order to investigate the aims of this chapter as set out in 5.2. The cells lines chosen for this purpose were MFE-280 and KLE cells, both isolated from poorly differentiated cancers with an epithelial phenotype reported to have non-functional ERα, whilst retaining normal 'wild-type' expression of PTEN and ARID1A (see 2.2.2). Several stable cell line variants were created as detailed in 5.3.2.1. For these studies Ishikawa cells were not used since they are ERα positive, with mutant PTEN and ARID1A and they were rapidly proliferating at baseline.

5.4.9 Knockdown of PTEN significantly increases cell proliferation in MFE-280 and KLE endometrial epithelial cancer cell lines

To determine whether silencing of PTEN promotes proliferative cellular activity in MFE-280 and KLE cells, PTEN protein expression was knocked down using RNA interference. Two lentiviral constructs were created, '1093' and '1672', each containing a different miRNA oligonucleotide sequence targeted against the *PTEN* gene; a lentivirus containing a scrambled miR oligonucleotide was used as a control (Table. 5-3).

Six new stable cell lines variants (MFE-280$^{(1093)}$, MFE-280$^{(1672)}$, MFE-280$^{(Scr\text{-}miR)}$, KLE$^{(1093)}$, KLE$^{(1672)}$ and KLE$^{(Scr\text{-}miR)}$) were created following lentiviral transduction. Knockdown efficiency was robust as evidenced by a decrease in protein expression of PTEN within the stably transduced cell lines compared to controls (representative Western blots, Figure. 5-9 A&B). miR-1093 demonstrated a statistically significant knockdown of PTEN protein compared to the scrambled miR control (Figure. 5-9 C&D), and visually it demonstrated lower expression of PTEN protein on Western blot analysis compared to miR-1672 in both the MFE-280 and KLE cells (Figure. 5-9 A&B).

Cell proliferation was then measured over a 7-day time course for the newly created MFE-280$^{(1093)}$, MFE-280$^{(Scr\text{-}miR)}$, KLE$^{(1093)}$ and KLE$^{(Scr\text{-}miR)}$ stable cell lines. Cell numbers were normalised to the percentage of cells initially seeded on day 1. Figure. 5-9 E&F demonstrate a statistically significant increase in cell proliferation with both the MFE-280$^{(1093)}$ and KLE$^{(1093)}$

PTEN knockdown cells compared with their scrambled miR control counterparts by the day 7 time point (*p<0.05 and **p<0.01 respectively).

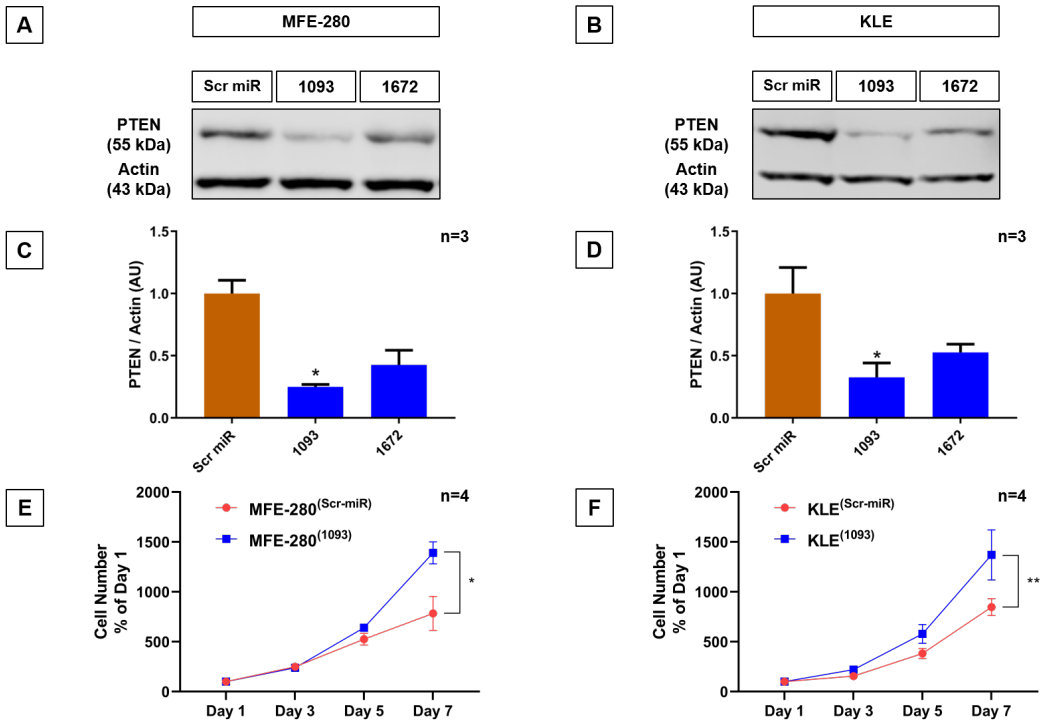

Figure 5-9: The effect of PTEN knockdown on proliferation of MFE-280 and KLE endometrial epithelial cancer cells. Two lentiviral constructs: i) pLenti6-cppt-emGFP-hPTEN-1093 ('1093') and ii) pLenti6-cppt-emGFP-hPTEN-1672 ('1672'), each containing a different miR oligonucleotide targeted against human *PTEN,* were analysed for their efficiency of PTEN protein knockdown compared to a control lentivirus (pLent6-cppt-CMV-emGFP-miR-NEG-control) containing a scrambled miR sequence (Scr miR). A, B) Western blot analysis of PTEN protein expression demonstrates successful knockdown of PTEN in the newly created MFE-280 and KLE stable cell lines with both miR oligonucleotides compared to the scrambled controls. C, D) Densitometry quantification of Western blot analyses demonstrates a significant PTEN knockdown effect with miR-1093 compared to the Scr miR control (n=3 cell passages) in (C) MFE-280 and (D) KLE cells. One-way ANOVA, *p<0.05. AU = Arbitrary units. The cell lines with miR-1093 were therefore taken forward for proliferation analysis. E, F) Cell proliferation of MFE-280$^{(1093)}$ and KLE$^{(1093)}$ PTEN knockdown cell lines, as assessed by the CyQuant direct proliferation assay, was significantly increased by day 7 compared to the Scr miR control cell lines. n=4, with x8 technical replicates in each. Two-way ANOVA, *p<0.05, **p<0.01.

5.4.10 Knockdown of ARID1A suggests a marginal trend towards increased cell proliferation in MFE-280 and KLE endometrial epithelial cancer cell lines

To determine whether silencing of ARID1A promotes cell proliferation in MFE-280 and KLE cells, ARID1A protein expression was knocked down using miRNAs. The *ARID1A* gene encodes two isoforms of protein (2285 and 2086 amino acids) although the relative expression and functional significance of the two isoforms are reportedly unclear (Wu and Roberts, 2013). Two lentiviral constructs were created, '1776' and '2233', each designed to contain a different miRNA oligonucleotide sequence targeted against both isoforms of the *ARID1A* mRNA, in addition to a control lentivirus containing a scrambled miR oligonucleotide (Table. 5-3).

Six new stable cell lines variants (MFE-280$^{(1776)}$, MFE-280$^{(2233)}$, MFE-280$^{(Scr\text{-}miR)}$, KLE$^{(1776)}$, KLE$^{(2233)}$ and KLE$^{(Scr\text{-}miR)}$) were created following lentiviral transduction. Knockdown efficiency was robust as evidenced by a decrease in protein expression of ARID1A within the stably transduced cell lines compared to controls (representative Western blots, Figure. 5-10 A&B). Interestingly, miR-1776 and miR-2233 both demonstrated statistically significant knockdown of ARID1A protein compared to the scrambled miR control in MFE-280 cells, when assessed by combined densitometry analysis of protein expression from n=3 cell passages (Figure. 5-10 C). miR-1776 was taken forward for proliferation analysis in MFE-280 cells as it gave the more statistically significant result with a p-value of 0.0128. In KLE cells, introduction of miR-2233 resulted in lower expression of ARID1A protein, both visually and by utilising Western blot densitometry, compared to miR-1776 (Figure. 5-10 B&D). These results were notable as they suggested differences in cellular machinery in the two cell lines.

Cell proliferation was measured over a 7-day time course for the newly created MFE-280$^{(1776)}$, MFE-280$^{(Scr\text{-}miR)}$, KLE$^{(2233)}$ and KLE$^{(Scr\text{-}miR)}$ stable cell lines. Cell numbers were normalised to the percentage of cells initially seeded on day 1 (Figure. 5-10 E&F). Whilst there was an apparent trend towards an increase in cell proliferation with both the MFE-280$^{(1776)}$ and KLE$^{(2233)}$ ARID1A knockdown cells compared with their scrambled miR control counterparts by the day 7 time point, this did not reach statistical significance in these experiments with n=4 cultures/conditions. Notably in both cell lines some residual protein expression was detectable.

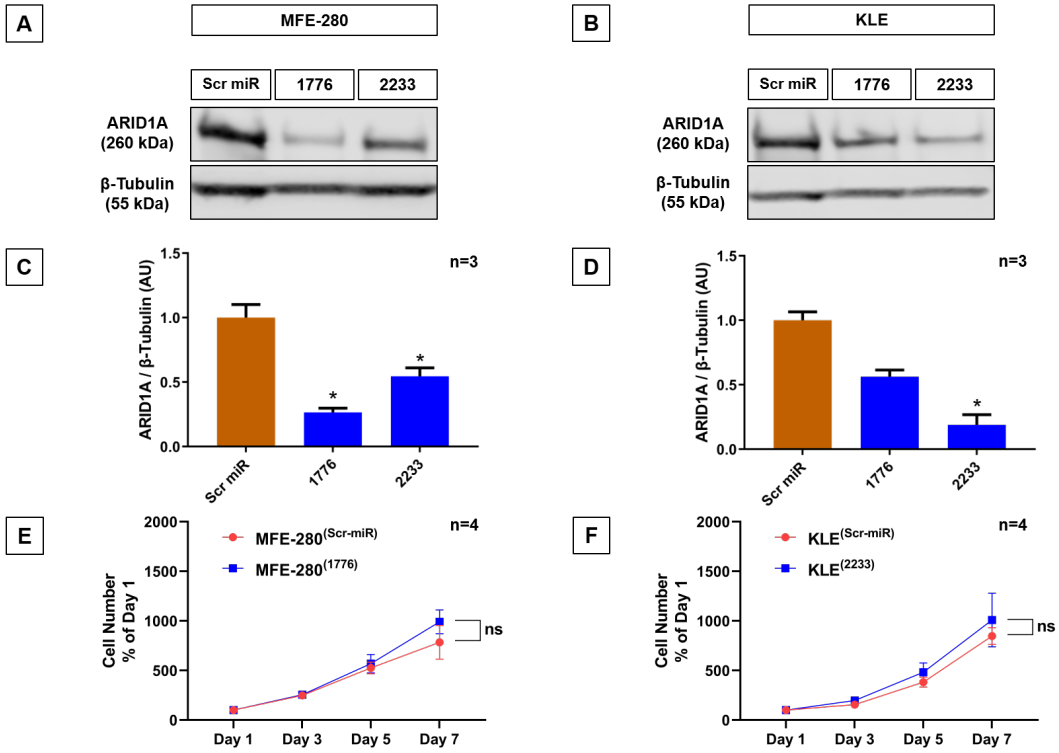

Figure 5-10: The effect of ARID1A knockdown on proliferation of MFE-280 and KLE endometrial cancer cells. Two lentiviral constructs: i) pLenti6-cppt-emGFP-hARID1A-1776 ('1776') and ii) pLenti6-cppt-emGFP-hARID1A-2233 ('2233'), each containing a different miR oligonucleotide targeted against human *ARID1A,* were analysed for their efficiency of protein knockdown compared to a control lentivirus (pLent6-cppt-CMV-emGFP-miR-NEG-control) containing a scrambled miR sequence. A, B) Western blot analysis of ARID1A protein expression demonstrates successful knockdown of ARID1A in the newly created MFE-280 and KLE stable cell lines with both miR oligonucleotides compared to the scrambled controls. C) Densitometry quantification of Western blot analyses demonstrates a significant ARID1A knockdown effect with miR-1776 and miR-2233 compared to the Scr miR control (n=3 cell passages) in MFE-280 cells, *p=0.0128 and *p=0.0136 respectively. D) Densitometry quantification of Western blot analyses demonstrates a significant ARID1A knockdown effect with miR-2233 compared to the Scr miR control (n=3 cell passages) in KLE cells. One-way ANOVA, *p<0.05. MFE-280 cells with miR-1776 and KLE cells with miR-2233 were both therefore taken forward for proliferation analysis. E, F) Cell proliferation of MFE-280$^{(1776)}$ and KLE$^{(2233)}$ ARID1A knockdown cell lines, as assessed by the CyQuant direct proliferation assay, suggests non-significant increases in percentage cell number by the day 7 time-point when compared to Scr miR controls. n=4, with x8 technical replicates in each. Two-way ANOVA, ns=non-significant.

5.4.11 Overexpression of oestrogen receptor alpha (ERα) does not increase cell proliferation in unstimulated MFE-280 or KLE endometrial epithelial cancer cells

To determine whether overexpression of oestrogen receptor alpha (ERα) promotes cellular proliferation in MFE-280 and KLE cells in the presence or absence of oestrogenic ligands, full length *ESR1* cDNA was stably introduced into MFE-280 and KLE cells via a lentiviral vector with an mCherry fluorescent tag (Table. 5-3). A control lentivirus containing an unmodified IRES construct was purchased from the Biomolecular core, The University of Edinburgh. Wild-type MFE-280 and KLE cells are known not to possess a functional ERα (see 2.2.2) and this was confirmed by Western blot (Figure. 5-11 A).

Four new stable cell lines variants (MFE-280$^{(ER\alpha+)}$, MFE-280$^{(IRES)}$, KLE$^{(ER\alpha+)}$ and KLE$^{(IRES)}$) were created following lentiviral transduction. Expression of ERα protein (and therefore successful genomic integration of *ESR1*) was evaluated by Western blot and compared with the Ishikawa endometrial epithelial cancer cell line, which retains a function ERα (representative Western blots, Figure. 5-11 A). Quantification of ERα protein expression was performed by Western blot densitometry (n=3 passages) and demonstrated significant overexpression of ERα protein in the new MFE-280$^{(ER\alpha+)}$ and KLE$^{(ER\alpha+)}$ stable cell lines, when compared to Ishikawa cells (Figure. 5-11 B&C). Notably expression in KLE cells was 15x higher than Ishikawa when compared to loading control (ß-tubulin).

Cell proliferation in medium without the addition of E_2 was then measured over a 7-day time course for the newly created MFE-280$^{(ER\alpha+)}$, MFE-280$^{(IRES)}$, KLE$^{(ER\alpha+)}$, KLE$^{(IRES)}$ stable cell lines. Cell numbers were normalised to the percentage of cells initially seeded on day 1. Figure. 5-11 D&E detail the results and show there was no statistical change in the increase in percentage cell proliferation for either the MFE-280$^{(ER\alpha+)}$ or KLE$^{(ER\alpha+)}$ ERα overexpressed cells compared with their control counterparts by the day 7 time point (p=non-significant).

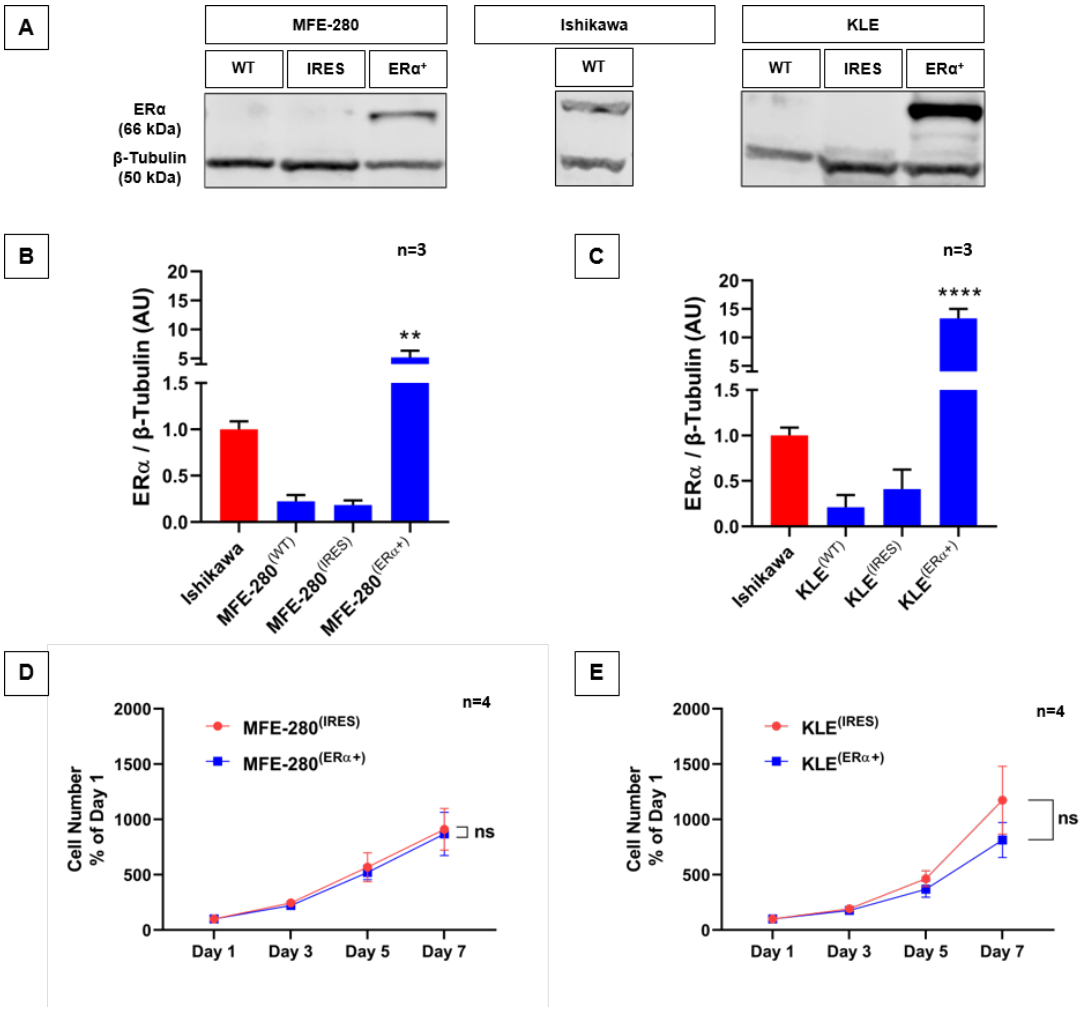

Figure 5-11: Overexpression of oestrogen receptor alpha (ERα) in MFE-280 and KLE endometrial epithelial cancer cells does not increase cell proliferation in an unstimulated environment. cDNA for the *ESR1* gene was inserted into a pDONR221-attB1-IRES-mcherry-attB2 plasmid prior to being Gateway cloned into the pLenti6-cppt-DEST-opre to produce the pLenti6-cppt-CMV-ESR1-IRES-mCherry-opre vector. MFE-280 and KLE cells were transduced with this lentiviral vector in order to stably overexpress ERα ("ERα^{+}"). Unmodified pLenti6-cppt-CMV-IRES-mCherry-opre was used as a negative control ("IRES"). A) Western blot protein analysis of transduced and wild-type (WT) cell lines for ERα expression. The Ishikawa endometrial cancer cell line retains ERα protein expression, unlike the MFE-280$^{(WT)}$ and KLE$^{(WT)}$ cell lines which do not. MFE-280$^{(ERα+)}$ and KLE$^{(ERα+)}$, stably express ERα protein unlike their control counterparts transduced with an unmodified lentivirus (MFE-280$^{(IRES)}$ and KLE$^{(IRES)}$). B,C) Densitometry quantification of Western blot analyses demonstrates significant overexpression of ERα protein within (B) MFE-280$^{(ERα+)}$ and (C) KLE$^{(ERα+)}$ cells compared to Ishikawa controls (n=3 cell passages). One-way AVOVA, **p<0.01, ****P<0.0001. Cell proliferation of MFE-280$^{(ERα+)}$ and KLE$^{(ERα+)}$ cells, as assessed by the CyQuant direct proliferation assay across multiple time points. D) Unstimulated MFE-280$^{(ERα+)}$ cell proliferation was not significantly altered at any time-point when compared to an unstimulated MFE-280$^{(IRES)}$ control. E) A non-significant trend towards reduced cell proliferation was seen by the day 7 time point in unstimulated KLE$^{(ERα+)}$ cells when compared

to unstimulated KLE$^{(IRES)}$ control cells. n=4, with x8 technical replicates in each. Two-way ANOVA, ns = non-significant.

5.4.12 Introduction of full length *ESR1* cDNA into MFE-280 and KLE cells produces a functional ERα capable of binding to exogenous ligands and activating ERE-dependent transcription

In the classical oestrogen receptor pathway, natural lipophilic ligands such as E_2 freely pass across the cell membrane into the cytoplasm. Once there they can bind to ERα causing a conformational change, form receptor dimers and recruit cofactors to blinding sites within the promotor regions of target genes, including the well-documented EREs (oestrogen receptor response elements) resulting in over/under expression of genes and altered cell responses. In order to assess if the transduced stable cell lines MFE-280$^{(ERα+)}$ and KLE$^{(ERα+)}$ contained a functional ERα, the impact of several known ligands for ERα were investigated using a luciferase reporter gene under the control of an oestrogen response element (in this case 3xERE-tk-luciferase) packaged within an adenovirus ('Ad-ERE-Luc').

MFE-280$^{(ERα+)}$, MFE-280$^{(IRES)}$, KLE$^{(ERα+)}$, KLE$^{(IRES)}$ and Ishikawa cell lines were transiently transfected with Ad-ERE-luc and treated with E_2 10^{-8}M, 4-Hydroxytamoxifen (4-OHT) 10^{-7}M and Propyl pyrazole triol (PPT) 10^{-8}M; concentrations were based on previous experience of using these ligands in reporter assays (Collins *et al.*, 2009; Gibson *et al.*, 2018). After 24 hours the cells were incubated with a luciferase substrate (Bright-Glo™ Luciferase Assay System) and luminescence was measured. E_2 and PPT increased ERE-dependent transcription in all three cell lines containing ERα (Figure. 5-12 A, B&C). This effect was abrogated by co-incubation with the anti-oestrogen, Fulvestrant (ICI 182,780), consistent with oestrogen receptor dependence. In contrast, incubation of the control cell lines containing an unmodified IRES construct with ligands, did not show any activation of ERE-dependent transcription of the reporter (Figure. 5-12 D&E).

When tamoxifen is used as antagonist therapy for ER$^+$ breast cancer it is reported to have partial agonist effect on the endometrium; it can also stimulate proliferation of Ishikawa cells, with a reportedly stronger affinity for ERα than 17β-Oestradiol (E_2). The ligand 4-Hydroxytamoxifen (4-OHT) is the active metabolite of tamoxifen and was used in the current study. At a concentration of 10^{-7}M the ligand had no impact on ERE-dependent transcription in Ishikawa cells and only a moderate (non-significant) response was in MFE-280$^{(ERα+)}$ and KLE$^{(ERα+)}$ cells (Figure. 5-12 A, B&C).

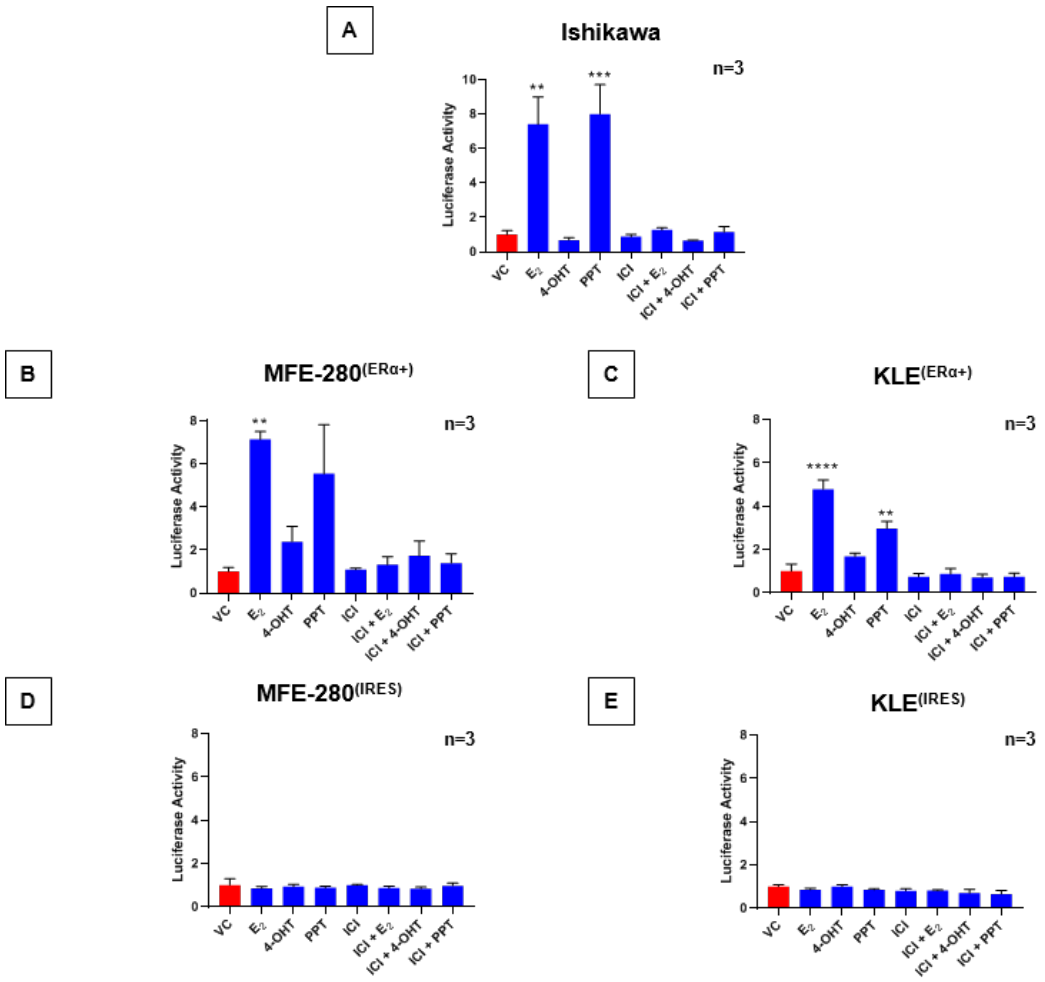

Figure 5-12: Transduced MFE-280$^{(ERα+)}$ and KLE$^{(ERα+)}$ cells possess a functional oestrogen receptor alpha (ERα). The presence of a functional ERα in MFE-280 and KLE cells stably transduced with the pLenti6-cppt-CMV-ESR1-IRES-mCherry-opre vector was confirmed by way of an oestrogen response element (ERE) reporter assay. Utilising a luciferase reporter gene under the control of an ERE (3× ERE-tk-luciferase) packaged within an adenovirus ('Ad-ERE-Luc'), known ligands for ERα (17β-Oestradiol (E_2) 10^{-8}M, 4-Hydroxytamoxifen (4-OHT) 10^{-7}M and Propyl pyrazole triol (PPT) 10^{-8}M) were assessed for their effect on ERE-dependent transcription. In addition, the ligands were also co-incubated with the antioestrogen Fulvestrant (ICI 182,780, 10^{-6}M) in order to block ERα activity. A, B, C) As expected in ERα positive cells ((A) Ishikawa, (B) MFE-280$^{(ERα+)}$ and (C) KLE$^{(ERα+)}$ luciferase activity (and therefore ERE activity) was significantly induced by E_2 and PPT, and to a lesser extent in the MFE-280$^{(ERα+)}$ and KLE$^{(ERα+)}$ cells with 4-OHT. This effect was abrogated when the ligands were co-incubated with ICI. D, E) ERα negative cells transduced with a control IRES lentivirus had no increase in luciferase activity. All data displayed consists of n=3 experiments, with x2 technical replicates in each. VC = Vehicle control. One-way ANOVA, **p<0.01, ***p<0.001, ****p<0.0001

5.4.13 Knockdown of PTEN together with overexpression of oestrogen receptor alpha (ERα) reduces proliferation in unstimulated MFE-280 but not KLE endometrial epithelial cancer cells

To determine whether the silencing of PTEN in combination with overexpression of ERα changes proliferative activity in MFE-280 and KLE cells, PTEN protein expression was knocked down and full length *ESR1* cDNA was stably introduced into MFE-280 and KLE cells via lentiviral vectors respectively.

Knockdown vectors together with their respective controls were tagged with emerald green fluorescent protein (EmGFP) and the overexpression vector and control with mCherry. Six new stable cell lines variants (MFE-280$^{(1093/ERα+)}$, MFE-280$^{(1672/ERα+)}$, MFE-280$^{(Scr\text{-}miR/IRES)}$, KLE$^{(1093/ERα+)}$, KLE$^{(1672/ERα+)}$ and KLE$^{(Scr\text{-}miR/IRES)}$ were created following lentiviral transduction. The cell lines were FACS sorted as per 5.3.2.2 to yield populations of double positive EmGFP^{+}/mCherry^{+} cells indicating genomic integration of both a knockdown and overexpression lentiviral vector into each cell (Figure. 5-13).

Knockdown efficiency was confirmed by a decrease in protein expression of PTEN compared to controls (representative Western blots, Figure. 5-14 A&B). miR-1093 demonstrated a more statistically significant knockdown of PTEN protein compared to miR-1672 (Figure. 5-14 C & D) by densitometry, and visually it demonstrated lower expression of PTEN protein on Western blot band analysis. Presence of ERα protein was confirmed by Western blot (Figure. 5-14 A & B) and quantification of ERα protein overexpression was performed by densitometry, demonstrated significant overexpression of ERα protein in the new MFE-280$^{(1093/ERα+)}$ and KLE$^{(1093/ERα+)}$ stable cell lines (Figure. 5-14 E & F).

Cell proliferation was then measured over a 7-day time course for the newly created MFE-280$^{(1093/ERα+)}$, MFE-280$^{(Scr\text{-}miR/IRES)}$, KLE$^{(1093/ERα+)}$ and KLE$^{(Scr\text{-}miR/IRES)}$ stable cell lines. Cell numbers were normalised to the percentage of cells initially seeded on day 1. Figure. 5-14 G & H shows that a statistically significant decrease in cell proliferation occurred in MFE-280$^{(1093/ERα+)}$ cells compared with control by the day 7 time point (***$p<0.001$) in the absence of exogenous oestrogens. There was a marginal trend towards an increase in cell proliferation in the corresponding KLE$^{(1093/ERα+)}$ cells

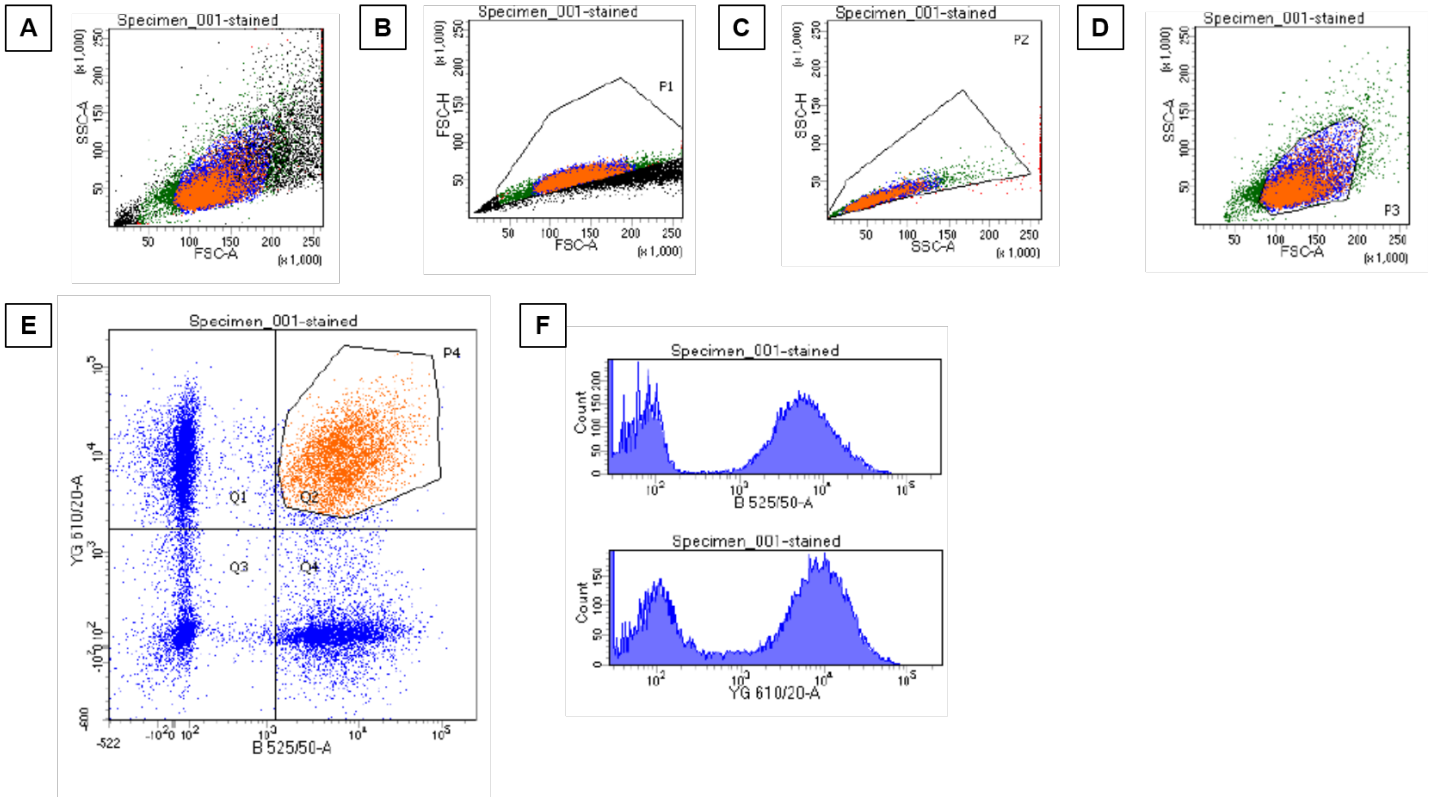

Figure 5-13: Representative gating strategy for FACS on a co-transduced cell line expressing EmGFP and mCherry fluorescent proteins. A) Total population of 'events' (i.e. all cell material, debris, single cells, double cells and clumps), in this example 24,931 events. B, C, D) Gating based on cell size and shape as determined by forward scatter area (FSC-A), forward scatter height (FSC-H), side scatter area (SSC-A) and side scatter height (SSC-H). This delineated a population of single cells, excluding clumps, doublets and cell debris. E, F) A blue laser (505 nm with filter 525/50) was used to detect EmGFP positive cells and a yellow-green laser (600 nm filter 610/20) was used to detect mCherry positive cells. Single cells were then sorted based on double positivity (E - orange upper, outer quadrant) with good separation noted between the cell populations as represented by the histograms (F). The final sorted, double positive population contained 4,295 events in this example (25.5 % of the parent population).

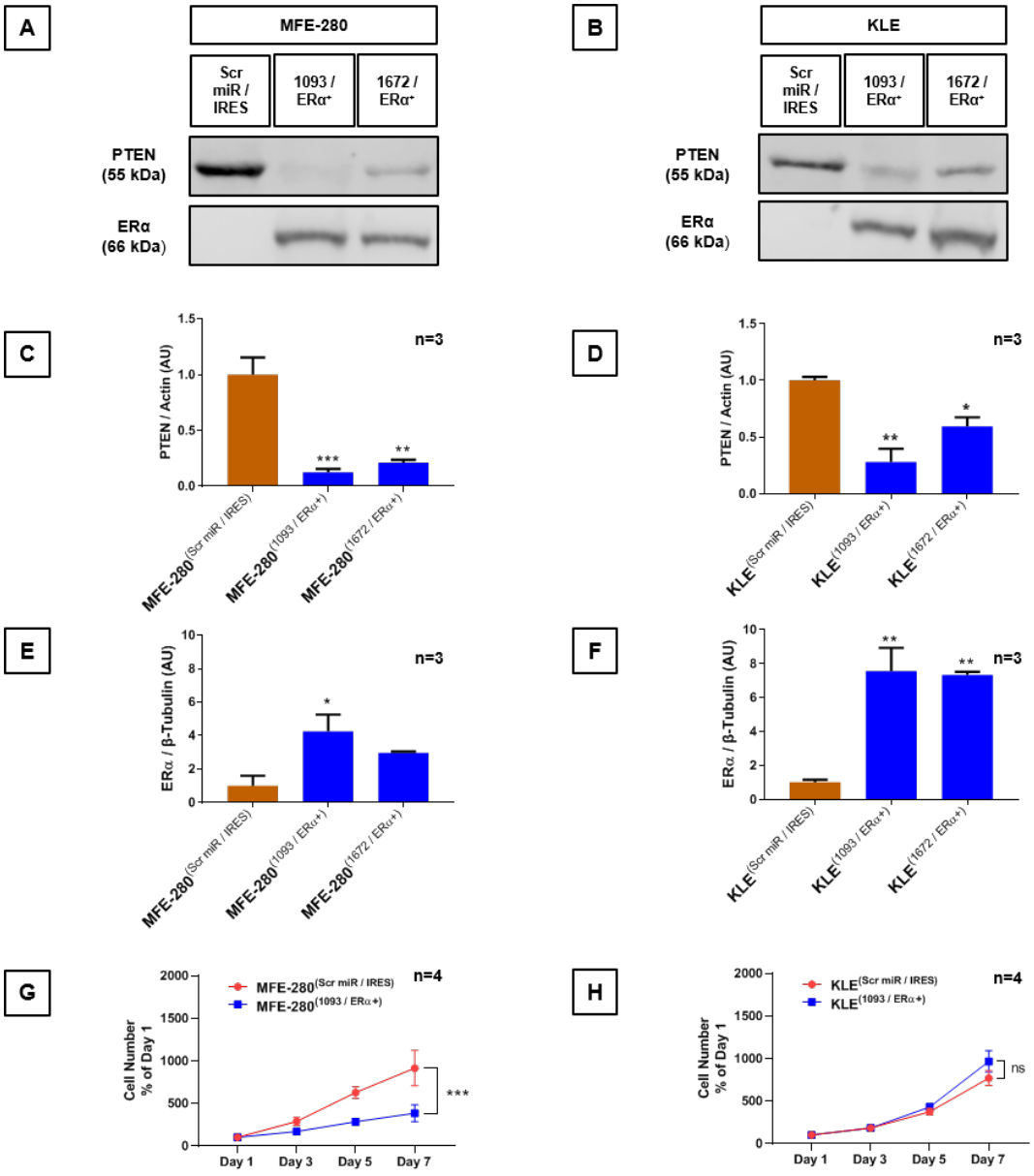

Figure 5-14: The effect of both PTEN knockdown and ERα overexpression on cell proliferation in unstimulated MFE-280 and KLE endometrial epithelial cells. Stably transduced MFE-280 and KLE cell lines were created using the following lentiviral constructs: i) pLenti6-cppt-emGFP-hPTEN-1093 ('1093') + pLenti6-cppt-CMV-ESR1-IRES-mCherry-opre and ii) pLenti6-cppt-emGFP-hPTEN-1672 ('1672') + pLenti6-cppt-CMV-ESR1-IRES-mCherry-opre. Each cell line was transduced with a different miR oligonucleotide targeted against the human *PTEN* gene in addition to full length cDNA for the *ESR1* gene. The stably transduced cell lines were analysed for their efficiency of PTEN protein knockdown compared to a transduced control cell line (pLent6-cppt-CMV-emGFP-miR-NEG-control + pLenti6-cppt-CMV-IRES-mCherry-opre). A, B) Western blot analysis of protein expression demonstrates both knockdown of PTEN and the presence of ERα in the transduced MFE-280 cells and KLE cells respectively compared to control. C, D) Densitometry quantification of PTEN Western blot analyses demonstrates a significant PTEN knockdown effect, with miR-1093 and miR-1672 compared to control in (C) MFE-280 and (D) KLE cells respectively (n=3 cell passages). E, F) Densitometry quantification of Western blot analyses demonstrates

significant overexpression of ERα protein within (E) MFE-280$^{(1093/ERα+)}$ and (F) KLE$^{(1093/ERα+)}$ **Continued.** and KLE$^{(1672/ERα+)}$ cells compared to controls (n=3 cell passages). The ERα+ cell lines with miR-1093 were taken forward for proliferation analysis since they had the more significant knockdown of PTEN and overexpression of ERα+. One-way ANOVA,*p<0.05, **P<0.01, ***P<0.001. E, F) Cell proliferation, as assessed by the CyQuant direct proliferation assay. In the unstimulated MFE-280$^{(1093/ ERα+)}$ cell line, percentage cell proliferation was significantly reduced compared to control by the day 7 time-point. In contrast, unstimulated KLE$^{(1093/ ERα+)}$ cells demonstrated a non-significant trend towards increased percentage proliferation compared to control by the day 7 time-point. n=4, with x8 technical replicates in each. Two-way ANOVA, ***p<0.001, ns = non-significant.

5.4.14 17β-Oestradiol (E_2) reduces cell proliferation at a 72-hour timepoint in MFE-280 and KLE cells when ERα is overexpressed regardless of PTEN status

This experiment formed part of a pilot designed to explore the effect on cell proliferation of combined knockdown of PTEN (using miR-1093) and overexpression of ERα when cells were incubated with E_2. Stably transduced MFE-280 (1093 / ERα$^+$, IRES / Scr miR, ERα$^+$, IRES, miR-1093, Scr miR) and KLE (1093 / ERα$^+$, IRES / Scr miR, ERα$^+$, IRES, miR-1093, Scr miR) cell line variants were incubated with vehicle control (VC, DMSO), E_2 (10^{-8}M), Fulvestrant (ICI 182,780, 10^{-6}M) or E_2 10^{-8}M + Fulvestrant 10^{-6}M and their effect on cell proliferation assessed at a 72 hour time-point. This experiment used a 72-hour time-point based on the knowledge of the doubling time of the MFE-280 and KLE 'wild-type' cells (Table. 5-2, 52 and 96 hours respectively) and because in MFE-280$^{(1093/ ERα+)}$ the first significant change in cell number between this cell line variant and control was detectable after 72 hours of growth (Figure. 5-14 G).

Incubation of cell line variants created to overexpress ERα with E_2 resulted in a reduction in cell number compared with VC that reached significance in KLE cells regardless of PTEN knockdown status (Figure. 5-15 B compared with F). In MFE-280 cells, the reduction in cell number was only significant when cells had reduced PTEN expression (Figure. 5-15 A). In all cultures the impact of E_2 was abrogated by co-incubation with Fulvestrant. Ishikawa cells (Figure. 5-15 M) (which retain a functional ERα), demonstrated a non-significant trend towards increased cell number when incubated with E_2 (10^{-8}M). Incubation with E_2 had no impact on the number of cells compared with those incubated with VC when cells had PTEN knockdown but remained ERα negative (Figure. 5-15 I, J) even though these cells showed higher rates of proliferation in the absence of E_2 compared with controls (see Figure. 5-10).

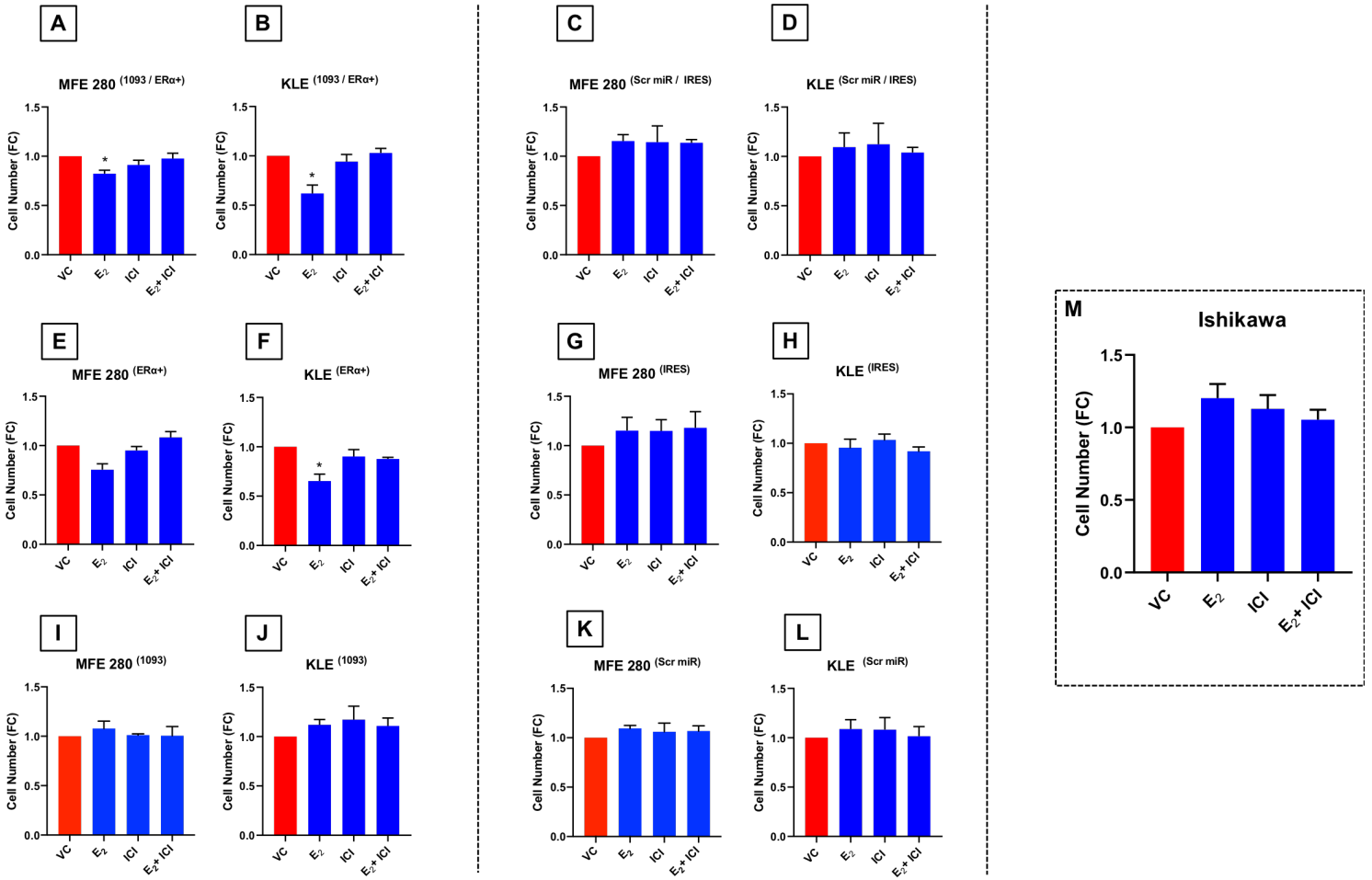

Figure 5-15: Cell proliferation in MFE-280 and KLE endometrial cells is reduced following the overexpression of a functional ERα when incubated with 17β-Oestradiol (E_2).

Continued. Ishikawa cells (M), stably transduced MFE-280 [(A) PTEN knockdown miR-1093 / ERα$^+$, (C) IRES / Scr miR, (E) ERα$^+$, (G) IRES, (I) PTEN knockdown miR 1093, (K) Scr miR] and KLE [(B) PTEN knockdown miR-1093 / ERα$^+$, (D) IRES / Scr miR, (F) ERα$^+$, (H) IRES, (J) PTEN knockdown miR-1093, (L) Scr miR] cell lines were incubated with 17β-Oestradiol (E_2, 10^{-8}M), Fulvestrant (ICI 182,780, 10^{-6}M) or a combination of both ligands. The effect of ligand incubation was assessed using the CyQuant direct proliferation assay after 72 hours. Cell lines with overexpression of ERα (A, B, E, F) demonstrated a reduction in cell proliferation when compared to vehicle control (VC) when incubated with E_2. This effect was found to be abrogated by co-incubation with Fulvestrant. Ishikawa cells (M) (which retain a functional ERα), demonstrated a non-significant trend towards increased cell proliferation when incubated with E_2 10^{-8}M. PTEN knockdown utilising miR-1093 did not appear to influence cell proliferation, in isolation or with overexpression of ERα, in either MFE-280 or KLE cells. MFE-280 and KLE data represent an n=3, with x8 technical replicates in each. Ishikawa data represent n=3, with x2 technical replicates in each. Date represented as a fold-change over vehicle control. One-sample *t* test with a hypothetical mean of 1, *p<0.05.

5.5 Discussion

To start to address the aims of the present study, we attempted to refine a technique to isolate a pure population of primary endometrial epithelial cells with which we could study the effect of silencing the expression of PTEN and ARID1A proteins. Primary cell isolation techniques were based upon published literature techniques (Chan *et al.*, 2004; Gargett *et al.*, 2009; Valentijn *et al.*, 2013). Endometrial Pipelle® biopsy samples were obtained from women undergoing surgery for benign disorders and were retrospectively dated by histopathology.

Due to the smaller numbers of cells in Pipelle® endometrial biopsy samples, it is difficult to conduct cell-based studies without first culturing and expanding these cells. We found that although we were able to isolate primary endometrial epithelial cells (Figure. 5-5 and 5-6), expansion of the cell population often resulted in cell death or senescence and allowed overgrowth of endometrial stromal cells (Figure. 5-7), regardless of the how pure the initial starting cultures seemed. Some cultures had minimal stromal contamination (Figure. 5.8) and anecdotally these cultures had greater starting numbers of isolated cells (potentially encouraging cell-cell interactions) or upon retrospective histological assessment, they were found to be from the early secretory phase of the menstrual cycle (plausibility at their maximal proliferative potential).

The observations above raise two points for future consideration: 1) How should primary endometrial epithelial cells be maintained culture? and 2) Should the 'normal' uterine physiological environment be considered when propagating these cells? Epithelial-cell function requires cellular polarity in which apical membrane surfaces have unique characteristics and cellular organelles are stratified (Munson *et al.*, 1990). In addition,

endometrial epithelial cells *in vivo* do not exist in isolation and the role of the stromal compartment may need to be considered when planning experiments. There is a suggested role for improving endometrial epithelial cell propagation by using an extra-cellular matrix derived from endometrial stromal cells which may maintain cell polarisation and enhance *in vitro* longevity (Munson *et al.*, 1990). Furthermore, several authors have investigated endometrial epithelial cells utilising model systems which propagate the cells *in vitro* at an air-liquid interface to maintain cellular polarity (Altman *et al.*, 1999; Li *et al.*, 2018; Rochon *et al.*, 2010).

There may be a role for immortalisation techniques which maintain the cellular phenotype to extend the culture longevity of primary endometrial epithelial cells. One such method with reported success in keratinocyte culture is Rho/ROCK immortalisation. Rho GTPases are a subfamily of the RAS superfamily of proteins that play essential roles in cell adhesion, cytokinesis, and cell migration (reviewed in Jaffe and Hall, 2005). Mammalian cells encode 2 Rho kinases, ROCK1 and ROCK2 (Chapman *et al.*, 2010) and it has been suggested that inhibition of ROCK greatly increases the cloning efficiency of human embryonic stem cells (Watanabe *et al.*, 2007) and human keratinocytes (Terunuma *et al.*, 2010).

An alternative avenue to pursue is that of 3D cell culture methods, which are suggested to mirror cellular phenotypes and gene expression *in vivo* more closely than 2D culture systems (Eritja *et al.*, 2010; Greaves *et al.*, 2017; Wang *et al.*, 2012). Moreover, 3D co-culture models can be used to assess the effect of one cell type on another and offer the opportunity to explore the interactions between different cells types (Greaves *et al.*, 2017). We have generated preliminary data to investigate a 3D hanging drop method of cell culture (Figure. 5-16) utilising the Ishikawa cell line as a proof of principle. This method of cell culture is proposed to have several advantages over traditional 2D methods, including: a more natural shape (retaining polarisation of cells), improved cell interface with culture media (as in physiological conditions, there is gradient availability of the media component, with upper layers of cells being highly exposed over the lower layers) and cell junctions are more prevalent than 2D systems (to enable improved cell to cell communications).

Another option to consider is the use of cellular organoids. Organoids are 3D structures generated *in vitro* from stem cells that self-organise through cell sorting into multicellular structures that have a functionality characteristic of the organ or tissue from which they were obtained (Deane *et al.*, 2017). They are a miniature and simplified version of their parent organ/tissue and may contain several differentiated cells types (Deane *et al.*, 2017). Endometrial organoids have been investigated, with promising results suggesting clonal

origins and physiologically appropriate responses to ovarian hormones (Boretto *et al.*, 2017; Turco *et al.*, 2017).

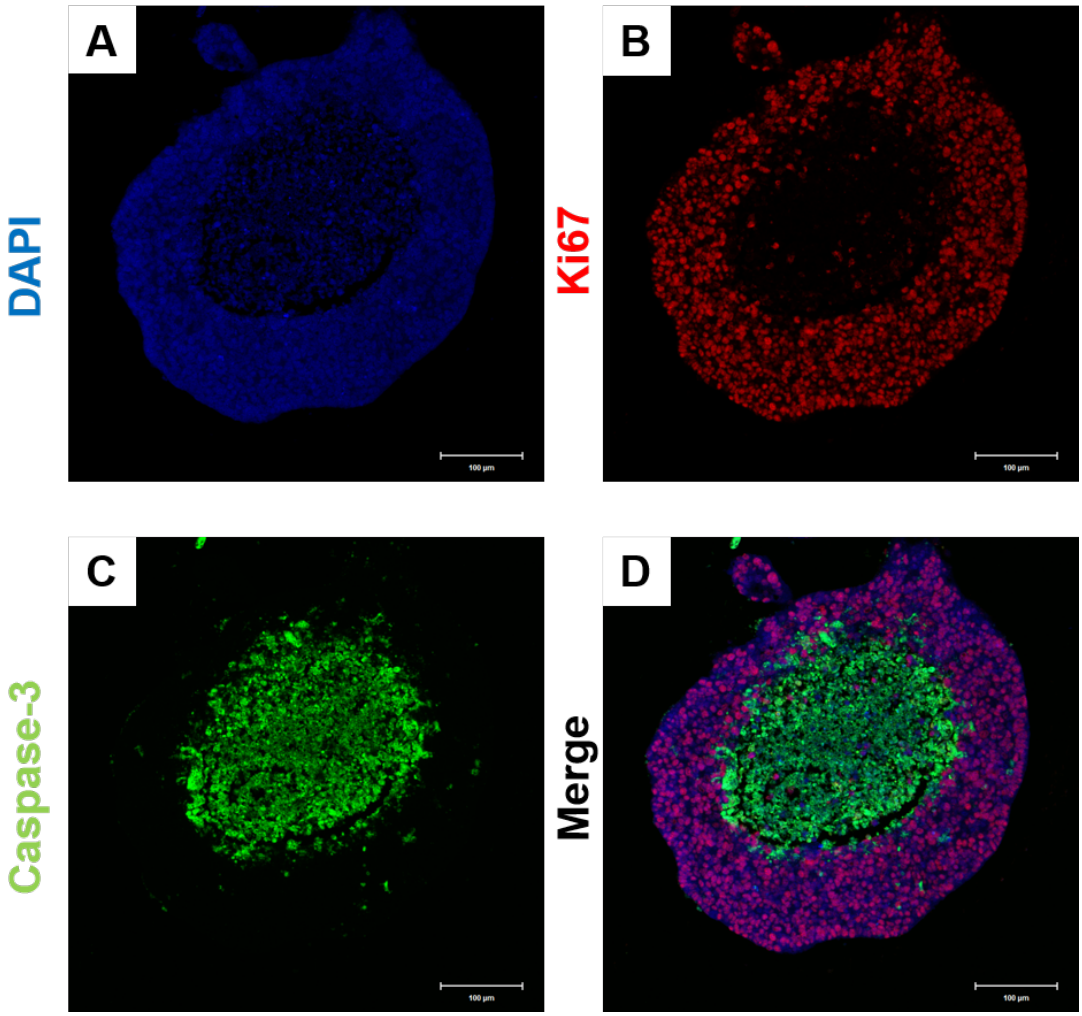

Figure 5-16: Double fluorescent immunocytochemistry of a 3D Ishikawa cell spheroid. Ishikawa cells were grown in a 3D hanging drop culture system (Perfecta 3D®, 3D Biomatrix Inc., Michigan, USA) as per manufacturer instructions. $1x10^3$ Ishikawa cells were initially seeded, and spheroids were harvested after 10 days in 3D monoculture. Spheroids were fixed (24 hours, 10 % neutral buffered formalin) prior to embedding (initially in agarose and subsequently paraffin), before sectioning for histology. Double fluorescent immunocytochemistry (see 2.5) was performed for Ki67 (MIB-1 Dako, M7240, 1:150,000 dilution) and cleaved caspase-3 (Cell signalling Tech, 9961, 1:500 dilution) using a dual Tyramide™ detection and amplification system (see 2.4.1), with DAPI (4,6-diamidino-2-phenylindole) nuclear counterstaining. Images were obtained using confocal microscopy. A) DAPI nuclear counterstaining of Ishikawa cells. B & C) In keeping with expectations of a gradient availability of media exposure, Ki67 staining demonstrates a proliferative outer ring of Ishikawa cells (B) and Cleaved caspase-3 staining demonstrates an internal apoptotic core of Ishikawa cells (C). D) Merged image. Scale bars - see individual figures.

Given the difficulties in reliably isolating and maintaining a population of pure endometrial epithelial cells, efforts were refocused on the use of cell lines. The human MFE-280 and KLE endometrial epithelial cancer cell lines were chosen for this purpose. These cells are both poorly differentiated and are slow to proliferate at baseline (Table. 5-2). They have been reported to lack a functional ERα protein, whilst retaining wild-type PTEN and ARID1A protein expression (Hackenberg *et al.*, 1998; Kwan *et al.*, 2016; Liang *et al.*, 2012; Qu *et al.*, 2019). We confirmed these findings by Western blot analysis in our study. Interestingly, Qu *et al,* reported that MFE-280 cells possess ERα mRNA raising the potential for post-translational modification in these cells (Qu *et al.*, 2019).

Both the unstimulated MFE-280 and KLE cell lines demonstrated increased cell proliferation with knockdown of PTEN protein when compared to controls (Figure. 5-9). This is in keeping with the known regulatory role that PTEN has in cell proliferation. Future work would aim to confirm the downstream implications of PTEN knockdown on the PI3K/Akt pathway in order to determine the mechanism by which PTEN exerts its effects in these cells. In addition, investigation of apoptosis should be also undertaken in order to corroborate that the changes seen in cell number are as a result of increased cell proliferation as opposed to reduced cell apoptosis.

Knockdown of ARID1A in unstimulated MFE-280 and KLE cells did not demonstrate a statistically significantly increase in cell proliferation as hypothesised (Figure. 5-10). This is in contrary to data presented by Ayhan and colleagues, who demonstrated an increased in cell proliferation in immortalised endometrial epithelial cells with knockdown of ARID1A (Ayhan *et al.*, 2015). Whilst this could be a limitation of cells type used in our study, it could also represent the efficiency of the protein knockdown in our study. Although we achieved a statistically significant knockdown of ARID1A protein expression (Figure. 5-10 C & D), some protein did still remain, and it may be that a minimal level of ARID1A protein is all that is required in order to influence a biological effect. Interestingly, Ayhan and colleagues also reported that compared to knockdown of either ARID1A or PTEN alone, the growth rate of endometrial epithelial cells was significantly elevated when both ARID1A and PTEN genes were silenced simultaneously (Ayhan *et al.*, 2015). They propose a gatekeeper role for ARID1A in preventing tumour progression despite the presence of PTEN mutation (Ayhan *et al.*, 2015).

When ERα was stably overexpressed in unstimulated KLE and MFE-280 cell lines, as anticipated cell proliferation was not significantly altered when compared to controls (Figure. 5-11). Work from the Saunders laboratory has previously shown that wild-type MFE-

280 cells do not respond to E_2 stimulation (Gibson *et al.*, 2018), however, these cells do have a Liver X receptor (LXR), that responds to a selective agonist, indicating that they have the necessary cellular machinery to drive a reporter assay (Gibson *et al.*, 2018). We therefore demonstrated that the overexpressed ERα in the MFE-280$^{(ER\alpha+)}$ and KLE$^{(ER\alpha+)}$ cells was functional by way of an ERE-luciferase reporter assay. This confirmed a significant increase in ERE-dependent transcription when the MFE-280$^{(ER\alpha+)}$ and KLE$^{(ER\alpha+)}$ cells were stimulated with the ligands E_2 and PPT (Figure. 5-12 B & C) compared to controls (Figure. 5-12 D & E). This was in keeping with a similar response seen in Ishikawa cells which are known to retain a functional ERα (Figure. 5-12 A). 4-Hydroxytamoxifen (4-OHT) had no impact on ERE-dependent transcription in Ishikawa cells and only a modest (non-significant) response in MFE-280$^{(ER\alpha+)}$ and KLE$^{(ER\alpha+)}$ cells (Figure. 5-12 A, B & C). This was unusual and not in keeping with published literature (Anzai *et al.*, 1989; Sakamoto *et al.*, 2002) and so a dose response experiment may be needed to further evaluate this, since a 10^{-7} M concentration of 4-OHT may be either too low to exert an effect, or too high that it becomes inhibitory.

Unexpectedly, co-transduction of MFE-280 and KLE cells to both knockdown PTEN (using miR-1093) and overexpress ERα demonstrated a significant reduction in cell proliferation in unstimulated MFE-280 cells but not the KLE cells (Figure. 5-14). This is despite baseline cell culture medium being phenol-red free and utilising charcoal stripped serum (CSFCS). This may suggest a difference in cellular machinery between the two cell lines. Stimulation with E_2 appeared to reduced cell proliferation at a 72-hour timepoint in all transduced cells with overexpression of ERα, regardless of PTEN knockdown status (although in MFE-280 cells this did not achieve statistical significance) (Figure 5-15. A, B, E, F). This was again unexpected. The overexpression of ERα may be too much for the basic proliferative machinery of these poorly differentiated EC cells (NB/ MFE-280$^{(ER\alpha+)}$ and KLE$^{(ER\alpha+)}$ cells had x5 and x15 the amount of ERα respectively, compared to Ishikawa cells (Figure. 5-11 B & C)).

Although the ERα overexpressed cells responded well in the reporter assay, a full response of genes implicated in proliferation would require co-factors e.g. steroid receptor coactivators (SRCs), to activate steroid hormone signalling and growth factor pathways in order to mount a proliferative response, which these cell lines may not possess (reviewed in Lonard and O'Malley, 2016). That being said, other groups have also reported inhibition of cellular growth with overexpression of ERα, not only in EC cells (Ali *et al.*, 2004; Webb *et al.*, 1992; ZHOU *et al.*, 2013) Ali and colleagues hypothesised that this effect may be due to modulation of angiogenic factors within the cells, which may ultimately function to limit blood

supply in ERα positive ECs and favourably limit tumour growth (Ali *et al.*, 2004). Webb *et al* suggest that saturation of the cellular capacity to mediate an oestrogen response and ER-dependent squelching occur at receptor titres well above those encountered in nature (Webb *et al.*, 1992). Clearly, further work needs to be undertaken to ascertain the exact mechanism responsible for the reduction in proliferation seen. Initially this may involve looking at several time-points, ligand doses, and modifying the level of ERα receptor titres.

In conclusion, data presented in this chapter confirm and extend existing literature on the proliferative effects of PTEN within endometrial epithelial cancer cells. The data also raises several further questions regarding the role of ARID1A and ERα in endometrial cell proliferation, which will form the basis for future research endeavours aiming to address mechanisms by which the normal endometrium transitions to neoplasia. Finally, preliminary work on 3D spheroid cell culture, may favourably lend itself to developing a robust technique for *in vitro* culture of primary endometrial epithelial cells able to model the physiological tissue environment.

6 Chapter 6

6 Final Discussion

6.1 Introduction

Endometrial cancer (EC) is the most common gynaecological malignancy in the United Kingdom (UK) and the 4th most common cancer to affect UK women after breast, lung and colorectal cancer (Cancer Research UK, 2018a). The incidence of EC is rising, with ~9000 new cases reported in the UK alone in 2015 (Kitson *et al.*, 2018). In the ten years between 1992 and 2012, the incidence of EC increased by 2 % every year in women under the age of 50 (Beavis *et al.*, 2016; MacKintosh and Crosbie, 2018). Furthermore, despite overall improvements in EC survival (Evans *et al.*, 2011), women continue to die from the disease, and projections envisage a potential rise of 19 % in mortality between 2014 to 2035 within the UK (Cancer Research UK, 2018).

The current obesity epidemic is playing a substantial role in driving this increase in EC incidence, such that every 5 kg/m^2 rise in body mass index (BMI) reportedly increases EC risk by 1.6-fold (Mackintosh and Crosbie, 2013). Other factors including delayed childbearing and a reduction in hysterectomy rates for benign disorders may also be contributing (Daniluk and Koert, 2016; MacKintosh and Crosbie, 2018). Surgery is, and has always been, the mainstay of treatment for early stage EC and takes the form of a total hysterectomy with bilateral salpingo-oophorectomy. There has been a progressive move towards the use of minimally invasive surgical (MIS) techniques, however, surgical intervention is not without risk, especially amongst obese individuals and in those with medical co-morbidities. In addition, ~120 women present annually in the UK with EC before the age of 45 years (Cancer Research UK, 2018; Farthing, 2006) and with age-specific incidence rates of EC rising steeply from around age 45-49, women of reproductive age are being seen more frequently, with requests to preserve fertility becoming commonplace.

At present, a screening programme for EC does not exist and there is not a standard or routine screening test available. Endometrial biopsy is a sensitive and specific test, but it can be uncomfortable and invasive. Since ~75 to 90 % of women with EC present with AUB as an early symptom (Kimura, Kamiura, *et al.*, 2004; Seebacher *et al.*, 2009), the majority of women are diagnosed when their EC is still confined to the uterus and have a >90 % five-year survival rate (Creasman *et al.*, 2006; Lewin *et al.*, 2010). The presence of early symptoms therefore affords secondary prevention, allowing detection of EC when surgical treatment can

stop it from progressing, although as mentioned above not all women will be candidates for surgical intervention. Women at risk of developing hereditary EC, e.g. those with Lynch syndrome, are normally invited for endometrial assessment at around age 30 to 35 years or 5 to 10 years prior to the earliest age of first diagnosis of a Lynch-associated cancer of any kind in the family (Lindor *et al.*, 2006), although this varies between institutions.

Current strategies for prevention of EC centre around reducing levels of obesity and counterbalancing un-opposed oestrogen exposure, e.g. progestin therapy (MacKintosh and Crosbie, 2018). A recent priority setting partnership, that brought together patients as well as health care professionals using a methodology established by the James Lind Alliance, provided an agreed list of the top-ten unanswered questions for EC research, helping to shape the future research agenda. Importantly, and of relevance to the current studies, these included the desire for development of a personalised risk score for developing EC (Wan *et al.*, 2016).

The studies contributing to this thesis centre around the condition endometrial hyperplasia (EH). This condition incorporates a heterogeneous group of endometrial lesions that can occur in response to oestrogenic stimulation. The variant, atypical hyperplasia / endometrioid intraepithelial neoplasia (EIN) is widely considered a true pre-malignant endometrial lesion, being a clonal proliferation of endometrial epithelial cells, and conferring a substantial risk of a concurrent or future EC when it is detected on endometrial biopsy (reviewed in Sanderson *et al.*, 2017). Historically, due to the heterogeneous nature of EH lesions, there has been considerable difficulty classifying them into clinically relevant and pathologically reproducible groups that correlate risk of malignancy with treatment options and clinical outcome. In addition, the mechanisms that drive progression of the endometrium from a benign to a neoplastic state are not fully understood. To that end, the studies presented herein aimed to use cellular and molecular approaches to further the capacity for earlier diagnosis of EC, through targeting and enhancing understanding of EH.

6.2 Aims and experimental approaches

The present studies addressed the following three aims:

- To evaluate the current pathological approaches used to classify EHs and predict progression to EC. Using a well characterised human archival EH tissue resource, the WHO94 and EIN/WHO2014 classification systems were investigated for their diagnostic reproducibility and capacity to predict progression to EC.

- To characterise key molecular changes within EH lesions so that they can be used to extend and enhance pathological classification of EH. Using the archival EH tissue resource, molecular changes pertinent to endometrial carcinogenesis were evaluated by immunohistochemistry with a view to potential use as a diagnostic / prognostic aid.

- To explore *in vitro* models of the endometrium and investigate the role of PTEN and ARID1A within endometrial proliferation. Utilising informative cell lines, the principles of RNA interference were employed to silence the protein expression of two frequently mutated tumour suppressors in ECs, PTEN and ARID1A. Cellular proliferation was investigated, both with and without a functional oestrogen receptor alpha (ERα).

6.3 The EIN/WHO2014 system of EH classification improves diagnostic reproducibility and better predicts progression to endometrial cancer compared to the WHO94 system

In chapter 3 it was demonstrated that the EIN/WHO2014 system of EH classification improves interobserver variability when compared to the WHO94 system of EH classification. A dual, blinded, expert gynaecological pathologist review of n=125 archival endometrial biopsy specimens was performed. Each pathologist was asked to record a diagnosis for each endometrial biopsy specimen utilising both the WHO94 and EIN/WHO2014 classification systems. The review diagnoses of each pathologist were compared to the original diagnosis for each specimen and also to each other. Interobserver percentage agreement for each of the expert pathologists and the original WHO94 based diagnosis was 56.0 % (n=70) and 48.8 % (n=61) respectively. When comparing the expert pathologists to each other, the percentage agreement was 52.1 % (n=64). Upon reclassification using the EIN/WHO2014 classification system, increased interobserver percentage agreement was noted between the two expert pathologists (67.2 %, n=84). Kappa (*k*) coefficient analysis was performed to account for any interobserver agreement occurring by chance, demonstrating an increase from 'fair' to 'moderate' agreement with the use of the EIN/WHO2014 classification system. This increase in interobserver variability echoed findings from other studies (Hecht *et al.*, 2005; Usubutun *et al.*, 2012), providing further validation of the EIN/WHO2014 system of EH classification.

Pathological interobserver variation is not a phenomenon unique to EH diagnoses, it has been studied extensively across numerous tissue types, e.g. Barratts oesophagus (Montgomery, 2005), breast hyperplasia (Jain *et al.*, 2011) and cutaneous melanoma (Eriksson *et al.*, 2013), to name but a few. Although diagnostic agreement is high in many key areas of pathology, increased levels of variability have been identified for diagnoses on the borderline between established entities (Allison *et al.*, 2014). In agreement with previous reports, the results summarised in chapter 3 identified significant morphological heterogeneity between EH lesions. The relationship between the presence of EH lesions and progression to EC is further complicated by evidence that EH lesions can be unstable; they may be shed spontaneously with menses, or they may be reversed by a change in the patient's hormonal milieu, whether through alterations in physiology (e.g. weight loss) or alterations produced iatrogenically (e.g. hormonal medications) (Gallos *et al.*, 2013; Terakawa *et al.*, 1997). The effects of endogenous hormones can also be problematic when accessing and classifying EH specimens. As such when analysing tissues partially treated with hormones and where there is difficulty in interpretation, hormonal therapy should be temporarily stopped, and a re-biopsy performed after 2-6 weeks (Mutter 2000).

Given the spatial and temporal alterations that occur in EH, together with the spectrum of morphological appearances often presented, it is unsurprising that diagnostic reproducibility varies so widely. In the case of EH, interobserver variation can have significant clinical implications. Since pre-malignant EH lesions are typically treated surgically with hysterectomy and other 'benign' EH variants offered conservative treatment or medical progestin therapy, diagnostic variation may result in some women being potentially overtreated or indeed undertreated. Whilst pathological classification helps to stratify EHs, with the EIN/WHO2014 system appearing to be superior to WHO94 in doing so, further avenues need to be pursued to ensure a robust diagnosis is made. To that end, the role of digital image analysis warrants further investigation.

The EIN system of classification was based upon innovative work by Jan Baak and the introduction of the morphometric D-score, which has consistently been demonstrated to have high diagnostic reproducibility (Baak *et al.*, 1988, 1992, 2001; Mutter, Baak, *et al.*, 2000; Orbo *et al.*, 2000). A reticence to adopt image analysis techniques often stems from a high initial cost outlay and the technical infrastructure required to set up such a service, although some would argue against this (Baak, Mutter, *et al.*, 2005). We investigated the role of digital image analysis in chapter 3, suggesting that the subjective non-quantitative estimates of the volume percentage stromal tissue compartment could be improved using computer-assisted

image analysis, such as that offered by the TissueGnostics Stratquest software. With advances in whole-slide scanning technologies and digital pathology becoming more mainstream, it is hoped that larger scale research studies and validation studies of diagnostic reproducibility using digital image analysis will provide alternate modalities to improve on what can be achieved currently with pathological classification alone. There is a reported national and global shortage of pathologists, due to poor recruitment in recent years (Bracey, 2017). In addition, workloads have increased, as has the complexity of diagnostic material (Bracey, 2017). Validated digitised analysis processes may offer a solution to these problems, working in parallel with a pathologist to help improve the accuracy, reliability and efficiency of histological testing. Further ahead in the future, application of automated artificial intelligence may offer more robust diagnostic reproducibility that is not currently achievable. In the interim, nationalised guidance on pathological approaches to EH classification, potentially with a stipulation for a dual-pathologist consensus on atypical hyperplasia / EIN diagnoses, may be beneficial.

As discussed above EC incidence increased sharply from around age 45-49 and what has previously been considered a predominantly postmenopausal disease is becoming an increasing concern for younger women of childbearing age, obese individuals and those with polycystic ovarian syndrome (PCOS). EIN may reside concurrently with EC or may precede EC by several years. Reports suggest that EC occurrences beyond 1 year of an EIN diagnosis are 45 times more likely than in EIN free women (Baak, Mutter, *et al.*, 2005). The ability to offer a comprehensive, evidence-based metric to women who may wish to retain their fertility is therefore essential. The EIN/WHO2014 classification system appears to offer this, and our data add to the body of evidence that a diagnosis of EIN confers an improvement on the prediction of a malignant outcome when compared with a WHO94 diagnosis of complex atypical hyperplasia.

6.4 Altered PAX2 and HAND2 protein expression in endometrial hyperplasia - steps forward towards identification of a diagnostic / prognostic panel?

Given the aforementioned challenges of achieving diagnostic reproducibility in EH, yet the clear clinical need for a reliable diagnosis, a role for tissue biomarker analysis is apparent. There exists an unmet need for a diagnostic test capable of: (i) differentiating neoplastic EIN lesions from benign hyperplasia and (ii) predicting progression of EH to EC. For example, a

pre-menopausal nulliparous patient with PCOS, found to have EIN on endometrial biopsy and who wishes to have future children would benefit from a prognostic test, able to predict the likelihood of her EIN progressing to EC *vs* EIN lesion involution, to guide her decision making. In addition, a diagnostic test may aid pathological analysis of sub-diagnostic EH lesions, as described by Owings *et al,* whereby crowding of cytologically suspicious glands is a concern; however, the overall lesion size may be insufficient for diagnosis (Owings and Quick, 2014). With this goal in mind, we endeavoured to characterise key molecular changes within EH lesions to extend and enhance pathological classification. I chose to focus on immunohistochemical markers since this technique is widely available in histopathological laboratories with validated methodologies, including the use of automated staining platforms.

In chapter 4, well characterised archival EH tissue samples (~105 samples) underwent immunohistochemical analysis for several key protein markers, established from current scientific literature to be pertinent to endometrial carcinogenesis (reviewed in Sanderson *et al.*, 2017). Individually, loss of PAX2 expression and altered HAND2 expression were significantly associated with a biopsy diagnosis of EIN. When subjected to hierarchical cluster analysis alongside PTEN protein expression, changes in PAX2 and HAND2 protein expression appeared to be the defining markers of each cluster group, with positivity for both proteins being highly suggestive of a benign EH diagnosis. *HAND2* has been suggested to be one of the most commonly hypermethylated and silenced genes in EC and increased *HAND2* methylation within premalignant lesions has been demonstrated (Jones *et al.*, 2013). Within our cohort 90 % of all the EH that progressed to EC demonstrated altered HAND2 protein expression.

Despite widespread suggestions that PTEN protein expression is a useful diagnostic marker of EIN (Colombo *et al.*, 2016), we demonstrated that although confluent PTEN-null glandular regions were significantly associated with an EIN lesion, overall loss of PTEN protein expression was not significantly associated with either a EIN or hyperplasia without atypia (HwA) diagnosis. This finding was supported by a recent meta-analysis which investigated the diagnostic accuracy of PTEN within EH lesions and reported low rates of sensitivity and specificity when PTEN was analysed across n=1736 EH specimens (Raffone, *et al.*, 2019).

The data presented in chapter 4 confirm and extend existing literature on the expression patterns of several key proteins within EH tissues. Utilising well characterised retrospectively classified samples using EIN/WHO2014 diagnostic criteria, the proteins PAX2

and HAND2 appear to lend themselves favourably to use in a diagnostic / prognostic panel and their expression warrants further investigation.

6.5 In an *in vitro* endometrial cell line model, knockdown of PTEN protein increases cellular proliferation

As previously discussed, several lines of evidence have demonstrated that PTEN protein regulates cell proliferation, tissue growth, and apoptosis via the PI3K/Akt/mTOR pathway (reviewed in Sansal and Sellers, 2004). PTEN mutations are widely considered to be both an early event and a frequent initiating event for endometrial carcinogenesis (Mutter *et al.*, 2001). However, they are not the rate-limiting event; several other steps of a multi–stage process are needed for EC to develop (Mutter *et al.*, 2014).

Data from chapter 4 demonstrated PTEN protein expression loss in 64/104 (58.7 %) of EH samples in the current study, which despite not being statistically associated with EH diagnosis, was still the largest change in protein expression of any of the markers investigated. In chapter 5 we utilised two endometroid epithelial cancer cell lines to investigate the effect that silencing of PTEN protein expression had on cell proliferation. In this *in vitro* model system, knockdown of PTEN expression using a lentiviral vector resulted in a significant increase in percentage cell number by day 7 in culture when compared to cells transfected with a control lentivirus in both of the transduced cell lines.

We hypothesised that there may be an association between PTEN expression loss and ERα, that may bestow a proliferative effect, since several lines of evidence have suggested that loss of *PTEN* can result in changes in tissue function through activation of ERα (Joshi *et al.*, 2012; Vilgelm *et al.*, 2006). To that end we both silenced PTEN and overexpressed ERα in two endometrioid epithelial cancer cell lines. In the absence of a ligand this co-manipulation resulted in a significant reduction in cell proliferation by day 7 in culture in MFE-280 cells when compared to control, however no significant effects were noted in KLE cell line. This this may be suggestive of alternated cellular machinery between the two cell lines. Furthermore, when these cells were stimulated with oestradiol (E_2) the opposite effect to what we expected was seen after 72 hours, with both co-manipulated cell lines demonstrating a significant reduction in cell proliferation. A similar effect was also observed in manipulated cell lines with ERα overexpression alone, without silencing PTEN. In retrospect, these results may demonstrate a limitation of the model system used, since both cell lines were developed

from grade 3 endometrioid tumours without a functional ERα. Despite the addition of functional ERα these cell lines may still lack all the necessary proliferation machinery e.g. steroid receptor coactivators (SRCs), to activate steroid hormone signalling and growth factor pathways in order to mount a proliferative response (reviewed in (Lonard and O'Malley, 2016).

6.6 Limitations

Whilst every effort was taken to ensure a vigorous methodological approach to the studies described herein, there are several limitations which should be taken into account. Firstly, the human EH tissue resource was obtained retrospectively from archival material. Whilst the quality of the archival tissue material was excellent, permitting comprehensive pathological classification, the associated clinical patient details were incomplete in several cases, e.g. complete body mass index (BMI) data. Moreover, the vast majority of the study population were of white Caucasian ethnicity, reflecting the fact that South East Scotland has a minority ethnic population, which was estimated at just over 4 % in the 2011 census (The Scottish Government, 2011).

Secondly, the number of EH cases that progressed to EC in this study was low (n=10 with tissue samples available for immunohistochemical analysis). This meant that simple observation and reflection on the immunohistochemical staining patterns was the ceiling of what could be realistically achieved in these cases. Whilst the primary outcome objective in chapter 3 was to analyse diagnostic pathological reproducibility, a secondary objective looked at progression to EC within the EH tissue cohort. The data generated regarding progression to EC in this study is limited by the absence of a power calculation and therefore true progression rates of EH to EC cannot be ascertained from this cohort. For future prospective studies to investigate rates of progression from EH to EC, an estimated sample size of EH cases to investigate would be ~3300 cases. This estimate is based upon the incidence of women developing EC being ~3.1 % and EH ~ 5 % (Cancer Research UK, 2018) and utilising an alpha value of 0.05 (i.e. false positive rate) and 80 % power (false negative rate).

Finally, as discussed in chapter 5, the mechanistic cellular arm of this study was limited by the known difficulties in obtaining primary human endometrial epithelial cells. Whilst cell lines provide a durable model system, they do not always provide a biological response close to an *in vivo* situation. Future *in vitro* work would focus on methods to obtain a pure population

of primary cells or consider using an organoid based model system able to recapitulate cellular processes and cellular arrangements as seen in the tissues (Deane *et al.*, 2017).

6.7 Future directions

The work presented in this thesis formed part of a pilot study based on an archival resource. A robust diagnostic/prognostic immunohistochemical panel requires independent validation using larger tissue resources which have linked clinical information, including data about subsequent development of EC. Importantly, this must also include a more diverse population than that in South East Scotland, as the risk of developing EC has been reported to vary according to ethnicity, although the reasons remain poorly understood (Setiawan *et al.*, 2007). In future endeavours it would also be useful to look at confirmed cases of endometrioid EC and then go back to review for pathology in archival biopsies prior to hysterectomy.

In the current study we obtained promising results using a digital pathology software platform, capable of analysing both the morphological proportions of different cellular compartments (stroma *vs.* epithelia) within tissues and evaluating the immunohistochemical staining pattern for different cellular markers. This software could also be used to quantify numbers of proliferating cells (via Ki67 interpretation) as well as other molecular markers, such as CTNNB1 (beta catenin) mutations, which have recently been reported as a predictor of disease-free survival in low-grade early EC (Kurnit *et al.*, 2017). The increasingly widespread use of slide-scanning technology will also mean that histology images could be shared between laboratories that may use alternative methods of tissue evaluation, i.e. the D-score, to see if a newer common diagnostic algorithm can be developed. As discussed in chapter 4, we found the scoring of PAX2 was sometimes challenging due to a 'cytoplasmic flare' effect, likely due to the use of a polyclonal primary antibody. The use of an automated system to segregate tissue compartments whilst analysing staining patterns would be very valuable under these circumstances.

In this study the challenges of maintaining a pure primary epithelial cell population limited their use for genomic manipulation in part due to limited amounts of starting material, but also most likely because the culture conditions had not been optimised for epithelial cells. This is a common problem reported by other groups and several recent advances in culture methodology, some reported from other tissue systems, may offer future promise including the growing of cells in media containing a ROCK inhibitor (Y-27632) in cultures at an air-liquid interface to promote cell polarisation (Li *et al.*, 2018). In the present study some

preliminary success was achieved in maintaining cells in 3D cultures using a hanging drop system. Once the epithelial cells have been established it will be important to revisit 3D culture systems that allow for interrogation of the stromal-epithelial cross talk that underpins the regulation of the normal endometrium, and which may be disturbed by excess unopposed oestrogens or mutations in other genes such as HAND2 which is expressed only in the stroma. Building on the work from chapter 4 utilising immunohistochemical HAC analysis, knockdown of HAND2 and PAX2 in a future cellular epithelial/stromal co-culture model system would allow functional validation of immunohistochemical data and allow permit further work aimed at unravelling a mechanism of action.

6.8 Conclusions

Endometrial hyperplasia (EH) represents a spectrum of morphological and cytological endometrial aberrations, and abnormal forms pose a significant risk of progression to endometrial cancer. Efforts to classify EH into clinically meaningful groups have historically suffered from poor diagnostic reproducibility, creating the potential for under- and over-treatment of the condition. Given the current observed increase in incidence of endometrial cancers, accurate and reproducible diagnosis of EH has a key role in the early detection and prevention of this disease. Whilst the EIN/WHO2014 classification system offers improvement on EH diagnostic reproducibly when compared to its predecessor WHO1994, it is not flawless, and efforts should be made to complement and improve pathological classification. This may, pending further validation, be with an immunohistochemical diagnostic panel and the studies presented herein suggest that HAND2 and PAX2 may lend themselves favourably to this. Furthermore, digital image analysis techniques and *in vitro* endometrial modelling have the capacity to extend our knowledge and assist in uncovering mechanisms which drive endometrial neoplasia.

7 References

Abu-Rustum NR, Zhou Q, Gomez JD, Alektiar KM, Hensley ML, Soslow RA, Levine DA, Chi DS, Barakat RR, Iasonos A. A nomogram for predicting overall survival of women with endometrial cancer following primary therapy: Toward improving individualized cancer care. *Gynecol Oncol* 2010;116:399–403.

Adams JM, Taylor AE, Schoenfeld DA, Crowley WF, Hall JE. The midcycle gonadotropin surge in normal women occurs in the face of an unchanging gonadotropin-releasing hormone pulse frequency. *J Clin Endocrinol Metab* 1994;79:858–64.

Agarwal ML, Agarwal A, Taylor WR, Stark GR. p53 controls both the G2/M and the G1 cell cycle checkpoints and mediates reversible growth arrest in human fibroblasts. *Proc Natl Acad Sci U S A* 1995;92:8493–7.

Ali IU, Schriml LM, Dean M. Mutational spectra of PTEN/MMAC1 gene: a tumor suppressor with lipid phosphatase activity. *J Natl Cancer Inst* 1999;91:1922–32.

Ali SH, O'Donnell AL, Mohamed S, Mousa S, Dandona P. Overexpression of estrogen receptor-α in the endometrial carcinoma cell line Ishikawa: inhibition of growth and angiogenic factors. *Gynecol Oncol* 2004;95:637–645.

Alkushi A, Lim P, Coldman A, Huntsman D, Miller D, Gilks CB. Interpretation of p53 immunoreactivity in endometrial carcinoma: establishing a clinically relevant cut-off level. *Int J Gynecol Pathol* 2004;23:129–37.

Allison KH, Reisch LM, Carney PA, Weaver DL, Schnitt SJ, O'Malley FP, Geller BM, Elmore JG. Understanding diagnostic variability in breast pathology: lessons learned from an expert consensus review panel. *Histopathology* 2014;65:240–51.

Allison KH, Tenpenny E, Reed SD, Swisher EM, Garica RL. Immunohistochemical Markers in Endometrial Hyperplasia: Is There a Panel With Promise? *Appl Immunohistochem Mol Morphol* 2008;16:329–343.

Allison KH, Upson K, Reed SD, Jordan CD, Newton KM, Doherty J, Swisher EM, Garcia RL. PAX2 loss by immunohistochemistry occurs early and often in endometrial hyperplasia. *Int J Gynecol Pathol* 2012;31:151–159.

Altman GB, Gown AM, Luchtel DL, Baker C. RANTES Production by Cultured Primate Endometrial Epithelial Cells. *Am J Reprod Immunol* 1999;42:168–174.

Alvarez T, Miller E, Duska L, Oliva E. Molecular profile of grade 3 endometrioid endometrial carcinoma: is it a type I or type II endometrial carcinoma? *Am J Surg Pathol* 2012;36:753–61.

Anzai Y, Holinka CF, Kuramoto H, Gurpide E. Stimulatory effects of 4-hydroxytamoxifen on proliferation of human endometrial adenocarcinoma cells (Ishikawa line). *Cancer Res* 1989;49:2362–5.

Arends M, Ibrahim M, Happerfield L, Frayling IM, Miller K. Interpretation of Immunohistochemical Analysis of MisMatch Repair (MMR) Protein Expression in Tissue Sections for Investigation of Suspected Lynch / Hereditary Non-Polyposis Colorectal Cancer (HNPCC) Syndrome. 2008. Available at: http://www.ukneqasicc.ucl.ac.uk/index.shtml.

Argenta PA, Kassing M, Truskinovsky AM, Svendsen CA. Bariatric surgery and endometrial pathology in asymptomatic morbidly obese women: a prospective, pilot study. *BJOG* 2013;120:795–800.

Ausems EWMA, van der Kamp J-K, Baak JPA. Nuclear Morphometry in the Determination of the Prognosis of Marked Atypical Endometrial Hyperplasia. *Int J Gynecol Pathol* 1985;4:180–185.

Ayhan A, Mao T-L, Suryo Rahmanto Y, Zeppernick F, Ogawa H, Wu R-C, Wang T-L, Shih I-M. Increased proliferation in atypical hyperplasia/endometrioid intraepithelial

neoplasia of the endometrium with concurrent inactivation of ARID1A and PTEN tumour suppressors. *J Pathol Clin Res* 2015;1:186–93.

Baak JP, Mutter GL, Robboy S, van Diest PJ, Uyterlinde AM, Ørbo A, Palazzo J, Fiane B, Løvslett K, Burger C, *et al.* The molecular genetics and morphometry-based endometrial intraepithelial neoplasia classification system predicts disease progression in endometrial hyperplasia more accurately than the 1994 World Health Organization classification system. *Cancer* 2005;103:2304–2312.

Baak JPA, van Diermen B, Steinbakk A, Janssen E, Skaland I, Mutter GL, Fiane B, Løvslett K. Lack of PTEN expression in endometrial intraepithelial neoplasia is correlated with cancer progression. *Hum Pathol* 2005;36:555–561.

Baak JPA, Mutter GL. EIN and WHO94. *J Clin Pathol* 2005;58:1–6.

Baak JPA, Nauta JJP, Wisse-Brekelmans ECM, Bezemer PD. Architectural and nuclear morphometrical features together are more important prognosticators in endometrial hyperplasias than nuclear morphometrical features alone. *J Pathol* 1988;154:335–341.

Baak JPA, Ørbo A, van Diest PJ, Jiwa M, de Bruin P, Broeckaert M, Snijders W, Boodt PJ, Fons G, Burger C, *et al.* Prospective multicenter evaluation of the morphometric D-score for prediction of the outcome of endometrial hyperplasias. *Am J Surg Pathol* 2001;25:930–935.

Baak JPA, Wisse-Brekelmans ECM, Fleege JC, van der Putten HWHM, Bezemer PD. Assessment of the Risk on Endometrial Cancer in Hyperplasia, by Means of Morphological and Morphometrical Features. *Pathol - Res Pract* 1992;188:856–859.

Bagcchi S. HAND2 methylation linked to endometrial cancer. *Lancet Oncol* 2013;14:e590.

Baker J, Obermair A, Gebski V, Janda M. Efficacy of oral or intrauterine device-delivered progestin in patients with complex endometrial hyperplasia with atypia or early endometrial adenocarcinoma: a meta-analysis and systematic review of the literature. *Gynecol Oncol* 2012;125:263–70.

Barbier CS, Becker KA, Troester MA, Kaufman DG. Expression of Exogenous Human Telomerase in Cultures of Endometrial Stromal Cells Does Not Alter Their Hormone Responsiveness1. *Biol Reprod* 2005;73:106–114.

Bartelmez GW. The phases of the menstrual cycle and their interpretation in terms of the pregnancy cycle. *Am J Obstet Gynecol* 1957;74:931–955.

Bates GW, Bowling M. Physiology of the female reproductive axis. *Periodontol 2000* 2013;61:89–102.

Beavis AL, Smith AJB, Fader AN. Lifestyle changes and the risk of developing endometrial and ovarian cancers: opportunities for prevention and management. *Int J Womens Health* 2016;8:151–67.

Berchuck A, Kohler MF, Marks JR, Wiseman R, Boyd J, Bast RC. The p53 tumor suppressor gene frequently is altered in gynecologic cancers. *Am J Obstet Gynecol* 1994;170:246–52.

Berends MJW, Hollema H, Wu Y, Van Sluis T Der, Mensink RGJ, Ten Hoor KA, Sijmons RH, De Vries EGE, Pras E, Mourits MJE, *et al.* MLH1 and MSH2 protein expression as a pre-screening marker in hereditary and non-hereditary endometrial hyperplasia and cancer. *Int J Cancer* 2001;92:398–403.

Bergeron C, Nogales FF, Masseroli M, Abeler V, Duvillard P, Müller-Holzner E, Pickartz H, Wells M. A multicentric European study testing the reproducibility of the WHO classification of endometrial hyperplasia with a proposal of a simplified working classification for biopsy and curettage specimens. *Am J Surg Pathol* 1999;23:1102–8.

Berthois Y, Katzenellenbogen JA, Katzenellenbogen BS. Phenol red in tissue culture media is a weak estrogen: implications concerning the study of estrogen-responsive cells in culture. *Proc Natl Acad Sci* 1986;83:2496–2500.

Beutler HK, Dockerty MB, Randall LM. Precancerous lesions of the endometrium. *Am J Obstet Gynecol* 1963;86:433–43.

Bobrowska K, Kamiński P, Cyganek A, Pietrzak B, Jabiry-Zieniewicz Z, Durlik M, Paczek L. High rate of endometrial hyperplasia in renal transplanted women. *Transplant Proc* 2006;38:177–9.

Bokhman J V. Two pathogenetic types of endometrial carcinoma. *Gynecol Oncol* 1983;15:10–17.

Boland CR, Thibodeau SN, Hamilton SR, Sidransky D, Eshleman JR, Burt RW, Meltzer SJ, Rodriguez-Bigas MA, Fodde R, Ranzani GN, *et al.* A National Cancer Institute Workshop on Microsatellite Instability for cancer detection and familial predisposition: development of international criteria for the determination of microsatellite instability in colorectal cancer. *Cancer Res* 1998;58:5248–57.

Bombail V, Collins F, Brown P, Saunders PTK. Modulation of ERα transcriptional activity by the orphan nuclear receptor ERRβ and evidence for differential effects of long- and short-form splice variants. *Mol Cell Endocrinol* 2010;314:53–61.

Bombail V, Gibson DA, Collins F, MacPherson S, Critchley HOD, Saunders PTK. A Role for the orphan nuclear receptor estrogen-related receptor alpha in endometrial stromal cell decidualization and expression of genes implicated in energy metabolism. *J Clin Endocrinol Metab* 2010;95:E224-8.

Bonadona V, Bonaïti B, Olschwang S, Grandjouan S, Huiart L, Longy M, Guimbaud R, Buecher B, Bignon Y-J, Caron O, *et al.* Cancer risks associated with germline mutations in MLH1, MSH2, and MSH6 genes in Lynch syndrome. *JAMA* 2011;305:2304–10.

Boretto M, Cox B, Noben M, Hendriks N, Fassbender A, Roose H, Amant F, Timmerman D, Tomassetti C, Vanhie A, *et al.* Development of organoids from mouse and human endometrium showing endometrial epithelium physiology and long-term expandability. *Development* 2017;144:1775–1786.

Bosse T, ter Haar NT, Seeber LM, Diest PJ v, Hes FJ, Vasen HFA, Nout RA, Creutzberg CL, Morreau H, Smit VT. Loss of ARID1A expression and its relationship with PI3K-Akt pathway alterations, TP53 and microsatellite instability in endometrial cancer. *Mod Pathol* 2013;26:1525.

Bracey T. Digital pathology. *Bull R Coll Surg Engl* 2017;99:93–96.

Briët JM, Hollema H, Reesink N, Aalders JG, Mourits MJE, ten Hoor KA, Pras E, Boezen HM, van der Zee AGJ, Nijman HW. Lymphvascular space involvement: an independent prognostic factor in endometrial cancer. *Gynecol Oncol* 2005;96:799–804.

Brinton LA, Felix AS, McMeekin DS, Creasman WT, Sherman ME, Mutch D, Cohn DE, Walker JL, Moore RG, Downs LS, *et al.* Etiologic heterogeneity in endometrial cancer: Evidence from a Gynecologic Oncology Group trial. *Gynecol Oncol* 2013;129:277–284.

ten Broeke SW, Brohet RM, Tops CM, van der Klift HM, Velthuizen ME, Bernstein I, Capellá Munar G, Gomez Garcia E, Hoogerbrugge N, Letteboer TGW, *et al.* Lynch syndrome caused by germline PMS2 mutations: delineating the cancer risk. *J Clin Oncol* 2015;33:319–25.

Buell-Gutbrod R, Cavallo A, Lee N, Montag A, Gwin K. Heart and Neural Crest Derivatives Expressed Transcript 2 (HAND2): a novel biomarker for the identification of atypical hyperplasia and Type I endometrial carcinoma. *Int J Gynecol Pathol* 2015;34:65–73. Available at: http://www.ncbi.nlm.nih.gov/pubmed/25473755.

Campbell RA, Bhat-Nakshatri P, Patel NM, Constantinidou D, Ali S, Nakshatri H. Phosphatidylinositol 3-kinase/AKT-mediated activation of estrogen receptor alpha: a new model for anti-estrogen resistance. *J Biol Chem* 2001;276:9817–24.

Cancer Research UK. Uterine cancer statistics. 2018. Available at: http://www.cancerresearchuk.org/health-professional/cancer-statistics/statistics-by-cancer-type/uterine-cancer/incidence#ref-1. Accessed March 07, 2018.

Carlson JW, Mutter GL. Endometrial intraepithelial neoplasia is associated with polyps and frequently has metaplastic change. *Histopathology* 2008;53:325–332.

Carter AJR, Nguyen CN. A comparison of cancer burden and research spending reveals

discrepancies in the distribution of research funding. *BMC Public Health* 2012;12:526.
Chan RWS, Schwab KE, Gargett CE. Clonogenicity of human endometrial epithelial and stromal cells. *Biol Reprod* 2004;70:1738–50.
Chandra V, Kim JJ, Benbrook DM, Dwivedi A, Rai R. Therapeutic options for management of endometrial hyperplasia. *J Gynecol Oncol* 2016;27:712–749.
Chapman S, Liu X, Meyers C, Schlegel R, McBride AA. Human keratinocytes are efficiently immortalized by a Rho kinase inhibitor. *J Clin Invest* 2010;120:2619–26.
Chi DS, Barakat RR, Palayekar MJ, Levine DA, Sonoda Y, Alektiar K, Brown CL, Abu-Rustum NR. The incidence of pelvic lymph node metastasis by FIGO staging for patients with adequately surgically staged endometrial adenocarcinoma of endometrioid histology. *Int J Gynecol Cancer* 2008;18:269–73.
Cinel L, Polat A, Aydin Ö, Düşmez D, Eğilmez R. Bcl-2, iNOS, p53 and PCNA expression in normal, disordered proliferative, hyperplastic and malignant endometrium. *Pathol Int* 2002;52:384–389.
Cirpan T, Terek MC, Mgoyi L, Zekioglu O, Iscan O, Ozsaran A. Immunohistochemical evaluation of PTEN protein in patients with endometrial intraepithelial neoplasia compared to endometrial adenocarcinoma and proliferative phase endometrium. *Eur J Gynaecol Oncol* 2006;27:389–92.
Coleman KM, Smith CL. Intracellular signaling pathways: nongenomic actions of estrogens and ligand-independent activation of estrogen receptors. *Front Biosci* 2001;6:D1379-91.
Collins F, MacPherson S, Brown P, Bombail V, Williams ARW, Anderson R a, Jabbour HN, Saunders PTK. Expression of oestrogen receptors, ERalpha, ERbeta, and ERbeta variants, in endometrial cancers and evidence that prostaglandin F may play a role in regulating expression of ERalpha. *BMC Cancer* 2009;9:330.
Colombo N, Creutzberg C, Amant F, Bosse T, González-Martín A, Ledermann J, Marth C, Nout R, Querleu D, Mirza MR, *et al.* ESMO-ESGO-ESTRO Consensus Conference on Endometrial Cancer: diagnosis, treatment and follow-up. *Ann Oncol* 2016;27:16–41.
Combs SE, Han G, Mani N, Beruti S, Nerenberg M, Rimm DL. Loss of antigenicity with tissue age in breast cancer. *Lab Investig* 2016;96:264–269.
Committee on Gynecologic Practice S of GO. The American College of Obstetricians and Gynecologists Committee Opinion no. 631. Endometrial intraepithelial neoplasia. *Obstet Gynecol* 2015;125:1272–8.
Creasman W. Revised FIGO staging for carcinoma of the endometrium. *Int J Gynaecol Obstet* 2009;105:109.
Creasman WT, Odicino F, Maisonneuve P, Quinn MA, Beller U, Benedet JL, Heintz APM, Ngan HYS, Pecorelli S. Carcinoma of the corpus uteri. FIGO 26th Annual Report on the Results of Treatment in Gynecological Cancer. *Int J Gynaecol Obstet* 2006;95 Suppl 1:S105-43.
Critchley HO, Wang H, Jones RL, Kelly RW, Drudy TA, Gebbie AE, Buckley CH, McNeilly AS, Glasier AF. Morphological and functional features of endometrial decidualization following long-term intrauterine levonorgestrel delivery. *Hum Reprod* 1998;13:1218–24.
Critchley HOD, Maybin JA. Molecular and cellular causes of abnormal uterine bleeding of endometrial origin. *Semin Reprod Med* 2011;29:400–9.
Critchley HOD, Saunders PTK. Hormone receptor dynamics in a receptive human endometrium. *Reprod Sci* 2009;16:191–9.
Daikoku T, Hirota Y, Tranguch S, Joshi AR, DeMayo FJ, Lydon JP, Ellenson LH, Dey SHK. Conditional loss of uterine Pten unfailingly and rapidly induces endometrial cancer in mice. *Cancer Res* 2008;68:5619–5627.
Daniluk JC, Koert E. Childless women's beliefs and knowledge about oocyte freezing for social and medical reasons. *Hum Reprod* 2016;31:2313–2320.
Deane JA, Cousins FL, Gargett CE. Endometrial organoids: in vitro models for endometrial

research and personalized medicine†. *Biol Reprod* 2017;97:781–783.
Deng Y, Chan SS, Chang S. Telomere dysfunction and tumour suppression: the senescence connection. *Nat Rev Cancer* 2008;8:450–8.
Donoghue JF, Lederman FL, Susil BJ, Rogers PAW. Lymphangiogenesis of normal endometrium and endometrial adenocarcinoma. *Hum Reprod* 2007;22:1705–13.
Dossus L, Allen N, Kaaks R, Bakken K, Lund E, Tjonneland A, Olsen A, Overvad K, Clavel-Chapelon F, Fournier A, *et al.* Reproductive risk factors and endometrial cancer: The European prospective investigation into cancer and nutrition. *Int J Cancer* 2010;127:442–451.
Downward J. Mechanisms and consequences of activation of protein kinase B/Akt. *Curr Opin Cell Biol* 1998;10:262–7.
Dumesic DA, Lobo RA. Cancer risk and PCOS. *Steroids* 2013;78:782–5.
Dunneram Y, Greenwood DC, Burley VJ, Cade JE. Dietary intake and age at natural menopause: results from the UK Women's Cohort Study. *J Epidemiol Community Health* 2018;72:733 LP-740.
Dunton CJ, Baak JP a, Palazzo JP, Van Diest PJ, McHugh M, Widra EA. Use of computerized morphometric analyses of endometrial hyperplasias in the prediction of coexistent cancer. *Am J Obstet Gynecol* 1996;174:1518–1521.
Dutertre M, Smith CL. Molecular mechanisms of selective estrogen receptor modulator (SERM) action. *J Pharmacol Exp Ther* 2000;295:431–7.
Eisen MB, Spellman PT, Brown PO, Botstein D. Cluster analysis and display of genome-wide expression patterns. *Proc Natl Acad Sci U S A* 1998;95:14863–8.
Elhafey AS, Papadimitriou JC, El-Hakim MS, El-Said AI, Ghannam BB, Silverberg SG. Computerized image analysis of p53 and proliferating cell nuclear antigen expression in benign, hyperplastic, and malignant endometrium. *Arch Pathol Lab Med* 2001;125:872–9.
Ellenson LH, Ronnett BM, Kurman RJ. Precursor Lesions of Endometrial Carcinoma. In: *Blaustein's Pathology of the Female Genital Tract*.Vol 7. Boston, MA: Springer US, 2011, 359–391.
Eriksson H, Frohm-Nilsson M, Hedblad M-A, Hellborg H, Kanter-Lewensohn L, Krawiec K, Lundh Rozell B, Månsson-Brahme E, Hansson J. Interobserver variability of histopathological prognostic parameters in cutaneous malignant melanoma: impact on patient management. *Acta Derm Venereol* 2013;93:411–6.
Eritja N, Llobet D, Domingo M, Santacana M, Yeramian A, Matias-Guiu X, Dolcet X. A Novel Three-Dimensional Culture System of Polarized Epithelial Cells to Study Endometrial Carcinogenesis. *Am J Pathol* 2010;176:2722–2731.
Erkanli S, Kayaselcuk F, Kuscu E, Bagis T, Bolat F, Haberal A, Demirhan B. Expression of survivin, PTEN and p27 in normal, hyperplastic, and carcinomatous endometrium. *Int J Gynecol Cancer* 2006;16:1412–1418.
Eshleman JR, Markowitz SD. Mismatch repair defects in human carcinogenesis. *Hum Mol Genet* 1996;5 Spec No:1489–94.
Esteller M, Catasus L, Matias-Guiu X, Mutter GL, Prat J, Baylin SB, Herman JG. hMLH1 promoter hypermethylation is an early event in human endometrial tumorigenesis. *Am J Pathol* 1999;155:1767–72.
Evans J, Catalano RD, Brown P, Sherwin R, Critchley HOD, Fazleabas AT, Jabbour HN. Prokineticin 1 mediates fetal-maternal dialogue regulating endometrial leukemia inhibitory factor. *FASEB J* 2009;23:2165–75.
Evans T, Sany O, Pearmain P, Ganesan R, Blann A, Sundar S. Differential trends in the rising incidence of endometrial cancer by type: data from a UK population-based registry from 1994 to 2006. *Br J Cancer* 2011;104:1505.
Fassbender A, Burney RO, O DF, D'Hooghe T, Giudice L. Update on Biomarkers for the Detection of Endometriosis. Biomed Res Int. 2015;2015:130854

Feldman S, Cook EF, Harlow BL, Berkowitz RS. Predicting endometrial cancer among older women who present with abnormal vaginal bleeding. *Gynecol Oncol* 1995;56:376–81.

Feldman S, Shapter A, Welch WR, Berkowitz RS. Two-Year Follow-Up of 263 Patients with Post/Perimenopausal Vaginal Bleeding and Negative Initial Biopsy. *Gynecol Oncol* 1994;55:56–59.

Ferenczy A, Gelfand M. The biologic significance of cytologic atypia in progestogen-treated endometrial hyperplasia. *Am J Obstet Gynecol* 1989;160:126–131.

Ferlay J, Soerjomataram I, Dikshit R, Eser S, Mathers C, Rebelo M, Parkin DM, Forman D, Bray F. Cancer incidence and mortality worldwide: sources, methods and major patterns in GLOBOCAN 2012. *Int J cancer* 2015;136:E359-86.

Fleischer AC, Kalemeris GC, Entman SS. Sonographic depiction of the endometrium during normal cycles. *Ultrasound Med Biol* 1986;12:271–7.

Gaide Chevronnay HP, Galant C, Lemoine P, Courtoy PJ, Marbaix E, Henriet P. Spatiotemporal coupling of focal extracellular matrix degradation and reconstruction in the menstrual human endometrium. *Endocrinology* 2009;150:5094–105.

Gallos I, Allazzam M, Clarke T, Faraj R, Rosenthal A, Smith P, Gupta J. Management of endometrial hyperplasia. London, 2016.

Gallos ID, Krishan P, Shehmar M, Ganesan R, Gupta JK. Relapse of endometrial hyperplasia after conservative treatment: a cohort study with long-term follow-up. Hum Reprod 2013;28:1231–6

Gallos ID, Yap J, Rajkhowa M, Luesley DM, Coomarasamy A, Gupta JK. Regression, relapse, and live birth rates with fertility-sparing therapy for endometrial cancer and atypical complex endometrial hyperplasia: a systematic review and metaanalysis. *Am J Obstet Gynecol* 2012;207:266.e1-12.

Gammon A, Jasperson K, Champine M. Genetic basis of Cowden syndrome and its implications for clinical practice and risk management. *Appl Clin Genet* 2016;Volume 9:83–92.

Garg K, Broaddus RR, Soslow RA, Urbauer DL, Levine DA, Djordjevic B. Pathologic scoring of PTEN immunohistochemistry in endometrial carcinoma is highly reproducible. *Int J Gynecol Pathol* 2012;31:48–56.

Garg K, Leitao MM, Wynveen C a, Sica GL, Shia J, Shi W, Soslow R a. P53 Overexpression in Morphologically Ambiguous Endometrial Carcinomas Correlates With Adverse Clinical Outcomes. *Mod Pathol* 2010;23:80–92.

Gargett CE, Schwab KE, Zillwood RM, Nguyen HPT, Wu D. Isolation and culture of epithelial progenitors and mesenchymal stem cells from human endometrium. *Biol Reprod* 2009;80:1136–45.

Garry R, Hart R, Karthigasu KA, Burke C. A re-appraisal of the morphological changes within the endometrium during menstruation: a hysteroscopic, histological and scanning electron microscopic study. *Hum Reprod* 2009;24:1393–401.

Gelb AB, Freeman VA, Astrow SH. Evaluation of methods for preserving PTEN antigenicity in stored paraffin sections. *Appl Immunohistochem Mol Morphol AIMM* 2011;19:569–73.

Georgescu M-M. PTEN Tumor Suppressor Network in PI3K-Akt Pathway Control. *Genes Cancer* 2010;1:1170–7.

Gibson D, Simitsidellis I, Collins F, Saunders PTK. Evidence of androgen action in endometrial and ovarian cancers. *Endocr Relat Cancer* 2014;21:203-18.

Gibson DA, Collins F, Cousins FL, Esnal Zufiaurre A, Saunders PTK. The impact of 27-hydroxycholesterol on endometrial cancer proliferation. *Endocr Relat Cancer* 2018;25:381–391.

Gibson DA, Saunders PTK. Estrogen dependent signaling in reproductive tissues - a role for estrogen receptors and estrogen related receptors. *Mol Cell Endocrinol* 2012;348:361–72.

Gibson DA, Saunders PTK. Endocrine disruption of oestrogen action and female reproductive tract cancers. *Endocr Relat Cancer* 2014;21:13-31.

van Gool IC, Eggink F a., Freeman-Mills L, Stelloo E, Marchi E, de Bruyn M, Palles C, Nout R a., de Kroon CD, Osse EM, *et al.* POLE Proofreading Mutations Elicit an Antitumor Immune Response in Endometrial Cancer. *Clin Cancer Res* 2015;21:3347–3355.

Greaves E, Critchley HOD, Horne AW, Saunders PTK. Relevant human tissue resources and laboratory models for use in endometriosis research. *Acta Obstet Gynecol Scand* 2017;96:644–658.

Greenblatt RB, Gambrell RD, Stoddard LD. The protective role of progesterone in the prevention of endometrial cancer. *Pathol Res Pract* 1982;174:297–318.

Grillo F, Bruzzone M, Pigozzi S, Prosapio S, Migliora P, Fiocca R, Mastracci L. Immunohistochemistry on old archival paraffin blocks: Is there an expiry date? *J Clin Pathol* 2017;70:988–993.

Gruber CJ, Tschugguel W, Schneeberger C, Huber JC. Production and actions of estrogens. *N Engl J Med* 2002;346:340–52.

Guan B, Mao T, Panuganti PK, Kuhn E, Kurman RJ, Maeda D, Chen E, Jeng Y, Wang T, Shih I. Mutation and loss of expression of ARID1A in uterine low-grade endometrioid carcinoma. *Am J Surg Pathol* 2011;35:625–32.

Guan B, Wang T-LL, Shih I-MM. ARID1A, a factor that promotes formation of SWI/SNF-mediated chromatin remodeling, is a tumor suppressor in gynecologic cancers. *Cancer Res* 2011;71:6718–27.

Gunderson CC, Fader AN, Carson KA, Bristow RE. Oncologic and Reproductive outcomes with progestin therapy in women with endometrial hyperplasia and grade 1 Adenocarcinoma: A systematic review. *Gynecol Oncol* 2012;125:477–482.

Gusberg SB, Kaplan AL. Precursors of corpus cancer. *Am J Obstet Gynecol* 1963;87:662–678.

Hackenberg R, Hawighorst T, Hild F, Schulz KD. Establishment of new epithelial carcinoma cell lines by blocking monolayer formation. *J Cancer Res Clin Oncol* 1997;123:669–673.

Hackenberg R, Loos S, Nia AH, Kunzmann R, Schulz KD. Expression of placental protein 14 by the new endometrial cancer cell line MFE-280 in vitro and by endometrial carcinomas in vivo. *Anticancer Res* 1998;18:1153–8.

Haines N. *Births by parents' characteristics in England and Wales: 2016*. 2017.

Hale GE, Hughes CL, Cline JM. Endometrial cancer: hormonal factors, the perimenopausal "window of risk," and isoflavones. *J Clin Endocrinol Metab* 2002;87:3–15.

Hamid AA, Mandai M, Konishi I, Nanbu K, Tsuruta Y, Kusakari T, Kariya M, Kita M, Fujii S. Cyclical change of hMSH2 protein expression in normal endometrium during the menstrual cycle and its overexpression in endometrial hyperplasia and sporadic endometrial carcinoma. *Cancer* 2002;94:997–1005.

Hardisson D, Moreno-Bueno G, Sánchez L, Sarrió D, Suárez A, Calero F, Palacios J. Tissue Microarray Immunohistochemical Expression Analysis of Mismatch Repair (hMLH1 and hMSH2 Genes) in Endometrial Carcinoma and Atypical Endometrial Hyperplasia: Relationship with Microsatellite Instability. *Mod Pathol* 2003;16:1148.

Harlow SD, Gass M, Hall JE, Lobo R, Maki P, Rebar RW, Sherman S, Sluss PM, de Villiers TJ, STRAW + 10 Collaborative Group. Executive summary of the Stages of Reproductive Aging Workshop + 10: addressing the unfinished agenda of staging reproductive aging. *J Clin Endocrinol Metab* 2012;97:1159–68.

Hayes MP, Wang H, Espinal-Witter R, Douglas W, Solomon GJ, Baker SJ, Ellenson LH. PIK3CA and PTEN Mutations in Uterine Endometrioid Carcinoma and Complex Atypical Hyperplasia. *Clin Cancer Res* 2006;12:5932–5935.

Hecht JL, Ince TA, Baak JPA, Baker HE, Ogden MW, Mutter GL. Prediction of endometrial carcinoma by subjective endometrial intraepithelial neoplasia diagnosis. *Mod Pathol* 2005;18:324–330.

Hecht JL, Mutter GL. Molecular and pathologic aspects of endometrial carcinogenesis. *J Clin Oncol* 2006;24:4783–91.

Heldring N, Pike A, Andersson S, Matthews J, Cheng G, Hartman J, Tujague M, Ström A, Treuter E, Warner M, *et al.* Estrogen receptors: how do they signal and what are their targets. *Physiol Rev* 2007;87:905–31.

Hendrickson MR, Kempson RL. Endometrial epithelial metaplasias: proliferations frequently misdiagnosed as adenocarcinoma. Report of 89 cases and proposed classification. *Am J Surg Pathol* 1980;4:525–42.

Horn LC, Schnurrbusch U, Bilek K, Hentschel B, Einenkel J. Risk of progression in complex and atypical endometrial hyperplasia: Clinicopathologic analysis in cases with and without progestogen treatment. *Int J Gynecol Cancer* 2004;14:348–353.

Horrée N, van Diest PJ, Sie-Go DMDS, Heintz APM. The invasive front in endometrial carcinoma: higher proliferation and associated derailment of cell cycle regulators. *Hum Pathol* 2007;38:1232–8.

Huang J, Zhao Y-L, Li Y, Fletcher JA, Xiao S. Genomic and functional evidence for an ARID1A tumor suppressor role. *Genes Chromosomes Cancer* 2007;46:745–50.

Isobe M, Emanuel BS, Givol D, Oren M, Croce CM. Localization of gene for human p53 tumour antigen to band 17p13. *Nature* 1986;320:84–5.

Jabbour HN, Kelly RW, Fraser HM, Critchley HOD. Endocrine regulation of menstruation. *Endocr Rev* 2006;27:17–46.

Jaffe AB, Hall A. RHO GTPASES: Biochemistry and Biology. *Annu Rev Cell Dev Biol* 2005;21:247–269.

Jain RK, Mehta R, Dimitrov R, Larsson LG, Musto PM, Hodges KB, Ulbright TM, Hattab EM, Agaram N, Idrees MT, *et al.* Atypical ductal hyperplasia: interobserver and intraobserver variability. *Mod Pathol* 2011;24:917–923.

Jeffus SK, Winham W, Hooper K, Quick CM. Secretory endometrial intraepithelial neoplasia. Kurman RJ, Ellenson LH, Ronnett BM (eds). *Int J Gynecol Pathol* 2014;33:515–6.

Johnson MH. Ovarian Function in the Adult. In: Johnson M, Everitt B (eds) *Essential Reproduction 6th Edition*. 6th Editio. Oxford: Blackwell Publishing, 2007, 146–168.

Joiner AK, Quick CM, Jeffus SK. Pax2 expression in simultaneously diagnosed WHO and EIN classification systems. *Int J Gynecol Pathol* 2015;34:40–6.

Jones A, Teschendorff AE, Li Q, Hayward JD, Kannan A, Mould T, West J, Zikan M, Cibula D, Fiegl H, *et al.* Role of DNA methylation and epigenetic silencing of HAND2 in endometrial cancer development. *PLoS Med* 2013;10:e1001551.

Joshi A, Wang H, Jiang G, Douglas W, Chan JSY, Korach KS, Ellenson LH. Endometrial tumorigenesis in Pten(+/-) mice is independent of coexistence of estrogen and estrogen receptor α. *Am J Pathol* 2012;180:2536–47.

Jovanovic AS, Boynton KA, Mutter GL. Uteri of women with endometrial carcinoma contain a histopathological spectrum of monoclonal putative precancers, some with microsatellite instability. *Cancer Res* 1996;56j:1917–1921.

Juric D, Castel P, Griffith M, Griffith OL, Won HH, Ellis H, Ebbesen SH, Ainscough BJ, Ramu A, Iyer G, *et al.* Convergent loss of PTEN leads to clinical resistance to a PI(3)Kα inhibitor. *Nature* 2015;518:240–244.

Kaaks R, Lukanova A, Kurzer MS. Obesity, endogenous hormones, and endometrial cancer risk: a synthetic review. *Cancer Epidemiol Biomarkers Prev* 2002;11:1531–43.

Kahraman K, Kiremitci S, Taskin S, Kankaya D, Sertcelik A, Ortac F. Expression pattern of PAX2 in hyperplastic and malignant endometrium. *Arch Gynecol Obstet* 2012;286:173–8.

Kandoth C, Schultz N, Cherniack AD, Akbani R, Liu Y, Shen H, Robertson a G, Pashtan I, Shen R, Benz CC, *et al.* Integrated genomic characterization of endometrial carcinoma. *Nature* 2013;497:67–73.

Kane SE, Hecht JL. Endometrial intraepithelial neoplasia terminology in practice: 4-year

experience at a single institution. *Int J Gynecol Pathol* 2012;31:160–165.
Kapucuoglu N, Aktepe F, Kaya H, Bircan S, Karahan N, Ciriş M, Çiriş M. Immunohistochemical expression of PTEN in normal, hyperplastic and malignant endometrium and its correlation with hormone receptors, bcl-2, bax, and apoptotic index. *Pathol Res Pract* 2007;203:153–62.
Kendall BS, Ronnett BM, Isacson C, Cho KR, Hedrick L, Diener-West M, Kurman RJ. Reproducibility of the Diagnosis of Endometrial Hyperplasia, Atypical Hyperplasia, and Well-Differentiated Carcinoma. *Am J Surg Pathol* 1998;22:1012–1019.
Key TJ, Pike MC. The dose-effect relationship between "unopposed" oestrogens and endometrial mitotic rate: its central role in explaining and predicting endometrial cancer risk. *Br J Cancer* 1988;57:205–12.
Kim H, Huang W, Jiang X, Pennicooke B, Park PJ, Johnson MD. Integrative genome analysis reveals an oncomir/oncogene cluster regulating glioblastoma survivorship. *Proc Natl Acad Sci U S A* 2010;107:2183–8.
Kim JJ, Chapman-Davis E. Role of progesterone in endometrial cancer. *Semin Reprod Med* 2010;28:81–90. Available at: http://www.ncbi.nlm.nih.gov/pubmed/20104432.
Kim JJ, Kurita T, Bulun SE. Progesterone action in endometrial cancer, endometriosis, uterine fibroids, and breast cancer. *Endocr Rev* 2013;34:130–62.
Kimura F, Watanabe J, Hata H, Fujisawa T, Kamata Y, Nishimura Y, Jobo T, Kuramoto H. PTEN immunohistochemical expression is suppressed in G1 endometrioid adenocarcinoma of the uterine corpus. *J Cancer Res Clin Oncol* 2004;130:161–168.
Kimura T, Kamiura S, Yamamoto T, Seino-Noda H, Ohira H, Saji F. Abnormal uterine bleeding and prognosis of endometrial cancer. *Int J Gynaecol Obstet* 2004;85:145–50.
King A. Uterine leukocytes and decidualization. *Hum Reprod Update* 2000;6:28–36.
Kitson SJ, Lindsay J, Sivalingam VN, Lunt M, Ryan NAJ, Edmondson RJ, Rutter MK, Crosbie EJ. The unrecognized burden of cardiovascular risk factors in women newly diagnosed with endometrial cancer: A prospective case control study. *Gynecol Oncol* 2018;148:154–160.
Klinge CM. Estrogen receptor interaction with estrogen response elements. *Nucleic Acids Res* 2001;29:2905–19.
Koch WH. Technology platforms for pharmacogenomic diagnostic assays. *Nat Rev Drug Discov* 2004;3:749–761.
Komm BS, Mirkin S. An overview of current and emerging SERMs. *J Steroid Biochem Mol Biol* 2014;143:207–222.
Korch C, Spillman MA, Jackson TA, Jacobsen BM, Murphy SK, Lessey BA, Jordan VC, Bradford AP. DNA profiling analysis of endometrial and ovarian cell lines reveals misidentification, redundancy and contamination. *Gynecol Oncol* 2012;127:241–8.
Kurman R, Carcangiu M, Herrington C, Young R. *WHO Classification of Tumours of Female Reproductive Organs*. 4th Edition. Lyon: IARC, 2014.
Kurman RJ, Kaminski PF, Norris HJ. *The behavior of endometrial hyperplasia. A long-term study of "untreated" hyperplasia in 170 patients.* Cancer 56 , 403–412 (1985).
Kurnit KC, Kim GN, Fellman BM, Urbauer DL, Mills GB, Zhang W, Broaddus RR. CTNNB1 (beta-catenin) mutation identifies low grade, early stage endometrial cancer patients at increased risk of recurrence. *Mod Pathol* 2017;30:1032–1041.
Kwan S-Y, Cheng X, Tsang YTM, Choi J-S, Kwan S-Y, Izaguirre DI, Kwan H-S, Gershenson DM, Wong K-K. Loss of ARID1A expression leads to sensitivity to ROS-inducing agent elesclomol in gynecologic cancer cells. *Oncotarget* 2016;7:56933–56943.
Lacey J V., Chia VM. Endometrial hyperplasia and the risk of progression to carcinoma. *Maturitas* 2009;63:39–44.
Lacey J V, Ioffe OB, Ronnett BM, Rush BB, Richesson DA, Chatterjee N, Langholz B, Glass AG, Sherman ME. Endometrial carcinoma risk among women diagnosed with endometrial hyperplasia: the 34-year experience in a large health plan. *Br J Cancer*

2008;98:45–53.
Lacey J V, Mutter GL, Nucci MR, Ronnett BM, Ioffe OB, Rush BB, Glass AG, Richesson DA, Chatterjee N, Langholz B, *et al.* Risk of subsequent endometrial carcinoma associated with endometrial intraepithelial neoplasia classification of endometrial biopsies. *Cancer* 2008;113:2073–81.
Lane DP. Cancer. p53, guardian of the genome. *Nature* 1992;358:15–6.
Latta E, Chapman WB. PTEN mutations and evolving concepts in endometrial neoplasia. *Curr Opin Obstet Gynecol* 2002;14:59–65.
Lee H, Choi HJ, Kang CS, Lee HJ, Lee WS, Park CS. Expression of miRNAs and PTEN in endometrial specimens ranging from histologically normal to hyperplasia and endometrial adenocarcinoma. *Mod Pathol* 2012;25:1508–1515.
Lessey BA, Ilesanmi AO, Castelbaum AJ, Yuan L, Somkuti SG, Chwalisz K, Satyaswaroop PG. Characterization of the functional progesterone receptor in an endometrial adenocarcinoma cell line (Ishikawa): progesterone-induced expression of the alpha1 integrin. *J Steroid Biochem Mol Biol* 1996;59:31–9.
Levin ER. Nuclear receptor versus plasma membrane oestrogen receptor. *Novartis Found Symp* 2000;230:41-50; discussion 50–5.
Lewin SN, Herzog TJ, Barrena Medel NI, Deutsch I, Burke WM, Sun X, Wright JD. Comparative performance of the 2009 international Federation of gynecology and obstetrics' staging system for uterine corpus cancer. *Obstet Gynecol* 2010;116:1141–9.
Lewis-Wambi JS, Jordan VC. Estrogen regulation of apoptosis: how can one hormone stimulate and inhibit? *Breast Cancer Res* 2009;11:206.
Li D, Li H, Wang Y, Eldomany A, Wu J, Yuan C, Xue J, Shi J, Jia Y, Ha C, *et al.* Development and characterization of a polarized human endometrial cell epithelia in an air–liquid interface state. *Stem Cell Res Ther* 2018;9:209.
Li Q, Kannan A, DeMayo FJ, Lydon JP, Cooke PS, Yamagishi H, Srivastava D, Bagchi MK, Bagchi IC. The antiproliferative action of progesterone in uterine epithelium is mediated by Hand2. *Science* 2011;331:912–916.
Liang H, Cheung LWT, Li J, Ju Z, Yu S, Stemke-Hale K, Dogruluk T, Lu Y, Liu X, Gu C, *et al.* Whole-exome sequencing combined with functional genomics reveals novel candidate driver cancer genes in endometrial cancer. *Genome Res* 2012;22:2120–9.
Lidor A, Ismajovich B, Confino E, David MP. Histopathological findings in 226 women with post-menopausal uterine bleeding. *Acta Obstet Gynecol Scand* 1986;65:41–3.
Lindahl B, Willén R. Endometrial hyperplasia following estrogen treatment without the addition of gestagen. A follow-up study after withdrawal of estrogens. *Anticancer Res* 1994;11:2071–3.
Lindor NM, Petersen GM, Hadley DW, Kinney AY, Miesfeldt S, Lu KH, Lynch P, Burke W, Press N. Recommendations for the care of individuals with an inherited predisposition to Lynch syndrome: a systematic review. *JAMA* 2006;296:1507–17.
Liu CL, Prapong W, Natkunam Y, Alizadeh A, Montgomery K, Gilks CB, van de Rijn M. Software tools for high-throughput analysis and archiving of immunohistochemistry staining data obtained with tissue microarrays. *Am J Pathol* 2002;161:1557–65.
Lonard DM, O'Malley BW. Molecular Pathways: Targeting Steroid Receptor Coactivators in Cancer. *Clin Cancer Res* 2016;22:5403–5407.
Lucas E, Chen H, Molberg K, Castrillon DH, Rivera Colon G, Li L, Hinson S, Thibodeaux J, Lea J, Miller DS, *et al.* Mismatch Repair Protein Expression in Endometrioid Intraepithelial Neoplasia/Atypical Hyperplasia: Should We Screen for Lynch Syndrome in Precancerous Lesions? *Int J Gynecol Pathol* 2018.
Luo J, Beresford S, Chen C, Chlebowski R, Garcia L, Kuller L, Regier M, Wactawski-Wende J, Margolis KL. Association between diabetes, diabetes treatment and risk of developing endometrial cancer. *Br J Cancer* 2014;111:1432–1439.
Mackenzie R, Talhouk A, Eshragh S, Lau S, Cheung D, Chow C, Le N, Cook LS, Wilkinson

N, McDermott J, *et al.* Morphologic and Molecular Characteristics of Mixed Epithelial Ovarian Cancers. *Am J Surg Pathol* 2015;39:1548–57.

Mackintosh ML, Crosbie EJ. Obesity-driven endometrial cancer: is weight loss the answer? *BJOG* 2013;120:791–4.

MacKintosh ML, Crosbie EJ. Prevention Strategies in Endometrial Carcinoma. *Curr Oncol Rep* 2018;20:101.

MacKintosh ML, Derbyshire AE, McVey RJ, Bolton J, Nickkho-Amiry M, Higgins CL, Kamieniorz M, Pemberton PW, Kirmani BH, Ahmed B, *et al.* The impact of obesity and bariatric surgery on circulating and tissue biomarkers of endometrial cancer risk. *Int J cancer* 2019;144:641–650.

Mansouri A, Stoykova A, Gruss P. Pax genes in development. *J Cell Sci Suppl* 1994;18:35–42.

Mao T-L, Ardighieri L, Ayhan A, Kuo K-T, Wu C-H, Wang T-L, Shih I-M. Loss of ARID1A expression correlates with stages of tumor progression in uterine endometrioid carcinoma. *Am J Surg Pathol* 2013;37:1342–8.

Mao T-L, Shih I-M. The roles of ARID1A in gynecologic cancer. *J Gynecol Oncol* 2013;24:376–81.

Matias-Guiu X, Prat J. Molecular pathology of endometrial carcinoma. *Histopathology* 2013;62:111–123.

Maybin JA, Critchley HOD. Menstrual physiology: implications for endometrial pathology and beyond. *Hum Reprod Update* 2015;21:748–61.

McCloskey C, Rada C, Bailey E, McCavera S, van den Berg HA, Atia J, Rand DA, Shmygol A, Chan Y-W, Quenby S, *et al.* The inwardly rectifying K+ channel KIR7.1 controls uterine excitability throughout pregnancy. *EMBO Mol Med* 2014;6:1161–1174.

McCluggage WG, Sumathi VP, Maxwell P. CD10 is a sensitive and diagnostically useful immunohistochemical marker of normal endometrial stroma and of endometrial stromal neoplasms. *Histopathology* 2001;39:273–8.

McConechy MK, Ding J, Cheang MC, Wiegand K, Senz J, Tone A, Yang W, Prentice L, Tse K, Zeng T, *et al.* Use of mutation profiles to refine the classification of endometrial carcinomas. *J Pathol* 2012;228:20–30.

McKinlay SM, Brambilla DJ, Posner JG. The normal menopause transition. *Maturitas* 1992;14:103–15.

Meng B, Hoang LN, McIntyre JB, Duggan M a., Nelson GS, Lee CH, Köbel M. POLE exonuclease domain mutation predicts long progression-free survival in grade 3 endometrioid carcinoma of the endometrium. *Gynecol Oncol* 2014;134:15–19.

Moley KH, Colditz GA. Effects of obesity on hormonally driven cancer in women. *Sci Transl Med* 2016;8:323ps3.

Monte NM, Webster KA, Neuberg D, Dressler GR, Mutter GL. Joint loss of PAX2 and PTEN expression in endometrial precancers and cancer. *Cancer Res* 2010;70:6225–32.

Montgomery E. Is There a Way for Pathologists to Decrease Interobserver Variability in the Diagnosis of Dysplasia? *Arch Pathol Lab Med* 2005;129:174–176.

Montz FJ, Bristow RE, Bovicelli A, Tomacruz R, Kurman RJ. Intrauterine progesterone treatment of early endometrial cancer. *Am J Obstet Gynecol* 2002;186:651–7.

Mourits MJ, De Vries EG, Willemse PH, Ten Hoor KA, Hollema H, Van der Zee AG. Tamoxifen treatment and gynecologic side effects: a review. *Obstet Gynecol* 2001;97:855–66.

Muller PAJ, Vousden KH. p53 mutations in cancer. *Nat Cell Biol* 2013;15:2.

Munro MG, Critchley HOD, Broder MS, Fraser IS, FIGO Working Group on Menstrual Disorders. FIGO classification system (PALM-COEIN) for causes of abnormal uterine bleeding in nongravid women of reproductive age. *Int J Gynaecol Obstet* 2011;113:3–13.

Munson L, Wilkinson JE, Schlafer DH. Effects of substrata on the polarization of bovine

endometrial epithelial cells in vitro. *Cell Tissue Res* 1990;261:155–161.
Murali R, Soslow RA, Weigelt B. Classification of endometrial carcinoma: more than two types. *Lancet Oncol* 2014;15:e268-78.
Mutter GL. Endometrial intraepithelial neoplasia (EIN): will it bring order to chaos? The Endometrial Collaborative Group. *Gynecol Oncol* 2000;76:287–290.
Mutter GL. Histopathology of genetically defined endometrial precancers. *Int J Gynecol Pathol* 2000;19:301–9.
Mutter GL. Endometrial Precancers : The Benign Endometrial Hyperplasia Sequence and EIN. *Pathology* 2008:1–22.
Mutter GL, Baak JPA, Crum CP, Richart RM, Ferenczy A, Faquin WC. Endometrial precancer diagnosis by histopathology, clonal analysis, and computerized morphometry. *J Pathol* 2000;190:462–469.
Mutter GL, Boynton KA, Faquin WC, Ruiz RE, Jovanovic AS. Allelotype mapping of unstable microsatellites establishes direct lineage continuity between endometrial precancers and cancer. *Cancer Res* 1996;56:4483–4486.
Mutter GL, Ince T a., Baak JP a, Kust G a., Zhou XP, Eng C. Molecular identification of latent precancers in histologically normal endometrium. *Cancer Res* 2001;61:4311–4314.
Mutter GL, Kauderer J, Baak JPA, Alberts D. Biopsy histomorphometry predicts uterine myoinvasion by endometrial carcinoma: a Gynecologic Oncology Group study. *Hum Pathol* 2008;39:866–874.
Mutter GL, Lin MC, Fitzgerald JT, Kum JB, Baak JP, Lees JA, Weng LP, Eng C. Altered PTEN expression as a diagnostic marker for the earliest endometrial precancers. *J Natl Cancer Inst* 2000;92:924–30.
Mutter GL, Lin MC, Fitzgerald JT, Kum JB, Eng C. Changes in endometrial PTEN expression throughout the human menstrual cycle. *J Clin Endocrinol Metab* 2000;85:2334–8.
Mutter GL, Monte NM, Neuberg D, Ferenczy A, Eng C. Emergence, involution, and progression to carcinoma of mutant clones in normal endometrial tissues. *Cancer Res* 2014;74:2796–802.
Mutter GL, Zaino RJ, Baak JPA, Bentley RC, Robboy SJ. Benign endometrial hyperplasia sequence and endometrial intraepithelial neoplasia. *Int J Gynecol Pathol* 2007;26:103–14.
Nieminen TT, Gylling A, Abdel-Rahman WM, Nuorva K, Aarnio M, Renkonen-Sinisalo L, Järvinen HJ, Mecklin J-P, Bützow R, Peltomäki P. Molecular Analysis of Endometrial Tumorigenesis: Importance of Complex Hyperplasia Regardless of Atypia. *Clin Cancer Res* 2009;15:5772 LP-5783.
Nilsson S, Mäkelä S, Treuter E, Tujague M, Thomsen J, Andersson G, Enmark E, Pettersson K, Warner M, Gustafsson JA. Mechanisms of estrogen action. *Physiol Rev* 2001;81:1535–65.
Nishida M. The Ishikawa cells from birth to the present. *Hum Cell* 2002;15:104–17.
Nishida M, Kasahara K, Kaneko M, Iwasaki H, Hayashi K. Establishment of a new human endometrial adenocarcinoma cell line, Ishikawa cells, containing estrogen and progesterone receptors. *Nihon Sanka Fujinka Gakkai Zasshi* 1985;37:1103–11.
Noyes RW, Hertig AT, Rock J. Dating the endometrial biopsy. *Am J Obstet Gynecol* 1975;122:262–3. Available at: http://www.ncbi.nlm.nih.gov/pubmed/1155504.
Ørbo A, Arnes M, Lyså LM, Straume B. Expression of PAX2 and PTEN Correlates to Therapy Response in Endometrial Hyperplasia. *Anticancer Res* 2015;35:6401–9.
Orbo A, Baak J, Kleivan I, Lysne S, Prytz P, Broeckaert M, Slappendel A, Tichelaar H. Computerised morphometrical analysis in endometrial hyperplasia for the prediction of cancer development. A long term retrospective study from northern Norway. *J Clin Pathol* 2000;53:697–703.
Orbo A, Nilsen MN, Arnes MS, Pettersen I, Larsen K. Loss of expression of MLH1, MSH2, MSH6, and PTEN related to endometrial cancer in 68 patients with endometrial

hyperplasia. *Int J Gynecol Pathol* 2003;22:141–8.
Ordi J, Bergeron C, Hardisson D, Mccluggage WG, Hollema H, Felix A, Soslow RA, Oliva E, Tavassoli FA, Alvarado-Cabrero I, *et al.* Reproducibility of current classifications of endometrial endometrioid glandular proliferations: Further evidence supporting a simplified classification. *Histopathology* 2014;64:284–292.
Owings R a., Quick CM. Endometrial Intraepithelial Neoplasia. *Arch Pathol Lab Med* 2014;138:484–491.
Ozkara SK, Corakci A. Significantly decreased P27 expression in endometrial carcinoma compared to complex hyperplasia with atypia (correlation with p53 expression). *Pathol Oncol Res* 2004;10:89–97.
Parkin DM, Boyd L. Cancers attributable to overweight and obesity in the UK in 2010. *Br J Cancer* 2011;105:S34–S37.
Pavlakis K, Messini I, Vrekoussis T, Panoskaltsis T, Chrissanthakis D, Yiannou P, Stathopoulos EN. PTEN-loss and nuclear atypia of EIN in endometrial biopsies can predict the existence of a concurrent endometrial carcinoma. *Gynecol Oncol* 2010;119:516–9.
Pernick N. Atrophy. 2017. Available at: http://www.pathologyoutlines.com/topic/uterusatrophy.html.
Poliseno L, Salmena L, Zhang J, Carver B, Haveman WJ, Pandolfi PP. A coding-independent function of gene and pseudogene mRNAs regulates tumour biology. *Nature* 2010;465:1033–8.
Poulogiannis G, Frayling IM, Arends MJ. DNA mismatch repair deficiency in sporadic colorectal cancer and Lynch syndrome. *Histopathology* 2010;56:167–79.
Qu W, Zhao Y, Wang X, Qi Y, Zhou C, Hua Y, Hou J, Jiang S-W. Culture characters, genetic background, estrogen/progesterone receptor expression, and tumorigenic activities of frequently used sixteen endometrial cancer cell lines. *Clin Chim Acta* 2019;489:225–232.
Quick CM, Laury AR, Monte NM, Mutter GL. Utility of PAX2 as a marker for diagnosis of endometrial intraepithelial neoplasia. *Am J Clin Pathol* 2012;138:678–84.
Raam S, Richardson GS, Bradley F, MacLaughlin D, Sun L, Frankel F, Cohen JL. Translocation of cytoplasmic estrogen receptors to the nucleus: Immunohistochemical demonstration utilizing rabbit antibodies to estrogen receptors of mammary carcinomas. *Breast Cancer Res Treat* 1983;3:179–199.
Raffone A, Travaglino A, Saccone G, Campanino MR, Mollo A, De Placido G, Insabato L, Zullo F. Loss of PTEN expression as diagnostic marker of endometrial precancer: A systematic review and meta-analysis. *Acta Obstet Gynecol Scand* 2019;98:275–286.
Raffone A, Travaglino A, Saccone G, Mascolo M, Insabato L, Mollo A, De Placido G, Zullo F. PAX2 in endometrial carcinogenesis and in differential diagnosis of endometrial hyperplasia: A systematic review and meta-analysis of diagnostic accuracy. *Acta Obstet Gynecol Scand* 2019;98:287–299.
Randall TC, Kurman RJ. Progestin treatment of atypical hyperplasia and well-differentiated carcinoma of the endometrium in women under age 40. *Obstet Gynecol* 1997;90:434–40.
Reed SD, Voigt LF, Newton KM, Garcia RH, Allison HK, Epplein M, Jordan D, Swisher E, Weiss NS. Progestin therapy of complex endometrial hyperplasia with and without atypia. *Obstet Gynecol* 2009;113:655–62.
Renehan AG, Soerjomataram I, Tyson M, Egger M, Zwahlen M, Coebergh JW, Buchan I. Incident cancer burden attributable to excess body mass index in 30 European countries. *Int J Cancer* 2010;126:692–702.
Rewcastle E, Varhaugvik AE, Gudlaugsson E, Steinbakk A, Skaland I, van Diermen B, Baak JP, Janssen EAM. Assessing the prognostic value of PAX2 and PTEN in endometrial carcinogenesis. *Endocr Relat Cancer* 2018;25:981–991.

Rex C, Bentley SJ. Exogenous hormones and their effects on the endometrium. In: *Robboy's Pathology of the Female Reproductive Tract*. 2nd Editio. Elsevir Health Sciences, 2009, 325–342.

Richardson GS, Dickersin GR, Atkins L, MacLaughlin DT, Raam S, Merk LP, Bradley FM. KLE: A cell line with defective estrogen receptor derived from undifferentiated endometrial cancer. *Gynecol Oncol* 1984;17:213–230.

Robson EJD, He S-J, Eccles MR. A PANorama of PAX genes in cancer and development. *Nat Rev Cancer* 2006;6:52–62.

Roche Molecular Systems. Universal ProbeLibrary Assay Design Center. 2017.

Rochon M-H, Fradette J, Fortin V, Tomasetig F, Roberge CJ, Baker K, Berthod F, Auger FA, Germain L. Normal Human Epithelial Cells Regulate the Size and Morphology of Tissue-Engineered Capillaries. *Tissue Eng Part A* 2010;16:1457–1468.

Rogers PAW. Structure and function of endometrial blood vessels. *Hum Reprod Update* 1996;2:57–62.

Ryan G, Steele-Perkins V, Morris JF, Rauscher FJ, Dressler GR. Repression of Pax-2 by WT1 during normal kidney development. *Development* 1995;121:867–875.

Saito Y, Swanson X, Mhashilkar AM, Oida Y, Schrock R, Branch CD, Chada S, Zumstein L, Ramesh R. Adenovirus-mediated transfer of the PTEN gene inhibits human colorectal cancer growth in vitro and in vivo. *Gene Ther* 2003;10:1961–9.

Sakamoto T, Eguchi H, Omoto Y, Ayabe T, Mori H, Hayashi S. Estrogen receptor-mediated effects of tamoxifen on human endometrial cancer cells. *Mol Cell Endocrinol* 2002;192:93–104.

Salman MC, Usubutun A, Boynukalin K, Yuce K. Comparison of WHO and endometrial intraepithelial neoplasia classifications in predicting the presence of coexistent malignancy in endometrial hyperplasia. *J Gynecol Oncol* 2010;21:97–101.

Sanderson PA, Critchley HOD, Williams ARW, Arends MJ, Saunders PTK. New concepts for an old problem: the diagnosis of endometrial hyperplasia. *Hum Reprod Update* 2017;23:232–254.

Sansal I, Sellers WR. The biology and clinical relevance of the PTEN tumor suppressor pathway. *J Clin Oncol* 2004;22:2954–63.

Sargent A, Fletcher S, Bray K, et al Cross-sectional study of HPV testing in self-sampled urine and comparison with matched vaginal and cervical samples in women attending colposcopy for the management of abnormal cervical screening BMJ Open 2019;9:e025388.

Sarmadi S, Izadi-Mood N, Sotoudeh K, Tavangar S. Altered PTEN expression; a diagnostic marker for differentiating normal, hyperplastic and neoplastic endometrium. *Diagn Pathol* 2009;4:41.

Schultheis AM, Martelotto LG, De Filippo MR, Piscuglio S, Ng CKY, Hussein YR, Reis-Filho JS, Soslow RA, Weigelt B. TP53 Mutational Spectrum in Endometrioid and Serous Endometrial Cancers. *Int J Gynecol Pathol* 2016;35:289–300.

Scully R, Bonfiglio T, Kurman R, Silverberg S, Wilkinson E. Histologic typing of female genital tract tumors. In: *International Histological Classification of Tumours*. 2nd Editio. New Yorl: Springer, 1994, 1–189.

Seebacher V, Schmid M, Polterauer S, Hefler-Frischmuth K, Leipold H, Concin N, Reinthaller A, Hefler L. The presence of postmenopausal bleeding as prognostic parameter in patients with endometrial cancer: a retrospective multi-center study. *BMC Cancer* 2009;9:460.

Semere LG, Ko E, Johnson NR, Vitonis AF, Phang LJ, Cramer DW, Mutter GL. Endometrial intraepithelial neoplasia: clinical correlates and outcomes. *Obstet Gynecol* 2011;118:21–8.

Setiawan VW, Pike MC, Kolonel LN, Nomura AM, Goodman MT, Henderson BE. Racial/ethnic differences in endometrial cancer risk: the multiethnic cohort study. *Am J*

Epidemiol 2007;165:262–70.
Shang Y. Hormones and cancer. *Cell Res* 2007;17:277–279.
Sherman AI, Brown S. The precursors of endometrial carcinoma. *Am J Obstet Gynecol* 1979;135:947–56.
Sherman BM, Korenman SG. Hormonal characteristics of the human menstrual cycle throughout reproductive life. *J Clin Invest* 1975;55:699–706.
Sherman ME, Bur ME, Kurman RJ. p53 in endometrial cancer and its putative precursors: Evidence for diverse pathways of tumorigenesis. *Hum Pathol* 1995;26:1268–1274.
Sikora MJ, Johnson MD, Lee A V., Oesterreich S. Endocrine response phenotypes are altered by charcoal-stripped serum variability. *Endocrinology* 2016;157:3760–3766.
Silva A, Yunes JA, Cardoso BA, Martins LR, Jotta PY, Abecasis M, Nowill AE, Leslie NR, Cardoso AA, Barata JT. PTEN posttranslational inactivation and hyperactivation of the PI3K/Akt pathway sustain primary T cell leukemia viability. *J Clin Invest* 2008;118:3762–74.
Simoncini T, Hafezi-Moghadam A, Brazil DP, Ley K, Chin WW, Liao JK. Interaction of oestrogen receptor with the regulatory subunit of phosphatidylinositol-3-OH kinase. *Nature* 2000;407:538–41.
Simpkins SB, Bocker T, Swisher EM, Mutch DG, Gersell DJ, Kovatich AJ, Palazzo JP, Fishel R, Goodfellow PJ. MLH1 promoter methylation and gene silencing is the primary cause of microsatellite instability in sporadic endometrial cancers. *Hum Mol Genet* 1999;8:661–666.
Simpson ER. Sources of estrogen and their importance. *J Steroid Biochem Mol Biol* 2003;86:225–30.
Skov BG, Broholm H, Engel U, Franzmann MB, Nielsen AL, Lauritzen AF, Skov T. Comparison of the reproducibility of the WHO classifications of 1975 and 1994 of endometrial hyperplasia. *Int J Gynecol Pathol* 1997;16:33–7.
Slomovitz BM, Coleman RL. The PI3K/AKT/mTOR pathway as a therapeutic target in endometrial cancer. *Clin Cancer Res* 2012;18:5856–64.
Soong R, Robbins PD, Dix BR, Grieu F, Lim B, Knowles S, Williams KE, Turbett GR, House AK, Iacopetta BJ. Concordance between p53 protein overexpression and gene mutation in a large series of common human carcinomas. *Hum Pathol* 1996;27:1050–1055.
Spencer CP, Whitehead MI. Endometrial assessment re-visited. *Br J Obstet Gynaecol* 1999;106:623–32.
Stambolic V, Suzuki A, de la Pompa JL, Brothers GM, Mirtsos C, Sasaki T, Ruland J, Penninger JM, Siderovski DP, Mak TW. Negative regulation of PKB/Akt-dependent cell survival by the tumor suppressor PTEN. *Cell* 1998;95:29–39.
Stambolic V, Tsao MS, Macpherson D, Suzuki A, Chapman WB, Mak TW. High incidence of breast and endometrial neoplasia resembling human Cowden syndrome in pten(+/-) mice. *Cancer Res* 2000;60:3605–3611.
Stauffer SR, Coletta CJ, Tedesco R, Nishiguchi G, Carlson K, Sun J, Katzenellenbogen BS, Katzenellenbogen J a. Pyrazole ligands: structure-affinity/activity relationships and estrogen receptor-alpha-selective agonists. *J Med Chem* 2000;43:4934–4947.
Steinbakk A, Malpica A, Slewa A, Gudlaugsson E, Janssen EAM, Arends M, Kruse AJ, Yinhua Y, Feng W, Baak JP. High frequency microsatellite instability has a prognostic value in endometrial endometrioid adenocarcinoma, but only in FIGO stage 1 cases. *Cell Oncol (Dordr)* 2011;34:457–65.
Steinbakk A, Malpica A, Slewa A, Skaland I, Gudlaugsson E, Janssen EAM, Løvslett K, Fiane B, Kruse AJ, Feng W, *et al.* Biomarkers and microsatellite instability analysis of curettings can predict the behavior of FIGO stage I endometrial endometrioid adenocarcinoma. *Mod Pathol* 2011;24:1262–71.
Stevens VL, Jacobs EJ, Patel A V., Sun J, Gapstur SM, McCullough ML. Body weight in early adulthood, adult weight gain, and risk of endometrial cancer in women not using

postmenopausal hormones. *Cancer Causes Control* 2014;25:321–328.
Stocco C, Telleria C, Gibori G. The molecular control of corpus luteum formation, function, and regression. *Endocr Rev* 2007;28:117–49.
Sun H, Enomoto T, Fujita M, Wada H, Yoshino K, Ozaki K, Nakamura T, Murata Y. Mutational Analysis of the PTEN Gene in Endometrial Carcinoma and Hyperplasia. *Am J Clin Pathol* 2001;115:32–38.
Sun H, Enomoto T, Shroyer KR, Ozaki K, Fujita M, Ueda Y, Nakashima R, Kuragaki C, Ueda G, Murata Y. Clonal analysis and mutations in the PTEN and the K-ras genes in endometrial hyperplasia. *Diagnostic Mol Pathol* 2002;11:204–211.
Sun J, Huang YR, Harrington WR, Sheng S, Katzenellenbogen JA, Katzenellenbogen BS. Antagonists selective for estrogen receptor alpha. *Endocrinology* 2002;143:941–7.
Sun M, Paciga JE, Feldman RI, Yuan Z, Coppola D, Lu YY, Shelley SA, Nicosia S V, Cheng JQ. Phosphatidylinositol-3-OH Kinase (PI3K)/AKT2, activated in breast cancer, regulates and is induced by estrogen receptor alpha (ERalpha) via interaction between ERalpha and PI3K. *Cancer Res* 2001;61:5985–91.
Sundar S, Balega J, Crosbie E, Drake A, Edmondson R, Fotopoulou C, Gallos I, Ganesan R, Gupta J, Johnson N, *et al.* BGCS uterine cancer guidelines: Recommendations for practice. *Eur J Obstet Gynecol Reprod Biol* 2017;213:71–97.
Szekely GJ, Rizzo ML. Hierarchical Clustering via Joint Between-Within Distances: Extending Ward's Minimum Variance Method. *J Classif* 2005;22:151–183.
Tabata T, Yamawaki T, Yabana T, Ida M, Nishimura K, Nose Y. Natural history of endometrial hyperplasia. Study of 77 patients. *Arch Gynecol Obstet* 2001;265:85–8.
Takeda T, Banno K, Okawa R, Yanokura M, Iijima M, Irie-Kunitomi H, Nakamura K, Iida M, Adachi M, Umene K, *et al.* ARID1A gene mutation in ovarian and endometrial cancers (Review). *Oncol Rep* 2016;35:607–13.
Talhouk A, McConechy MK, Leung S, Li-Chang HH, Kwon JS, Melnyk N, Yang W, Senz J, Boyd N, Karnezis a N, *et al.* A clinically applicable molecular-based classification for endometrial cancers. *Br J Cancer* 2015;113:299–310.
Terakawa N, Kigawa J, Taketani Y, Yoshikawa H, Yajima a, Noda K, Okada H, Kato J, Yakushiji M, Tanizawa O, *et al.* The behavior of endometrial hyperplasia: a prospective study. Endometrial Hyperplasia Study Group. *J Obstet Gynaecol Res* 1997;23:223–30.
Terunuma A, Limgala RP, Park CJ, Choudhary I, Vogel JC. Efficient procurement of epithelial stem cells from human tissue specimens using a Rho-associated protein kinase inhibitor Y-27632. *Tissue Eng Part A* 2010;16:1363–1368.
The Scottish Government. Ethnic Group Demographics - 2011 Census. *People Soc Demogr* 2011. Available at: https://www2.gov.scot/Topics/People/Equality/Equalities/DataGrid/Ethnicity/EthPopMig. Accessed January 27, 2019.
Toki T, Shimizu M, Takagi Y, Ashida T, Konishi I. CD10 is a marker for normal and neoplastic endometrial stromal cells. *Int J Gynecol Pathol* 2002;21:41–7.
Tong G-X, Melamed J, Mansukhani M, Memeo L, Hernandez O, Deng F-M, Chiriboga L, Waisman J. PAX2: a reliable marker for nephrogenic adenoma. *Mod Pathol* 2006;19:356–63.
Tornehave D, Hougaard DM, Larsson L. Microwaving for double indirect immunofluorescence with primary antibodies from the same species and for staining of mouse tissues with mouse monoclonal antibodies. *Histochem Cell Biol* 2000;113:19–23.
Treloar AE, Boynton RE, Behn BG, Brown BW. Variation of the human menstrual cycle through reproductive life. *Int J Fertil* 1967;12:77–126.
Trimble CL, Kauderer J, Zaino R, Silverberg S, Lim PC, Burke JJ, Alberts D, Curtin J, Mackey D. Concurrent endometrial carcinoma in women with a biopsy diagnosis of atypical endometrial hyperplasia. *Cancer* 2006;106:812–819.
Trimble CL, Method M, Leitao M, Lu K, Ioffe O, Hampton M, Higgins R, Zaino R, Mutter

GL, Society of Gynecologic Oncology Clinical Practice Committee. Management of Endometrial Precancers. *Obstet Gynecol* 2012;120:1160–1175.

Turco MY, Gardner L, Hughes J, Cindrova-Davies T, Gomez MJ, Farrell L, Hollinshead M, Marsh SGE, Brosens JJ, Critchley HO, *et al.* Long-term, hormone-responsive organoid cultures of human endometrium in a chemically defined medium. *Nat Cell Biol* 2017;19:568–577.

Turner KJ, Macpherson S, Millar MR, McNeilly AS, Williams K, Cranfield M, Groome NP, Sharpe RM, Fraser HM, Saunders PTK. Development and validation of a new monoclonal antibody to mammalian aromatase. *J Endocrinol* 2002;172:21–30.

Upson K, Allison KH, Reed SD, Jordan CD, Newton KM, Swisher EM, Doherty J a., Garcia RL. Biomarkers of progestin therapy resistance and endometrial hyperplasia progression. *Am J Obstet Gynecol* 2012;207:36.e1-36.e8.

UpToDate inc. The menstrual cycle. 2019:Graphic 62189 Version 4.0. Available at: https://www-uptodate-com.ezproxy.is.ed.ac.uk/contents/image?imageKey=ENDO%2F62189&topicKey=ENDO%2F7418&search=menstrual cycle&source=outline_link&selectedTitle=1~150. Accessed January 16, 2018.

Usubutun A, Mutter GL, Saglam A, Dolgun A, Ozkan EA, Ince T, Akyol A, Bulbul HD, Calay Z, Eren F, *et al.* Reproducibility of endometrial intraepithelial neoplasia diagnosis is good, but influenced by the diagnostic style of pathologists. *Mod Pathol* 2012;25:877–884.

Valentijn AJJ, Palial K, Al-Lamee H, Tempest N, Drury J, Von Zglinicki T, Saretzki G, Murray P, Gargett CEE, Hapangama DKK. SSEA-1 isolates human endometrial basal glandular epithelial cells: phenotypic and functional characterization and implications in the pathogenesis of endometriosis. *Hum Reprod* 2013;28:2695–2708.

VanDusen NJ, Casanovas J, Vincentz JW, Firulli BA, Osterwalder M, Lopez-Rios J, Zeller R, Zhou B, Grego-Bessa J, De La Pompa JL, *et al.* Hand2 Is an Essential Regulator for Two Notch-Dependent Functions within the Embryonic Endocardium. *Cell Rep* 2014;9:2071–2083.

Vilar E, Gruber SB. Microsatellite instability in colorectal cancer—the stable evidence. *Nat Rev Clin Oncol* 2010;7:153–162.

Vilgelm A, Lian Z, Wang H, Beauparlant SL, Klein-Szanto A, Ellenson LH, Di Cristofano A. Akt-mediated phosphorylation and activation of estrogen receptor alpha is required for endometrial neoplastic transformation in Pten+/- mice. *Cancer Res* 2006;66:3375–80.

Vineis P, Schatzkin A, Potter JD. Models of carcinogenesis: an overview. *Carcinogenesis* 2010;31:1703–9.

Voss MA, Ganesan R, Ludeman L, McCarthy K, Gornall R, Schaller G, Wei W, Sundar S. Should grade 3 endometrioid endometrial carcinoma be considered a type 2 cancer—A clinical and pathological evaluation. *Gynecol Oncol* 2012;124:15–20.

Wakeling AE, Dukes M, Bowler J. A potent specific pure antiestrogen with clinical potential. *Cancer Res* 1991;51:3867–73.

Wan YL, Beverley-Stevenson R, Carlisle D, Clarke S, Edmondson RJ, Glover S, Holland J, Hughes C, Kitchener HC, Kitson S, *et al.* Working together to shape the endometrial cancer research agenda: The top ten unanswered research questions. *Gynecol Oncol* 2016;143:287–293.

Wang H, Pilla F, Anderson S, Martinez-Escribano S, Herrer I, Moreno-Moya JM, Musti S, Bocca S, Oehninger S, Horcajadas JA. A novel model of human implantation: 3D endometrium-like culture system to study attachment of human trophoblast (Jar) cell spheroids. *Mol Hum Reprod* 2012;18:33–43.

Watanabe K, Ueno M, Kamiya D, Nishiyama A, Matsumura M, Wataya T, Takahashi JB, Nishikawa SS, Nishikawa SS, Muguruma K, *et al.* A ROCK inhibitor permits survival of dissociated human embryonic stem cells. *Nat Biotechnol* 2007;25:681–6.

Webb P, Lopez GN, Greene GL, Baxter JD, Kushner PJ. The limits of the cellular capacity to mediate an estrogen response. *Mol Endocrinol* 1992;6:157–67.

Weber AM, Belinson JL, Piedmonte MR. Risk factors for endometrial hyperplasia and cancer among women with abnormal bleeding. *Obstet Gynecol* 1999;93:594–8.

Welshons W V., Wolf MF, Murphy CS, Jordan VC. Estrogenic activity of phenol red. *Mol Cell Endocrinol* 1988;57:169–178.

Werner HMJ, Berg A, Wik E, Birkeland E, Krakstad C, Kusonmano K, Petersen K, Kalland KH, Oyan AM, Akslen L a, *et al.* ARID1A loss is prevalent in endometrial hyperplasia with atypia and low-grade endometrioid carcinomas. *Mod Pathol* 2012;26:428–434.

Whitaker L, Critchley HOD. Abnormal uterine bleeding. *Best Pract Res Clin Obstet Gynaecol* 2016;34:54–65.

Whitehead MI, Lane G, Dyer G, Townsend PT, Collins WP, King RJ. Oestradiol: the predominant intranuclear oestrogen in the endometrium of oestrogen-treated postmenopausal women. *Br J Obstet Gynaecol* 1981;88:914–8.

Wiegand KC, Lee AF, Al-Agha OM, Chow C, Kalloger SE, Scott DW, Steidl C, Wiseman SM, Gascoyne RD, Gilks B, *et al.* Loss of BAF250a (ARID1A) is frequent in high-grade endometrial carcinomas. *J Pathol* 2011;224:328–33.

Wiegand KC, Shah SP, Al-Agha OM, Zhao Y, Tse K, Zeng T, Senz J, McConechy MK, Anglesio MS, Kalloger SE, *et al.* ARID1A mutations in endometriosis-associated ovarian carcinomas. *N Engl J Med* 2010;363:1532–43.

Wiencke JK, Zheng S, Jelluma N, Tihan T, Vandenberg S, Tamgüney T, Baumber R, Parsons R, Lamborn KR, Berger MS, *et al.* Methylation of the PTEN promoter defines low-grade gliomas and secondary glioblastoma. *Neuro Oncol* 2007;9:271–9.

Wise MR, Jordan V, Lagas A, Showell M, Wong N, Lensen S, Farquhar CM. Obesity and endometrial hyperplasia and cancer in premenopausal women: A systematic review. *Am J Obstet Gynecol* 2016;214:689.e1-689.e17.

Woo YL, Cheah PL, Shahruddin SI, Omar SZ, Arends M. The immunohistochemistry signature of mismatch repair (MMR) proteins in a multiethnic Asian cohort with endometrial carcinoma. *Int J Gynecol Pathol* 2014;33:554–9.

Wu H, Chen Y, Liang J, Shi B, Wu G, Zhang Y, Wang D, Li R, Yi X, Zhang H, *et al.* Hypomethylation-linked activation of PAX2 mediates tamoxifen-stimulated endometrial carcinogenesis. *Nature* 2005;438:981–987.

Wu JN, Roberts CWM. ARID1A mutations in cancer: another epigenetic tumor suppressor? *Cancer Discov* 2013;3:35–43.

Xiong Y, Xiong YY, Zhou YF. Expression and significance of beta-catenin, Glut-1 and PTEN in proliferative endometrium, endometrial intraepithelial neoplasia and endometrioid adenocarcinoma. *Eur J Gynaecol Oncol* 2010;31:160–4.

Yamamoto S, Tsuda H, Takano M, Tamai S, Matsubara O. PIK3CA mutations and loss of ARID1A protein expression are early events in the development of cystic ovarian clear cell adenocarcinoma. *Virchows Arch* 2012;460:77–87.

Zaino R, Carinelli S, Ellenson L. Uterine corpus: epithelial tumors and precursors. In: Kurman RJ, Carcangiu ML, Herrington C, Young R (eds) *World Health Organisation Classification of Tumors of Female Reproductive Organs, 4th Edn*. 4th ed. Lyon, France: International Agency for Research on Cancer (IARC) Press, 2014, 125–135.

Zhang G, Hou X, Gao S. Stimulation of peroxisome proliferator-activated receptor γ inhibits estrogen receptor α transcriptional activity in endometrial carcinoma cells. *Oncol Rep* 2015;33:1227–1234.

Zheng W, Baker HE, Mutter GL. Involution of PTEN-null endometrial glands with progestin therapy. *Gynecol Oncol* 2004;92:1008–13.

Zhou J, Teng R, Xu C, Wang Q, Guo J, Xu C, Li Z, Xie S, Shen J, Wang L. Overexpression of ERα inhibits proliferation and invasion of MKN28 gastric cancer cells by suppressing β-catenin. *Oncol Rep* 2013;30:1622–1630.

8 Appendix 1

- Details of MRC-CIR archival endometrial hyperplasia tissue resources used for optimisation experiments.

Number	WHO94	WHO2014	Study number	Block number
1	Atypical hyperplasia	EIN	CA9/100	1999-1632
2	Complex atypical hyperplasia	Proliferative	CA73/02	2001-1562
3	Complex atypical hyperplasia	EIN	CA200	2006-1584
4	Complex atypical hyperplasia	EIN	CA52/01	2000-2690
5	Complex atypical hyperplasia	EC	CA55/01	2000-3080
6	Complex hyperplasia	EIN	CA264	2009-1956
7	Complex hyperplasia	EIN	CA264	2009-1957
8	Complex hyperplasia	EC	CA183	2005-2084
9	Complex hyperplasia	EIN	CA265	2009-1964
10	Complex hyperplasia	Cervix	CA265	2009-1965
11	Complex hyperplasia	EC	CA187	2006-111
12	Complex hyperplasia	EC	CA188	2006-112
13	Complex hyperplasia	EC	CA124	2003-2759
14	Hyperplasia with atypia	HwA	CA208	2006-3478
15	Hyperplasia with atypia	EIN	CA220	2007-1682
16	Hyperplasia with atypia	EC	CA204	2006-2724

9 Appendix 2

- Application form to South East Scotland HSS Bioresource
- Approval letter from South East Scotland HSS Bioresource

Appendix 2

SR465

REQUEST FOR ACCESS TO SOUTH EAST SCOTLAND HSS (formerly SAHSC) BIORESOURCE

This application form is for the purpose of making a request to collect, use and process tissue/data via the HSS (SAHSC) BioResource. The tissue/data must be utilised within the laboratory and by personnel that fall under the supervision of the Principal Investigator listed on the application. Any transfer of tissue/data to personnel or laboratories that are not under the supervision of the indicated PI requires the following:

- An explanation of the need to transfer the tissue/data and benefit to the investigator's research
- A copy of the enclosed BioResource agreement form signed by the collaborator

The South East Scotland HSS (SAHSC) BioResource does not supply tissue/data solely for distribution to third party researchers, those researchers should apply to the BioResource directly.

The requested information is necessary in order to document your request for permission to collect, or access tissue/data and to ensure that the South East Scotland HSS (SAHSC) BioResource operates within the guidelines of the Tissue Act Scotland, 2006.

When submitting a written request for permission to collect or access tissue/data:

- Please print neatly or type.
- Patient identity is confidential. Samples will be coded and supplied with a minimum data set.
- Researchers are required to cover the cost of transport of their samples and supply appropriate customs declarations if applicable.
- For additional information please contact the South East Scotland HSS (SAHSC) BioResource at frances.rae@luht.scot.nhs.uk, craig.marshall@luht.scot.nhs.uk, or rie.tissuegovernance@luht.scot.nhs.uk
- Please send completed request forms and proof of ethical approval where applicable to Frances Rae with a copy to Craig Marshall at the above e-mail address.
- Application will then be sent to the appropriate Scientific Review Committee for consideration and approval. No tissue or data will be released prior to approval being granted.

Appendix 2

REQUEST FORM.

Name & Address of PI: e-mail address:	Professor Philippa Saunders Director, Postgraduate Research, CMVM. Professor of Reproductive Steroids, MRC Centre for Inflammation Research, The Queen's Medical Research Institute, 47 Little France Crescent Edinburgh EH16 4TJ 0131-242-6388 (office) p.saunders@ed.ac.uk
Study Title: Ethical Status:	Early Diagnosis and Treatment Strategies for Endometrial Cancer N/A
Sponsor:	N/A
Funding Body:	Cancer Research UK / Edinburgh Cancer Research Centre
Material/Data Requested: Please be specific as to the nature of the material/data and indicate exactly the type and quantity eg fresh frozen, paraffin embedded, archival or prospective etc. If the request is for sections, please specify quantity, thickness of sections required, and type of slide eg plain or adhesive.	We would like to request endometrial tissue samples and have access to anonymised patient medical history data stored within NHS Lothian and the Department of Pathology at the Royal Infirmary of Edinburgh. Via our NHS Lothian/Clinical collaborator – Professor Alistair Williams, Chair of Gynaecological Pathology, a patient cohort of interest has been identified. These patients underwent endometrial sampling and/or surgery between the years 2004-2009 and were diagnosed with the condition endometrial hyperplasia (Now also referred to as Endometrial Intraepithelial Neoplasia – EIN). From this patient cohort we would like to obtain the original index diagnostic tissue sample(s), any prior / subsequent tissue samples taken in the diagnostic/treatment timeline and also anonymised demographic/medical history information about these patients from their medical records (paper or electronic.) These data/tissue sections will be used within the University of Edinburgh for further research into the classification and understanding of the condition endometrial hyperplasia/EIN by examining expression of putative biomarkers of the condition.

	This will involve immunohistochemical staining for proteins previously identified as diagnostic of 1) the proliferation status of cells within the tissue; 2) response to steroids [e.g. receptor proteins] 3) epithelial-mesenchymal transition 4) mismatch repair activity 5) inflammation. Information from this study will be analysed and correlated along with the medical history data and patient demographics. If unstained slides are provided, we would like the archival tissue to be from FFPE blocks, cut at 5 microns and on adhesive glass slides. There are 143 patients within our identified cohort and we would initially require 50 unstained sections from the index diagnostic biopsy of each patient. From a subset of the cohort (unknown quantity at present) we would also want 50 unstained sections from selected pre and post index biopsy samples along the diagnostic timeline in order to map disease progression. Medical history and demographic data would include: age, BMI, parity, hormone use, family history, past medical history, past surgical history, smoking status and other relevant risk factor(s) data for development of endometrial hyperplasia/EIN.
Synopsis of project (100 – 200 words approximately):	Endometrial cancer is a common malignancy of the uterine lining; rates are rising and there is an increasing incidence of pre-menopausal disease which is more difficult to diagnose. Sex-steroids (especially unopposed oestrogens) have been shown to play a crucial role in the development of endometrial cancer, with lifetime exposure influencing cell proliferation in normal and malignant endometrial tissue. A recent integrated genomic and proteomic analysis has provided new insights into the biology and classification of endometrial cancer. This project will investigate endometrial pre-malignant neoplasia using a range of methods in order to develop improved strategies for earlier diagnosis and treatment. In 1994 The World Health Organisation (WHO) classified the condition known as ‘Endometrial Hyperplasia’. The WHO classification of endometrial hyperplasia consists of four categories, of which complex hyperplasia with nuclear atypia is considered to have the greatest risk of progression to endometrioid endometrial carcinoma. However, there is often considerable variability amongst pathologists when diagnosing specimens using the WHO nomenclature A new classification of the endometrial intraepithelial neoplasia (EIN) was published in 2000. It has been claimed that the EIN system better predicts disease progression. We wish to investigate the following:

	(i) What are the key cellular changes that characterise these precursor lesions of endometrioid endometrial carcinomas? (ii) What are the patterns of expression of steroid receptors and steroid responsive genes in the precursor lesions of endometrioid endometrial carcinomas and can they predict responsiveness to therapies designed to interrupt the precursor-cancer transition?
If tissue collection is prospective, estimated number of patients to be consented.	N/A
Material disposal or storage plan:	1) Slides would be physically stored within the University of Edinburgh, MRC Centre for Inflammation Research and if no longer required, sensitive disposal would be undertaken in line with the University of Edinburgh guidelines on disposal of human tissue waste. 2) Electronically stored (Slides scanned) on secure server as a future reference library.
Date Required:	ASAP
Shipping Address (if different to above):	Saunders Lab, West-Block MRC Centre for Inflammation Research, The Queen's Medical Research Institute, 47 Little France Crescent Edinburgh, EH16 4TJ

AGREEMENT FOR USE OF TISSUE/DATA.

The recipient agrees that any tissue/data provided by the South East Scotland HSS (SAHSC) BioResource will only be used for the purposes specified in this application and will only be used for the common good in scientific research or education. The recipient shall maintain retrievable records linking the material and accompanying data to the terms of acquisition. The recipient agrees not to attempt to obtain information identifying the individuals donating tissues/data to the South East Scotland HSS (SAHSC) BioResource. The recipient agrees they shall not sell any portion of the tissues/data provided by the South East Scotland HSS (SAHSC) BioResource, or products directly extracted from tissue material (e.g. protein, mRNA or DNA). The recipient also agrees that they shall not transfer tissue/data (or any portion thereof) supplied by the South East Scotland HSS (SAHSC) BioResource to third parties without prior written permission of the South East Scotland HSS (SAHSC) BioResource. Any subsequent transfer that may be made to other parties, with prior agreement from the South East Scotland HSS (SAHSC) BioResource, will require signature of this agreement between the final recipients of the material and the South East Scotland HSS (SAHSC) BioResource.

Appendix 2

The recipient understands that while the South East Scotland HSS (SAHSC) BioResource attempts to avoid providing tissues that are contaminated with highly infectious agents eg hepatitis or HIV, all tissues should be handled as if potentially infectious. The individuals who have supplied tissue to the South East Scotland HSS
(SAHSC) BioResource have not agreed to have clinical tests performed on this tissue, therefore, the recipient agrees not to perform such tests on the tissues supplied by the South East Scotland HSS (SAHSC) BioResource. The recipient acknowledges that the institution where the tissue/data will be used follows the relevant Human Tissue Authority or appropriate local regulations for handling human specimens and will instruct their staff to abide by those rules. The recipient further agrees to assume all responsibility for informing and training personnel in the potential risks and safety procedures for the handling of human tissues.

Tissues are provided as a service to the research community without warranty of merchantability or fitness for a particular purpose or any other warranty, express or implied. The South East Scotland HSS (SAHSC) BioResource accepts no responsibility for any injury (including death), damages or loss that may arise either directly or indirectly from their use.
The recipient agrees to acknowledge the contributions of the South East Scotland HSS (SAHSC) BioResource in all publications resulting from the use of these tissues/data
The institution agrees to assume all risks and responsibility in connection with receipt, handling, storage and use of tissue/data from the South East Scotland HSS (SAHSC) BioResource. It further agrees to indemnify and hold harmless the South East Scotland HSS (SAHSC) BioResource from any claim costs, damages or expenses resulting from the use of the tissue/data provided by the South East Scotland HSS (SAHSC) BioResource. The undersigned warrant that they have authority to execute this agreement on behalf of the recipient institution.

By my signature I agree to the terms set out in the above agreement

Name of Principal Investigator:	Professor Philippa TK Saunders
Institution:	The University of Edinburgh
Signature:	

Appendix 2

NHS LOTHIAN SAHSC BIORESOURCE
SAMPLE REQUEST ANSWER FORM

Sample Request number:	SR465
Name of Researcher:	Professor Philippa Saunders
Address of Researcher:	Director, Postgraduate Research CMVM MRC CIR QMRI Edinburgh
Study Title:	Early Diagnosis and Treatment Strategies for Endometrial Cancer
Ethical status:	13/ES/0126
Material Requested	Release and use of the followng is approved in principle for the purposes of this project:, but we will be unable to meet the requirement for 50 sections from the blocks. Anonymised archival endometrial tissue samples and linked patient medical history data as described on the request form. Paraffin sections will be supplied, but the number of slides will be significantly less than 50, and further discussion with Prof Williams will be necessary.

REQUEST AUTHORISED

Date:	12-Feb-2015
Authorised by:	Frances Rae

REQUEST REJECTED

Date:	
Authorised by:	
Reason	

10 Appendix 3

- Sample histopathology scoring proforma for endometrial hyperplasia samples.

Appendix 3

Sample number: **Date reviewed:** **Reviewer:**				
Adequate endometrial tissue for diagnosis?	**YES**	**NO**	**Only if NO: Tick all that apply**	
	□	□	Inadequate Quality	□
			Processing / technical problems	□
			Other: Specify	
Diagnosis:				
Benign Endometrium	**YES**	**NO**	**Only if YES: only tick one**	
	□	□	Atrophic	□
			Inactive	□
			Proliferative	□
			Disordered Proliferative	□
			Secretory (including progestin & OCP effect)	□
			Menstrual	□
			Endometritis	□
			Other: Specify	
Endometrial Hyperplasia	□	**WHO 2014**	Hyperplasia without Atypia	□
			Endometrioid intraepithelial neoplasia (EIN)	□
	□	**WHO 1994**	Simple, non-atypical hyperplasia	□
			Complex non-atypical hyperplasia	□
			Simple atypical hyperplasia	□
			Complex atypical hyperplasia	□
Malignant Neoplasm	□	□	Endometrial neoplasm	□
			Type: Specify	
			Other malignant neoplasm	□
			Type: Specify	
Polyp:				
Endometrial polyp	**YES**	**NO**	**Only if YES: only tick one**	
	□	□	Atrophic	□
			Functional	□
			Hyperplastic	□
Notes:				

11 Appendix 4

Published paper:

Peter A. Sanderson, Hilary O.D. Critchley, Alistair R.W. Williams, Mark J. Arends, Philippa T.K. Saunders; New concepts for an old problem: the diagnosis of endometrial hyperplasia, Human Reproduction Update, Volume 23, Issue 2, 1 March 2017, Pages 232–254.

Human Reproduction Update, Vol.23, No.2 pp. 232–254, 2017
Advanced Access publication on December 5, 2016 doi:10.1093/humupd/dmw042

human reproduction update

New concepts for an old problem: the diagnosis of endometrial hyperplasia

Peter A. Sanderson[1], Hilary O.D. Critchley[2], Alistair R.W. Williams[3], Mark J. Arends[4,5], and Philippa T.K. Saunders[1,*]

[1]MRC Centre for Inflammation Research, The University of Edinburgh, The Queen's Medical Research Institute, 47 Little France Crescent, Edinburgh EH16 4TJ, UK [2]MRC Centre for Reproductive Health, The University of Edinburgh, The Queen's Medical Research Institute, 47 Little France Crescent, Edinburgh EH16 4TJ, UK [3]Division of Pathology, The Royal Infirmary of Edinburgh, 51 Little France Crescent, Edinburgh EH16 4SA, UK [4]Division of Pathology, Edinburgh Cancer Research Centre, Western General Hospital, Crewe Road South, Edinburgh EH4 2XR, UK [5]Centre for Comparative Pathology, The University of Edinburgh, Easter Bush, Midlothian EH25 9RG, UK

*Correspondence address. E-mail: p.saunders@ed.ac.uk

Submitted on May 2, 2016; resubmitted on October 24, 2016; editorial decision on October 27, 2016; accepted on October 31, 2016

TABLE OF CONTENTS

BACKGROUND: Endometrial hyperplasia (EH) is a uterine pathology representing a spectrum of morphological endometrial alterations. It is predominantly characterized by an increase in the endometrial gland-to-stroma ratio when compared to normal proliferative endometrium. The clinical significance of EH lies in the associated risk of progression to endometrioid endometrial cancer (EC) and 'atypical' forms of EH are regarded as premalignant lesions. Traditional histopathological classification systems for EH exhibit wide and varying degrees of diagnostic reproducibility and, as a consequence, standardized patient management can be challenging.

OBJECTIVE AND RATIONALE: EC is the most common gynaecological malignancy in developed countries. The incidence of EC is rising, with alarming increases described in the 40–44-year-old age group. This review appraises the current EH classification systems used to stratify women at risk of malignant progression to EC. In addition, we summarize the evidence base regarding the use of immunohistochemical biomarkers for EH and discuss an emerging role for genomic analysis.